TRACING PALEOZOIC SILICICLASTIC SEDIMENT DISPERSAL TO THE FORT WORTH AND MIDLAND BASINS: IMPLICATIONS FOR PALEOGEOGRAPHY AND ORGANIC MATTER ACCUMULATION

by

OHOOD BADER ALSALEM

Presented to the Faculty of the Graduate School of

The University of Texas at Arlington in Partial Fulfillment

of the Requirements

for the Degree of

DOCTORAL OF PHILOSOPHY IN EARTH AND ENVIRONMNTAL SCIENCES

THE UNIVERSITY OF TEXAS AT ARLINGTON

May, 2019

In loving memory of the two beloved men in my life:

Bader Jasem Alsalem
(May 11, 1941 – December 8, 1997)
A father, a teacher, and a great man,

Faisal Hesham Almughrabi
(August 29, 1977 – March 19, 2019)
A husband, a friend, and a life partner.

ACKNOWLEDGEMENTS

It all started as a little girl's dream, with faith, hard work, confidence and self-motivation, that dream became true – Ohood

I would first like to express my deep gratitude to all those who had encouraged and assisted me for years to complete this work. Special appreciation goes to my advisor, Prof. Majie Fan, for her continual guidance and extreme support during these years. I highly appreciate the great amount of time and patience that Prof. Fan has put on teaching me new methods, lab techniques and inspiring my research thoughts. I will always be grateful to her for helping me to develop my understanding of basin analysis and sediment provenance, and their importance to modern researche. Her continuous encouragement has increased my confidence in myself, which prepared me very well for my dissertation defense. She gave me several chances to attend different conferences that helped me to increase my knowledge and interact with others to gain new thoughts regarding my research. Also with her guidance, my writing skills had tremendously improved and I was able to published two articles even before getting my PhD degree. Prof. Fan has always believed in me and my skills, and she has been a good teacher, advisor, and a great friend to me and to my family. I will always remember the great time me and my family had with her lovely family during thanksgiving. Her commitment to her students is what makes her a great advisor. I am so grateful for the journey we had together, as it gave me an opportunity to develop my ability as an independent researcher and polish my skills for the future. Without her continuous support, I wouldn't be able to accomplish this work with such a great success.

I would also like to thank my committee members, including Prof. Xiangyang Xie, for his continuous advising and help in collecting the data used in Chapter 2 and 4, Prof. Asish R. Basu, for his help in processing and interpreting the REEs data presented in Chapter 3, Prof. Merlynd Nestell and Dr. Matthew Loocke for their time, comments, and guidance throughout the preparation and review of this dissertation.

Many thanks to the committee members of the scholarship in Kuwait University for providing me the financial support for my master and PhD degrees at the University of Texas at Arlington. This honorable scholarship provided me a great opportunity to conduct research that is very significant and to pursue my academic dream. I look forward to joining in my former professors at the Department of Earth and Environmental Sciences in Kuwait University, and to bringing all the knowledge I had learned through my seven years of study in the USA.

I will always be thankful to my academic advisers at the General Consulate at the Embassy of Kuwait, Mrs. Karla Petty and Mr. Marcelo Ostria for their help throughout the years of my graduate studies.

I am so grateful to Dr. Jasem Alawadhi for believing in me since day one, and encouraging me to apply for the scholarship to pursue my graduate studies. Also I would like to thank my former professors at the Department of Earth and Environmental Sciences in the Kuwait University: Dr. Maryam Alkuwairan for her continuous encouragement and endless support that she provided me from a distance, Dr. Dhary Alkandary and his wife Aroub Alkandary, for the good days that our families had together, Dr. Yaqoub Alrefaei and his wife Hanan Alsharah for providing the help and support when I need it, and to the five wonderful women: Dr. Adeeba Alhurban, Dr. Fowzia Abdullah, Dr. Fozya Alruwayeh, Ms. Suad Qabazard and Ms. Huda Qabazard, who had inspired me and supported me for years since my undergraduate study in Kuwait University.

***

Great thanks to my office mate and friend, Lu Zhu, for her endless help in teaching me some of the lab work. Lu is a great friend; she has never stopped encouraging me since we met. She was a good listener and a problems solver. She never complained listening to my problems every morning and she was always willing to help me to find the best solutions. I will always remember her sharing her delicious snacks with me so I wouldn't starve while working late. Special thanks also go to my friend, Hepeng Tian, for his help in some of the lab work, cutting and crushing some

of my samples, and helping me with my references list. I enjoied working with him, sharing the knowledge, new ideas and thoughts regarding our projects. Many thanks also to my friend, Puloma Chakrabarty, for her help in teaching me the REEs and Nd isotope calculations, and for all the great time she shared with me as she never stopped putting a big smile on my face and changing my bad mood. I also would like to thank Min Gao and Jenna West, for being good friends and great support during my first years at the University of Texas at Arlington, and the entire Department of Earth and Environmental Sciences, including faculty, staff, and students for making a productive academic environment and creating a home away from home.

I would like to express my gratitude to my friends, members of the Saudi Students Club at Arlington: Mousa Almotairi, Reem Alsogaih, Aohud Binbuhaer, Noura Alkhaldi and Hanof Alkhaldi, for all the activities, events and good time we had together. It was an honor to work with all of them and I am so glad that I got the chance to show other people our beautiful middle-eastern culture.

Special thanks are extended to all the inspiring ladies in my life and to all my friends here in the USA, specially Ashwaq Almotairi, Shaikha Aldousari, Aseel Alsaleh, Haneen Almuzani, Sumiah Attiah, and Hanaa Tayara, and to all my friends in the State of Kuwait, specially Dr. Abeer Almaimouni, Nouf Aloraini, Noura Sabeel, Afrah Alajmi, Hiba Abyan, Fatma Alotaibi, Laila Aldousary, Bashayer Aldhifery, Munira Almansour, Jomana AsdAllah and Sakeena Faraidoun, for their endless support and for being constant sources of motivation and inspiration. Each of them is an extraordinary woman who kept inspiring me with her success stories. I wouldn’t be able to reach this point without all the love and support I got from them throughout those years.

***

Kindly I want to thank my mother Shaikha Almezel, my two adorable sisters Amna and Ghosoon Alsalem, my wonderful brother Mobarak Alsalem, my sweet sister-in-law Shaymaa Alradhan, my lovely nephew Abdualaziz Alsalem, and all my other sisters, nephews, nieces, aunts

and cousins for their unconditional support regardless of the distance. I highly appreciate all the positive energy and love I've been blessed with. This study could not have been completed without this encouragement and support. Also I won't forget my two beautiful kids, Wasan and Yousef, for adding joy and fulfilment in my life and sharing my journey far from home.

Lastly and most importantly, with a grieved heart I want to express my heartiest gratitude to my beloved husband Faisal Almughrabi, who has shockingly passed away recently. Faisal was not only my life partner and father of our two adorable kids, but also my best friend and my perfect companion, with whom I shared a loving home, dreams and passion for art and music. He always believed in me, and he always supported and encouraged me to pursue my dreams, and for all of that and the sacrifices he had made to ensure that my dreams will come true, I will forever cherish the memory with thankfulness and endless love for my lifetime.

April 22, 2019

ABSTRACT

TRACING PALEOZOIC SILICICLASTIC SEDIMENT DISPERSAL TO THE FORT WORTH AND MIDLAND BASINS: IMPLICATIONS FOR PALEOGEOGRAPHY AND ORGANIC MATTER ACCUMULATION

Ohood Bader Alsalem, Ph.D.

The University of Texas at Arlington, 2019

Supervising Professor: Majie Fan

The Fort Worth and Midland Basins in central and West Texas are major petroleum-producing systems in North America. The provenances of the thick Paleozoic sedimentary rocks in both basins are poorly constrained, although they are important to the understanding of these petroleum systems. The siliciclastic grains of the upper Paleozoic in the two basins were proposed to be derived from local sources, including the basin-bounding Ouachita-Marathon orogen and crystalline basement-cored Ancestral Rocky Mountains, or distal source of the Appalachian highland. The distal source requires a transcontinental river system routing along the Appalachian-Ouachita forelands. Here I applied several provenance-tracking methods, including detrital zircon U-Pb geochronology and Lu-Hf isotope composition, sandstone petrography, and mudstone rare-earth element compositions, to the Paleozoic strata in the Fort Worth and Midland Basins in order to reconstruct sediment dispersal patterns in the southern margin of Laurentia, and test the sediment routing hypotheses. The data show that during the Cambrian, sediments were transported by local rivers from basement rocks exposed on the Texas Arch to the northwest of the basins. During the Pennsylvanian-early Permian, sediments were transported by a transcontinental river from the Appalachians in the front of the Appalachian-Ouachita orogen and by local rivers draining the peri-Gondwana terranes incorporated in the Ouachita-Marathon orogen. The late Paleozoic sediment

dispersal may be assisted by another transcontinental river linking the Midland Basin and Appalachians through the midcontinent area. These rivers may have brought abundant nutrients into the two basins, promoted algal bloom and contributed organic matter enrichment in the basins.

Table of Contents

List of Illustrations

List of Tables

Chapter 1 INTRODUCTION

Subduction of the southern margin of Laurentia underneath Gondwana and the subsequent collision between the two continents caused the Alleghanian-Ouachita-Marathon orogenies and flexural subsidence of several peripheral foreland basins in eastern and southern Laurentia during the late Paleozoic. The Fort Worth and Midland Basins in Texas, U.S.A., evolved from a passive margin tectonic setting to a contractional tectonic setting during the late Paleozoic. Both basins are major oil-producing regions in the world. Numerous studies have been conducted on the Paleozoic basin fill in the two basins in order to understand the petroleum systems, yet the provenances of the basin fill and the paleogeography before and during the Laurentia-Gondwana collision remain poorly constrained. Sediment dispersal patterns along the southern margin of Laurentia are fundamental to the understanding of the paleogeography, and tectonic configuration before and during the collision, intracontinental responses to Laurentia-Gondwana collision and organic matter accumulation.

This dissertation includes three projects presented in Chapters 2, 3 and 4. Chapter 2 is entitled *Paleozoic sediment dispersal before and during the collision between Laurentia and Gondwana in the Fort Worth Basin, USA*. It determines sediment provenance of Cambrian and Pennsylvanian sandstones in the Fort Worth Basin using detrital zircon U-Pb geochronology. This work was published in Geosphere in 2018. The citation is Alsalem, O.B., Fan, M., Zamora, J., Xie, X., and Griffin, W.R., 2018, Paleozoic sediment dispersal before and during the collision between Laurentia and Gondwana in the Fort Worth Basin, USA: Geosphere, v. 14, no. 1. doi:10.1130/GES01480.1. GSA states “An author has the right to use his or her article or a portion of the article in a thesis or dissertation without requesting permission from GSA, provided the bibliographic citation and the GSA copyright credit line are given on the appropriate pages”.

Chapter 3 in entitled *Paleozoic sediment dispersal to the Fort Worth Basin: Constraints from sandstone petrography and mudstone REEs*. Chapter 2 concludes different sediment dispersal patterns between the Cambrian and Middle Pennsylvanian, but cannot determine when the Middle Pennsylvanian dispersal pathway began because of the lack of sandstone in the Mississippian and Lower

Pennsylvanian in the Fort Worth Basin. This chapter applies sandstone petrography and mudstone rare-earth element concentrations to test the interpretation of sediment dispersal pathways in Chapter 2, and determine the timing of the earliest change of sediment provenance.

Chapter 4 is entitled *Paleozoic sediment dispersal before and during the collision between Laurentia and Gondwana in the Midland Basin*. In this chpter, I determine sediment provenance of the Cambrian and Pennsylvanian sandstones in the Midland Basin using detrital zircon U-Pb ages and Lu-Hf isotopic data.

Chapter 2 PALEOZOIC SEDIMENT DISPERSAL BEFORE AND DURING THE COLLISION BETWEEN LAURENTIA AND GONDWANA IN THE FORT WORTH BASIN, USA

Ohood B. Alsalem[1], Majie Fan[1], Juan Zamora[1], Xiangyang Xie[2], and William R. Griffin[3]

[1]Department of Earth and Environmental Sciences, The University of Texas at Arlington, Arlington, Texas 76019, USA

[2]School of Geology, Energy, and the Environment, Texas Christian University, Fort Worth, Texas 76129, USA

[3]Department of Geosciences, The University of Texas at Dallas, Richardson, Texas 75080, USA

ABSTRACT

We report detrital zircon U-Pb ages in the Fort Worth Basin (southern USA) aimed at understanding sediment dispersal patterns on the southern margin of Laurentia before and during the Laurentia-Gondwana collision. The ages from two Cambrian fluvial-marginal marine sandstone and six Pennsylvanian deltaic-fluvial sandstone samples span from Archean to early Paleozoic time. In the Cambrian sandstones, 80% of zircons are of Mesoproterozoic age (1.451–1.325 Ga) and 18% are of Grenvillian age. The high abundance of the Mesoproterozoic population suggests that the grains were dispersed by a local river draining the midcontinent granite-rhyolite province located in the Texas Arch to the northwest of the Fort Worth Basin. In the Pennsylvanian sandstones, 26% of zircons are of Archean–early Mesoproterozoic age, 47% are of Grenvillian age, 15% are of Neoproterozoic–earliest Paleozoic age (800–500 Ma), and 10% are of early Paleozoic age (500–318 Ma), indicating a different dispersal pattern during the Pennsylvanian relative to the Cambrian. Compared to other early Paleozoic detrital zircon records on the southern margin of Laurentia, our Pennsylvanian sandstones have a distinct age peak at ca. 650–550 Ma, which we interpreted to be a result of transport by local rivers draining a peri-Gondwana terrane, most likely the Sabine terrane in the Ouachita orogen. The high abundance of Grenvillian zircons reflects either direct transport from the Appalachians by an axial river or recycling from Mississippian–Pennsylvanian sedimentary rocks incorporated in the Ouachita

orogenic front. The similarity of detrital zircon age distributions in the Fort Worth Basin, the Arkoma Basin, and the southern Appalachian forelands seems to favor sediment dispersal by a major river with headwaters in the southern Appalachians.

2. 1 INTRODUCTION

Subduction of the southern Laurentian margin underneath Gondwana and the subsequent collision between the two continents caused the Alleghanian-Ouachita-Marathon orogenies and flexural subsidence of several peripheral foreland basins in southern Laurentia during the late Paleozoic (e.g., Walper, 1982; Erlich and Coleman, 2005; Thomas, 2006; Elebiju et al., 2010). The contractional tectonics may have accumulated enough intracontinental stress to reactivate paleotransform faults in western Laurasia, leading to the basement-involved Ancestral Rocky Mountain (ARM) orogeny (Dickinson, 2000; Dickinson and Lawton, 2003). Sediment dispersal patterns and paleogeographic reconstruction of the southern margin of Laurentia are fundamental to the understanding of the tectonic configuration before and during the collision, as well as the intracontinental responses to the collision.

In north-central Texas, U.S.A., the Fort Worth Basin evolved from a passive margin to a foreland basin during the late Paleozoic (Thomas, 1977; Walper, 1982). Numerous studies have been conducted on the Paleozoic basin-fill in the Fort Worth Basin in order to understand petroleum systems of the region (e.g., Morris, 1974; Pollastro et al., 2003, 2007; Hentz et al., 2012), yet, the provenances of the basin-fill and the paleogeography before and during the collision remain poorly constrained. Two hypotheses have been proposed to explain the provenance of the Paleozoic basin fill in the Fort Worth Basin. Graham et al., (1975) proposed that the Paleozoic highland of the Appalachians funneled sediments into its foreland, and the sediments were then transported by a large axial river and dispersed into remnant ocean basins. This idea was further supported by neodymium isotope studies in the Arkoma Basin in Oklahoma and Arkansas, and Marathon Basin in West Texas (Gleason et al., 1994; 1995); detrital zircon U-Pb ages in the Marathon foreland in West Texas (Gleason et al., 2007); and $^{40}Ar/^{39}Ar$ analysis of detrital muscovite in the Black Warrior Basin in Alabama (Uddin et al., 2016). As

summarized in Archer and Greb (1995), the most direct physical evidence for the river system is Early Pennsylvanian paleovalleys with 20-70 m of incision and south-southwestward paleoflow directions in the central Appalachian basin, Kentucky, and Indiana. Other studies have suggested that the large river originated in the Appalachians, instead of flowing through the Appalachian-Ouachita foreland, drained through or around the Illinois Basin before entering the Ouachita front (Thomas, 1977; Sharrah, 2006; Xie et al., 2016). However, based on fractional volume of sand and interpretation of westward and southwestward propagation of deltas, the siliciclastic detritus in the Fort Worth Basin have been suggested to be from local sources, including the basin-bounding Ouachita orogen to the east and the basement-involved ARM uplifts to the north of the basin (Lovick et al., 1982; Walper, 1982; Hentz et al., 2012).

This study determines sediment provenance of Cambrian and Pennsylvanian sandstones in the Fort Worth Basin in southern Laurentia using detrital zircon U-Pb ages. By combining our data with published detrital zircon data in eastern and southern Laurentia, we infer dispersal patterns of siliciclastic sediments on the southern margin of Laurentia, and reconstruct the paleogeography before and during the suturing between Gondwana and Laurentia.

2. 2 GEOLOGICAL SETTING

The Fort Worth Basin is a foreland basin formed on the southern Laurentian continental shelf during the late Paleozoic Ouachita orogeny (e.g., Graham et al, 1975; Walper, 1977; Nelson et al, 1982; Thomas and Viele, 1983). The basin is bounded by the basement-involved Red River and Muenster uplifts to the north, the Ouachita thrust belt to the east, the Llano uplift to the south, and it shallows gently toward the Bend Arch to the west (Figure 2-1).

After the Neoproterozoic rifting of the supercontinent Rodinia, the southern margin of Laurentia gradually evolved into a passive margin of the Iapetus Ocean during the early Cambrian (Houseknecht and Matthews, 1985; Poole et al., 2005; Cawood and Nemchin, 2001). In association with the opening of the Iapetus Ocean, a rift zone was initiated in southern Oklahoma (Keller and Stephenson, 2007; Hanson et al., 2013) and formed the southern Oklahoma aulacogen in the vicinity of

the Fort Worth Basin (Burke, 1977; Perry, 1989). The closure of the Iapetus Ocean started during the Early Ordovician, and was associated with the separation of several arc terranes (e.g., Avalonia, Ganderia, Carolinia, Meguma, Suwannee) from the continental margin of northern Gondwana (e.g., Nance et al., 2002; Keppie et al., 2003; Murphy et al., 2006; Nance and Linnemann, 2008; Pollock et al., 2009; van Staal et al., 2009; Mueller et al., 2014). These terranes were later accreted to Laurentia during the closure of the Iapetus and Rheic Oceans and suturing between Gondwana and Laurentia as early as the Early Devonian. By the Late Devonian, Laurentia, Baltica, and Avalonia-Carolina had collided to form Laurussia. The suturing mechanism between Laurussia and Gondwana has long been debated. Whereasmost studies have agreed that the southern margin of Laurentia subducted underneath Gondwana (e.g., Thomas, 2004; Poole et al., 2005; Nance and Linnemann, 2008), other studies have suggested that the Laurentian plate was the upper plate before the collision (e.g., Domeier and Torsvik, 2014). The final closure of the Rheic Ocean resulted in the complete burial of the Laurentian platform by thick synorogenic sedimentation during the Pennsylvanian in the newly formed foreland basins (e.g., Hatcher, 1989; Viele and Thomas, 1989; Thomas, 2004).

The Alleghanian orogeny that occurred in southeastern Laurentia is the youngest orogenic event in the Appalachian orogen (Nance et al., 2010). The Ouachita orogeny occurred in southern Laurentia and represents the southwestward extension of the Alleghanian orogeny (Loomis et al., 1994; Poole et al., 2005), or is possibly coeval with the Alleghanian orogeny (Thomas, 1977; Robinson et al., 2012). The Ouachita orogen extends from Mississippi westward to southeastern Oklahoma, bends southward in eastern Texas, and is contiguous with the Marathon uplift in western Texas (Graham et al., 1975; Houseknecht and Matthews, 1985; Loomis et al., 1994; Poole et al., 2005) (Figure 2-1). Today, the mountains are mostly buried underneath Mesozoic and Cenozoic strata of the Gulf Coastal Plains (Houseknecht and Matthews, 1985; Loomis et al., 1994), and exposed only in the Marathon and Solitario uplifts in West Texas and in the Ouachita Mountains in Arkansas and Oklahoma (Thomas and Viele, 1983; Noble, 1993) (Figure 2-1).

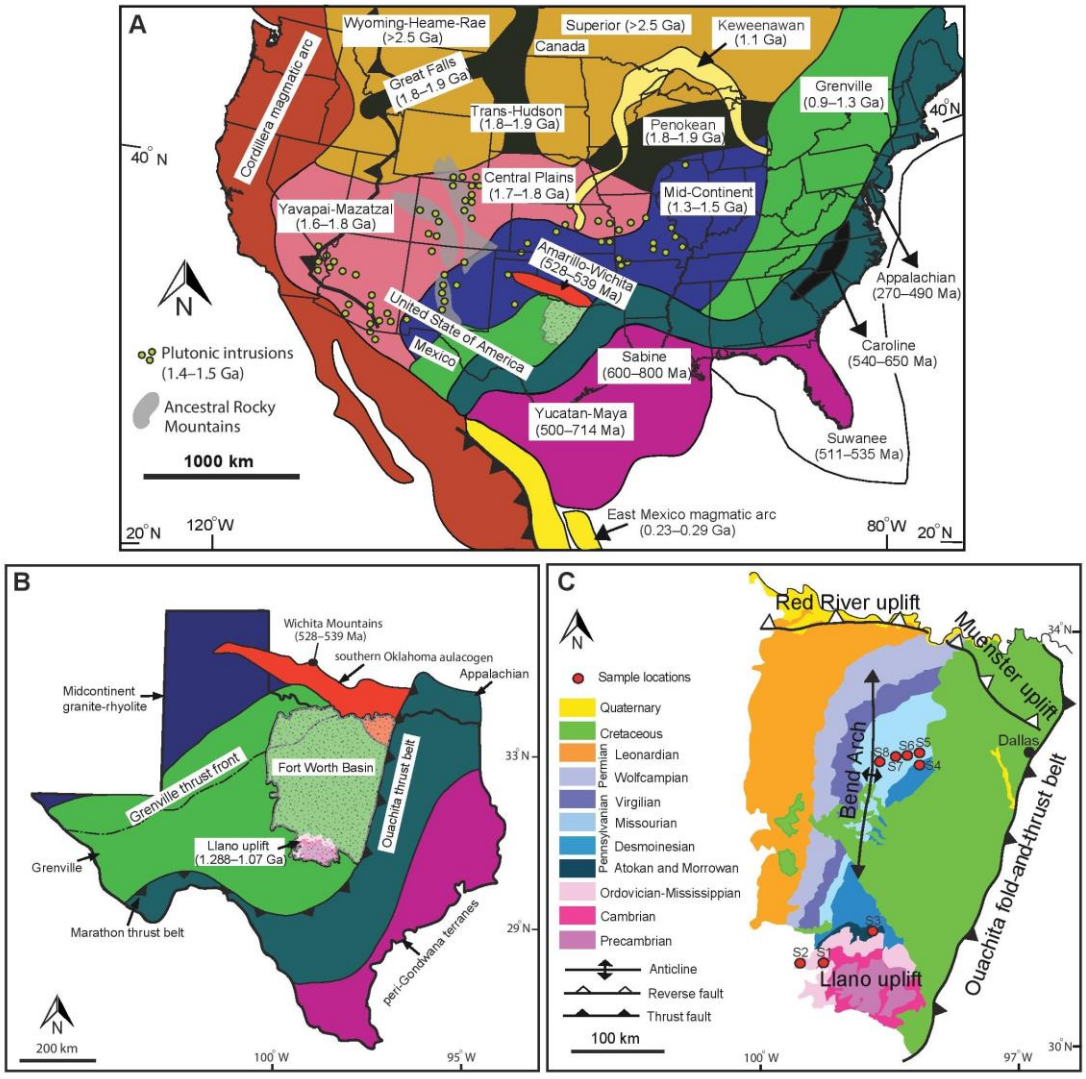

Figure 2-1 (A) Map showing the main basement provinces and study area in North America. Fort Worth Basin is shown in a stippled pattern. Modified after Sims and Petermar (1986), Mueller et al. (2002), and Dickinson and Gehrels (2009). (B) Map showing tectonic provinces and distribution of surface exposures of Precambrian and Cambrian rocks in Texas. Modified after Thomas (2006), Stoeser et al. (2007), and Whitmeyer and Karlstrom (2007). (C) Geological map of the Fort Worth Basin. Modified after Barnes (1992) North America stages follow Rohde (2005).

Contractional tectonics during the late Paleozoic also reactivated rift-related faults of the southern Oklahoma aulacogen and formed the northwest-striking Red River and Muenster uplifts as part of the Amarillo–Wichita uplift (Walper, 1982; Keller et al., 1989; Montgomery et al., 2005; Elebiju et al., 2010; Alsalem et al., 2017). Reactivation of early Paleozoic normal faults also caused the initial rise of the basement-involved Llano uplift in southern Laurentia (Erlich and Coleman, 2005). Exhumation of the Llano uplift continued into the Late Pennsylvanian, which may have tilted the strata in the Fort Worth Basin westward (Thomas, 2003). The Fort Worth Basin may have experienced exhumation during the late Permian-Jurassic as a result of the opening of the Gulf of Mexico (Jarvie et al., 2005; Ewing, 2006; Stern and Dickinson, 2010).

2. 3 STRATIGRAPHY

The Cambrian–lower Permian sedimentary rocks in the Fort Worth Basin are up to ~3.7 km thick (Montgomery et al., 2005). In north-central Texas, the late Cambrian strata unconformably overlie Proterozoic gneiss and schist as well as granitic intrusions (Stenzel, 1935). The Paleozoic strata are unconformably overlain by Lower Cretaceous strata in the eastern part of the Fort Worth Basin (Figure 2-1C). Based on depositional environments and tectonic histories, Montgomery et al. (2005) divided the Paleozoic strata in the Fort Worth Basin roughly into three intervals: (1) late Cambrian to Ordovician platform strata deposited in a passive continental margin; (2) Mississippian shallow marine rocks deposited during the exhumation of the Amarillo-Wichita uplift; and (3) Pennsylvanian–lowermost Permian interbedded shallow marine and deltaic deposition associated with the development of Ouachita orogen. The Paleozoic strata thin rapidly toward the southwest and crop out in the Llano uplift (Turner, 1957; Moore, 1959; Feray and Brooks, 1966; Erlich and Coleman, 2005; Montgomery et al., 2005; Alsalem et al., 2017). Below we briefly describe the clastic units that we sampled. The lithofacies of each sample and the sample locations are summarized in Table 2-1.

Table 2-1 Location and sample description of the sandstone samples used for detrital zircon geochronology in this study, Fort Worth Basin, USA

Sample no.	Sample name	Formation (Group)	Epoch	Latitude (°N)	Longitude (°W)	Elevation (m)	Sample description	References
S1	Lower Hickory	Riley (Moore Hollow)	Late Middle Cambrian	30.8371	99.1171	491	Cross-bedded, coarse- to medium-grained, angular to subangular, poorly sorted quartzose sandstone	Bridge et al., 1947; Barnes and Bell, 1977
S2	Upper Hickory	Riley (Moore Hollow)	Late Cambrian	30.7653	99.4051	521	Coarse-grained, moderately to well-sorted, well-rounded quartzose sandstone with iron-oxide ooids and cement	Barnes and Schofield, 1964; Randolph, 1991; Wilson, 2001
S3	Big Saline	Big Saline (Bend)	Middle Pennsylvanian	31.1377	98.5795	397	Medium-grained, subangular quartzose sandstone	Flippin, 1982
S4	Dobbs Valley	Grindstone Creek (Strawn)	Middle Pennsylvanian	32.7050	98.0688	234	Large-scale trough cross-bedded sandstone	Brown et al., 1973
S5	Brazos River	Brazos River (Strawn)	Middle Pennsylvanian	32.7554	98.0562	285	Small-scale trough cross-bedded, ripple cross-laminated, or planar-laminated sandstone	Brown et al., 1973
S6	Lake Pinto	Mineral Wells (Strawn)	Middle Pennsylvanian	32.7828	98.1802	270	Cross-bedded, coarse-grained sandstone	Plummer and Hornberger, 1935
S7	Turkey Creek	Mineral Wells (Strawn)	Late Pennsylvanian	32.7679	98.3125	325	Cross-bedded, coarse-grained sandstone	Plummer and Hornberger, 1935
S8	Colony Creek	Colony Creek Shale (Canyon)	Late Pennsylvanian	32.7529	98.5197	386	Cross-bedded or massive, fine-grained sandstone	Brown et al., 1973

Two sandstone samples (S1 and S2) were collected from the Hickory Sandstone Member of the upper Cambrian Riley Formation in the south side of the Fort Worth Basin (Figure 2-1C; Table 2-1). The member comprises fluvial–shallow marine sandstone deposited in a shallow epicratonic embayment on the Texas platform (Goolsby, 1957; Cornish, 1975; Krause, 1996; Teran, 2007). The thickness of the member reaches up to 168 m in paleotopographic lows (Barnes and Bell, 1977). The Hickory Sandstone is subdivided into upper, middle, and lower subunits (Figure 2-2). The lower subunit was interpreted to be braided stream deposits grading upward into tidal flat and intertidal estuarine deposits, the middle subunit consists of fluvial-influenced, shallow subtidal estuarine and shoreface deposits, and the upper subunit consists of estuarine–shallow marine deposits (Goolsby, 1957; Cornish, 1975; Krause, 1996). Primary depositional cross-beds within the Hickory Sandstone suggest that sediments were mostly transported from north-northwest to south-southeast (Wilson, 1962; Cornish, 1975; Krause, 1996; Cook, 2009). Our samples were collected from the lower and upper subunits.

One Pennsylvanian sandstone sample (S3) was collected from the Big Saline Formation in the southwestern part of the Fort Worth Basin (Figure 2-1C; Table 2-1). Cheney (1940) and Turner (1957) proposed that the Big Saline is a formation within the Middle Pennsylvanian Bend Group, and that this formation overlies the Early Pennsylvanian Marble Falls Formation (Figure 2-2). The formation consists of predominantly limestone with thin beds of deltaic sandstone and mudstone in the southwestern part of the basin, and becomes interbedded with sandstone and conglomerate of the Bend

conglomerate in the northern part of the basin (Turner, 1957; Thompson, 1982; Flippin, 1982). Lithofacies distribution of the Lower Pennsylvanian Bend Group suggests that the paleorivers flowed from the Ouachita orogen and Muenster uplift toward the northwest and southwest (Hentz et al., 2012).

The other five Pennsylvanian samples (S4–S8) were collected from the northwestern part of the Fort Worth Basin (Figure 2-1C; Table 2-1). Four of the samples were collected from different sandstone members of the upper Middle Pennsylvanian–lower Upper Pennsylvanian Strawn Group, and one sample was from an unnamed sandstone unit in the Upper Pennsylvanian Canyon Group. The Strawn Group consists of interbedded marine limestone and mudstone, and deltaic conglomerate and sandstone (Brown et al., 1973). The lower part of the Strawn Group contains fan deltas and shallow marine deposits, and the upper part of the Strawn Group contains deltaic-fluvial deposits (Brown et al., 1973). These rocks thicken eastward and reach up to 1370 m thick in front of the Ouachita orogen (Alsalem et al., 2017). Maps of fractional volume of sand in the Strawn and Canyon Groups suggest that the sandstones were most likely sourced from east-northeast of the basin (Brown et al., 1973).

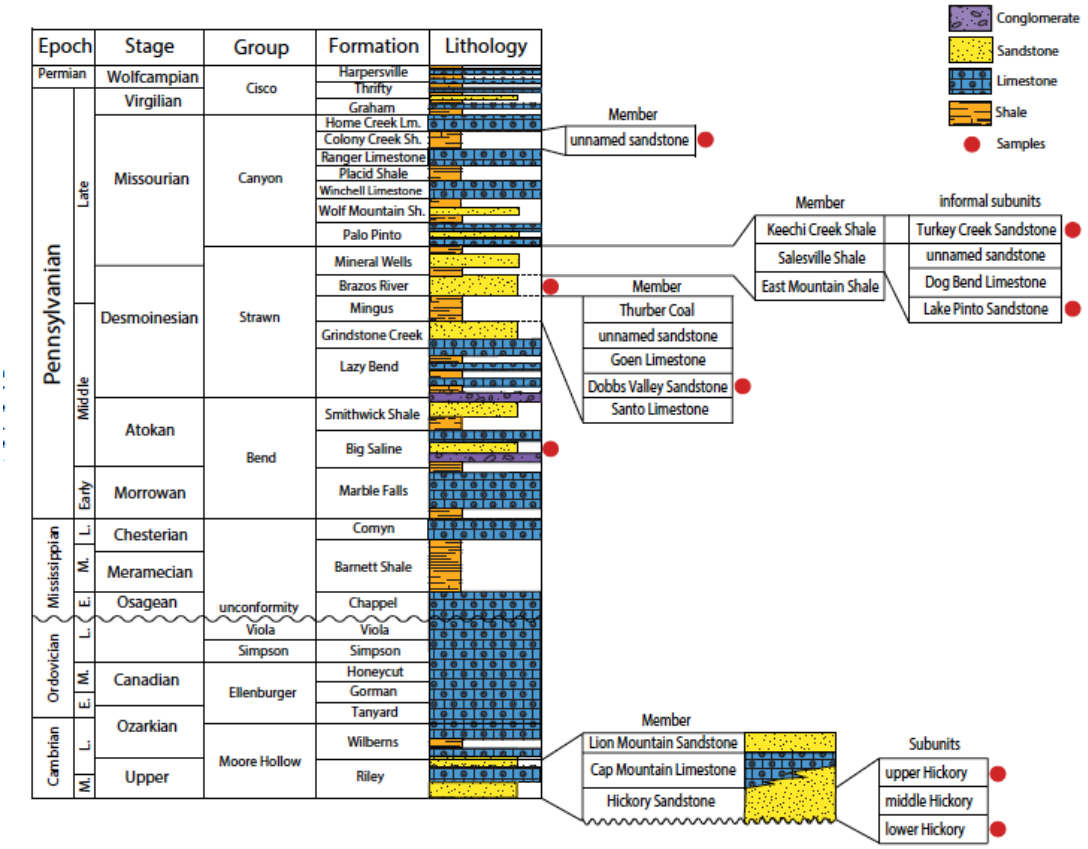

Figure 2-2 Generalized stratigraphic column of the Fort Worth Basin. Modified after Brown et al. (1973), Flippin (1982), Krause (1996), Pollastro (2003), and Hill et al. (2007). North America stages follow Rohde (2005). E., M., L.—Early, Middle, Late; Lm.—Limestone; Sh.—Shale.

2. 4 METHODS

Zircon crystals were extracted from samples by traditional methods of crushing and grinding, followed by separation with a Frantz magnetic separator and heavy liquids following the method of Dickinson and Gehrels (2008). U-Pb analyses of ~100 single zircon grains per sample were conducted by laser ablation–multi-collector–inductively coupled plasma mass spectrometry (LAMC- ICPMS) at the Arizona LaserChron Center (Tucson, Arizona, USA; see Appendix A). The analyses involved ablation of zircon with a Photon Machine Analyte G2 excimer laser using a spot diameter of 35 μm. For samples with smaller grain sizes, the laser beam size was reduced to 25 μm in diameter. Zircon

grains were randomly selected for analysis to avoid bias in size or shape. The ablated material was carried in helium gas into the plasma source of a Nu HR ICPMS, which was equipped with a flight tube of sufficient width that U, Th, and Pb isotopes were measured simultaneously. All measurements were made in static mode, using Faraday detectors with 3 × 1011 Ω resistors for ^{238}U, ^{232}Th, and $^{208\text{-}207\text{-}206}Pb$, and discrete dynode ion counters for ^{204}Pb and ^{202}Hg. Ion yields were ~0.8 mV per ppm. Each analysis consisted of one 15 s integration on peaks with the laser off (for backgrounds), fifteen 1 s integrations with the laser firing, and a 30 s delay to purge the previous sample and prepare for the next analysis. The ablation pit was ~15 μm in depth.

Common Pb correction was accomplished by measuring $^{206}Pb/^{204}Pb$ and assuming an initial Pb isotopic composition from Stacey and Kramers (1975), and uncertainties of 1.0% for $^{206}Pb/^{204}Pb$ and 0.3% for $^{207}Pb/^{204}Pb$. Subtraction of ^{204}Hg was accomplished by using the measured ^{202}Hg and natural $^{202}Hg/^{204}Hg$ ratio (4.34). Uncertainty in this value of $^{202}Hg/^{204}Hg$ is not significant because of the low intensities of Hg observed. Fractionation of $^{206}Pb/^{238}U$ and $^{206}Pb/^{207}Pb$ during ablation was monitored by analyzing fragments of a large concordant zircon crystal standard from Sri Lanka that has a known age of 563.5 ± 3.2 Ma (Gehrels et al., 2008). The uncertainty arising from this calibration correction, combined with the uncertainty from decay constants, age of the primary standard, and common Pb isotopic composition, contributes 1% systematic error to the $^{206}Pb/^{238}U$ and $^{206}Pb/^{207}Pb$ ages (2σ). R33 was used as a secondary standard to ensure that data were reliable. For all samples reported herein, the average $^{206}Pb/^{238}U$ age of the R33 analyses was within 2% of the known age.

The $^{206}Pb/^{207}Pb$ ages are used for grains older than 900 Ma, and $^{206}Pb/^{238}U$ ages are used for grains younger than 900 Ma. Grains with ages older than 400 Ma were filtered by 20% discordance and 5% reverse discordance. Age groups were determined by identifying three or more grains with overlapping $^{206}Pb/^{238}U$ and $^{206}Pb/^{207}Pb$ ages in the aggregate data set. After filtering the data for discordance, normalized relative age probability diagrams were constructed from least-discordant data (Figure 2-3). Quantitative comparisons of detrital zircon ages were conducted using the Kolmogorov-Smirnov (K-S) test (Press et al., 1986). The test compares two age distributions to determine if they are

from the same sources by measuring the probability (*P*). A *P*-value < 0.05 rejects the null hypothesis that the two samples are statistically indistinguishable. However, the K-S test results might imply different sources when, for example, the two samples are dominated by the same two age populations but in slightly varying proportions (e.g., Dickinson et al., 2010). Therefore, visual comparison of age spectra was used along with the K-S test.

2. 5 RESULTS

The detrital zircon U-Pb dates range from Archean (3.635 Ga) to Pennsylvanian (318 Ma) (Appendix A). As would be expected from their different tectonic setting, the two Cambrian samples have different age distributions compared to the Pennsylvanian samples, and the distributions of the six Pennsylvanian samples are similar to each other. Because the Cambrian samples show relatively simple age distributions compared to the Pennsylvanian samples, here we classify zircon populations based on the Pennsylvanian samples. Based on known ages of major magmatic terranes in North America (e.g., Thomas et al., 2004; Dickinson and Gehrels, 2009; Soreghan et al., 2002; Gehrels et al., 2011) and the abundance of zircons from each terrane in our samples, a total of 1002 dates are divided into five populations (Figure 2-3): Archean–Paleoproterozoic (3.634–1.825 Ga) zircons of population A, late Paleoproterozoic–early Mesoproterozoic (1.825–1.300 Ga) zircons of population B, middle Mesoproterozoic–early Neoproterozoic (1.300–0.900 Ga) zircons of population C, Neoproterozoic–early Paleozoic (800–500 Ma) zircons of population D, and Paleozoic (500–318 Ma) zircons of population E. The six Pennsylvanian samples include 11.5% population A, 15.0% population B, 46.8% population C, 15.3% population D, and 10.3% population E zircons. The remaining 1.1% of the zircons are of 900–800 Ma age. Given that zircons of this age group do not have well-defined magmatic terranes in Laurentia and the content is very low in our samples, they are excluded from the discussion. The two Cambrian samples have 79.9% population B, 17.7% population C, and 2.4% population D zircons. Zircons of population B in the two Cambrian samples are in a tight age range of 1.451–1.325 Ga. Zircons of population D are only present in the upper subunit of the Hickory Sandstone, and have a tight age range of 535–508 Ma.

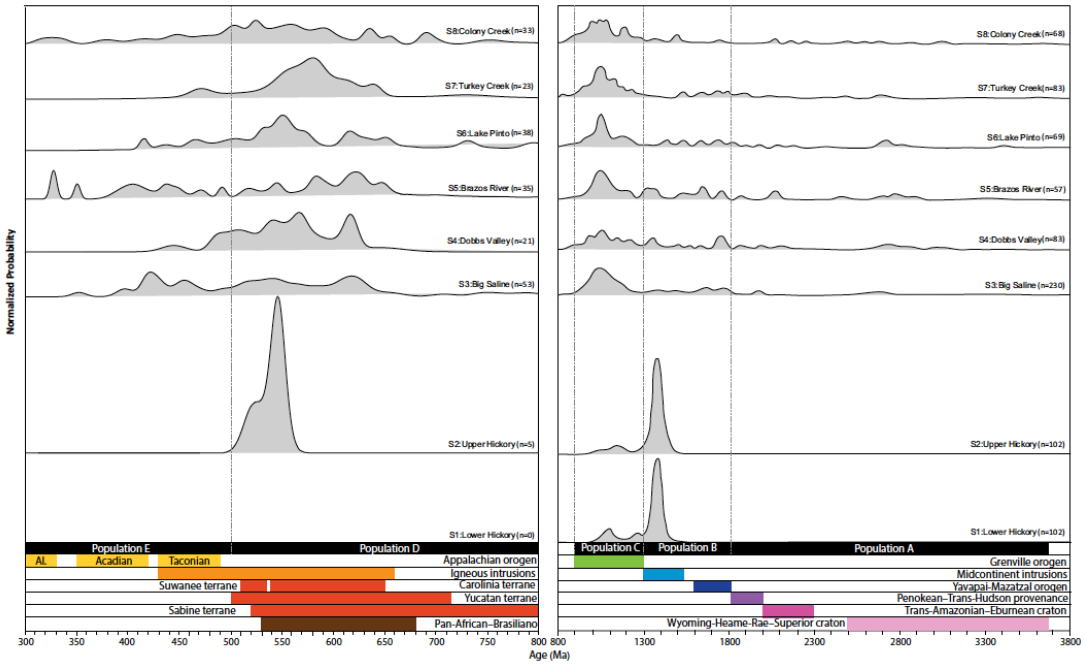

Figure 2-3 Normalized detrital zircon U-Pb age probability plots for the two Cambrian and six Pennsylvanian sandstones of the Fort Worth Basin. Different provinces and durations of zircon subpopulations A–E are shown at the bottom. Al.—Alleghanian. n denotes the number of concordant detrital zircon ages obtained for each sample.

2. 6 POTENTIAL ZIRCON SOURCES

2. 6.1 Archean and Paleoproterozoic (>1.825 Ga)

Potential sources of zircons from population A (3.634–1.825 Ga) mainly include the Archean Wyoming-Heame-Rae and Superior provinces (3.600–2.500 Ga), the Paleoproterozoic Penokean–Trans-Hudson provinces (2.000–1.800 Ga), and the Great Falls tectonic zone (ca. 1.86 Ga) in the interior of Laurentia. Potential sources of zircons from population A (3.634–1.825 Ga) mainly include the Archean Wyoming-Heame-Rae and Superior provinces (3.600– 2.500 Ga), the Paleoproterozoic Penokean–Trans-Hudson provinces (2.000–1.800 Ga), and the Great Falls tectonic zone (ca. 1.86 Ga) in the interior of Laurentia (Figure 2-1A) (e.g., Hoffman, 1988; Frost et al., 2000; Mueller et al., 2002; Whitmeyer and Karlstrom, 2007). Although these sources were distal to the Fort Worth Basin and were not exhumed during the Paleozoic, zircons of this population have been found in a wide range of

Proterozoic to lower Paleozoic strata of North America (e.g., Stewart et al., 2001; Gehrels et al., 2011; LaMaskin et al., 2011; May et al., 2013), particularly in the lower Paleozoic strata in southern Laurentia, including the Ordovician–Lower Pennsylvanian strata in the Appalachian foreland basins (Eriksson et al., 2004; Park et al., 2010); Middle Ordovician–Pennsylvanian strata in the Ouachita foreland basins in Oklahoma and Arkansas (Sharrah, 2006; Pickell, 2012); late Mesoproterozoic strata in western Texas (Spencer et al., 2014); and Cambrian–Ordovician strata in southern New Mexico (Gleason et al., 2007; Amato and Mack, 2012). About 2.1% of zircons in the Pennsylvanian samples are of 2.300–2.000 Ga age. This subgroup of zircons was originally formed by the Trans-Amazonian–Eburian orogenic events in the Gondwana margin (Trompette, 2000), and has been found in the Devonian–Pennsylvanian strata in the Appalachian foreland basin, reflecting recycling from various peri-Gondwana terranes (Thomas et al., 2004; Park et al., 2010; Mueller et al., 2014).

2. 6.2 Late Paleoproterozoic-Early Mesoproterozoic (1.825-1.300 Ga)

Zircons of population B (1.825–1.300 Ga) were formed in the Yavapai-Mazatzal orogenic belt (1.825–1.600 Ga) and the granite-rhyolite province (1.585–1.300 Ga) distributed in the southwestern and midcontinent regions of North America (Figure 2-1A). The granite-rhyolite province was formed by anorogenic magmatism (e.g., Hoffman, 1988; Van Schmus et al., 1996; Barnes et al., 2002). Bickford et al. (2015) suggested that the magmatism occurred across the continent with a westward-younging trend during 1.5–1.4 Ga, and that younger magmatism (1.390–1.340 Ga) was a major event only in the south-central midcontinent. The late Paleoproterozoic–early Mesoproterozoic basement was exhumed by a Transcontinental Arch during the Cambrian–Mississippian, and the arch extended from Minnesota southwestward to New Mexico (Billo, 1985; Sloss, 1988). The basement was also exhumed by the ARM orogeny during the Pennsylvanian–early Permian in Colorado, Arizona, New Mexico, and Oklahoma (e.g., Kluth, 1986). Zircons of this population represent a significant component in Mesoproterozoic–lower Permian strata in western USA (Stewart et al., 2001; Dickinson and Gehrels, 2003; Gehrels et al., 2011; Amato and Mack, 2012). A small amount of zircons of this population was also found in the Middle Ordovician–Pennsylvanian siliciclastic rocks in Oklahoma and Arkansas

(Sharrah, 2006; Pickell, 2012) and the Neoproterozoic–Pennsylvanian strata in the Appalachian foreland basins (Eriksson et al., 2004; Park et al., 2010).

2. 6.3 Mesoproterozoic (1.300-0.900 Ga)

Zircons of population C (1.300–0.900 Ga) were formed during the Grenville orogeny when several continent-continent collisions formed the supercontinent Rodinia (e.g., Dalziel, 1997; Hoffman, 1991; Borg and DePaolo, 1994; Torsvik et al., 1996; Unrug, 1995; Whitmeyer and Karlstrom, 2007). The Grenville basement was located in the eastern margin of Laurentia during the Paleozoic, and currently extends from Fennoscandia through Canada to the southeastern USA and forms much of the West Texas and eastern New Mexico basement (Mezger et al., 1993; Dalziel, 1997; Moecher and Samson, 2006; Barnes et al., 2002). Grenville basement was also redistributed to the Precordillera region in South America during the early Paleozoic (Thomas et al., 2002). Zircons of Grenvillian age are very fertile and have been documented as a predominant population in many Neoproterozoic to Paleozoic strata in southeastern Laurentia, particularly in the Appalachian foreland basins (Eriksson et al., 2004; Becker et al., 2005; Moecher and Samson, 2006; Gleason et al., 2007); the Ouachita Mountains in Oklahoma and Arkansas (Gleason et al., 2002); and the Precambrian rocks in West Texas (Shannon et al., 1997; Mosher, 1998; Bickford et al., 2000; Grimes and Copeland, 2004; Spencer et al., 2014).

2. 6.4 Neoproterozoic-Earliest Paleozoic (800-500 Ma)

Zircons of population D (800–500 Ma) were formed in two major tectonomagmatic units with overlapping ages: the peri-Gondwana terranes (800 to ca. 500 Ma), and magmatism on the eastern and southern margins of Laurentia associated with the breakup of Rodinia (760–550 Ma). The major peri-Gondwana terranes (800–500 Ma) include the Avalonian-Carolinian- Uchee terranes (650–540 Ma) in the southern Appalachian Mountains (Rast and Skehan, 1983; Williams and Hatcher, 1982; Murphy et al., 1992; Mueller et al., 1994; Keppie et al., 1996; Thompson et al., 1996; Steltenpohl et al., 2008); the Suwannee terrane (535–511 Ma) in the Florida subsurface (Opdyke et al., 1987; Mueller et al., 1994; Murphy et al., 2004; Martens et al., 2010); the Sabine terrane (800–600 Ma; Thomas, 2013) in eastern

Texas and the western Louisiana subsurface (Granata, 1963; Gleason et al., 2007; Nunn, 2012); and the Yucatan-Maya terrane (714–500 Ma) in southeastern Mexico (Rankin et al., 1989; Mueller et al., 1994; Thomas et al., 2004). These terranes were accreted to Laurentia before and during the Appalachian-Ouachita orogenies (ca. 490–260 Ma) (Samson et al., 2001; Murphy et al., 2004; Mueller et al., 2014).

The breakup of Rodinia was associated with two magmatic events in southeastern Laurentia, including a failed rift event at 760–700 Ma and the opening of the Iapetus Ocean at 620–550 Ma (Hatcher, 1989; Su et al., 1994; Aleinikoff et al., 1995; Rankin et al., 1997; Walsh and Aleinikoff, 1999; Cawood and Nemchin, 2001). In the vicinity of the Fort Worth Basin, granitic bodies of ca. 539–528 Ma age were formed in the southern Oklahoma aulacogen (Lambert et al., 1988; Hames et al., 1995; Hogan and Gilbert, 1998; Spencer et al., 2014; Thomas et al., 2016) and exposed in the Amarillo-Wichita uplift and Arbuckle Mountains during the early Paleozoic (Johnson et al., 1988; Gilbert and Denison, 1993). Igneous intrusions related to the opening of the Iapetus Ocean or extension of the southern Oklahoma aulacogen were also found in New Mexico and southern Colorado (Hogan and Gilbert, 1998; Cawood and Nemchin, 2001; McMillan and McLemore, 2004) and were exhumed during the Pennsylvanian–early Permian ARM orogeny (Ye et al., 1996; Dickinson and Lawton, 2003). Small amounts of zircon of population D (800–500 Ma) have been documented in Paleozoic strata in the Grand Canyon region of Arizona (Gehrels et al., 2011), and in lower Paleozoic strata in southeastern Laurentia, including in the Appalachian foreland basins and the Arkoma Basin (Eriksson et al., 2004; Becker et al., 2005; Moecher and Samson, 2006; Sharrah, 2006; Gleason et al., 2007).

2. 6.5 Paleozoic (500-318 Ma)

Zircons of population E (500–318 Ma) were mainly formed during the Appalachian orogeny (ca. 490–270 Ma). The tectonomagmatic units of the Appalachian orogeny that occurred in eastern Laurentia include the Taconic (490–430 Ma), Acadian (420–350 Ma), and Alleghanian (330–270 Ma) orogenies (Hatcher, 1989; Miller et al., 2000). Zircons of this population have been documented in lower Paleozoic strata in the Appalachian foreland basins (Eriksson et al., 2004; Thomas et al., 2004; Park et al., 2010), Mississippian–lower Permian strata in the Grand Canyon region (Gehrels et al.,

2011), and Ordovician–Pennsylvanian strata in Oklahoma and Arkansas (Gleason et al., 2002; Sharrah, 2006). Some grains in this population are of Mississippian age and were derived from volcanic arcs formed during the subduction of southern Laurentia beneath Gondwana. Evidence of volcanic activity of Mississippian age has been documented in sedimentary rocks in Oklahoma and Arkansas (Niem, 1977; Shaulis et al., 2012) and in the Marathon uplift (Imoto and McBride, 1990).

2. 7 PROVENANCE INTERPRETATION

The two Cambrian samples have 79.9% population B, 17.7% population C, and 2.4% population D zircons. The predominance of zircons from the granite- rhyolite province of population B suggests that the Cambrian paleorivers mainly drained the granite-rhyolite province. The Grenvillian zircons of population C may be directly derived from the Grenville basement or recycled from older sedimentary rocks exposed in the drainage of the paleorivers. Zircons of 535–508 Ma (population D) were most likely directly sourced from the southern Oklahoma aulacogen (Figure 2-3).

The six Pennsylvanian samples include 11.5% population A, 15.0% population B, 46.8% population C, 15.3% population D, and 10.3% of population E zircons. Zircons of the Archean–Paleoproterozoic population and the late Paleoproterozoic– early Mesoproterozoic population (populations A and B) were recycled from Neoproterozoic–Paleozoic sedimentary rocks on the southern margin of Laurentia. Some grains of the late Paleoproterozoic–early Mesoproterozoic population may be directly derived from the ARM region in western Laurentia. The Grenvillian zircons (population C) were directly derived from the Grenville basement, which was exhumed in the Appalachians during the late Paleozoic, or recycled from the Neoproterozoic–Paleozoic sedimentary rocks on the southern margin of Laurentia. The Grenvillian zircons account for nearly half of the grains, suggesting that they were most likely directly derived from the Grenville basement by a major river. Zircons of the Neoproterozoic–earliest Paleozoic population (population D) were derived from the peri-Gondwana terranes (800–500 Ma) and the basin-bounding Amarillo-Wichita uplift and Arbuckle Mountains (ca. 539–528 Ma). The closest peri-Gondwana terrane to the Fort Worth Basin is the Sabine terrane located in the subsurface of east Texas and Louisiana (Figure 2-1). Because our Pennsylvanian samples contain

only eight grains of 539–528 Ma age, the local ARM terranes are not a major source of zircons of this population. The Paleozoic zircons (population E) were recycled from Paleozoic strata or directly transported from the Appalachians by a transcontinental river. Only a few zircons in this population are of Mississippian age, which were recycled from the Mississippian sedimentary rocks in Oklahoma and Arkansas.

2. 8 DISCUSSION

2. 8.1 Sediment dispersal during the Cambrian

We suggest that the abundant zircons derived from the granite-rhyolite province were transported by paleorivers draining the Texas Arch during the Cambrian (Figure 2-4). The Texas Arch was a Cambro-Ordovician structural high on the flanks of the larger Transcontinental Arch (Figure 2-4) near the study area (e.g., Adams, 1954; Wright, 1979; Billo, 1985), and may have remained as a positive topographic feature during the Early Mississippian (Ruppel, 1985). Uplift of the Transcontinental Arch exhumed both the Yavapai-Mazatzal and granite-rhyolite provinces distributed in the southwestern and midcontinent of North America (e.g., Hoffman, 1988; Van Schmus et al., 1993; Dickinson and Gehrels, 2009). Because the granite-rhyolite province was mostly to the south and east of the Yavapai-Mazatzal province, our data suggest that the paleorivers had headwaters only on the south limb of the Texas Arch. Our inference is consistent with previous interpretations that the lower subunit of the Hickory Sandstone was deposited in braided rivers flowing toward the southeast based on stratigraphic architecture, paleocurrent directions, and sandstone compositions (Wilson, 1962; Cornish, 1975; Krause, 1996; McBride et al., 2002). Our interpretation is further supported by the observation that these zircons are in a tight age range (1.451–1.325 Ga), indicating that they were from southwestern Laurentia because the Proterozoic anorogenic magmatism has a westward-younging trend (Bickford et al., 2015). Although the upper subunit of the Hickory Sandstone was deposited in an estuarine–shallow marine environment, the similarity of zircon age distributions of the two Cambrian samples suggests that the grains were mainly transported by fluvial process, and that other depositional processes, such as longshore drift, did not influence the zircon populations.

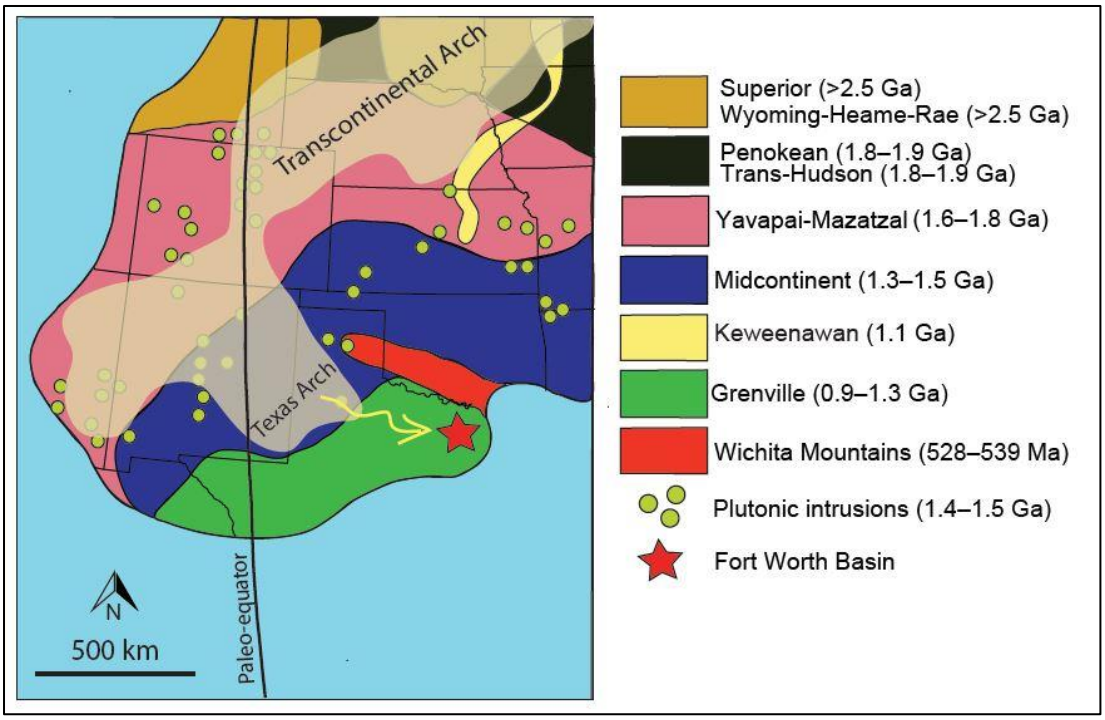

Figure 2-4 Paleogeographic map showing basement provinces in southern Laurentia and our inferred southeastward sediment dispersal (yellow) from the Texas Arch (light brown) to the Fort Worth Basin (red star) during the Late Cambrian. Basement province map is modified after Thomas (2006), Stoeser et al. (2007), and Whitmeyer and Karlstrom (2007).

We suggest that the Grenvillian zircons were directly sourced from Grenville basement exposed on the south limb of the Texas Arch (Figure 2-4). The Llano uplift, which bounds the Fort Worth Basin to the south (Figure 2-1), is the closest source for the Grenvillian zircons. However, basin subsidence modeling suggests that the Llano uplift was not exhumed until the Ouachita orogeny during the late Paleozoic (Erlich and Coleman, 2005). Based on detrital zircon geochronology, Spencer et al. (2014) proposed that the Llano uplift was the main source of Grenvillian zircon to West Texas during the Cambrian. This observation is in contrast to the results of our Cambrian samples. Only 17.7% of zircons are of Grenvillian age, and the ages of these zircons are 1.295–1.040 Ga. The Llano uplift contains Grenville basement (1.360–1.232 Ga) and Proterozoic plutons (1.288–1.070 Ga) (Mosher, 1998). If the Llano uplift was the source for the Grenvillian zircons, we would expect the ages of the

Grenvillian zircons in the Fort Worth Basin to be 1.360–1.070 Ga. However, the age range of the Grenvillian zircons in the two Cambrian samples is tight, and the ages are in the younger end of the basement age in the Llano uplift. The Grenvillian zircons were not recycled from older sedimentary strata because our samples do not contain any zircons from the Yavapai-Mazatzal and Archean basement provinces (Figure 2-3). Proterozoic sedimentary rocks, such as in West Texas (Spencer et al., 2014), have zircons from the Grenville, Yavapai-Mazatzal, and Archean basements. Recycling of the older sedimentary rocks should not contribute only Grenvillian zircons.

2. 8.2 Sediment dispersal during the Pennsylvanian

The high abundance (47%) of Grenvillian zircons in the Pennsylvanian sandstones cannot be simply explained by recycling from Proterozoic–lower Paleozoic strata. Although abundant Grenvillian zircons have been found in the Mesoproterozoic and Cambrian rocks in West Texas and lower Paleozoic strata in southern Laurentia (Figure 2-5A; Gleason et al., 2002; Gehrels et al., 2011; Amato and Mack, 2012; Spencer et al., 2014), P-values of K-S tests conducted on all zircon grains older than 900 Ma in our samples versus these Proterozoic–lower Paleozoic strata are $\leqslant$0.05 (Table 2-2), indicating that it is very unlikely that the zircon populations are from the same sources or that recycling from the older strata is not a major contributor to sediments in the Fort Worth Basin. We conducted K-S tests on only the grains older than 900 Ma because our samples have high abundance of zircon of 680–520 Ma (Figure 2-5), which may have been added to the Pennsylvanian river system from a local peri-Gondwana source, explaining the low *P*-values. K-S tests were performed on all grains older than 900 Ma, assuming that no significant amount of these zircons was dispersed from a local peri-Gondwana source. This assumption can be tested only when future study directly constrains the detrital zircon age distribution of the peri-Gondwana terrane.

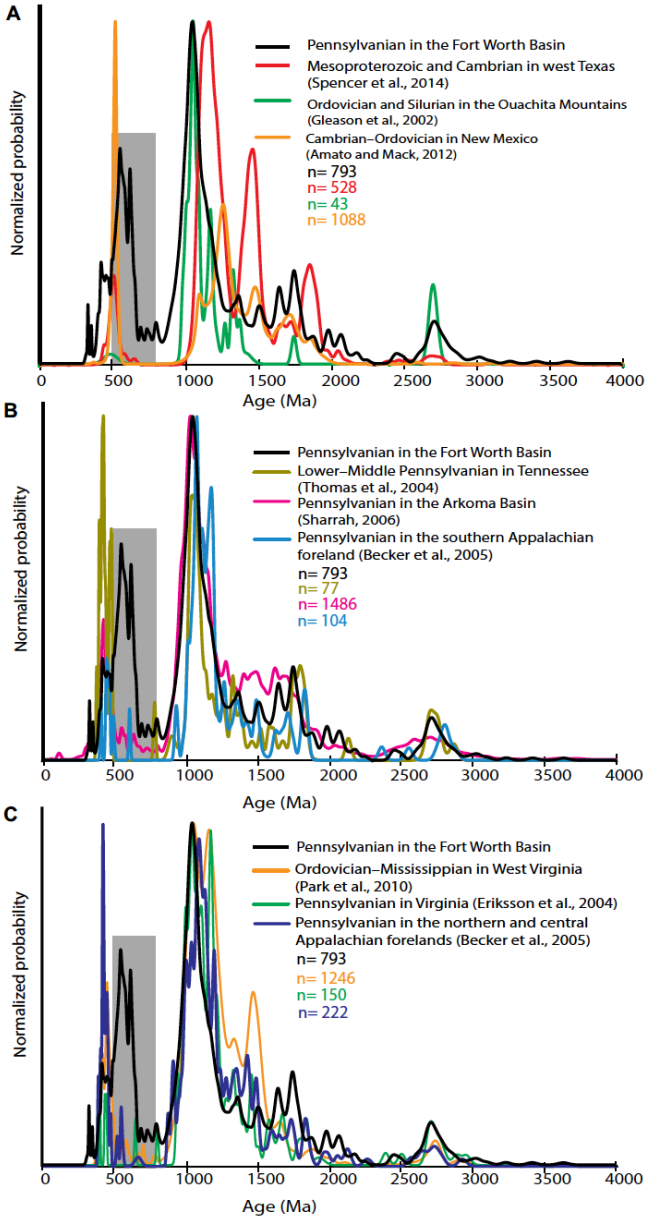

Figure 2-5 Normalized U-Pb age probability plots comparing our data to those of other studies. (A) Our Pennsylvanian samples in the Fort Worth Basin and other Mesoproterozoic–lower Paleozoic strata in southern Laurentia. (B) Our Pennsylvanian samples in the Fort Worth Basin, Pennsylvanian strata in Tennessee and the Arkoma Basin, and Permian strata in the Delaware Basin. (C) Our Pennsylvanian samples in the Fort Worth Basin and lower Paleozoic strata in the Appalachian forelands. Grey areas highlight the differences in detrital zircon population D between our samples and other Paleozoic strata. n is the total number of zircon data presented in each study.

Table 2-2 Results of Kolmogorov-Smirnov tests for detrital zircons older than 900 Ma in strata of different ages summarized in this study

	Fort Worth basin (this study)	West Texas (Spencer et al., 2014)	Ouachita Mountains (Gleason et al., 2002)	Arkoma basin (Sharrah, 2006)	New Mexico (Amato and Mack, 2012)	Tennessee (Thomas et al., 2004)	West Virginia (Park et al., 2010)	Virginia (Eriksson et al., 2004)	Central Appalachian foreland (Becker et al., 2005)	Southern Appalachian foreland (Becker et al., 2005)
Fort Worth basin		0.000	**0.068**	**0.310**	0.000	**0.942**	0.000	0.016	0.048	0.011
West Texas	0.000		0.000	0.000	0.000	0.000	0.000	0.000	0.000	0.000
Ouachita Mountains	**0.068**	0.000		0.038	0.000	**0.209**	**0.069**	**0.602**	**0.099**	**0.218**
Arkoma basin	**0.310**	0.000	0.038		0.000	**0.645**	0.000	0.007	0.026	0.021
New Mexico	0.000	0.000	0.000	0.000		0.000	0.000	0.000	0.000	0.000
Tennessee	**0.942**	0.000	**0.209**	**0.645**	0.000		0.008	**0.210**	**0.524**	**0.234**
West Virginia	0.000	0.000	**0.069**	0.000	0.000	0.008		**0.444**	**0.320**	**0.358**
Virginia	0.016	0.000	**0.602**	0.007	0.000	**0.210**	**0.444**		**0.236**	**0.851**
Central Appalachian foreland	0.048	0.000	**0.099**	0.026	0.000	**0.524**	**0.320**	**0.236**		**0.752**
Southern Appalachian foreland	0.011	0.000	**0.218**	0.021	0.000	**0.234**	**0.358**	**0.851**	**0.752**	

Previous studies have suggested that a late Paleozoic river flowed along the Appalachian-Ouachita foreland and brought Grenville basement detritus to the remnant ocean basins (Graham et al., 1975; Archer and Greb, 1995; Gleason et al., 1994, 1995, 2007). Others, however, have suggested that the paleoriver or another paleoriver entered the Ouachita foreland during the Early Pennsylvanian by draining through the Illinois Basin (Thomas, 1997; Archer and Greb, 1995; Sharrah, 2006). The paleoriver draining the Illinois Basin (Archer and Greb, 1995) would have had its drainage mostly in the Laurentia continental interior rather than the Appalachians, and cannot explain the high abundance of Grenvillian zircons and low abundance of zircons of Archean–early Mesoproterozoic age. Furthermore, comparison of our detrital zircon data and data from the Pennsylvanian sedimentary rocks in the central Appalachian foreland suggests that the paleoriver did not have a major catchment in the central Appalachians. Zircons from the Paleozoic strata in the central Appalachian foreland have two Grenvillian peaks (Figure 2-5C; Eriksson et al., 2004; Becker et al., 2005; Park et al., 2010), including one at 0.980–1.090 Ga representing the Ottawan orogeny (Rivers, 1997; Heumann et al., 2006) and one at 1.160–1.190 Ga representing the Shawinigan orogeny (Chiarenzelli et al., 2010; McLelland et al., 2010). The Grenvillian zircons in our Pennsylvanian samples are mostly in the age range of 0.980–1.090 Ga (Figure 2-5), and the low abundance of zircons of 1.160–1.190 Ga in our samples and the Pennsylvanian strata in the Ouachita foreland (Sharrah, 2006) suggest that the central Appalachians and Ouachita foreland were unlikely to have been connected by a paleodrainage. *P*-values of K-S tests

conducted on zircon grains older than 900 Ma in our data versus the data of Ordovician–Mississippian strata in Virginia, West Virginia, and Pennsylvania (Eriksson et al., 2004; Becker et al., 2005; Park et al., 2010) are all <0.05 (Figure 2-5C; Table 2-2), further indicating the difference in zircon provenances.

We suggest that the abundant Grenvillian zircons were directly derived from the southern Appalachian Mountains via a major river (Figure 2-6). The zircon populations in our Pennsylvanian samples are very similar to those in the Pennsylvanian sandstones in the Arkoma Basin (Sharrah, 2006). The *P*-value of a K-S test conducted on the two groups of samples is 0.3 (Figure 2-5B; Table 2-2; Sharrah, 2006), suggesting that sediments in the Fort Worth Basin and Ouachita foreland were from the same source, and that the two basins were most likely connected. Although the Amarillo-Wichita uplift induced by the ARM orogeny could have acted as a topographic barrier between the two regions, isopach maps of the Mississippian and Pennsylvanian strata in the Fort Worth Basin show that the Muenster uplift did not cause significant flexural subsidence, and thus was not a major topographic feature during the Pennsylvanian (Alsalem et al., 2017).

The alternative explanation of the abundant Grenvillian zircons is that they were recycled from the Ordovician–Lower Pennsylvanian sandstones that were incorporated in the Alleghanian and Ouachita orogenic fronts when Laurentia and Gondwana experienced oblique collision during the late Paleozoic. Local rivers draining the southern Appalachian orogenic front delivered detritus southward and southwestward and stored the Grenvillian zircons temporarily in the Mississippian–Lower Pennsylvanian sandstones deposited in the remnant Rheic Ocean. During the suturing between Gondwana and Laurentia, these sandstones were incorporated in the orogenic wedge and eroded. Local rivers draining the newly formed orogenic wedge delivered the Grenvillian zircons farther southwestward. This alternative explanation is possible given that the Grenvillian zircons are abundant in lower Paleozoic rocks and tend to survive recycling. However, we do not prefer this explanation based on three lines of evidence. First, large axial rivers commonly exist in the forelands of long orogenic belts, such as the Ganges River in the Himalayan foreland (Graham et al., 1975). It is very likely such an axial river existed in the southern Appalachian and Ouachita forelands based on the plate

tectonic setting. Second, the Mississippian–Lower Pennsylvanian strata deposited in the remnant Rheic Ocean along the Appalachian-Ouachita orogen are dominantly fine-grained siliciclastic sediments and carbonates (e.g., Cline, 1960; Pashin, 1994), thus they are unlikely to represent major sources of coarse sediments in the Fort Worth Basin. The *P*-value of a K-S test conducted on zircon grains older than 900 Ma in our data versus the data of the Ordovician–Silurian strata in the Ouachita Mountains (Gleason et al., 2002) is only 0.07 (Figure 2-5A; Table 2-2), suggesting that recycling of older strata cannot explain the zircon age distribution in the Fort Worth Basin. Finally, the Mississippian Stanley Group in the Ouachita Mountains has tuffs of 329–321 Ma age (Shaulis et al., 2012), and only one zircon in our Pennsylvanian samples is younger than 330 Ma, suggesting that the flysch deposits in the Ouachita trough were not the major sources of zircons in the Fort Worth Basin.

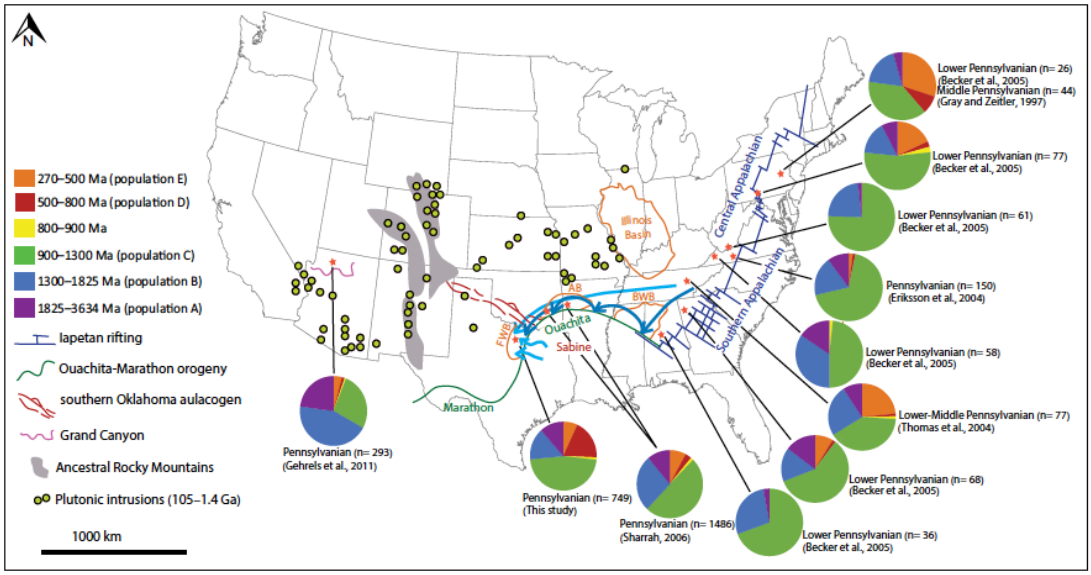

Figure 2-6 Relative abundance of zircons of populations A–E in southern and eastern Laurentia during the Pennsylvanian and the inferred paleodraiange of the rivers (blue lines) that brought sediments to the Fort Worth Basin. The ages below the pie graphs represent the ages of the strata with detrital zircon studies. n is the total number of zircon data presented in each study. FWB—Fort Worth Basin; AB—Arkoma Basin; BWB—Black Warrior Basin. The long light blue arrow represents our inferred axial river from the southern Appalachians, and the short light blue arrows represent the inferred rivers from

the Sabine terrane in the Ouachita orogen. Short arched dark blue arrows represent potential sediment recycling of upper Paleozoic sediments through intermediate steps. See text for details.

2. 8.3 Missing Signal of the Amarillo-Wichita Uplift and ARM Orogen

The abundant Grenvillian zircons cannot be derived from the ARM orogen the Amarillo-Wichita uplift bounding the Fort Worth Basin to the northeast is the nearest ARM uplift to our study site. The uplift has Cambrian igneous rock of 535 ± 10 Ma and the granite-rhyolite basement of 1.399–1.363 Ga (Thomas et al., 2012, 2016). Erosion of the Amarillo-Wichita uplift should have contributed zircons of these two populations into the Fort Worth Basin, however zircons of 535 ± 10 Ma are present in our Cambrian samples, but not in our Pennsylvanian samples. Zircons of the granite-rhyolite province only contribute a small proportion (~5.6%) to our Pennsylvanian samples. Based on the low abundance, and possible contribution of zircons of the same age from the peri-Gondwana terranes, we suggest that the Amarillo-Wichita uplift did not provide significant amounts of sediment into the Fort Worth Basin during the Middle- and Late Pennsylvanian. This interpretation is consistent with the eastward shift of the basin depocenter and dominant control of the Ouachita orogen on basin subsidence during the Middle- and Late Pennsylvanian (Alsalem et al., 2017). The ARM orogeny mainly influenced western Laurentia and reached its maximum during the Middle Pennsylvanian (Kluth and Coney, 1981). The ARM orogeny in western Laurentia exposed the Yavapai-Mazatzal basement, however our samples have only 9.0% zircons of 1.825–1.600 Ga, further suggesting that ARM-involved sources were not a major source of sediments for the Fort Worth Basin during the Pennsylvanian. Recycling of sedimentary cover in the ARM orogen is also unlikely a major source of sediments because the ARM orogen is to the northeast of the Fort Worth Basin and could not have caused westward delta propagation (Brown et al., 1973).

2. 8.4 Signal of the Sabine Uplift

Our Pennsylvanian samples have a zircon age peak at ca. 650–500 Ma and a small proportion of zircons of 650–820 Ma age (Figure 2-3). Igneous and metamorphic rocks of these ages have not been documented in the vicinity of the Fort Worth Basin. Zircons of these ages were formed in Gondwana

during the Pan-Africa orogeny in Africa and the Brasiliano orogeny in South America, and these orogenies began at ca. 820 Ma and were completed by ca. 500 Ma (Hoffman, 1999; Schaaf et al., 2002). Possible sources of these zircons include the peri-Gondwana terranes accreted to the Laurentia margin before and during the Ouachita orogeny. Although Neoproterozoic zircons are found in the Avalonia, Carolinia, and Suwannee terranes (Opdyke et al., 1987; Murphy et al., 1992, 2004; Mueller et al., 1994), zircons of ca. 650–540 Ma age were absent in the central and southern Appalachian forelands (Figure 2-5; Eriksson et al., 2004; Thomas et al., 2004; Park et al., 2010), suggesting that these terranes were not likely sources of the Neoproterozoic zircons in our Pennsylvanian samples. The Yucatan-Maya terranes were not accreted to Laurentia along the Ouachita-Marathon belt until the early Permian (Pindell, 1985; Viele and Thomas, 1989; Dickinson and Lawton, 2001), thus they were also not likely the source of the Neoproterozoic zircons.

The only known peri-Gondwana terrane near the Fort Worth Basin is the Sabine terrane, which exists in the subsurface of east Texas and Louisiana today (Figure 2-1). We infer that zircons of ca. 650–500 Ma age in our Pennsylvanian samples were from the Sabine terrane. The interpretation is consistent with the inferred westward delta propagation direction based on fractional volume of sand distribution of the Strawn and Canyon Groups (Brown et al., 1973). Thomas (2013) suggested that the synorogenic sandstones in the Arkoma Basin have a distinctive detrital zircon age group of 800–600 Ma, which may be derived from the Sabine terrane. Our samples also have more zircons of 800–650 Ma compared to the other Pennsylvanian sandstones summarized in Figure 2-5, supporting the interpretation that local rivers draining the Sabine terrane delivered zircons of 820–500 Ma. Presently, there are no age constraints for basement rocks underlying the upper Paleozoic sedimentary cover in the Sabine terrane. Future dating of the basement rocks can verify our inference about the zircon signal of the Sabine terrane.

2. 9 CONCLUSIONS

In this chapter we utilize detrital zircon U-Pb geochronology to understand sediment dispersal and reconstruct paleogeography on the southern margin of Laurentia before and during the suturing of Laurentia and Gondwana. We suggest that detrital zircons in the Cambrian Hickory Sandstone were transported by local rivers draining the Texas Arch located to the northwest of the Fort Worth Basin and that the Llano uplift was not an active source during the Cambrian. Detrital zircons of the six Pennsylvanian sandstones contain 26% Archean–Mesoproterozoic grains, 47% Grenvillian grains, and 26% Neoproterozoic and early Paleozoic grains. The Archean–Mesoproterozoic grains in these Pennsylvanian sandstones were recycled from the lower Paleozoic strata distributed in southern Laurentia. The high abundance of Grenvillian zircons and the similarity of detrital zircon age distributions between our samples and the Pennsylvanian strata in the Arkoma Basin suggests sediment dispersal by a major river flowing in the Ouachita foreland to the remnant ocean basin. Comparison of detrital zircon age distributions in the Pennsylvanian strata in the Fort Worth and Arkoma Basins with those in the Appalachian forelands suggest that the headwaters of the river was limited to the southern Appalachians during the Pennsylvanian. Our Pennsylvanian samples have abundant zircons of 820–500 Ma age, which were transported by local rivers from the Sabine terrane incorporated in the Ouachita orogen. Therefore, both distal sediment dispersal from the southern Appalachians and local sediment dispersal from the Ouachita orogen contributed sedimentation in the Fort Worth Basin during the Pennsylvanian.

2. 10 ACKNOWLEDGMENTS

This research was funded by the Gulf Coast Section SEPM. We thank Mark Pecha for assisting the analysis of detrital zircon U-Pb ages. We thank Drs. Emily Finzel and Peter Mueller and Associate Editor Terry Pavlis for the constructive comments that help to improve the work.

2. 11 REFERENCES CITED

Adams, J.E., 1954, Mid-Paleozoic paleogeography of central Texas: Oklahoma City Geological Society, The Shale Shaker Digest I, v. I-V, p. 238-241.

Aleinikoff, J.N., Zartman, R.E., Walter, M., Rankin, D.W., Lyttle, P.T., and Burton, W.C., 1995, U-Pb ages of metarhyolites of the Catoctin and Mount Rogers Formations, central and southern Appalachians: Evidence for two pulses of Iapetan rifting: American Journal of Science, v. 295, p. 428-454.

Alsalem, O.B., Fan, M., Xie, X., 2017, Late Paleozoic Subsidence and Burial History of the Fort Worth Basin: American Association of Petroleum Geologists Bulletin, , v. 101, no. 11, p. 1813-1833, doi: 10.1306/01251716016.

Amato, J.M., and Mack, G.H., 2012, Detrital zircon geochronology from the Cambrian-Ordovician Bliss Sandstone, New Mexico: Evidence for contrasting Grenville-age and Cambrian sources on opposite sides of the Transcontinental Arch: Geological Society of America Bulletin, v. 124, p. 1826-1840.

Archer, A.W., and Greb, S.F., 1995, An Amazon-Scale Drainage System in the Early Pennsylvanian of Central North America: The Journal of Geology, v. 103, p. 611-628.

Barnes, V.E., 1992, Geologic Map of Texas: Bureau of Economic Geology, The University of Texas at Austen Map SM0003, Scale 1:500,000, 4 sheets.

Barnes, V.E., and Bell, W.C., 1977, The Moore Hollow Group of Central Texas: The University of Texas at Austin, Bureau of Economic Geology, Report of Investigations no. 88, 169 p.

Barnes, V.E. and Schofield, D.A., 1964, Potential low-grade iron ore and hydraulic-fracturing sand in Cambrian sandstones, northwestern Llano Region, Texas: Bureau of Economic Geology, University of Texas, report of investigation, no. 53, 58 p.

Barnes, M.A., Anthony, E.Y., Williams, I., and Asquith, G.B., 2002, Architecture of a 1.38–1.34 Ga granite–rhyolite complex as revealed by geochronology and isotopic and elemental geochemistry of subsurface samples from West Texas, USA: Precambrian Research, v. 119, p. 9-43.

Becker, T.P., Thomas, W.A., Samson, S.D., and Gehrels, G.E., 2005, Detrital zircon evidence of Laurentian crustal dominance in the lower Pennsylvanian deposits of the Alleghanian clastic wedge in eastern North America: Sedimentary Geology, v. 182, p. 59-86.

Bickford, M.E., Soegaard, K., Nielsen, K.C., and McLelland, J.M., 2000, Geology and geochronology of Grenville-age rocks in the Van Horn and Franklin Mountains area, West Texas: Implications for the tectonic evolution of Laurentia during the Grenville: Geological Society of America Bulletin, v. 112, p.1134-1148.

Bickford, M.E., Van Schmus, W.R., Karlstrom, K.E., Mueller, P.A., Kamenov, G.D., 2015, Mesoproterozoic–trans-Laurentian magmatism: a synthesis of continent-wide age distributions, new SIMS U–Pb ages, zircon saturation temperatures, and Hf and Nd isotopic compositions: Precambrian Res, v. 265, p. 286-312.

Billo, S.M., 1985, The Transcontinental Arch and its Relation to the Colorado oil and mineral belt: Journal of Petroleum Geology, v. 8, p. 343-352.

Borg, S.G., and DePaolo, D.J., 1994, Laurentia, Australia, and Antarctica as a Late Proterozoic supercontinent: constraints from isotopic mapping: Geology, v. 22, p. 307-310.

Bridge, J., Barnes, V.E. and Cloud, P.E., 1947, Stratigraphy of the Upper Cambrian, Llano Uplift, Texas: Geological Society of America Bulletin, v. 58, p. 109-124.

Briggs, G., 1960, Paleocurrent study of the Brazos River Sandstone Member of the Garner Formation, Palo Pinto County, Texas [M.S. Thesis], Southern Methodist University, 20 p.

Brown, L.F., Cleaves, II, A.W., and Erxleben, A.W., 1973, Pennsylvanian depositional systems in North-Central Texas: A guide for interpreting terrigenous clastic facies in a cratonic basin: The University of Texas at Austin, Bureau of Economic Geology, Guidebook No. 14, 122 p.

Burke, K., 1977, Aulacogens and continental breakup: Annual Review of Earth and Planetary Sciences, v. 5, p. 371-396.

Carlson, M.P., 1999. Transcontinental Arch—A pattern formed by rejuvenation of local features across central North America: Tectonophysics, v. 305, p. 225-233.

Cawood, P.A., and Nemchin, A.A., 2001, Source regions for Laurentian margin sediments: Constraints from U/Pb dating of detrital zircon in the Newfoundland Appalachians: Geological Society of America Bulletin, v. 113, p. 1234-1246.

Cheney, M.G., 1940, Geology of north-central Texas: American Association of Petroleum Geologists Bulletin, v. 24, p. 65-118.

Chiarenzelli, J., Regan, S., Peck, W.H., Selleck, B.W., Cousens, B., Baird, G.B., and Shrady, C.H., 2010, Shawinigan arc magmatism in the Adirondack Lowlands as a consequence of closure of the Trans-Adirondack backarc basin: Geosphere, v. 6, p. 900-916.

Cline, L.M., 1960, Stratigraphy of the Late Paleozoic Rocks of the Ouachita Mountains, Oklahoma: Oklahoma Geological Survey Bulletin, v. 85, 113 p.

Cocks, L.R.M., and Torsvik, T.H., 2011, The Palaeozoic geography of Laurentia and western Laurussia: A stable craton with mobile margins: Earth-Science Reviews, v. 106, p. 1-51.

Cook, T.D., 2009, Facies Description and Interpretation of the Upper Lower Hickory Sandstone, Riley Formation, Central Texas [M.S. Thesis], Texas A&M University, TX, 112 p.

Cornish, F.G., 1975, Tidally-influenced deposits of the Hickory Sandstone, Cambrian, central Texas [M.S. Thesis], The University of Texas at Austin, TX, 186 p.

Dalziel, I.W., 1997, OVERVIEW: Neoproterozoic-Paleozoic geography and tectonics: Review, hypothesis, environmental speculation: Geological Society of America Bulletin, v. 109, p. 16-42.

Dickinson, W.R., 2000, Geodynamic interpretation of Paleozoic tectonic trends in oriented oblique to the Mesozoic Klamath-Sierran continental margin in California, in Soreghan, M.J., and Gehrels, G.E., eds., Paleozoic and Triassic Paleogeography and Tectonics of Western Nevada and Northern California: Geological Society of America Special Paper 347, p. 209-245.

Dickinson, W.R., and Gehrels, G.E., 2003, U–Pb ages of detrital zircons from Permian and Jurassic eolian sandstones of the Colorado Plateau, USA: paleogeographic implications: Sedimentary Geology, v. 163, p. 29-66.

Dickinson, W.R., and Gehrels, G.E., 2008, U-Pb ages of detrital zircons in relation to paleogeography: Triassic paleodrainage networks and sediment dispersal across southwest Laurentia: Journal of Sedimentary Research, v. 78, p. 745-764.

Dickinson, W.R., and Gehrels, G.E., 2009, U-Pb ages of detrital zircons in Jurassic eolian and associated sandstones of the Colorado Plateau: Evidence for transcontinental dispersal and intraregional recycling of sediment: Geological Society of America Bulletin, v. 121, p. 408-433.

Dickinson, W.R., and Lawton, T.F., 2001, Carboniferous to Cretaceous assembly and fragmentation of Mexico: Geological Society of America Bulletin, v.113, p. 1142-1160.

Dickinson, W.R., and Lawton, T.F., 2003, Sequential suturing as the ultimate control for Pennsylvanian Ancestral Rocky Mountains deformation: Geology, v. 31, p. 609-612.

Dickinson, W.R., Gehrels, G., and Stern, R., 2010, Late Triassic Texas uplift preceding Jurassic opening of the Gulf of Mexico: evidence from U-Pb ages of detrital zircons: Geosphere, v. 6, p. 641-662.

Domeier, M. and Torsvik, T.H., 2014, Plate tectonics in the late Paleozoi: Geoscience Frontiers, v. 5, p. 303-350.

Elebiju, O.O., Keller, G.R., and Marfurt, K.J., 2010, Case History: Investigation of links between Precambrian basement structure and Paleozoic strata in the Fort Worth basin, Texas, U.S.A., using high-resolution aeromagnetic, HRAM data and seismic attributes: Geophysics, v. 75, p. B157-B168.

Erlich, R. N., and J. L. Coleman, 2005, Drowning of the Upper Marble Falls Carbonate Platform (Pennsylvanian), central Texas: A case of conflicting 'signals?': Sedimentary Geology, v.175, p. 479-499.

Eriksson, K.A., Campbell, I.H., Palin, J.M., Allen, C.M., and Bock, B., 2004, Evidence for multiple recycling in Neoproterozoic through Pennsylvanian sedimentary rocks of the central Appalachian Basin: The Journal of geology, v. 112, p. 261-276.

Ewing, T.E., 2006, Mississippian Barnett Shale, Fort Worth Basin, north-central Texas: Gas-shale play with multi–trillion cubic foot potential [Discussion], American Association of Petroleum Geologists Bulletin, v. 90, p. 963-966.

Feray, D.E., and Brooks, J.E., 1966, Pennsylvanian Canyon stratigraphy of north-central Texas: Southern Methodist University, Journal Graduate Research Center, v. 35, p. 91-104.

Flippin, J.W., 1982, The stratigraphy, structure, and economic aspects of the Paleozoic strata in Erath County, North-Central Texas, in C. A. Martin, ed., Petroleum Geology of the Fort Worth Basin and Bend Arch Area: Dallas Geological Society, p. 129-155.

Frost, B.R., Chamberlain, K.R., Swapp, S., Frost, C.D., and Hulsebosch, T.P., 2000, Late Archean structural and metamorphic history of the Wind River Range: evidence for a long-lived active margin on the Archean Wyoming Craton: Geological Society of American, Bulletin, v. 112, p. 564-578.

Gehrels, G.E., Valencia, V., and Ruiz, J., 2008, Enhanced precision, accuracy, efficiency, and spatial resolution of U-Pb ages by laser ablation–multicollector–inductively coupled plasma–mass spectrometry: Geochemistry Geophysics Geosystems, v. 9, Q03017, doi:10.1029/2007GC001805.

Gehrels, G.E., Blakey, R., Karlstrom, K.E., Timmons, J.M., Dickinson, W.R., and Pecha, M., 2011, Detrital zircon U-Pb geochronology of Paleozoic strata in the Grand Canyon, Arizona: Lithosphere, v. 3, p. 183-200.

Gilbert, M.C., and Denison, R.E., 1993, Late Proterozoic to Early Cambrian basement of Oklahoma, in Reed, J.C., Jr., Bickford, M.E., Houston, R.S., Link, P.K., Rankin, D.W., Sims, P.K., and Van Schmus, W.R., eds., Precambrian: Conterminous U.S.: Geological Society of America, The Geology of North America, v. C-2, p. 303-314.

Goolsby, J.L., 1957, A study of the Hickory Sandstone [M.S. Thesis], Texas A&M University, TX, 92 p.

Graham, S.A., Dickinson, W.R., and Ingersoll, R.V., 1975, Himalayan– Bengal model for flysch dispersal in the Appalachian–Ouachita system: Geological Society of America Bulletin, v. 86, p. 273-286.

Granata Jr, W.H., 1963, Cretaceous stratigraphy and structural development of the Sabine Uplift area, Texas and Louisiana, in Report on Selected North Louisiana and South Arkansas oil and gas fields and Regional Geology: Shreveport Geological Society Reference Report, v. 5, p. 50-95.

Grimes, S.W., and Copeland, P., 2004, Thermochronology of the Grenville Orogeny in West Texas: Precambrian Research, v. 131, p. 23-54.

Gleason, J.D., Patchett, P.J., Dickinson, W.R., and Ruiz, J., 1994, Nd isotopes link Ouachita turbidites to Appalachian sources: Geology, v. 22, p. 347-350.

Gleason, J.D., Patchett, P.J., Dickinson, W.R., and Ruiz, J., 1995, Nd isotopic constraints on sediment sources of the Ouachita-Marathon fold belt: Geological Society of America Bulletin, v. 107, p. 1192-1210.

Gleason, J.D., Finney, S.C., and Gehrels, G.E., 2002, Paleotectonic implications of a mid‐to late‐Ordovician provenance shift, as recorded in sedimentary strata of the Ouachita and southern Appalachian mountains: The Journal of geology, v. 110, p. 291-304.

Gleason, J.D., Gehrels, G.E., Dickinson, W.R., Patchett, P.J., and Kring, D.A., 2007, Laurentian sources for detrital zircon grains in turbidite and deltaic sandstones of the Pennsylvanian Haymond Formation, Marathon assemblage, West Texas, USA: Journal of Sedimentary Research, v. 77, p. 888-900.

Hames, W.E., Hogan, J.P., and Gilbert, M.C., 1995, Revised granite-gabbro age relationships, Southern Oklahoma Aulacogen: Basement Tectonics 12, volume 6 of the series Proceedings of the International Conferences on Basement Tectonics, p. 247-249.

Hanson, R.E., Puckett, R.E., Keller, G.R., Brueseke, M.E., Bulen, C.L., Mertzman, S.A., Finegan, S.A., and McCleery, D.A., 2013, Intraplate magmatism related to opening of the southern

Iapetus Ocean: Cambrian Wichita igneous province in the Southern Oklahoma rift zone: Lithos, v. 174, p. 57-70.

Hatcher, R.D. Jr. 1989, Tectonic synthesis of the U.S. Appalachians, in Hatcher, R.D., Jr., W.A. Thomas, and G.W. Viele, eds., The Appalachian-Ouachita Orogen in the United States: Geological Society of America Decade of North American Geology, v. F2, p. 29-41.

Hentz, T.C., Ambrose, W.A., and Carr, D.L., 2012, Reservoir system of the Pennsylvanian lower Atoka Group (Bend Conglomerate), northern Fort Worth Basin, Texas: High-resolution facies distribution, structural controls on sedimentation, and production trends: American Association of Petroleum Geologists Bulletin, v. 96, p. 1301-1332.

Heumann, M.J., Bickford, M.E., Hill, B.M., McLelland, J.M., Selleck, B.W., and Jercinovic, M.J., 2006, Timing of anatexis in metapelites from the Adirondack lowlands and southern highlands: A manifestation of the Shawinigan orogeny and subsequent anorthosite-mangerite-charnockite-granite magmatism: Geological Society of America Bulletin, v. 118, p. 1283-1298.

Hill, R.J., Jarvie, D.M., Zumberge, J., Henry, M., and Pollastro, R.M., 2007, Oil and gas geochemistry and petroleum systems of the Fort Worth Basin: American Association of Petroleum Geologists Bulletin, v. 91, p. 445-473.

Hoffman, P.F., 1988, United Plates of America, the birth of a craton-Early Proterozoic assembly and growth of Laurentia: Annual Review of Earth and Planetary Sciences, v. 16, p. 543-603.

Hoffman, P.F., 1991, Did the breakout of Laurentia turn Gondwanaland inside-out: Science, v. 252, p. 1409-1412.

Hogan, J.P., and Gilbert, M.C., 1998, The Southern Oklahoma aulacogen: A Cambrian analog for Mid-Proterozoic AMCG (anorthosite-mangerite-charnockite-granite) complexes?: Basement Tectonics 12, volume 6 of the series Proceedings of the International Conferences on Basement Tectonics, p. 39-78.

Houseknecht, D.W., and Matthews, S.M., 1985, Thermal Maturity of Carboniferous Strata, Ouachita Mountains: American Association of Petroleum Geologists Bulletin, v. 69, p. 335-345.

Imoto, N., and McBride, E.F., 1990, Volcanism recorded in the Tesnus Formation, Marathon uplift, Texas, in LaRoche, T.M., and Higgins, L., eds., Marathon Thrust Belt: Structure, Stratigraphy, and Hydrocarbon Potential: West Texas Geological Society and SEPM, Permian Basin Section, Field Seminar, p. 93-98.

Jarvie, D.M., Hill, R.J., and Pollastro, R.M., 2005, Assessment of the gas potential and yields from shales: The Barnett Shale model: Oklahoma Geological Survey Circular, v. 110, p. 37-50.

Johnson, K.S., Amsden, T.W., Denison, R.E., Dutton, S.P., Goldstein, A.G., Rascoe, B. Jr., Sutherland, P.K., and Thompson, D.M., 1988, Southern Midcontinent region, in Sloss, L.L., ed., Sedimentary cover—North American craton: U.S.: Geological Society of America, The Geology of North America, v. D-2, p. 307-359.

Keller, G.R., and Stephenson, R.A., 2007, The Southern Oklahoma and Dniepr-Donets aulacogens: A comparative analysis, in Hatcher, R.D., Jr., Carlson, M.P., McBride, J.H., and Martínez Catalán, J.R., eds., 4-D Framework of Continental Crust: Geological Society of America Memoir 200, p. 127-143, doi:10.1130/2007.1200(08).

Keller, G.R., Kruger, J.M., Smith, K.J., and Voight, M.R., 1989, The Ouachita system: A geophysical overview, in Hatcher, R.D., Thomas, W.A., and Viele, G.W., eds., The Appalachian-Ouachita Orogen in the United States: Geological Society of America, The Geology of North America, F-2, p. 689-693.

Keppie, J.D., Dostal, J., Murphy, J.B., and Nance, R.D., 1996, Terrane transfer between eastern Laurentia and western Gondwana in the early Paleozoic: Constraints on global reconstructions: Geological Society of America Special Papers 304, p. 369-380.

Keppie, J.D., Nance, R.D., Murphy, J.B., and Dostal, J., 2003, Tethyan, Mediterranean, and Pacific analogues for the Neoproterozoic–Paleozoic birth and development of peri-Gondwanan terranes and their transfer to Laurentia and Laurussia: Tectonophysics, v. 365, p. 195-219.

Kluth, C.F., 1986, Plate tectonics of the Ancestral Rocky Mountains: Part III. Middle Rocky Mountains, in Peterson, J.A., ed., Paleotectonics and Sedimentation in the Rocky Mountain Region: American Association of Petroleum Geologists Memoir, v. 41, p. 353-369.

Kluth, C.F., and P.J. Coney, 1981, Plate tectonics of the Ancestral Rocky Mountains: Geology, v. 9, p. 10-15.

Krause, S.J., 1996, Stratigraphic framework, Facies analysis, and depositional history of the Middle to Late Cambrian Riley Formation, central Texas [M.S. Thesis], The University of Texas at Austin, TX, 172 p.

LaMaskin, T.A., Vervoort, J.D., Dorsey, R.J., and Wright, J.E., 2011, Early Mesozoic paleogeography and tectonic evolution of the western United States: Insights from detrital zircon U-Pb geochronology, Blue Mountains Province, northeastern Oregon: Geological Society of America Bulletin, v. 123, p. 1939-1965.

Lambert, D.D., Unruh, D.M., and Gilbert, M.C., 1988, Rb\\Sr and Sm\\Nd isotopic study of the Glen Mountains Layered Complex: initiation of rifting within the Southern Oklahoma aulacogen: Geology, v. 16, p. 13-17.

Loomis, J., Weaver, B., and Blatt, H., 1994, Geochemistry of Mississippian tuffs from the Ouachita Mountains, and Implications for the Tectonic of the Ouachita orogen, Oklahoma and Arkansas: Geological Society of America Bulletin, v.106, p. 1158-1171.

Lovick, G.P., Mazzini, C.G., and Kotila, D.A., 1982, Atokan Clastics of Fort Worth Basin--Depositional Environments in a Foreland Basin [abs.]: American Association of Petroleum Geologists Bulletin, v. 66, p. 246.

Martens, U., Weber, B., and Valencia, V.A., 2010, U/Pb geochronology of Devonian and older Paleozoic beds in the southeastern Maya block, Central America: Its affinity with peri-Gondwanan terranes: Geological Society of America Bulletin, v. 122, p. 815-829.

May, S.R., Gray, G.G., Summa, L.L., Stewart, N.R., Gehrels, G.E., and Pecha, M.E., 2013, Detrital zircon geochronology from the Bighorn Basin, Wyoming, USA: implications for

tectonostratigraphic evolution and paleogeography: Geological Society of America, Bulletin, v. 125, p. 1403-1422.

McBride, E.F., Abdel-Wahab, A.A., and Milliken, K.L., 2002, Petrography and diagenesis of a half-billion-yearold cratonic sandstone (Hickory), Llano region, Texas: University of Texas, Austin, Bureau of Economic Geology, Report of Investigation No. 264, 77 p.

McLelland, J., Selleck, B., and Bickford, M.E., 2010, Review of the Proterozoic evolution of the Grenville Province, its Adirondack outlier, and the Mesoproterozoic inliers of the Appalachians, in Tollo, R.P., Bartholomew, M.J., Hibbard, J.P., and Karabinos, P.M., eds., From Rodinia to Pangea: The Lithotectonic Record of the Appalachian Region: Geological Society of America Memoir, v. 206, p. 21-49, doi:10.1130/2010.1206(02).

McMillan, N.J., and McLemore, V.T., 2004, Cambro-Ordovician magmatism and extension in New Mexico and Colorado: New Mexico Bureau of Geology and Mineral Resources, Bulletin, v. 160, 11 p.

Mezger, K., Essene, E.J., Van der Pluijm, B.A., and Halliday, A.N., 1993, U-Pb geochronology of the Grenville Orogen of Ontario and New York: constraints on ancient crustal tectonics: Contributions to Mineralogy and Petrology, v. 114, p. 13-26.

Miller, C.F., Hatcher, R.D., Jr., Ayers, J.C., Coath, C.D., and Harrison, T.M., 2000, Age and zircon inheritance of eastern Blue Ridge plutons, southwestern North Carolina and northeastern Georgia, with implications for magma history and evolution of the southern Appalachian orogen: American Journal of Science, v. 300, p. 142-172.

Moecher, D.P., and Samson, S.D., 2006, Differential zircon fertility of source terranes and natural bias in the detrital zircon record: Implications for sedimentary provenance analysis: Earth and Planetary Science Letters, v. 247, p. 252-266.

Montgomery, S.L., Jarvie, D.M., Bowker, K.A., and Pollastro, R.M., 2005, Mississippian Barnett Shale, Fort Worth basin, north-central Texas: Gas-shale play with multi–trillion cubic foot potential: American Association of Petroleum Geologists Bulletin, v. 89, p. 155-175.

Moore, W.L., 1959, Pennsylvanian Foraminifera from the Big Saline Formation of the Llano Uplift of Texas [Ph.D. Dissertation], University of Wisconsin, 184 p.

Morris, R.C. 1974, Sedimentary and tectonic history of Ouachita Mountains, in W. R. Dickinson, ed., Tectonics and Sedimentation, Society of Economic Paleontologists and Mineralogists Special Publication, v. 22, p. 120-142.

Mosher, S., 1998, Tectonic evolution of the southern Laurentian Grenville orogenic belt: Geological Society of America Bulletin, v. 110, no. 11, p. 1357-1375.

Mueller, P.A., Heatherington, A.L., Wooden, J.L., Shuster, R.D., Nutman, A.P., and Williams, I.S., 1994, Precambrian zircons from the Florida basement: A Gondwanan connection: Geology, v. 22, p. 119-122.

Mueller, P.A., Heatherington, A.L., Kelly, D.M., Wooden, J.L. and Mogk, D.W., 2002, Paleoproterozoic crust within the Great Falls tectonic zone: Implications for the assembly of southern Laurentia: Geology, v. 30, p. 127-130.

Mueller, P.A., Heatherington, A.L., Foster, D.A., Thomas, W.A., and Wooden, J.L., 2014, The Suwannee suture: Significance for Gondwana-Laurentia terrane transfer and formation of Pangaea: Gondwana Research, v. 26, p. 365-373.

Murphy, J.B., Pe-Piper, G., Keppie, J.D,. and Piper, D.J., 1992, Correlation of Neoproterozoic III sequences in the Avalon Composite Terrane of mainland Nova Scotia: tectonic implications: Atlantic Geology, v. 28, p. 143-151.

Murphy, J.B., Pisarevsky, S.A., Nance, R.D., and Keppie, J.D., 2004, Neoproterozoic—Early Paleozoic evolution of peri-Gondwanan terranes: implications for Laurentia-Gondwana connections: International Journal of Earth Sciences, v. 93, p. 659-682.

Murphy, J.B., Gutierrez-Alonso, G., Nance, R.D., Fernandez-Suarez, J., Keppie, J.D., Quesada, C., Strachan, R.A., and Dostal, J., 2006, Origin of the Rheic Ocean: Rifting along a Neoproterozoic suture?: Geology, v. 34, p. 325-328.

Nance, R.D., and Linnemann, U., 2008, The Rheic Ocean: origin, evolution, and significance: Geological Society of America Today, v. 18, p. 4-12.

Nance, R.D., Murphy, J.B., and Keppie, J.D., 2002, A Cordilleran model for the evolution of Avalonia: Tectonophysics, v. 352, p. 11-31.

Nance, R.D., Gutiérrez-Alonso, G., Keppie, J.D., Linnemann, U., Murphy, J.B., Quesada, C., Strachan, R.A., and Woodcock, N.H., 2010, Evolution of the Rheic ocean: Gondwana Research, v. 17, p. 194-222.

Nelson, K.D., Lillie, R. J., de Voogd, B., Brewer, J. A., Oliver, J. E. , Kaufman, S., Brown, L., and, Viele, G.W., 1982, COCORP seismic reflection profiling in the Ouachita Mountains of western Arkansas geometry and geologic interpretation: Tectonics, v. 1, p. 413-430.

Niem, M.R., 1977, Mississippian pyroclastic flow and ash-fall deposits in the deep-marine Ouachita flysch basin, Oklahoma and Arkansas: Geological Society of America Bulletin, v. 88, p. 49-61.

Noble, P.J., 1993, Paleoceanographic and tectonic implications of a regionally extensive Early Mississippian hiatus in the Ouachita system, southern mid-continental United States: Geology, v. 21, p. 315-318.

Nunn, J.A., 2012, Burial and thermal history of the Haynesville shale: Implications for overpressure, gas generation, and natural hydrofracture: Gulf Coast Association of Geological Societies, v. 1, p. 81-96.

Opdyke, N.D., Jones, D.S., MacFadden, B.J., Smith, D.L., Mueller, P.A., and Shuster, R.D., 1987, Florida as an exotic terrane: Paleomagnetic and geochronologic investigation of lower Paleozoic rocks from the subsurface of Florida: Geology, v. 15, p. 900-903.

Park, H., Barbeau Jr, D.L., Rickenbaker, A., Bachmann‐Krug, D., and Gehrels, G., 2010, Application of foreland basin detrital‐zircon geochronology to the reconstruction of the southern and central Appalachian orogen: The Journal of Geology, v.118, p. 23-44.

Pashin, J.C., 1994, Cycles and stacking patterns in Carboniferous rocks of the Black Warrior foreland basin: Gulf Coast Association of Geological Societies Transactions, v. 44, p. 555-563.

Perry, W.J., 1989, Tectonic Evolution of the Anadarko Basin Region, Oklahoma, Evolution of sedimentary basins-Anadarko Basin, chapter A: Department of the Interior, US Geological Survey, 19 p.

Pickell, M.J., 2012, Detrital Zircon Geochronology of Middle Ordovician Siliciclastic Sediment on the Southern Laurentian Shelf [M.S. Thesis], Texas A&M University, TX, 128 p.

Pindell, J.L., 1985, Alleghenian reconstruction and subsequent evolution of the Gulf of Mexico, Bahamas, and Proto‐Caribbean: Tectonics, v. 4, p. 1-39.

Plummer, F.B., and Hornberger, J., 1935, Geology of Palo Pinto County, Texas, University of Texas at Austin: University of Texas Bulletin, no. 3534, 237 p.

Pollastro, R. M., 2003, Geological and production characteristics utilized in assessing the Barnett Shale continuous (unconventional) gas accumulation, Barnett–Paleozoic total petroleum system, Fort Worth basin, Texas: Barnett Shale Symposium: Ellison Miles Geotechnology Institute at Brookhaven College, Dallas, Texas, 6 p.

Pollastro, R.M., Hill, R.J., Jarvie, D.M. and Henry, M.E., 2003, Assessing undiscovered resources of the Barnett-Paleozoic total petroleum system, Bend Arch–Fort Worth basin province, Texas: AAPG Southwest Section Meeting, Fort Worth, TX, 18 p.

Pollastro, R.M., Jarvie, D.M., Hill, R.J., and Adams, C.W., 2007, Geologic framework of the Mississippian Barnett Shale, Barnett-Paleozoic total petroleum system, Bend arch–Fort Worth Basin, Texas: American Association of Petroleum Geologists Bulletin, v. 91, p. 405-436.

Pollock, J.C., Hibbard, J.P., and Sylvester, P.J., 2009, Early Ordovician rifting of Avalonia and birth of the Rheic Ocean: U–Pb detrital zircon constraints from Newfoundland: Journal of the Geological Society, v. 166, p. 501-515.

Poole, F.G., Perry, W.J., Madrid, R.J., and Martinez, R.A., 2005, Tectonic synthesis of the Ouachita-Marathon-Sonora orogenic margin of southern Laurentia: Stratigraphic and structural

implications for timing of deformational events and plate-tectonic model: Geological Society of America Special Papers, v. 393, p. 543-596.

Press, W.H., Flannery, B.P., Tenkolsky, S.A., and Vetterling, W.T., 1986, Numerical recipes: Cambridge, U.K., Cambridge University Press, 818 p.

Randolph, L.C., 1991, The effects of faults on the groundwater system in the Hickory sandstone aquifer in central Texas [Ph.D. Dissertation], Texas A&M University, 102 p.

Rankin, D.W., Drake, A.A., Jr., Glover, L., III, Goldsmith, R., Hall, L.M., Murray, D.P., Ratcliffe, N.M., Read, J.F., Secor, D.T., Jr., and Stanley, R.S., 1989, Pre-orogenic terranes, in Hatcher, R.D., Jr., Thomas, W.A., and Viele, G.W., eds. The Appalachian-Ouachita Orogen in the United States: Geological Society of America, Geology of North America, v. F-2, p. 7-100.

Rankin, D.W., Tollo, R.P., Aleinikoff, J.A., and Ayuso, R.A., 1997, Manhattan Prong A-type metagranites with feldspar Pb isotope affinities to Laurentia and zircon ages of ;563 Ma: Support for late Neoproterozoic Iapetian rifting [abs.]: Geological Society of America Abstracts with Programs, v. 29, p. 74.

Rast, N., and Skehan, J.W., 1983, The evolution of the Avalonian plate: Tectonophysics, v. 100, p. 257-286.

Rivers, T., 1997, Lithotectonic elements of the Grenville province: Precambrian Research, v. 86, p. 117-154.

Robinson, D.M., Bailey, R.M. and Goodliffe, A.M., 2012, Structure of the Alleghanian Thrust Belt under the Gulf Coastal Plain of Alabama: Gulf Coast Association of Geological Societies Transactions, v. 1, p. 44-54.

Ruppel, S.C., 1985, Stratigraphy and petroleum potential of pre-Pennsylvanian rocks, Palo Duro Basin, Texas Panhandle: University of Texas at Austin. Bureau of Economic Geology, Report of investigations No. 147, p. 71-73.

Samson, S.D., Secor, D.T., and Hamilton, M.A., 2001, Wandering Carolina: tracking exotic terranes with detrital zircons [abs.]: Geological Society of America Abstracts with Programs, v. 33, p. 263.

Schaaf, P., Weber, B., Weis, P., Gross, A., Ortega-Gutiérrez, F., and Köhler, H., 2002, The Chiapas Massif (Mexico) revised: New geologic and isotopic data for basement characteristics, in Miller, H., ed., Contributions to Latin American Geology: Neues Jahrbuch für Geologie und Paläontologie Abhandlung, v. 225, p. 1-23.

Shannon, W.M., Barens, C.G. and Bickford, M.E., 1997, Grenville magmatism in West Texas: Petrology and geochemistry of the Red Bluff granitic suite: Journal of Petrology, v. 38, no. 10, p. 1279-1305.

Sharrah, K.L., 2006, Comparative Study of the Sedimentology and Provenance of the Atoka Formation in the Frontal Ouachita Thrust Belt, Oklahoma [Ph.D. Dissertation], University of Tulsa, 268 p.

Shaulis, B.J., Lapen, T.J., Casey, J.F., and Reid, D.R., 2012, Timing and rates of flysch sedimentation in the Stanley Group, Ouachita Mountains, Oklahoma and Arkansas, U.S.A.: constraints from U-Pb zircon ages of subaqueous ash-flow tuffs: Journal of Sedimentary Research, v. 82, p. 833-840.

Sims, P.K. and Petermar, Z.E., 1986, Early Proterozoic Central Plains orogen: A major buried structure in the north-central United States: Geology, v. 14, p.488-491.

Sloss, L.L., 1988, Tectonic evolution of the craton in Phanerozoic time, in Sloss, L.L., ed., Sedimentary Cover; North America Craton: Geological Society of America, Geology of North America, v. D-2, p. 25-51.

Soreghan, M.J., Soreghan, G.S., and Hamilton, M., 2002, Paleowinds inferred from detrital-zircon geochronology of upper Paleozoic loessite, western equatorial Pangea: Geology, v. 30, p. 695-698.

Spencer, C.J., Prave, A.R., Cawood, P.A., and Roberts, N.M., 2014, Detrital zircon geochronology of the Grenville/Llano foreland and basal Sauk Sequence in West Texas, USA: Geological Society of America Bulletin, v.126, p. 1117-1128.

Stacey, J.T., and Kramers, 1., 1975, Approximation of terrestrial lead isotope evolution by a two-stage model: Earth and planetary science letters, v. 26, p. 207-221.

Steltenpohl, M.G., Mueller, P.M., Heatherington, A.L., Hanley, T.B. and Wooden, J.L., 2008, Gondwanan/peri-Gondwanan origin for the Uchee terrane, Alabama and Georgia: Carolina zone or Suwannee terrane (?) and its suture with Grenvillian basement of the Pine Mountain window: Geosphere, v. 4, p. 131-144.

Stenzel, H. B., 1935, Precambrian structural conditions in the Llano region: The Geology of Texas, V. II, Structural and Economic Geology University of Texas Bureau of Economics Geology Bulletin, v. 3401, p. 74-79.

Stern, R.J., and Dickinson, W.R., 2010, The Gulf of Mexico is a Jurassic backarc basin: Geosphere, v. 6, p. 739-754.

Stewart, J.H., Gehrels, G.E., Barth, A.P., Link, P.K., Christie-Blick, N., and Wrucke, C.T., 2001, Detrital zircon provenance of Mesoproterozoic to Cambrian arenites in the western United States and northwestern Mexico: Geological Society of America Bulletin, v. 113, p. 1343-1356.

Stoeser, D.B., Green, G.N., Morath, L.C., Heran, W.D., Wilson, A.B., Moore, D.W., and Van Gosen, B.S., 2007, Preliminary Integrated Geologic Map Databases for the United States Central States: Montana, Wyoming, Colorado, New Mexico, Kansas, Oklahoma, Texas, Missouri, Arkansas, and Louisiana: U.S. Geological Survey Open-File Report 2005-1351, version 1.0, http://pubs.usgs.gov/of/2005/1351/.

Su, Q., Goldberg, S.A., and Fullagar, P.D., 1994, Precise U-Pb zircon ages of Neoproterozoic plutons in the southern Appalachian Blue Ridge and their implications for initial rifting of Laurentia: Precambrian Research, v. 68, p. 81-95.

Teran, I.A.P., 2007, Stratal architecture and sedimentology of a portion of the Upper Cambrian Hickory Sandstone, Central Texas, USA [M.S. Thesis], Texas A&M University, 87 p.

Thomas, J.D., 2003, Integrating Synsedimentary Tectonics with Sequence Stratigraphy to Understand the development of the Fort Worth Basin: American Association of Petroleum Geologists Search and Discovery, AAPG Southwest Section Meeting, Ruidoso, New Mexico, p. 149-157.

Thomas, W.A., 1977, Evolution of Appalachian Ouachita salients and recesses from reentrants and promontories in the continental margin: American Journal of Science, v. 277, p. 1233-1278.

Thomas, W.A., 1997, Nd isotopic constraints on sediment sources of the Ouachita-Marathon fold belt: Alternative Interpretation and Reply: Geological Society of America Bulletin v. 109, p. 779-787.

Thomas, W.A., 2004, Genetic relationship of rift-stage crustal structure, terrane accretion, and foreland tectonics along the southern Appalachian-Ouachita orogen: Journal of Geodynamics, v. 37, p. 549-563.

Thomas, W.A., 2006, Tectonic inheritance at a continental margin: Geological Society of America Today, v. 16, p. 4-11.

Thomas, W.A., 2013, The Sabine and Coahuila terranes at the southern margin of Laurentia [abs.]: Geological Society of America Abstracts with Programs, v. 45, p. 293.

Thomas, W. A., and Viele, G. W., 1983, Tectonic history of the Ouachita orogen: Geology, v. 11, p. 482-483.

Thomas, W.A., Astini, R.A. and Bayona, G., 2002, Ordovician collision of the Argentine Precordillera with Gondwana, independent of Laurentian Taconic orogeny: Tectonophysics, v. 345, p. 131-152.

Thomas, W.A., Becker, T.P., Samson, S.D., and Hamilton, M.A., 2004, Detrital zircon evidence of a recycled orogenic foreland provenance for Alleghanian clastic ‐ wedge sandstones: The Journal of Geology, v. 112, p. 23-37.

Thomas, W.A., Tucker, R.D., Astini, R.A., and Denison, R.E., 2012, Ages of pre-rift basement and synrift rocks along the conjugate rift and transform margins of the Argentine Precordillera and Laurentia: Geosphere, v. 8, p. 1366-1383, doi: 10 .1130 /GES00800 .1 .

Thomas, W.A., Gehrels, G.E., and Romero, M.C., 2016, Detrital zircons from crystalline rocks along the Southern Oklahoma fault system, Wichita and Arbuckle Mountains, USA: Geosphere, v. 12, p. 1224-1234, doi:10.1130/GES01316.1.

Thompson, M.D., 1982, Atoka Group (Lower to Middle Pennsylvanian), Northern Fort Worth Basin, Texas: terrigenous depositional systems, diagenesis, and reservoir distribution and quality: The University of Texas at Austin, Bureau of Economic Geology Report of Investigations No. 125, 62 p.

Thompson, M.D., Hermes, O.D., Bowring, S.A., Isachsen, C.E., Besancon, J.R., and Kelly, K.L., 1996, Tectonostratigraphic implications of Late Proterozoic U-Pb zircon ages in the Avalon Zone of southeastern New England: Geological Society of America Special Paper 304, p. 179-192.

Torsvik, T.H., Smethurst, M.A., Meert, J.G., Van der Voo, R., McKerrow, W.S., Brasier, M.D., Sturt, B.A., and Walderhaug, H.J., 1996, Continental break-up and collision in the Neoproterozoic and Palaeozoic—a tale of Baltica and Laurentia: Earth-Science Reviews, v. 40, p. 229-258.

Trompette, R., 2000, Gondwana evolution; its assembly at around 600 Ma: Comptes Rendus, Academie des Sciences-Series 2, Earth and Planetary Science, v. 330, p. 305-315.

Turner, G. L., 1957, Paleozoic stratigraphy of the Fort Worth Basin, Joint Field Trip Guidebook: Abilene Geological Society, Fort Worth Geological Society, p. 57-77.

Uddin, A., Hames, W.E., Peavy, T., Pashin, J.C., 2016, Detrital History of the Lower Pennsylvanian Pottsville Formation in the Cahaba Synclinorium of Alabama, U.S.A.: SEPM Society for Sedimentary Geology: Journal of Sedimentary Research, v. 86, p. 1287-1297.

Unrug, R., 1995, Rodinia and Gondwana: A record of supercontinent configuration change, in Yoshida, M., and Santosh, M., eds., India and Antarctica during the Precambrian: Geological Society of India Memoir 34, p. 1-9.

Van Schmus, W.R., Bickford, M.E., Sims, P.K., Anderson, J.L., Shearer, C.K., and Treves, S.B., 1993, Proterozoic geology of the western midcontinent region, in Reed, J.C., Bickford, M.E., Houston, R.S., Link, P.K., Rankin, D.W., Sims, P.K., and Van Schmus, W.R., eds., Precambrian Conterminous U.S.: Geological Society of America, The Geology of North America, v. C-2, p. 239-259.

Van Schmus, W.R., Bickford, M.E., and Turek, A., 1996, Proterozoic geology of the east-central Midcontinent basement: Geological Society of America, Special Paper 308, p. 7-32.

Van Staal, C.R., Whalen, J.B., Valverde-Vaquero, P., Zagorevski, A., and Rogers, N., 2009, Pre-Carboniferous, episodic accretion-related, orogenesis along the Laurentian margin of the northern Appalachians: Geological Society Special Publications [London], v. 327, p. 271-316.

Viele, G.W., and Thomas, W.A., 1989, Tectonic synthesis of the Ouachita orogenic belt, in Hatcher, R.D., Jr., Thomas, W.A., and Viele, G.W., eds., The Appalachian-Ouachita orogen in the United States: Geological Society of America, The Geology of North America, v. F-2, p. 695-728.

Walper, J.L., 1977, Paleozoic tectonics of the southern margin of North America: Gulf Coast Association of Geological Societies Transactions, v. 27, p. 230-241.

Walper, J.L., 1982, Plate tectonic evolution of the Fort Worth Basin: in C.A. Martin, ed., Petroleum Geology of the Fort Worth Basin and Bend Arch Area: Dallas Geological Society, p. 237-251.

Walsh, G.J., and Aleinikoff, J.N., 1999, U-Pb zircon age of metafelsite from the Pinney Hollow Formation; implications for the development of the Vermont Appalachians: American Journal of Science, v. 299, p. 157-170.

Whitmeyer, S.J., and Karlstrom, K.E., 2007, Tectonic model for the Proterozoic growth of North America: Geosphere, v. 3, p. 220-259.

Williams, H., and Hatcher, R.D., 1982, Suspect terranes and accretionary history of the Appalachian orogen: Geology, v. 10, p. 530-536.

Wilson, J.S., 2001, High-resolution stratigraphic and structural characterization of the fault-partitioned hickory sandstone aquifer, Mason county, central Texas [Ph.D. dissertation], Texas A&M University, TX, 151 p.

Wilson, W.F., 1962, Sedimentary petrology and sedimentary structures of the Cambrian Hickory Sandstone Member, Central Texas [M.S. Thesis], The University of Texas at Austin, TX, 229 p.

Wright, W. F., 1979, Petroleum geology of the Permian Basin: West Texas Geological Society Publication 79-71, 98 p.

Xie, X., Cains, W., and Manger, W.L., 2016, U–Pb detrital zircon evidence of transcontinental sediment dispersal: provenance of Late Mississippian Wedington Sandstone member, NW Arkansas: International Geology Review, v. 58, p. 1951-1966.

Ye, H., Royden, L., Burchfiel, C., and Schuepbach, M., 1996, Late Paleozoic deformation of interior North America: the greater Ancestral Rocky Mountains: American Association of Petroleum Geologists Bulletin, v. 80, p. 1397-1432.

Chapter 3 SANDSTONE PETROGRAPHY AND REEs CONSTRAINTS ON PALEOZOIC SEDIMENT DISPERSAL TO THE FORT WOTH BASIN

ABSTRACT

The Fort Worth Basin in north-central Texas is a major shale-gas producer, yet its Paleozoic sediments dispersal patterns and their influences on hydrocarbon enrichment in the basin remain under debate. Herein we apply sandstone petrography and mudstone rare-earth elements (REEs) to determine provenance of the Paleozoic sedimentary rocks in the Fort Worth Basin and understand the sediment dispersal patterns on the southern margin of Laurentia before and during the Laurentia-Gondwana collision. The sandstone composition changes from the Cambrian ($Q_{91}F_6L_3$) to the Pennsylvanian and early Permian ($Q_{87}F_2L_{11}$), suggesting more continental input from the Laurentian craton during the Cambrian, but more input from the recycled orogen during the Middle Pennsylvanian-early Permian. The Paleozoic mudstone samples show enrichment of L REEs, flat distributions of HREE, and negative Eu anomalies after the data is normalized to Chondrite, consistent with the REE pattern of average upper crust. The Middle Pennsylvanian-earliest Permian samples have lower REEs contents, less LREEs, and larger negative Eu anomalies compared to the Cambrian-Early Pennsylvanian samples, reflecting long distance transport of detritus from the Appalachians and erosion of peri-Gondwana terranes in the vicinity of the Fort Worth Basin. These changes of sediment provenance recorded in sandstone petrography and mudstone REEs patterns confirm the interpretation of Appalachian-derived sediments based on detrital zircon geochronology, and further clarify that the change of sediment provenance to the Fort Worth Basin occurred as early as the Middle Pennsylvanian.

3. 1 INTRODUCTION

During the late Paleozoic, subduction of the southern margin of Laurentia underneath Gondwana and their subsequent collision formed the Alleghanian-Ouachita-Marathon orogenies on

Laurentia (Walper, 1982; Erlich and Coleman, 2005; Thomas, 2006; Elebiju et al., 2010). Flexural subsidence induced by the orogenies formed several peripheral foreland basins in southern Laurentia, including, from east to west, the Black Warrior, Arkoma, Fort Worth, and Val Verde Basins (e.g., Walper, 1982; Thompson, 1988; Erlich and Coleman, 2005; Thomas, 2006; Alsalem et al., 2017). Because of limited rock exposure and post-Paleozoic erosion of the orogenies, the timing of suturing and the suturing process of the two continents remain poorly understood. In addition, the collisional tectonics on the plate margin may have accumulated enough intracontinental stress and caused the basement-involved Ancestral Rocky Mountains (ARM) Orogeny in western Laurasia (Dickinson, 2000; Dickinson and Lawton, 2003). Sedimentary rocks in peripheral foreland basins are important archives of orogenic processes. Therefore, sediment provenance in southern Laurentia holds the key to reconstruct the collisional process between the two continents.

As a foreland basin of the Ouachita orogen, the Fort Worth Basin in north-central Texas, U.S.A., has excellent hydrocarbon potential. Numerous studies have been conducted on the basin fill in order to understand the petroleum system (e.g., Morris, 1974; Pollastro et al, 2003, 2007; Hentz et al., 2012), yet the provenance of basin fill and the paleogeography before and during the collision remain poorly constrained. Current understanding of the Paleozoic sediment provenance in the Fort Worth Basin includes two schools of thought. Graham et al. (1975) proposed that sediment eroded from the Appalachians was transported by a large axial river along the Appalachian-Ouachita forelands and dispersed into a remnant ocean basin during the Paleozoic. This idea was further supported by a detrital zircon study in the Marathon foreland in West Texas (Gleason et al., 2007), and neodymium isotope studies of the deep-water deposits in the Arkoma and Marathon Basins (Gleason et al., 1994; 1995). Mudstone εNd values in these basins increased from a range of -16 to -13 to a range of -10 to -6 at ~450 Ma, suggesting arrival of the juvenile arc signature of the Taconic Orogeny in the Appalachians (Gelason et al., 1994; Patchett et al., 1999). Debate exists regarding whether such a large river existed only in the Appalachian foreland (Archer and Greb, 1995; Thomas, 1997; Thomas et al., 2017),

extended from the Appalachian foreland to the Ouachita foreland (Alsalem et al., 2018), or drained through or around the Illinois Basin before entering the Ouachita front during the late Paleozoic (Sharrah, 2006). However, other studies suggest that the basement-involved Muenster uplift to the north of the Fort Worth Basin was the primary sediment source as early as the Mississippian (Loucks and Stephen, 2007) and remained as a source during the Early Pennsylvanian (Hentz et al., 2012), with the Ouachita fold-and-thrust belt, located to the east of the Fort Worth Basin, became the main source of sediment during the Late Mississippian-Late Pennsylvanian (e.g., Walper, 1982; Grayson et al., 1991; Noble, 1993; Pollastro, 2003).

A detrital zircon study conducted in the Fort Worth Basin shows that the clastic sediments in the Cambrian strata were dispersed from the Laurentian craton, whereas the sediments in the Middle and Late Pennsylvanian strata were transported both from the Appalachians by a transcontinental river and from the peri-Gondwana Sabine terrane incorporated in the Ouachita orogen by local rivers (Alsalem et al., 2018). However, due to the high fertility of Grenvillian zircon in sediment recycling (Moecher and Samson, 2006), and that the Mississippian and Lower Pennsylvanian strata in the Fort Worth Basin are dominated by mudstone and carbonate that are not suitable for detrital zircon study, additional evidence is needed to test the competing hypotheses of sediment provenance, and constrain the timing of the earliest arrival of Gondwana sediments.

This study determines sediment provenance of Paleozoic siliciclastic rocks in the Fort Worth Basin using sandstone petrography analysis and mudstone rare-earth element (REEs) compositions. By combining our data with published detrital zircon data in eastern and southern Laurentia, we infer any changes in sediments dispersal patterns to the Fort Worth Basin and reconstruct the paleogeography before and during the Ouachita orogeny.

3. 2 GEOLOGICAL SETTINGS

The Fort Worth Basin is a foreland basin formed on the southern Laurentian continental shelf during the late Paleozoic Ouachita Orogeny (e.g., Walper, 1977; Nelson et al, 1982; Thomas and Viele,

1983). The basin is bounded by the basement-involved Red River and Muenster uplifts of ARM to the north, the Ouachita thrust belt to the east, the Llano uplift to the south, and it shallows gently toward the Bend Arch to the west (Figure 3-1).

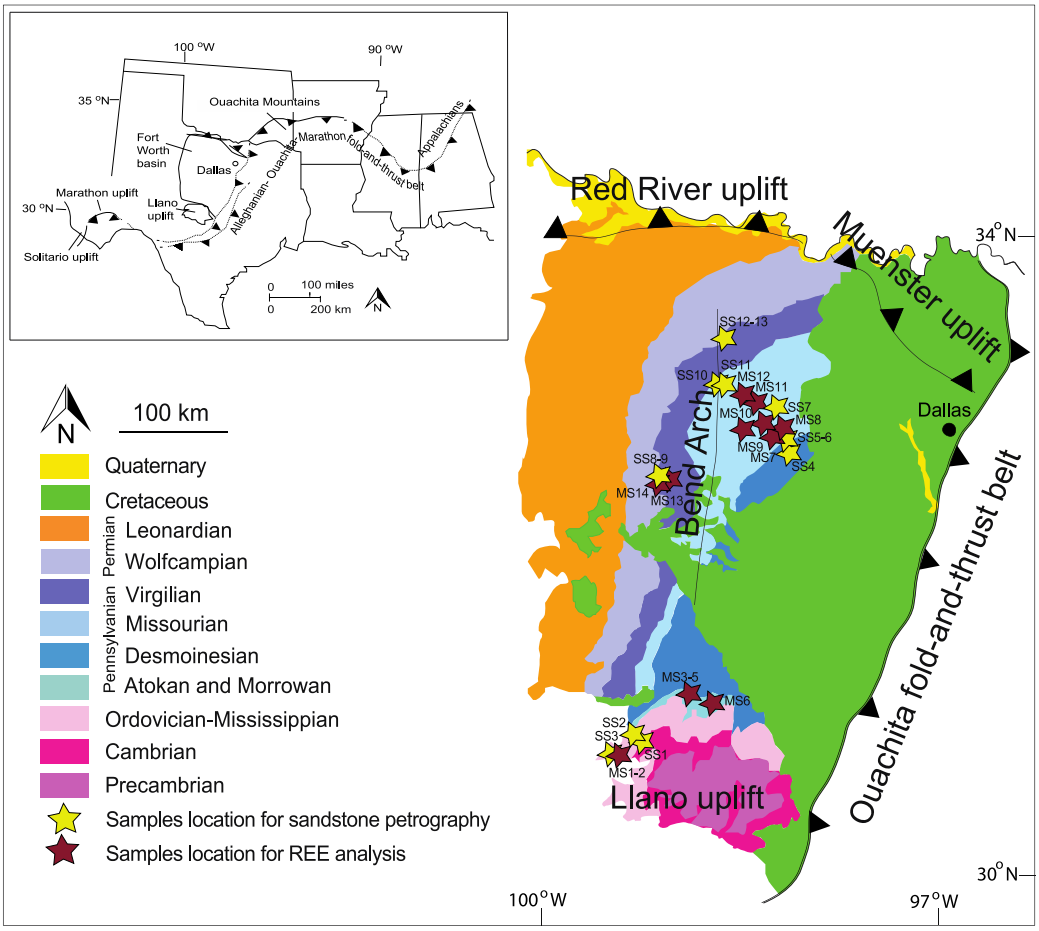

Figure 3-1 Geological map of the Fort Worth Basin. Modified after Barnes (1992) North America stages following Rohde (2005).

After the Neoproterozoic rifting of the supercontinent Rodinia, the southern margin of Laurentia gradually evolved into a passive margin of the Iapetus Ocean during the Early Cambrian (Houseknecht and Matthews, 1985; Poole et al., 2005; Cawood and Nemchin, 2001). The rifting process formed a failed rift zone in southern Oklahoma (Keller and Stephenson, 2007; Hanson et al., 2013).

The suturing between Gondwana and Laurentia started as early as the Early Devonian when several peri-Gondwana arc terranes (e.g., Avalonia, Ganderia, Carolinia, Meguma, Suwannee) were accreted to Laurentia (e.g., Nance et al., 2002; Keppie et al., 2003; Murphy et al., 2006; Nance and Linnemann, 2008; Pollock et al., 2009; van Staal et al., 2009; Mueller et al., 2014). By the Late Devonian, Laurentia, Baltica, and Avalonia-Carolina had collided to form the large Laurentia landmass. The suturing mechanism between Laurentia and Gondwana has long been debated. Whereas most studies agreed that the southern margin of Laurentia subducted underneath Gondwana (e.g., Thomas, 2004; Poole et al., 2005; Nance and Linnemann, 2008), other studies suggest that Laurentia was the upper plate before the collision (e.g., Domeier and Torsvik, 2014). The final suturing resulted in the complete burial of the Laurentian passive margin deposits by thick synorogenic sedimentation during the Pennsylvanian in the newly formed foreland basins (e.g., Hatcher, 1989; Viele and Thomas, 1989; Thomas, 2004).

The Ouachita orogen extends from Mississippi westward to southeastern Oklahoma, bends southward in eastern Texas, and is contiguous with the Marathon uplift in western Texas (Graham et al., 1975; Houseknecht and Matthews, 1985; Loomis et al., 1994; Poole et al., 2005) (Figure 3-1). The Ouachita Orogeny is the southwestward extension of the Alleghanian Orogeny (Loomis et al., 1994; Poole et al., 2005), or is only coeval with the Alleghanian Orogeny (Thomas, 1977; Robinson et al., 2012). Today, the Ouachita orogen is mostly buried underneath Mesozoic and Cenozoic strata of the Gulf Coastal Plains (Houseknecht and Matthews, 1985; Loomis et al., 1994), and exposed only in the Marathon and Solitario uplifts in West Texas and in the Ouachita Mountains in Arkansas and Oklahoma (Thomas and Viele, 1983; Noble, 1993) (Figure 3-1).

Contractional tectonics during the late Paleozoic also reactivated rift-related faults of the southern Oklahoma aulacogen and formed the northwest-striking Red River and Muenster uplifts as part of the Amarillo–Wichita uplift (Walper, 1982; Keller et al., 1989; Montgomery et al., 2005; Elebiju et al., 2010; Alsalem et al., 2017). Reactivation of early Paleozoic normal faults also caused the initial rise of the basement-involved Llano uplift in southern Laurentia (Erlich and Coleman, 2005).

Exhumation of the Llano uplift continued into the Late Pennsylvanian, which may have tilted the strata in the Fort Worth Basin westward (Thomas, 2003). The Fort Worth Basin may have experienced exhumation during the late Permian-Jurassic as a result of opening of the Gulf of Mexico (Jarvie et al., 2005; Ewing, 2006; Stern and Dickinson, 2010).

3. 3 STRATIGRAPHY

The Cambrian-lower Permian sedimentary rocks in the Fort Worth Basin are up to ~3.5 km thick (Alsalem et al., 2017). The Paleozoic strata unconformably overlie Proterozoic gneiss and schist, and granitic intrusions, and are unconformably overlain by Lower Cretaceous strata in the eastern part of the Fort Worth Basin (Figure 3-2). Based on depositional environments and tectonic histories, Montgomery et al. (2005) divided the Paleozoic strata in the Fort Worth Basin into three intervals: 1) Upper Cambrian to Ordovician platform strata deposited in a passive continental margin; 2) Mississippian shallow marine rocks deposited during the exhumation of the Amarillo–Wichita uplift; and 3) Pennsylvanian-lowermost Permian interbedded shallow marine and deltaic and fluvial deposits associated with the development of Ouachita orogen.

The samples used for this study were collected from siliciclastic rocks in Cambrian, Mississippian and Pennsylvanian strata. The Cambrian samples were from the Hickory Sandstone Member of the Riley Formation in the Moore Hollow Group, which is exposed in the southern part of the Fort Worth Basin. The Riley Formation is subdivided into three members, including, from bottom to top, the Hickory Sandstone Member, Cap Mountain Limestone Member and Lion Mountain Sandstone Member (Cloud et al., 1945; Cornish, 1975; Barnes and Bell, 1977). The Hickory Sandstone Member is subdivided into upper, middle, and lower subunits (Figure 3-2). The lower subunit was interpreted to be braided stream deposits grading upward into tidal flat and intertidal estuarine deposits, the middle subunit consists of fluvial-influenced, shallow subtidal estuarine and shoreface deposits, and the upper subunit consists of estuarine-shallow marine deposits (Goolsby, 1957; Cornish, 1975; Krause, 1996).

The Mississippian samples are from the Barnett Shale deposited in a marine environment. The Pennsylvanian strata include the Bend, Strawn, Canyon and Cisco Groups. The Lower to Middle Pennsylvanian Bend Group includes the Marble Falls, Big Saline, and Smithwick Formations. Marble Falls is further divided into two members. The lower part of the Marble Falls Member (Morrowan Stage) is composed of carbonate (Kier, 1980). The upper part of the Marble Falls Member (Atokan Stage) is composed of carbonate and shale (Erlich and Coleman, 2005). The Middle Pennsylvanian Bend Group is composed of conglomerate, sandstone, shale, and thin layers of limestone (Turner, 1957; Thompson, 1988; Montgomery et al., 2005). The Strawn Group is composed of thinly interbedded limestone and shale, with some sandstone, conglomerate, and coal beds (Turner, 1957; Brown et al., 1979). The Canyon Group is composed of interlayered limestone, mudstone and sandstone (Turner, 1957; Brown et al., 1979). The Cisco Group consists primarily of mudstone and sandstone, and this group extends into the earliest Permian (Turner, 1957; Brown et al., 1979).

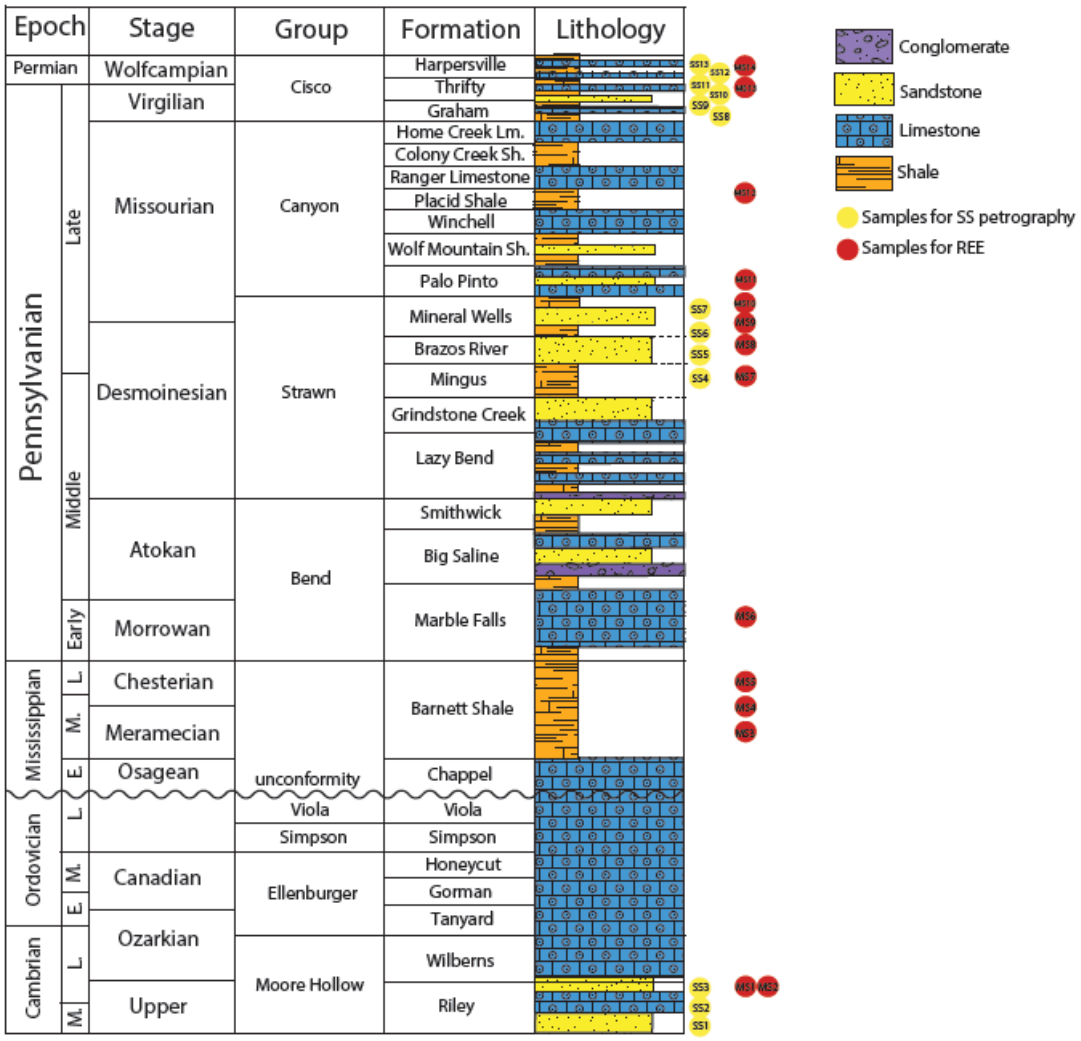

Figure 3-2 Generalized stratigraphic column of the Fort Worth Basin. Modified from Alsalem et al. (2018). North America stages follow Rohde (2005). E., M., L.—Early, Middle, Late; Lm.—Limestone; Sh.—Shale.

3. 4 SAMPLES

3.4.1 Sandstone Petrography

Three sandstone samples (SS1-SS3) were collected from the lower, middle and upper part of the Hickory Sandstone Member of the Riley Formation in the southern part of the Fort Worth Basin, four Pennsylvanian sandstone samples (SS4-SS7) were collected from the Strawn and Canyon Groups

in the northwestern part of the basin, and six Late Pennsylvanian-early Permian samples (SS8-SS13) were collected from the Cisco Group in the northwestern part of the Fort Worth Basin (Figures 3-1/2; Table 3-1).

Table 3-1 Location and samples description of the sandstone samples used for sandstone petrography in this study, Fort Worth Basin, USA

Sample #	Sample name	Formation (Group)	Epoch	Latitude (°N)	longitude (°W)	Elevation (m)	Sample Description	References
SS1	Lower Hickory	Riley (Moore Hollow)	Late Middle Cambrian	30.8371	99.1171	491	Cross-bedded, coarse- to medium-grained, angular to subangular, poorly sorted quartzose sandstone	Bridge et al., 1947; Barnes and Bell, 1977
SS2	Middle Hickory	Riley (Moore Hollow)	Late Cambrian	30.8381	99.1532	496	Cross-bedding, fine- to medium-grained sandstone, well rounded to sub angular, poorly sorted, thinly beddded, argillaceous, silty and micaceous	Barnes and Bell, 1977; Randolph, 1991; Wilson, 2001
SS3	Upper Hickory	Riley (Moore Hollow)	Late Cambrian	30.7653	99.4051	521	Coarse-grained, moderately to well sorted, well rounded quartzose sandstone with iron-oxide ooids and cement	Barnes and Schofield, 1964; Randolph, 1991; Wilson, 2001
SS4	Dobbs Valley	Mingus (Strawn)	Middle Pennsylvanian	32.7050	98.0688	234	Large-scale trough cross-bedded sandstone	Brown et al., 1973
SS5	Lower Brazos River	Brazos River (Strawn)	Middle Pennsylvanian	32.7554	98.0562	283	Small-scale trough cross-bedded, ripple cross-laminated, or planar-laminated sandstone	Brown et al., 1973
SS6	Upper Brazos River	Brazos River (Strawn)	Middle Pennsylvanian	32.7554	98.0562	285	Small-scale trough cross-bedded, ripple cross-laminated, or planar-laminated sandstone	Brown et al., 1973
SS7	Devils Hollow	Mineral Wells (Strawn)	Middle Pennsylvanian	32.7828	98.1802	270	Massively bedded, calcareous sandstone, highly bioturbated, and bears a few marine fossils	Teo, 1991
SS8	Cisco1	(Cisco)	Late Pennsylvanian-early Permian	32.4417	98.9799	473	Fine- to medium-grained, trough-cross-bedded sandstones that exhibit no vertical textural or sedimentary structural variations	Brown et al., 1973
SS9	Cisco2	(Cisco)	Late Pennsylvanian-early Permian	32.4417	98.9799	470		
SS10	Cisco3	(Cisco)	Late Pennsylvanian-early Permian	33.0511	98.5473	348		
SS11	Cisco5	(Cisco)	Late Pennsylvanian-early Permian	33.0356	98.5165	350		
SS12	Cisco6	(Cisco)	Late Pennsylvanian-early Permian	33.3652	98.4929	341		
SS13	Cisco7	(Cisco)	Late Pennsylvanian-early Permian	33.36518	98.4929	340		

3.4.2 Rare Earth Elements

Two mudstone samples (MS 1-2) were collected from the upper part of the Hickory Sandstone Member of the Riley Formation, three mudstone samples (MS 3-5) were collected from the Mississippian Barnett Shale, nine Pennsylvanian samples (MS 6-14) were collected from different formations of the Bend, Strawn, Canyon and Cisco Groups in the northwestern part of the Fort Worth Basin (Figures 3-1/2; Table 3-2).

Table 3-2 Location of the mudstone samples used for REEs study in the Fort Worth Basin, USA

Sample no.	Sample name	Formation (Group)	Epoch	Latitude (°N)	longitude (°W)	Elevation (m)
MS1-2	Upper Hickory	Riley (Moore Hollow)	Late Cambrian	30.7653	99.4054	523
MS3-5	Barnett Shale	Barnett Shale	Middle Mississippian	31.1649	98.6933	452
MS6	Marble Falls	Marble Falls (Bend)	Early-Middle Pennsylvanian	31.0323	98.5776	384
MS7	Dobbs Valley	Mingus (Strawn)	Middle Pennsylvanian	32.6827	98.1117	239
MS8	Brazos River	Brazos River (Strawn)	Middle Pennsylvanian	32.7554	98.0562	285
MS9	Lake Pinto	Mineral Wells (Strawn)	Middle Pennsylvanian	32.7828	98.1802	270
MS10	Turkey Creek	Mineral Wells (Strawn)	Late Pennsylvanian	32.7679	98.3125	325
MS11	Palo Pinto	Palo Pinto (Canyon)	Late Pennsylvanian	32.9138	98.2426	8
MS12	Placid Shale	Placid Shale (Canyon)	Late Pennsylvanian	32.9772	98.3395	12
MS13	Cisco	Thrifty and Graham (Cisco)	Late Pennsylvanian	32.4598	98.8954	6
MS14	Cisco	Harpersville (Cisco)	Late Pennsylvanian - early Permian	32.40236	98.98294	8

3. 5 METHODS

3. 5.1 Sandstone Petrography

Standard thin sections were made from the 13 sandstone samples. The thin sections were stained for potassium and calcium feldspar and were point counted using the Gazzi-Dickenson point counting method. The method reduces the effects of grain-size biases on composition by identifying the composition of the sand-sized components in a given grain (Ingersoll et al., 1984). In this study, a total of 450 counts per slide were obtained for each thin section. The results were grouped following table 3 and plotted on various provenance ternary plots (Figure 3-3) after Dickinson and Suczek (1979) to determine the tectonic setting under which the Paleozoic sandstones were deposited. Three main provenance types are identified in these plots, including continental block, magmatic arc and recycled orogen (Figure 3-3).

Qt in the QtFL plot includes both monocrystalline and polycrystalline quartz and reflects the stability of grains, which is the combined result of weathering, provenance relief, transport mechanism,

and source rock composition. Lt in the QmFLt plot includes all the lithic fragments and polycrystalline quartz, emphasizing the grain size of source rock, because finer grained rocks yield more lithic fragments in the sand-size range (Dickinson and Suezek, 1979; Dickinson et al., 1983; Dickinson, 1985).

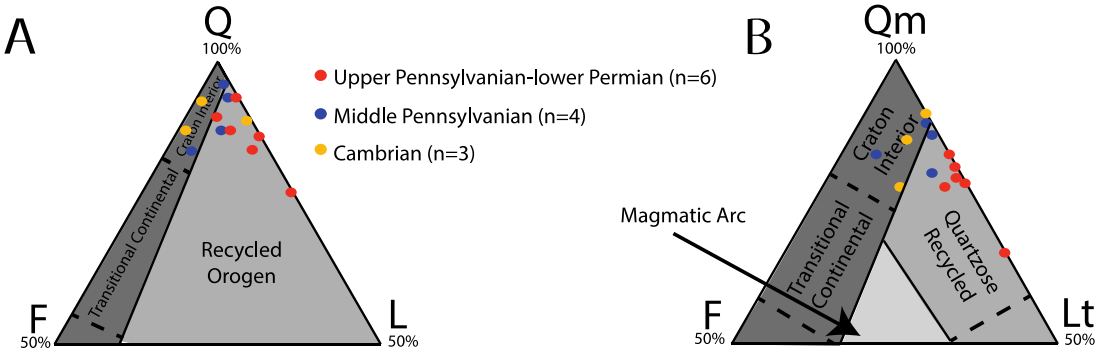

Figure 3-3 Ternary diagrams showing mean framework modes for sandstone derived from different types of provenances. A) Triangular QFL plot, Q is total quartzose grains; F is total feldspar grains; L is total unstable lithic fragments. B) Triangular Q_mFL_t plot, Q_m is monocrystalline quartz grains; F is total feldspar grains; L_t is total lithic fragments and polycrystalline quartz. Modified after Dickinson and Suczek (1979).

3. 5.2 Rare Earth Elements

The fourteen mudstone samples were pretreated for REEs analysis following the procedures of solid sample digestion by Potts et al. (2014). These samples were powdered using a ceramic mortar and pestle, and the tools were cleaned through between samples to avoid contamination. About 250 mg of whole-rock samples were weighed and digested by mixture of double distilled HNO_3 and HF acid with a volume ratio of 3:2 in Teflon beaker on a hot plate. The digests were then dried on a hot plate and heated to 195 ^oC to decompose and evaporate fluorides, chlorides and perchlorates because residual fluorides can precipitate REEs, and chlorides can form diatomic ionic species in the inductively coupled plasma that interfere with the determination of some of the REEs. The residues were then dissolved with 2 ml of HCl for overnight to ensure that carbonate was completely dissolved. The residual was then heated to 150 ^oC to evaporate chloride.

For column chemistry treatment, the samples were passed through two column volumes of water, then conditioned with 10 ml 0.25 N HCl. Then 0.25 ml sample solution was injected into column, and rinsed three times with 0.1 ml 0.25 N HCl followed by another rinse using 0.75 ml 0.25 N HCl. After this step, and REEs began to elute and the solutions were collected. The solutions were dried down on the hotplate and treated with H_2O_2 to remove organic material. The treated solution was dried down for analysis. REEs analysis were conducted using an Inductively Coupled Plasma Mass Spectrometry (ICP-MS) at the Boston University. The ICP-MS analysis has a routine precision of 1-2% relative standard deviation, which is 100*SD/mean result, for most trace elements in solution.

3. 6 RESULTS

3. 6.1 Sandstone Petrography

Petrographic observation shows that in all the samples, the feldspar and lithic grains appear to be weathered or partially dissolved, the samples generally lack matrix, and the grains are subangular to subrounded (Figure 3-4). The three Cambrian sandstone samples (SS1-SS3) are generally fine- to medium-grained (Figure 3-4 A & B). These samples are classified as quartz arenite with an average composition of $Q_{91}F_6L_3$ (Table 3-3). These samples are in the craton interior field on both the QFL and QmFLt plots (Figure 3-3). They are dominated by monocrystalline quartz, and majority of the monocrystalline quartz grains show straight extinction with weak or absent undulatory extinction. The feldspars are all K-feldspar.

The four Middle Pennsylvanian samples (SS4-SS7) are generally fine-grained (Figure 3-4 C & D). These samples are also classified as quartz arenite and have an average composition of $Q_{91}F_4L_5$ (Table 3-3). These samples are in the craton interior and recycled orogen fields on both the QFL and QmFLt plots (Figure 3-3). They are dominated by monocrystalline quartz, and contain small percentages of polycrystalline quartz, chert, feldspar and rock fragments. The feldspars contain both K-feldspar and plagioclase.

The six Upper Pennsylvanian-lowermost Permian sandstone samples (SS8-SS13) are generally fine-grained (Figure 3-4 E & F). These samples have more lithics and are classified as sublitharenite with an average composition of $Q_{87}F_2L_{11}$ (Table 3-3). The composition of the lithics are difficult to identify because of diagenesis. These samples are in the recycled orogen field on both the QFL and QmFLt plots (Figure 3-3). Their mineral compositions are similar to those of the Middle Pennsylvanian samples, but contain higher percentages of chert and rock fragments.

Table 3-3 Petrographic analysis results of the sandstones in the Fort Worth Basin

Minerals	Samples												
	SS1	**SS2**	**SS3**	**SS4**	**SS5**	**SS6**	**SS7**	**SS8**	**SS9**	**SS10**	**SS11**	**SS12**	**SS13**
Quartz													
Monocrystalline	347	402	409	368	372	387	398	356	351	297	353	377	362
Polycrystalline	21	2	3	12	4	11	21	20	22	19	16	18	16
Chert	-	-	-	10	5	13	14	20	3	9	8	12	10
Novacolite	-	-	-	17	-	20	-	16	15	92	33	13	20
K-feldspar	52	29	-	3	20	1	-	18	2	-	-	-	12
Plagioclase	-	-	-	19	33	2	4	6	7	-	-	-	8
Rock fragments	-	1	45	14	18	5	16	8	43	14	26	14	17
Cement													
Hematite	-	-	79	2	7	9	18	6	277	8	4	15	36
Carbonate			280	52	147	-	232	7	-	-	-	-	-

3. 6.2 Rare Earth Elements

The REEs contents of all our samples are typically less than 10 ppm except a few light rare earth elements (LREEs) in the Cambrian and Mississippian samples (Table 3-4). The REEs data are normalized to Chondrite and Post Archaen Australian Shale (PAAS) following Taylor and McLennan (1981) to identify the potential sources (Figure 3-5; Table 3-4). The REEs contents of the Middle Pennsylvanian-earliest Permian samples are generally lower than those of the Cambrian-Early Pennsylvanian samples. The chondrite-normalized patterns of all samples are characterized by enrichment of LREEs and negative Eu anomalies (Table 3-4). The Eu anomalies are between 0.2-0.7 for the Middle Pennsylvanian-earliest Permian samples, but are very small (<0.1) for the Cambrian-

Early Pennsylvanian samples. PAAS is a good representation of upper crustal material. The PAAS-normalized patterns are characterized by slight depletion of LREEs. The Middle Pennsylvanian-earliest Permian samples are more depleted in LREEs compared to the Cambrian-Early Pennsylvanian samples. The Cambrian samples show positive Ce anomalies. The Mississippian-Middle Pennsylvanian samples show negative Ce anomalies. The Late Pennsylvanian-earliest Permian samples do not show Ce anomalies.

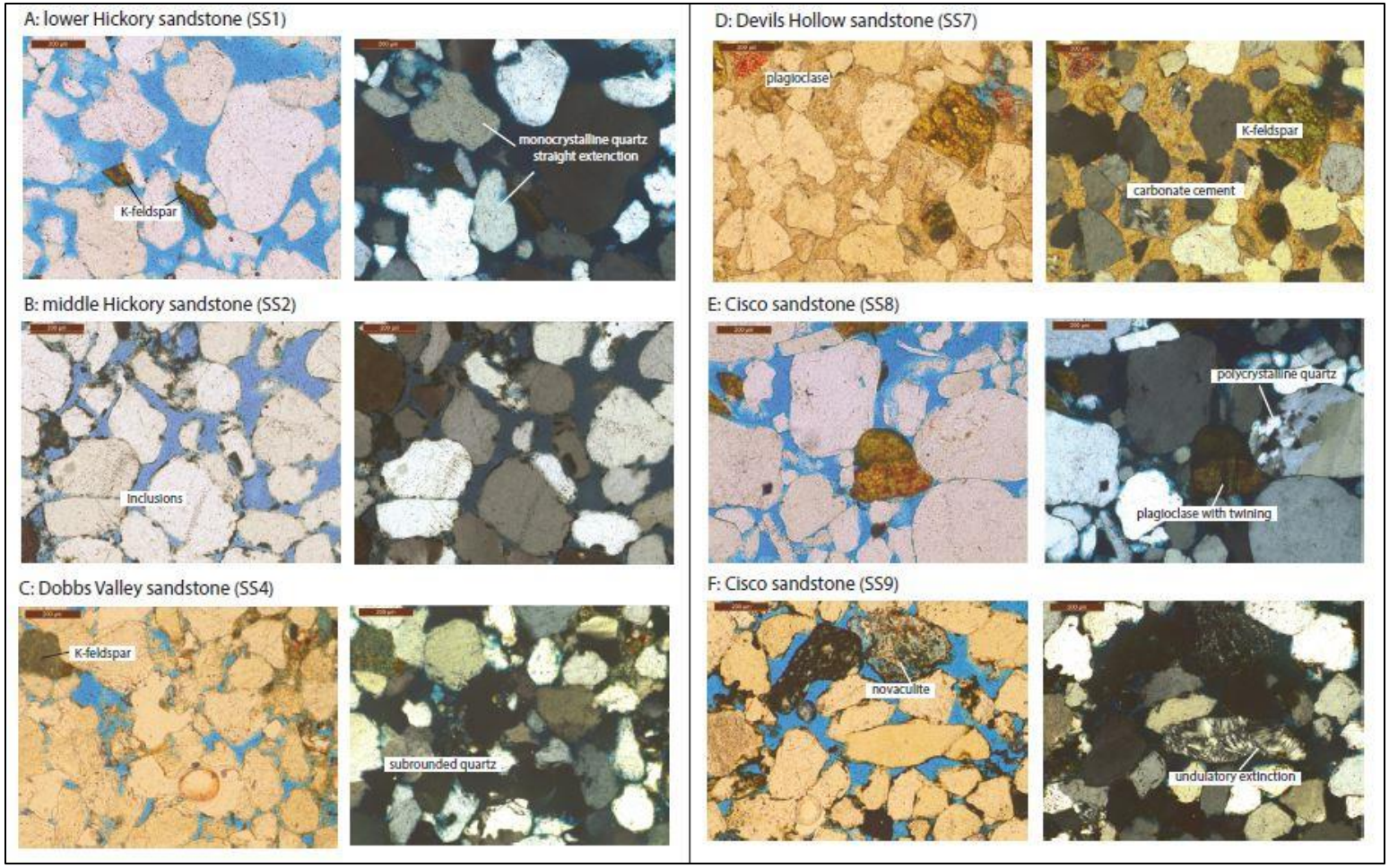

Figure 3-4 Photos of petrographic thin sections of sandstone samples in the Fort Wort Basin.

Table 3-4 REEs data for the mudstone samples in the Fort Worth Basin.

Samples Name	Cisco 1	Cisco 2	Canyon 1	Canyon 2	Strawn 1	Strawn 2	Strawn 3	Strawn 4	Marble Falls	Barnett Shale 1	Barnett Shale 2	Barnett Shale 3	Upper Hickory 1	Upper Hickory 2
REE (ppm)														
La	1.4	1.4	2.0	1.1	2.9	3.0	1.4	2.0	32.9	34.9	7.7	14.7	4.9	21.4
Ce	2.5	4.2	4.3	2.4	6.3	5.8	2.4	4.6	35.3	40.0	14.5	23.5	19.0	53.4
Pr	0.3	0.6	0.8	0.3	1.1	1.0	0.3	0.7	6.2	7.3	2.4	5.1	1.9	4.3
Nd	1.6	3.1	3.5	1.9	5.7	4.3	1.9	3.2	22.9	27.7	10.2	21.5	8.6	18.6
Sm	0.3	0.7	0.7	0.4	1.3	0.9	0.4	0.7	3.9	4.6	2.2	4.6	2.1	4.2
Eu	0.0	0.1	0.1	0.1	0.3	0.2	0.1	0.1	0.7	0.9	0.5	1.0	0.4	1.0
Tb	0.0	0.1	0.1	0.0	0.2	0.1	0.0	0.1	0.5	0.7	0.4	0.8	0.4	0.8
Gd	0.2	0.5	0.5	0.3	1.3	0.7	0.3	0.6	3.5	4.6	2.3	5.0	2.2	4.7
Dy	0.2	0.6	0.5	0.3	1.2	0.7	0.3	0.6	2.8	3.9	2.4	4.8	2.5	4.6
Ho	0.1	0.1	0.1	0.1	0.2	0.2	0.1	0.1	0.6	0.8	0.5	1.0	0.5	1.0
Er	0.1	0.4	0.3	0.2	0.6	0.4	0.1	0.4	1.5	2.2	1.6	2.7	1.5	2.7
Yb	0.2	0.6	0.4	0.2	0.5	0.5	0.2	0.5	1.3	1.7	1.9	2.3	1.7	3.0
Lu	0.0	0.1	0.1	0.0	0.1	0.1	0.0	0.1	0.2	0.2	0.3	0.4	0.3	0.5
(La/Sm)N	2.8	1.3	1.8	1.8	1.4	2.2	2.2	1.8	5.3	4.7	2.2	2.0	1.5	3.1
(Ce/Yb)N	3.3	1.9	2.8	2.9	3.4	2.8	3.1	2.6	7.4	6.3	2.0	2.7	2.9	4.7
(Gd/Yb)N	0.7	0.7	1.0	1.0	2.1	1.0	1.1	1.0	2.2	2.2	0.9	1.7	1.0	1.3
Eu/Eu*	0.7	0.4	0.4	0.6	0.2	0.3	0.5	0.3	0.1	0.0	0.1	0.0	0.1	0.1
Ce/Ce*	0.8	1.1	0.9	0.9	0.8	0.8	0.7	0.9	0.6	0.6	0.8	0.7	1.5	1.3
Gd/Gd*	0.7	0.8	0.8	0.8	1.0	0.8	0.8	0.8	1.0	1.0	0.9	1.0	0.9	1.0
La/Lu	4.7	1.6	3.5	3.6	4.1	3.8	4.5	3.0	18.6	14.7	2.6	4.3	1.8	4.9
Note: Eu/Eu* = EuN/(SmN x GdN)1/2 , Ce/Ce* = CeN /(LaN2/3x NdN1/3), Gd/Gd*= GdN/(0.33SmN + 0.67TbN), where N is chondrite-normalized value.														

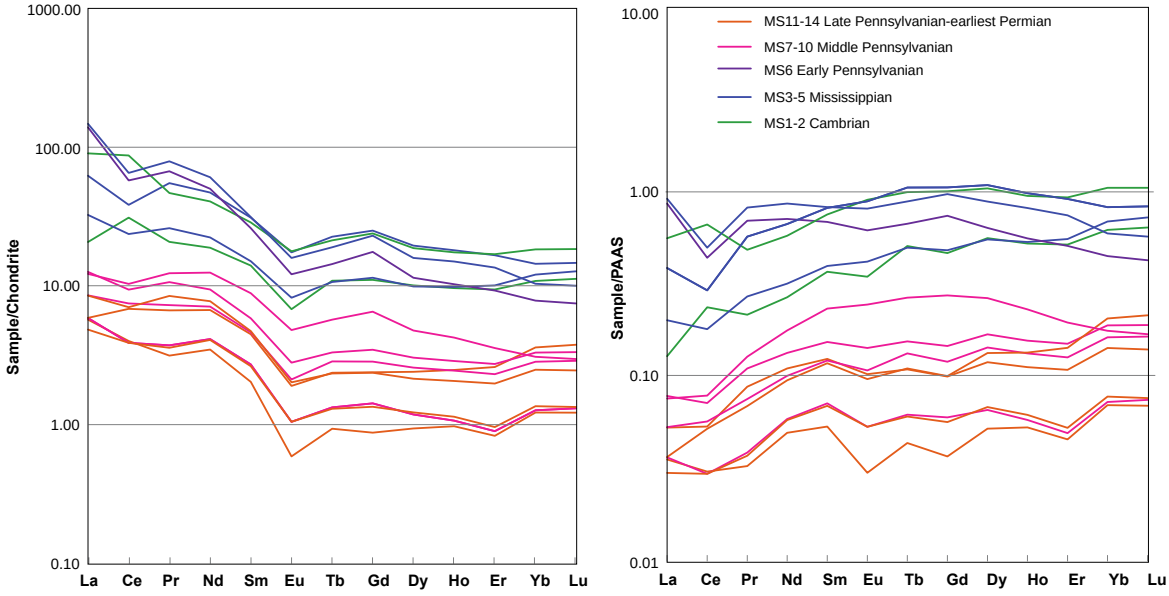

Figure 3-5 REEs patterns normalized to chondrite and Post Archean Australian Shale (PAAS) (Taylor and McLennan, 1985).

3. 7 DATA INTERPRETATION

3. 7.1 Sandstone Petrography

The lack of feldspar and lithics in the Cambrian sandstones seems not consistent with the interpretation that zircon grains were mostly from direct erosion of Precambrian basement rock in the Texas Arch (Alsalem et al., 2018) by local braided rivers (Goolsby 1957; Cornish 1975; Krause 1996) in Chapter 2. However, the partial dissolution of feldspar grains clearly suggests the influence of diagenesis on these samples. The chert grains in the Middle Pennsylvanian-earliest Permian samples were from the Paleozoic Arkansas Novaculite that are commonly distributed in the Ouachita Mountains of Arkansas and Oklahoma (Baker, 1974; Keller et al., 1985; Haley, 1993; Etchieson, 1997) and in the Marathon uplift of West Texas (McBride and Thomas, 1970). The presence of these grains suggests sediment recycling of Paleozoic strata in the Ouachita, and likely Marathon orogen. The change from contribution of craton interior in the Cambrian to recycled orogen in the Middle Pennsylvanian is consisit with the interpretation of detrital zircon geochronology in Chapter 2 that Appallachian and

Ouachita orogens both provided detritus into the Fort Worth Basin during the Pennsylvanain. This change in sediment provenance is associated with the change of depositional environment from braided river and marginal marine environment to mixed shallow marine, deltaic and fluvial environment (Brown et al., 1973). The increase of lithics fraction from the Middle Pennsylvanian to the Late Pennsylvanian samples may suggest decease of transport distance or increase of local sources (Folk, 1980). Given that detrital zircon data suggest that the sediments were from the Appalachians as well as the basin-bounding Ouachita orogen, the increase of lithics fraction most likely suggests more input from the Ouachita orogen. These grains derived from local sources are most likely subangular given the short transport distance. However, given there is no detrital zircon data for the Cisco Group, this interpretation based on sandstone petrography cannot be directly tested.

3. 7.2 Rare Earth Elements

The overall decrease of REEs content from the Cambrian-Early Pennsylvanian to the Middle-Late Pennsylvanian cannot be a result of changing sediment grain size or carbonate content. Culler et al. (1987) found that REEs content is ~20% higher in mudstones than in sandstones. All our samples are mudstone, and do not have obvious changes in grain size. Carbonate rocks often have a low REEs content, usually <10 ppm, and their REEs pattern is generally similar to that of clastic rocks (Taylor and McLennan, 1985). The samples with highest carbonate content are the samples from the Mississippian Barnett Shale and Early Pennsylvanian Marble Falls Formation, but they do not show low REE content compared to the other samples (Figure 3-5).

The chondrite-normalized REEs patterns of all our samples are generally similar to the pattern of average upper crust (Taylor and McLennan, 1985), including enrichment of LREEs and negative Eu anomalies (Figure 3-5), suggesting our samples contain mostly sediments eroded from continental crust. The depletion of LREEs and larger negative Eu anomaly in the Middle Pennsylvanian-earliest Permian samples compared to the Cambrian-Early Pennsylvanian samples suggest mixing of sediments from another source that will be further discussed in the following section.

The Cambrian samples show positive Ce anomalies, whereas the Mississippian and Pennsylvanian samples show negative Ce anomalies. Changes in the Ce anomaly is related to redox condition dictated by the changes in sea level that affect the chemical condition of the water (Wilde et al., 1996; Holser, 1997). During a transgression, the bottom water would become more anoxic, whereas it would become more oxic during a regression. In anoxic conditions, the Ce is depleted leading to a negative Ce anomaly, whereas the Ce anomaly will be more positive in rocks that formed in oxic conditions (Wilde et al., 1996). The change of Ce anomaly is consistent with the change of depositional environment from braided river-marginal marine with oxic condition in the Cambrian to isolated deep marine environment and presence of black shale in anoxic condition during the Mississippian (Loucks and Ruppel, 2007).

3. 8 DISCUSSION

Our sandstone petrography data suggest increase of sediment provenance from recycled orogen, most likely the Appalachian and Ouachita orogens, during the Middle Pennsylvanian. The mudstone REEs data further clarify that the change of sediment provenance occurred at the beginning of the Middle Pennsylvanian. We further discuss the potential source that caused the change of REEs signature. We compare the REEs pattern of our samples with Paleozoic sediments derived from typical Laurentian crustal source (Dorais et al., 2009), Paleozoic sediments derived primarily from the Appalachian highland in the central Appalachian foreland basin (Shatzel and Stewart, 2012), and Pan-African granite in Africa (Ukaegbu and Beka, 2008) in order to infer the source (Figure 3-6). Our Cambrian-Early Pennsylvanian REEs patterns are similar to those of the Laurentian crust and Appalachian foreland, despite that the REEs contents are generally lower.

Depleted mantle and mid-ocean ridge basalt (MORB) are characterized by depletion of LREEs and lack of Eu anomaly relative to chondrite (Salters and Stracke, 2004). Despite that addition of materials from source with depleted mantle composition can explain the slight depletion of LREEs in our Middle-Late Pennsylvanian samples, it cannot explain the higher Eu anomaly in these samples.

Significant negative Eu anomalies can be resulted by two processes, including crustal materials suffered long transport and recycling because of decomposition of high-temperature minerals during transport (Gao and Wedephol, 1995) and addition of material derived from Pan-Africa volcanic rocks (Figure 3-6). The peri-Gondwana terranes are characterized by the Pan-African basement (870-550 Ma), which was formed by a protracted orogenic cycle associated mostly with accretion and collision of crustal blocks to form supercontinent Gondwana (Kroner and Stern, 2004). In the vicinity of the Fort Worth Basin, the peri-Gondwana terrane is most likely the Sabine terrane in east Texas and Louisianan border (Alsalem et al., 2018). There is no REEs data published for basement rocks of this terrane as it is buried subsurface. Therefore, its REEs pattern has to be inferred from other late Neoproterozoic Gondwana rocks in Gondwana. In addition to the Neoproterozoic Pan-Africa granite from the Obudu Plateau in southeastern Nigeria (Ukaegbu and Beka, 2008), the volcanic-intrusion belt of late Neoproterozoic age in Wadi Ranga area in Egypt also has Pan-Africa granite that shows similar negative Eu anomaly as the one in Nigeria (Gharib and Ahmed, 2012). Therefore, it is likely that the erosion of the Sabine terrane caused the negative Eu anomaly in our Middle Pennsylvanian-earliest Permian samples. We suggest both of the processes may have occurred to cause the large negative Eu anomaly in our Middle-Late Pennsylvanian samples because detrital zircon data suggest long transport of Appalachian sediments and Pan-Africa Neoproterozoic rocks in the Ouachita (Alsalem et al., 2018). We suggest that the depletion in LREEs was possibly caused by erosion of felsic volcanic rocks (Miller and Mittlefehldt, 1982). Some young felsic metavolcanics in Wadi Ranga area show depletion of LREEs (Gharib and Ahmed, 2012).

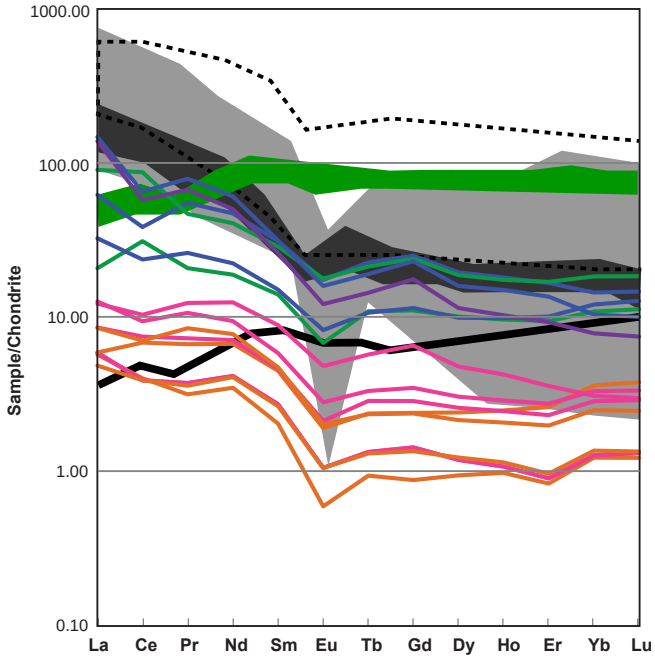

Figure 3-6 REEs patterns in the Fort Worth Basin are compared with the REEs patterns of Paleozoic sediments derived from Laurentia crustal source (Dorais et al., 2009; in dark grey band), Paleozoic sediments in the Appalachian foreland basin (Shatzel and Stewart 2012; in dashed black polygon), Pan-African granite in Africa (Ukaegbu and Beka, 2008; in light grey band), and MORB (in green band) and depleted mantle (in thick black line) (Salters and Stracke, 2004).

3. 9 CONCLUSIONS

We apply sandstone petrography and mudstone REEs pattern to determine provenance of the Paleozoic sedimentary rocks in the Fort Worth Basin in order to understand the sediment dispersal patterns on the southern margin of Laurentia before and during the Laurentia-Gondwana collision in the Paleozoic. The sandstone composition changed from continental input from Laurentian craton during the Cambrian to recycled orogen during the Middle Pennsylvanian-earliest Permian. The Chondrite-normalized mudstone REEs patterns in the Fort Worth Basin are generally similar to average upper crust. The Middle Pennsylvanian-earliest Permian samples have less LREEs, and larger Eu anomalies compared to the Cambrian-Early Pennsylvanian samples, reflecting addition of material transported by long distance from the Appalachians and/or erosion of peri-Gondwana terranes in the

vicinity of the Fort Worth Basin. These data support the interpretation of Appalachian- and Ouachita-derived sediments based on detrital zircon geochronology, and further clarify that the change of sediment provenance to the Fort Worth Basin occurred as early as the Middle Pennsylvanian.

3. 10 ACKNOWLEDGMENTS

I would like to thank AAPG Grants-in-Aid program for a graduate student research grant.

3. 11 REFERENCES CITED

Alsalem, O.B., Fan, M., and Xie, X., 2017, Late Paleozoic subsidence and burial history of the Fort Worth basin: American Association of Petroleum Geologists Bulletin, v. 101, p. 1813-1833, doi: 10.1306/01251716016.

Alsalem, O.B., Fan, M., Zamora, J., Xie, X., and Griffin, W.R., 2018, Paleozoic sediment dispersal before and during the collision between Laurentia and Gondwana in the Fort Worth Basin, USA: Geosphere, v. 14, p.325-342, doi:10.1130 /GES01480.1.

Archer, A.W., and Greb, S.F., 1995, An Amazon-Scale Drainage System in the Early Pennsylvanian of Central North America: The Journal of Geology, v. 103, p. 611-628.

Baker, C. M., 1974, A Study of Aboriginal Novaculite Exploitation in the Ouachita Mountains of South-Central Arkansas [M.A. Thesis], University of Arkansas, Fayetteville, AR.

Barnes, V.E., 1992, Geologic Map of Texas: Bureau of Economic Geology, The University of Texas at Austen Map SM0003, Scale 1:500,000, 4 sheets.

Barnes, V.E., and Bell, W.C., 1977, The Moore Hollow Group of Central Texas: The University of Texas at Austin, Bureau of Economic Geology, Report of Investigations No. 88, 169 p.

Brown, L.F., Cleaves, II, A.W., and Erxleben, A.W., 1973, Pennsylvanian depositional systems in North-Central Texas: A guide for interpreting terrigenous clastic facies in a cratonic basin: The University of Texas at Austin, Bureau of Economic Geology, Guidebook No. 14, 122 p.

Cawood, P.A., and Nemchin, A.A., 2001, Source regions for Laurentian margin sediments: Constraints from U/Pb dating of detrital zircon in the Newfoundland Appalachians: Geological Society of America Bulletin, v. 113, p. 1234-1246.

Cloud , P. E., Barnes, V. E. , and Bridge , Josiah, 1945, Stratigraphy of the Ellenburger group in central Texas - a progress report: University Texas Publications, Austin, No. 4301, p. 133-161.

Cornish, F.G., 1975, Tidally-influenced deposits of the Hickory Sandstone, Cambrian, central Texas [M.S. Thesis], The University of Texas at Austin, TX, 186 p.

Dickinson, W.R., 2000, Geodynamic interpretation of Paleozoic tectonic trends oriented oblique to the Mesozoic Klamath-Sierran continental margin in California: Geological Society of America, Special Paper 347: Paleozoic and Triassic paleogeography and tectonics of western Nevada and Northern California, p. 209-245.

Dickinson, W.R, and Lawton, T.F., 2003, Sequential intercontinental suturing as the ultimate control for Pennsylvanian Ancestral Rocky Mountains deformation: Geology, v. 31, p. 609-612.

Dickinson, W.R. and Suczek, Ch.A., 1979, Plate Tectonics and sandstone composition: American Association of Petroleum Geologists Bulletin, v. 63, p. 2164-2182.

Domeier, M. and Torsvik, T.H., 2014, Plate tectonics in the late Paleozoi: Geoscience Frontiers, v. 5, p. 303-350.

Dorais, M.J., Wintsch, R.P., Nelson, W.R., and Tubrett, M., 2009, Insights into the Acadian orogeny, New England Appalachians: a provenance study of the Carrabassett and Kittery formations, Maine: Atlantic Geology, v. 45, p. 50-71.

Elebiju, O.O., Keller, G.R., and Marfurt, K.J., 2010, Case History: Investigation of links between Precambrian basement structure and Paleozoic strata in the Fort Worth basin, Texas, U.S.A., using high-resolution aeromagnetic, HRAM data and seismic attributes: Geophysics, v. 75, p. B157-B168.

Erlich, R. N., and J. L. Coleman, 2005, Drowning of the Upper Marble Falls Carbonate Platform (Pennsylvanian), central Texas: A case of conflicting 'signals?': Sedimentary Geology, v. 175, p. 479-499.

Etchieson, M., 1997, Prehistoric Novaculite Quarries in the Ouachita Mountains: Paper presented at the Annual Meeting of the Society for American Archaeology, Nashville, Tennessee, Web published at http://www.fs.fed.us/oonf/history/nova/ novaculite.htm.

Ewing, T.E., 2006, Mississippian Barnett Shale, Fort Worth Basin, north-central Texas: Gas-shale play with multi–trillion cubic foot potential [Discussion], American Association of Petroleum Geologists Bulletin, v. 90, p. 963-966.

Folk, R.L.,1980, Pertrology of Sedimentary Rocks: Hemphill Publishing Co., Austin, Texas, U.S.A, 182, 123 p.

Gao, S., and Wedepohl, K.H., 1995, The negative Eu anomaly in Archean sedimentary rocks: Implications for decomposition, age and importance of their granitic sources: Earth and Planetary Science Letters, v. 133, p.81-94.

Gharib, M.E., and Ahmed, A.H., 2012, Late Neoproterozoic volcanics and associated granitoids at Wadi Ranga, south Eastern Desert, Egypt: a transition from subduction related to intra-arc magmatism. Lithos, v. 155, p.236-255.

Gleason, J.D., Patchett, P.J., Dickinson, W.R., and Ruiz, J., 1994, Nd isotopes link Ouachita turbidites to Appalachian sources: Geology, v. 22, p. 347-350.

Gleason, J.D., Patchett, P.J., Dickinson, W.R., and Ruiz, J., 1995, Nd isotopic constraints on sediment sources of the Ouachita-Marathon fold belt: Geological Society of America Bulletin, v. 107, p. 1192-1210.

Gleason, J.D., Gehrels, G.E., Dickinson, W.R., Patchett, P.J., and Kring, D.A., 2007, Laurentian sources for detrital zircon grains in turbidite and deltaic sandstones of the Pennsylvanian

Haymond Formation, Marathon assemblage, West Texas, USA: Journal of Sedimentary Research, v. 77, p. 888-900.

Goolsby, J.L., 1957, A study of the Hickory Sandstone [M.S. Thesis], Texas A&M University, TX, 92 p.

Graham, S.A., Dickinson, W.R., and Ingersoll, R.V., 1975, Himalayan– Bengal model for flysch dispersal in the Appalachian–Ouachita system: Geological Society of America Bulletin, v. 86, p. 273-286.

Grayson, R.C. Jr., Merill, G.K., Pranter, M.J., and Lambert, L.L., 1991, Carboniferous geology and tectonic history of the southeastern Fort Worth (foreland) Basin and Concho platform, Texas: Dallas Geological Society, Dallas, Texas, Field Trip No. 13, 67 pp.

Hanson, R.E., Puckett, R.E., Keller, G.R., Brueseke, M.E., Bulen, C.L., Mertzman, S.A., Finegan, S.A., and McCleery, D.A., 2013, Intraplate magmatism related to opening of the southern Iapetus Ocean: Cambrian Wichita igneous province in the Southern Oklahoma rift zone: Lithos, v. 174, p. 57-70.

Hatcher, R.D. Jr. 1989, Tectonic synthesis of the U.S. Appalachians, in Hatcher, R.D., Jr., W.A. Thomas, and G.W. Viele, eds., The Appalachian-Ouachita Orogen in the United States: Geological Society of America Decade of North American Geology, v. F2, p. 29-41.

Hentz, T.C., Ambrose, W.A., and Carr, D.L., 2012, Reservoir system of the Pennsylvanian lower Atoka Group (Bend Conglomerate), northern Fort Worth Basin, Texas: High-resolution facies distribution, structural controls on sedimentation, and production trends: American Association of Petroleum Geologists Bulletin, v. 96, p. 1301-1332.

Holser, W.T., 1997, Evaluation of the application of rare-earth elements to paleoceanography: Palaeogeography, Palaeoclimatology, Palaeoecology, v. 132, p. 309-323.

Houseknecht, D.W., and Matthews, S.M., 1985, Thermal Maturity of Carboniferous Strata, Ouachita Mountains: American Association of Petroleum Geologists Bulletin, v. 69, p. 335-345.

Ingersoll, R.V., Bullard, T.F., Ford, R.L., Grimm, J.P., Pickle, J.D., and Sares, S.W., 1984, The effect of grain size on detrital modes: a test of the Gazzi-Dickinson point-counting method: Journal of Sedimentary Research, v. 54, p.103-116.

Jarvie, D.M., Hill, R.J., and Pollastro, R.M., 2005, Assessment of the gas potential and yields from shales: The Barnett Shale model: Oklahoma Geological Survey Circular, v. 110, p. 37-50.

Keller, G.R., and Stephenson, R.A., 2007, The Southern Oklahoma and Dniepr-Donets aulacogens: A comparative analysis, in Hatcher, R.D., Jr., Carlson, M.P., McBride, J.H., and Martínez Catalán, J.R., eds., 4-D Framework of Continental Crust: Geological Society of America Memoir 200, p. 127–143, doi:10.1130/2007.1200(08).

Keller, G.R., Kruger, J.M., Smith, K.J., and Voight, M.R., 1989, The Ouachita system: A geophysical overview, in Hatcher, R.D., Thomas, W.A., and Viele, G.W., eds., The Appalachian-Ouachita Orogen in the United States: Geological Society of America, The Geology of North America, F-2, p. 689-693.

Keller, W.D., Stone, C.G., and Hoersch, A.L., 1985, Textures of Paleozoic chert and novaculite in the Ouachita Mountains of Arkansas and Oklahoma and their geological significance: Geological Society of America Bulletin, v. 96, p. 1353-1363.

Keppie, J.D., Nance, R.D., Murphy, J.B., and Dostal, J., 2003, Tethyan, Mediterranean, and Pacific analogues for the Neoproterozoic–Paleozoic birth and development of peri-Gondwanan terranes and their transfer to Laurentia and Laurussia: Tectonophysics, v. 365, p. 195-219.

Kier, R.S.,1980, Depositional history of the Marble Falls Formation of the Llano region, Central Texas: West Texas Geological Society Publication 80-73, Guidebook to the Annual Field Trip, p. 59-75.

Krause, S.J., 1996, Stratigraphic framework, Facies analysis, and depositional history of the Middle to Late Cambrian Riley Formation, central Texas [M.S. Thesis], The University of Texas at Austin, TX, 172 p.

Loucks, R.G., and Ruppel, S.C., 2007, Mississippian Barnett Shale: Lithofacies and depositional setting of a deep-water shale-gas succession in the Fort Worth Basin, Texas: American Association of Petroleum Geologists Bulletin, v. 91, p. 579-601, doi:10.1306/11020606059.

Loomis, J., Weaver, B., and Blatt, H., 1994, Geochemistry of Mississippian tuffs from the Ouachita Mountains, and Implications for the Tectonic of the Ouachita orogen, Oklahoma and Arkansas: Geological Society of America Bulletin, v. 106, p. 1158-1171.

McBride E.F. and Thomson, A., 1970, The Caballos Novaculite, Marathon region, Texas: The Geological Society of America Special Paper 122, 129 p.

Miller, C.F., and Mittlefehldt, D.W., 1982, Depletion of light rare-earth elements in felsic magmas: Geology, v. 10, p. 129-133.

Moecher, D.P., and Samson, S.D., 2006, Differential zircon fertility of source terranes and natural bias in the detrital zircon record: Implications for sedimentary provenance analysis: Earth and Planetary Science Letters, v. 247, p. 252-266.

Montgomery, S.L., Jarvie, D.M., Bowker, K.A., and Pollastro, R.M., 2005, Mississippian Barnett Shale, Fort Worth basin, north-central Texas: Gas-shale play with multi–trillion cubic foot potential: American Association of Petroleum Geologists Bulletin, v. 89, p. 155-175.

Morris, R.C. 1974, Sedimentary and tectonic history of Ouachita Mountains, in W. R. Dickinson, ed., Tectonics and Sedimentation, Society of Economic Paleontologists and Mineralogists Special Publication, v. 22, p. 120-142.

Mueller, P.A., Heatherington, A.L., Foster, D.A., Thomas, W.A., and Wooden, J.L., 2014, The Suwannee suture: Significance for Gondwana-Laurentia terrane transfer and formation of Pangaea: Gondwana Research, v. 26, p. 365-373.

Murphy, J.B., Gutierrez-Alonso, G., Nance, R.D., Fernandez-Suarez, J., Keppie, J.D., Quesada, C., Strachan, R.A., and Dostal, J., 2006, Origin of the Rheic Ocean: Rifting along a Neoproterozoic suture?: Geology, v. 34, p. 325-328.

Nance, R.D., and Linnemann, U., 2008, The Rheic Ocean: origin, evolution, and significance: Geological Society of America Today, v. 18, p. 4-12.

Nance, R.D., Murphy, J.B., and Keppie, J.D., 2002, A Cordilleran model for the evolution of Avalonia: Tectonophysics, v. 352, p. 11-31.

Nelson, K.D., Lillie, R. J., de Voogd, B., Brewer, J. A., Oliver, J. E. , Kaufman, S., Brown, L., and, Viele, G.W., 1982, COCORP seismic reflection profiling in the Ouachita Mountains of western Arkansas geometry and geologic interpretation: Tectonics, v. 1, p. 413-430.

Noble, P.J., 1993, Paleoceanographic and tectonic implications of a regionally extensive Early Mississippian hiatus in the Ouachita system, southern mid-continental United States: Geology, v. 21, p. 315-318.

Pollastro, R. M., 2003, Geological and production characteristics utilized in assessing the Barnett Shale continuous (unconventional) gas accumulation, Barnett–Paleozoic total petroleum system, Fort Worth basin, Texas: Barnett Shale Symposium: Ellison Miles Geotechnology Institute at Brookhaven College, Dallas, Texas, 6 p.

Patchett, P.J., Ross, G.M., and Gleason, J.D., 1999, Continental drainage in North America during the Phanerozoic from Nd isotopes: Science, v. 283, p. 671-673.

Pollastro, R.M., Hill, R.J., Jarvie, D.M. and Henry, M.E., 2003, Assessing undiscovered resources of the Barnett-Paleozoic total petroleum system, Bend Arch-Fort Worth basin province, Texas: AAPG Southwest Section Meeting, Fort Worth, TX, 18 p.

Pollastro, R.M., Jarvie, D.M., Hill, R.J., and Adams, C.W., 2007, Geologic framework of the Mississippian Barnett Shale, Barnett-Paleozoic total petroleum system, Bend arch–Fort Worth Basin, Texas: American Association of Petroleum Geologists Bulletin, v. 91, p. 405-436.

Pollock, J.C., Hibbard, J.P., and Sylvester, P.J., 2009, Early Ordovician rifting of Avalonia and birth of the Rheic Ocean: U–Pb detrital zircon constraints from Newfoundland: Journal of the Geological Society, v. 166, p. 501-515.

Poole, F.G., Perry, W.J., Madrid, R.J., and Martinez, R.A., 2005, Tectonic synthesis of the Ouachita-Marathon-Sonora orogenic margin of southern Laurentia: Stratigraphic and structural implications for timing of deformational events and plate-tectonic model: Geological Society of America Special Papers, v. 393, p. 543-596.

Potts, P.J., Webb, P.C., and Thompson, M., 2015, Bias in the determination of Zr, Y and rare earth element concentrations in selected silicate rocks by ICP‐MS when using some routine acid dissolution procedures: Evidence from the GeoPT proficiency testing programme: Geostandards and Geoanalytical Research, v. 39, p.315-327.

Robinson, D.M., Bailey, R.M. and Goodliffe, A.M., 2012, Structure of the Alleghanian Thrust Belt under the Gulf Coastal Plain of Alabama: Gulf Coast Association of Geological Societies Transactions, v. 1, p. 44-54.

Rohde, R.A., 2005, Geologic Timeline, GeoWhen Database, http://www.stratigraphy.org /bak/geowhen /timelinestages.html (last accessed 10 April 2019).

Salters, V.J., and Stracke, A., 2004, Composition of the depleted mantle: Geochemistry, Geophysics, Geosystems, v. 5, doi:10.1029/2003GC000597.

Schatzel, S.J., and Stewart, B.W., 2012, A provenance study of mineral matter in coal from Appalachian Basin coal mining regions and implications regarding the respirable health of underground coal workers: a geochemical and Nd isotope investigation: International Journal of Coal Geology, v. 94, p.123-136.

Sharrah, K.L., 2006, Comparative Study of the Sedimentology and Provenance of the Atoka Formation in the Frontal Ouachita Thrust Belt, Oklahoma [Ph.D. Dissertation], University of Tulsa, 268 p.

Stern, R.J., and Dickinson, W.R., 2010, The Gulf of Mexico is a Jurassic backarc basin: Geosphere, v. 6, p. 739-754.

Taylor, S.R. and McLennan, S.M., 1985, The continental crust: its composition and its evolution [B]: Blackwell, Oxford, 312 p.

Teo, W.S., 1991, Elemental geochemistry of shales in Pennsylvanian cyclothems, midcontinent North America [Ph.D. Dissertation], Texas Tech University, Texas, 179 p.

Thomas, J.D., 2003, Integrating Synsedimentary Tectonics with Sequence Stratigraphy to Understand the development of the Fort Worth Basin: American Association of Petroleum Geologists Search and Discovery, AAPG Southwest Section Meeting, Ruidoso, New Mexico, p. 149-157.

Thomas, W.A., 1977, Evolution of Appalachian Ouachita salients and recesses from reentrants and promontories in the continental margin: American Journal of Science, v. 277, p. 1233-1278.

Thomas, W.A., 1997, Nd isotopic constraints on sediment sources of the Ouachita-Marathon fold belt: Alternative Interpretation and Reply: Geological Society of America Bulletin v. 109, p. 779-787.

Thomas, W.A., 2004, Genetic relationship of rift-stage crustal structure, terrane accretion, and foreland tectonics along the southern Appalachian-Ouachita orogen: Journal of Geodynamics, v. 37, p. 549-563.

Thomas, W.A., 2006, Tectonic inheritance at a continental margin: Geological Society of America today, v. 16, p. 4-11.

Thomas, W.A., Gehrels, G.E., Greb, S.F., Nadon, G.C., Satkoski, A.M., and Romero, M.C., 2017, Detrital zircons and sediment dispersal in the Appalachian foreland: Geosphere, v. 13, p. 2206-2230, doi: 10.1130/GES01525.1.

Thomas, W. A., and Viele, G. W., 1983, Tectonic history of the Ouachita orogen: Geology, v. 11, p. 482-483.

Thompson, M.D., 1982, Atoka Group (Lower to Middle Pennsylvanian), Northern Fort Worth Basin, Texas: terrigenous depositional systems, diagenesis, and reservoir distribution and quality:

The University of Texas at Austin, Bureau of Economic Geology Report of Investigations No. 125, 62 p.

Turner, G. L., 1957, Paleozoic stratigraphy of the Fort Worth Basin, Joint Field Trip Guidebook: Abilene Geological Society, Fort Worth Geological Society, p. 57-77.

Ukaegbu, V.U., and Beka, F.T., 2008, Rare-earth elements as source indicators of Pan-African granites from Obudu Plateau, Southeastern Nigeria: Chinese Journal of Geochemistry, v. 27, p.130-134.

Van Staal, C.R., Whalen, J.B., Valverde-Vaquero, P., Zagorevski, A., and Rogers, N., 2009, Pre-Carboniferous, episodic accretion-related, orogenesis along the Laurentian margin of the northern Appalachians: Geological Society Special Publications [London], v. 327, p. 271-316.

Viele, G.W., and Thomas, W.A., 1989, Tectonic synthesis of the Ouachita orogenic belt, in Hatcher, R.D., Jr., Thomas, W.A., and Viele, G.W., eds., The Appalachian-Ouachita Orogen in the United States: Geological Society of America, The Geology of North America, v. F-2, p. 695-728.

Walper, J.L., 1977, Paleozoic tectonics of the southern margin of North America: Gulf Coast Association of Geological Societies Transactions, v. 27, p. 230-241.

Walper, J.L., 1982, Plate tectonic evolution of the Fort Worth Basin: in C.A. Martin, ed., Petroleum Geology of the Fort Worth Basin and Bend Arch Area: Dallas Geological Society, p. 237-251.

Wilde, P., Quinby-Hunt, M.S., and Erdtmann, B.D., 1996, The whole-rock cerium anomaly: a potential indicator of eustatic sea-level changes in shales of the anoxic facies: Sedimentary Geology, v. 101, p.43-53.

Chapter 4 TRACING PALEOZOIC SILICICLASTIC SIDEMENT DISPERDAL TO THE MIDLAND BASIN IN WEST TEXAS USING DETRITAL ZIRCON

ABSTRACT

The Midland Basin region in West Texas evolved from continental margin during the early Paleozoic to the southwestern part of the Alleghanian-Ouachita-Marathon orogen belt during the late Paleozoic. Sediment provenance is important to the reconstruction of sediment dispersal pathways and paleogeography caused by changing tectonic setting. Herein I study the detrital zircon U-Pb ages and Hf isotope compositions of two samples collected from the Cambrian and Late Pennsylvanian fluvial and deltaic sandstones in the Midland Basin to constrain sediment provenances. The Cambrian sample contains predominantly grains derived from the Proterozoic midcontinent Granite-Rhyolite province and a small portion of Grenville grains, and the εHf values are between +5 and +20, suggesting that the paleoriver mainly drained the Proterozoic basement that was exposed in the Texas Arch to the north of the basin. The Pennsylvanian sample contain grains ranging from Archean to late Paleozoic age, and is characterized by a large Grenville population with two peaks at ~1.02 Ga and ~1.15 Ga and a large Neoproterozoic-early Paleozoic (800-500 Ma) population. The εHf values range from -24 to +12. By comparing the detrital zircon signature with potential sources and Paleozoic clastic rocks in southern Laurentia, I suggest that the Late Pennsylvanian sediments were dispersed by a transcontinental river along the Appalachian-Ouachita foreland and regional rivers draining the peri-Gondwana terranes in the Ouachita thrust belt. The nutrients brought by the river may have enhanced marine productivity and caused organic matter enrichment.

4. 1 INTRODUCTION

During the late Paleozoic, the Alleghanian-Ouachita-Marathon orogenies and several peripheral foreland basins were formed in southern Laurentia by the subduction of Laurentian margin underneath Gondwana and their subsequent collision (e.g., Walper, 1982; Erlich and Coleman, 2005;

Thomas, 2006; Elebiju et al., 2010) (Figure 4-1). During the same time, the Ancestral Rocky Mountains (ARM) Orogeny formed several basement-involved uplifts in the interior of southwestern Laurentia, as a result of reactivation of paleotransform faults by intracontinental stress accumulation induced by the contractional tectonics (Dickinson and Lawton, 2003), or by flat slab subduction (Ye et al., 1996), or by the combined effect of collision, subduction under the western margin and transpressional deformation along the southwestern margin (Leary et al., 2017). These tectonic processes should have changed the landscape and sediment dispersal pattern in southern Laurentia. Reconstruction of sediment dispersal pathways through sediment provenance study provides critical understanding to the paleogeography and tectonic configuration.

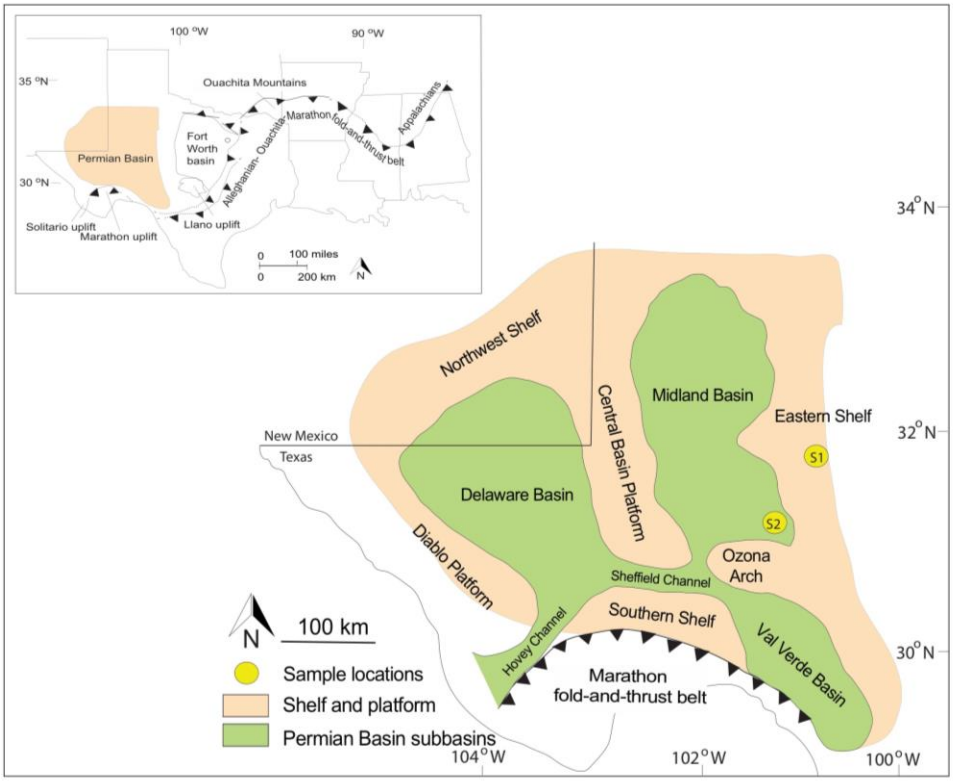

Figure 4-1 Location of the Permian Basin and its subbasins and basin-bounding units in southern U.S.A. Also shown are the other major sedimentary basin mentioned in this study. Modified from Dutton et al., (2000).

In West Texas and southeastern New Mexico, U.S.A., the Permian Basin was formed on the Laurentian continental shelf during the collision of Laurentia and Gondwana. The basin is divided into several subbasins, among which, the Delaware Basin to the west and the Midland Basin to the east are the two largest (Figure 4-1). Since 1920, the Permian Basin has produced more than 30 Bbbl of oil and more than 75 Tcf of natural gas, and numerous studies have been conducted on the sedimentary and petrophysical characteristics of the hydrocarbon-bearing lower Permian strata in order to enhance hydrocarbon exploration and production (e.g., Broadhead and King, 1988; Tyler and Banta, 1989; Ball, 1995; Broadhead et al., 2004; Dutton et al., 2005; Merrill et al., 2015), yet the sediment provenance of the Paleozoic basin-fill, the tectonic setting, and the paleogeography before and during the formation of the Permian Basin remain poorly constrained.

The provenance of the Paleozoic siliciclastic detritus in the Permian Basin is highly debated, and most of the provenance studies focus on the middle Permian Delaware Mountain Group in the Delaware Basin. These studies suggested that the middle Permian detritus were derived from five different local sources, including: 1) the basement-cored uplifts of the ARM located to the north-northwest of the basin based on the arkosic composition of sandstones in the Northwest Shelf region (King 1948; Hull, 1957; Breg, 1979; Watson, 1979; Williamson, 1979; Mazzullo et al., 1991); 2) the Arbuckle-Wichita uplifts, the easternmost extension of the ARM, to the northeast of the basin (Hull et al., 1957; Watson, 1979), which is consistent with the NE-SW trended middle Permian submarine channels in the Delaware Basin (Payne, 1976); 3) local sources within the basin, including the Northwest Shelf and the Central Basin Platform based on stratigraphic correlations of the Bell Canyon and Cherry Canyon Formations in the Guadalupe Mountains (Newell et al., 1953; Bozanich, 1979); 4) contribution from a southern source, including mainly the Ouachita-marathon orogenic system based on limited presence of sandstones and conglomerates in the Glass Mountains (King, 1948); and 5) contribution from east and northeast by recycling Pennsylvanian sandstones in Oklahoma and Colorado (Newell at al., 1953), or Permian Whitehorse Group in Kansas, Oklahoma and northern part of Texas

by a southwestward eolian system (Kocurek and Kirkland, 1998). Two recent detrital zircon provenance studies made improvement on the provenance interpretation. Soreghan and Soreghan (2013) suggested that the middle Permian sediments in the northwestern part of Delaware Basin were mainly transported from the Ouachita orogenic belt by local rivers with the assistance of eolian deflation of fluvial sediments. Xie et al. (2019) suggested that majority of the middle Permian sediments in the central and southern parts of the Delaware Basin were derived from the Appalachian foreland by a transcontinental river, and from the Ouachita orogenic belt and peri-Gondwanan terranes incorporated in the orogenic belt by local rivers. In addition to these studies to the middle Permian strata, provenance of the other Paleozoic strata remains unexplored.

Paleozoic sediments derived from the Appalachians contributed to Pennsylvanian sedimentation in the Fort Worth Basin (Alsalem et al., 2018), and may have provided siliciclastic grains to the Midland Basin. Graham et al. (1975) proposed that the Paleozoic highland of the Appalachians poured sediments into its foreland, and then the sediments were transported by a large axial river flowed along the Appalachian and Ouachita forelands, and dispersed sediments into remnant ocean basins. These sediments may have made to the Permian Basin because of juvenile neodymium isotope composition and abundant Grenvillian and Appalachian detrital zircons were also documented in the Pennsylvanian strata in the Marathon foreland and hinterland (Gleason et al., 1994; 1995; Gleason et al., 2007) and middle Permian strata in the Delaware Basin (Xie et al., 2019). However, detrital zircon data are lacking from the older strata in the Permian Basin, hindering our understanding to when and how Appalachian detritus made to the basin.

This study determines sediment provenance of Cambrian and Pennsylvanian sandstones in the Midland Basin in southern Laurentia using detrital zircon U-Pb ages and Lu-Hf isotopic data. By combining my data with published detrital zircon data in eastern and southern Laurentia, I infer sediment dispersal patterns of siliciclastic sediments on the southern margin of Laurentia, and reconstruct the paleogeography before and during the suturing between Gondwana and Laurentia.

4. 2 GELOLGICAL SETTING

As the two largest subbasins of the Permian Basin, the Midland Basin is separated from the Delaware Basin to the west by the NW-trending, basement-involved Central Basin Platform (Figure 4-1). The Midland Basin is bounded to the east by the Eastern Shelf, to the south by the E-W trending Ozona Arch, an easterly extension of the southern Central Basin Platform, and to the north by the Northern Shelf (Figure 4-1). The different orientations of the Central Basin Platform and Ozona Arch suggest that they likely formed by different tectonic mechanisms (Yang and Dorobek, 1995).

The precursor of the Permian Basin is the Tobosa Basin on the southern Laurentian margin (Galley, 1958; Adams, 1965). The Tobosa Basin formed as a result of subsidence relative to its peripheral shelf areas during the Cambrian and Ordovician (Galley, 1958; Robinson, 1988) by weak crustal extension and gradual thermal cooling (Horak, 1985; Miall, 2008; Merrill et al., 2015). During the Early Ordovician, several arc terranes (e.g., Avalonia, Ganderia, Carolinia, Meguma, Suwannee) were separated from the continental margin of northern Gondwana (e.g., Murphy et al., 2002, 2006; Nance et al., 2002; Keppie et al., 2003; Nance and Linnemann, 2008; Pollock et al., 2009; van Staal et al., 2009). These terranes were later accreted to Laurentia during the gradual closure of the Rheic Ocean and suturing between Gondwana and Laurentia. The southern margin of Laurentia began to subduct underneath Gondwana as early as the Early Devonian, and the final closure of the Rheic Ocean resulted in the complete burial of Laurentia shelf during the Pennsylvanian (e.g., Hatcher, 1989; Viele and Thomas, 1989; Thomas, 2004). During the Mississippian-early Permian, the southwestward subduction of Laurentia beneath Gondwana formed the Ouachita-Marathon-Sonora orogenic belt to the south of the Permian Basin (Poole et al., 2005). The Ouachita Orogeny is the southwestward extension of the Alleghanian Orogeny (Loomis et al., 1994; Poole et al., 2005), which is the youngest deformation in the Appalachian orogen (Nance et al., 2010). The collisional tectonics further reactivated pre-existing faults in the Permian Basin, and caused uplift along high-angle to vertical fault systems and subsidence

in the centers of the Midland and Delaware Basins (Dutton et al., 2005; Scholle et al., 2007; Miall, 2008; Poole et al., 2005).

4. 3 STRATIGRAPHY

The Paleozoic basin-fill of the Midland Basin contains primarily carbonate and shale, and the total thickness is ~4 km (Galley, 1958; Robinson, 1988). Based on the tectonic history, the Paleozoic strata were divided into three major stratigraphic units: 1) the Cambrian to Devonian unit deposited in a passive continental margin; 2) the Mississippian to middle Permian unit deposited during the Ouachita-Marathon orogeny; and 3) the late Permian unit representing the post-orogenic deposition (Adams, 1965; Ward et al., 1986, Robinson, 1988; Sarg et al., 1999).

The Cambrian-Devonian system represents deposition in the ancestral Tobosa Basin (Galley, 1958; Robinson, 1988). The basal Cambrian siliciclastic sedimentary rocks unconformably overlie Precambrian crystalline basement, and are overlain by strata of the Ordovician System (Figure 4-2) (Robinson, 1988). The Upper Cambrian consists of interbedded sandstone, limestone and shale that were deposited in the southeastern part of the basin during a marine transgression (Galley, 1958). The system grades upward into the carbonate-dominated deposit of the Lower Ordovician-Lower Devonian (e.g., Galley, 1958; Wright, 1979; Robinson, 1988; Frenzel et al., 1988; Ruppel, 2008), and the black mudstone of the Middle to Upper Devonian Woodford Formation (Montgomery, 1998).

The Mississippian System mainly contains carbonate of shallow marine environment (Robinson, 1988; Montgomery, 1998). Deposition of the Pennsylvanian System was strongly influenced by tectonism related to the Ouachita-Marathon Orogeny and the ARM Orogeny (Wright, 2006). The Pennsylvanian Morrowan to Desmoinesian Series consists of shallow marine carbonate and a minor amount of shale of the Atoka and Strawn Groups; the Missourian Series consists of shale and marine carbonate of the Canyon Group, and the Virgilian Series only consists of black shale of the Cisco Group in the basin (Wright, 2006; Wright, 2011). The Pennsylvanian System is up to ~920 m thick. On the Eastern Shelf and eastern periphery of the Val Verde Basin, Desmoinesian and Missourian

alluvial and deltaic siliciclastics are distributed (Wright, 2011), and nine cycles of carbonate-siliciclastic sequences deposited during highstand-lowstand cycles were defined for the Virgilian (Brown et al., 1990).

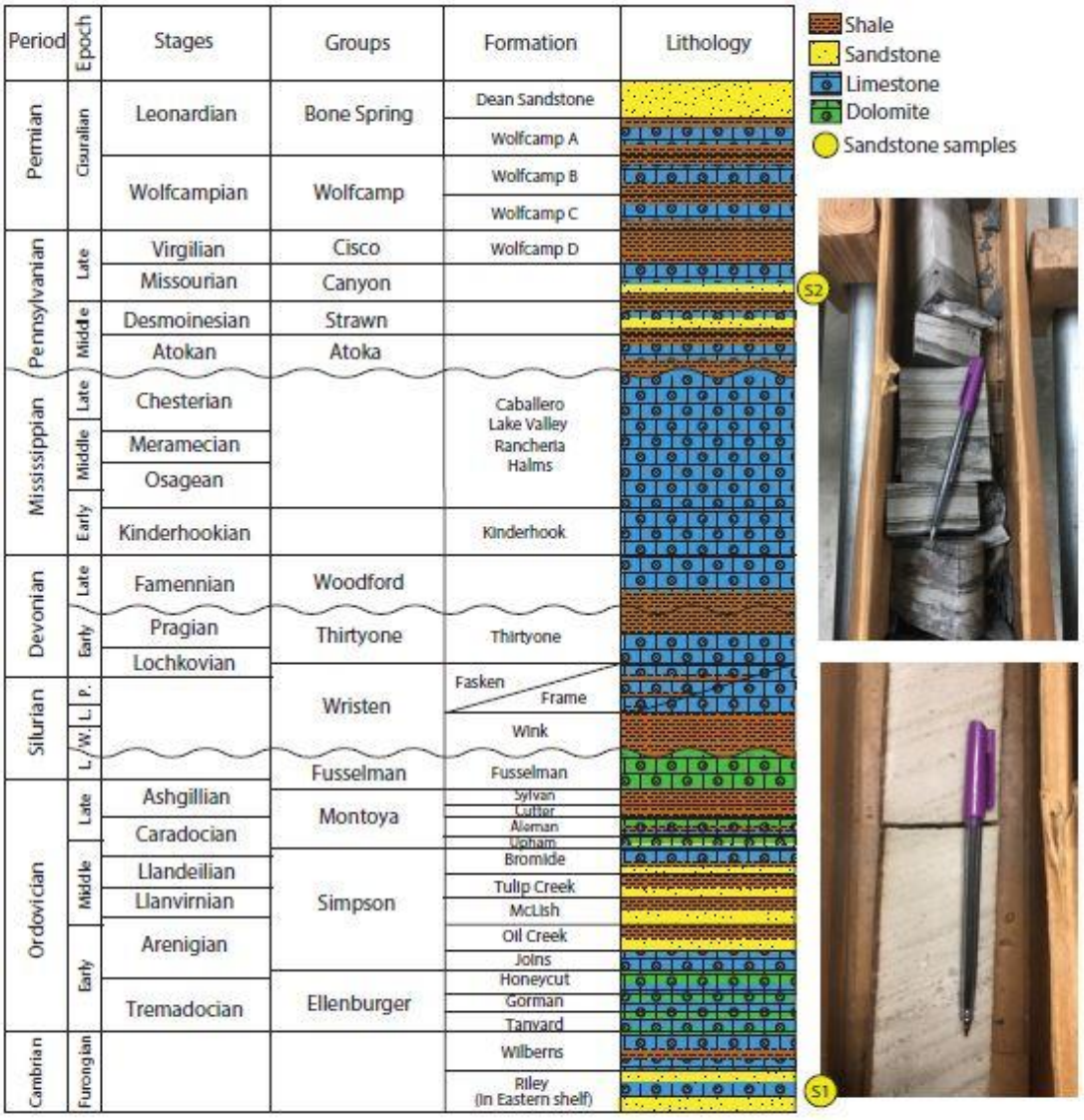

Figure 4-2 Stratigraphic column of the basin fill in the Midland Basin and the pictures of the two core samples used for this study. Modified from Robinson (1988); Yang and Dorobek (1995); Dutton et al. (2004); Pope (2004); Jones (2009); Loucks (2010); Merrill et al. (2015); and Murphy (2015).

The Permian system grades upward from an interbedded siliciclastic and carbonate unit to an evaporite unit. During the early Permian, the basin was deep and tectonically stable, allowing deposition of interbedded sandstone, shale and thick carbonate in the center, which were surrounded by reefs and carbonate shelves (Robinson, 1988). By the late Permian, evaporitic sabkha conditions existed over the entire Midland Basin (Robinson, 1988). The total thickness of the Permian System in the Permian Basin is up to ~5200 m. The Permian strata are unconformably overlain by the Triassic continental deposits.

4. 4 MATERIALS AND METHODS

For this study, I collected two sandstone samples from the core lab in the Bureau of Economic Geology in Austin. One sample was collected from the upper part of the Cambrian Riley Formation in the Eastern Shelf, and the other sample was from the Late Pennsylvanian Canyon Group in the southern part of the basin (Figure 4-1; Table 4-1). The Cambrian sandstone is cross-bedded, coarse- to medium-grained, quartzose and poorly sorted (Figure 4-2), most likely deposited in fluvial environment. The Pennsylvanian sample is fine-grained and poorly sorted (Figure 4-2). In the core, the sandstone grades upward into siltstone, and is in erosional contact with the underlying shale (Figure 4-2). The sandstone was most likely deposited in deltaic environment.

The two sandstone samples were processed for detrital zircon U-Pb geochronology and Lu–Hf isotope analysis to determine the sediment provenance. Zircon crystals were extracted from samples by traditional methods of crushing and grinding, followed by separation with a Frantz magnetic separator and heavy liquid.

The U-Pb geochronology and Hf isotopic analyses of 70-300 zircon grains in each sample were conducted concurrently using a laser ablation multi-collector inductively coupled plasma mass spectrometry (LA-MC-ICPMS) at the Washington State University. An Analyte G2 193 nm excimer laser was connected to the Element 2 high resolution ICPMS. The laser parameters include 10 Hz repetition rate ~5.5 J/cm^2 power and 25-35 μm laser spot. Zircon grains were randomly selected for analysis to avoid bias in size or shape. U-Pb measurement followed the method of Chang et al. (2006).

A 30-second blank measurement of He and Ar carrier gasses (laser off) before each analysis was used to measure background, followed by 300 scans across masses ^{202}Hg, ^{204}Pb+Hg, ^{206}Pb, ^{207}Pb, ^{208}Pb, ^{232}Th, ^{235}U, and ^{238}U during ~30 seconds laser ablation period. Data were processed offline using the Iolite software (Paton et al., 2011). The zircon standards used in this study were Plesovice (337 Ma; Sláma et al., 2008) and FC1 (1099 Ma; Paces and Miller, 1993). The ^{206}Pb/^{238}U ratios of unknown analyses were corrected using Plesovice, and the ^{206}Pb/^{207}Pb ratios were corrected using FC1. Zircon 91500 (1065 Ma; Wiedenbeck et al., 1995) and Temora 2 (417 Ma; Black et al., 2004) were used as quality control standards. Common Pb correction was performed using the ^{207}Pb method (Williams, 1998). U-Pb ages were calculated using Isoplot (Ludwig, 2003). Zircon U-Pb data are in Appendix B.

Following analyses of U-Pb ages, the Lu-Hf isotope composition of zircon crystals was determined at the Radiogenic Isotope and Geochronology Lab (RIGL) at Washington State University. Analyses were conducted using a ThermoFinnigan Neptune plus mass spectrometer coupled to an Analyte G2 193 nm excimer laser, using a spot size of 30 μm, a laser fluence of ~7 J/cm^2, and repetition rate of 10 Hz. This study used the same instrument configuration, operating parameters, and data reduction methods outlined by Fisher et al. (2014a), with the exception that U-Pb ages were not simultaneously determined. In this "dedicated Hf" method, the output from the ablation cell was mixed with N_2 gas and delivered directly to the Neptune MC-ICPMS. To reduce inter-laboratory bias, the Plešovice zircon standard (^{176}Hf/^{177}Hf = 0.282482 ± 13, Sláma et al., 2008) was regularly analyzed between sample blocks and used to correct the measured ^{176}Hf/^{177}Hf of unknowns. Given the potentially large range of (Lu+Yb)/Hf in zircon samples, accurate correction for the isobaric interference of ^{176}Yb and ^{176}Lu on ^{176}Hf is imperative, and should be assessed using quality control zircons interspersed with samples (Fisher et al., 2014b). Over the course of this study, 10 analyses of the Z145 sinthetic zircon (S-MC-ICPMS ^{176}Hf/^{177}Hf = 0.282135 ± 7, Fisher et al, 2011) yielded a ^{176}Hf/^{177}Hf value of 0.282133 ± 23 (2σ), 3 analyses of the Temora-2 zircon (S-MC-ICPMS ^{176}Hf/^{177}Hf = 0.282686 ± 8, Woodhead and Hergt, 2005) yielded a ^{176}Hf/^{177}Hf value of 0.282687 ± 28 (2σ), and analyses of the 91500 zircon

(S-MC-ICPMS $^{176}Hf/^{177}Hf = 0.282306 \pm 8$, Blichert-Toft, 2008) yielded a $^{176}Hf/^{177}Hf$ value of 0.282324 ± 26 (2σ). Analyses of these quality control zircons agree well with published S-MC-ICPMS isotope compositions of purified Hf from these zircons, attesting to the accuracy of the interference correction methods employed.

Internal 2σ precision was typically ~ 1.2 ε_{Hf}. Analyses with less than 25 ratios, and/or internal 2δ uncertainty over 2 ε_{Hf} units were discarded and not presented here. Present day ε_{Hf} values were calculated using the CHUR parameters reported by Bouvier et al. (2008). Laser ε_{Hf} values are reported with 2σ uncertainty in Appendix C.

The $^{206}Pb/^{207}Pb$ ages are used for grains older than 900 Ma, and $^{206}Pb/^{238}U$ ages are used for grains younger than 900 Ma. Ages older than 400 Ma were filtered by 20% discordance and 5% reverse discordance. Age groups were determined by identifying three or more grains with overlapping $^{206}Pb/^{238}U$ and $^{206}Pb/^{207}Pb$ ages in the aggregate data set. Kernel density estimation (KDS) was used to evaluate final abundance to avoid analytical bias due to quantity and quality (Vermeesch, 2012; Vermeesch et al., 2016) (Figure 1-3). Hafnium data are presented using Hf evolution diagrams (Figure 4-3), where initial $^{176}Hf/^{177}Hf$ ratios are expressed in εHf notation, which represents the Hf isotopic composition at the time of zircon crystallization relative to the chondritic uniform reservoir (CHUR) (Bouvier et al., 2008). εHf data of grains with 20-40% U-Pb discordance are also shown in Figure 4-3.

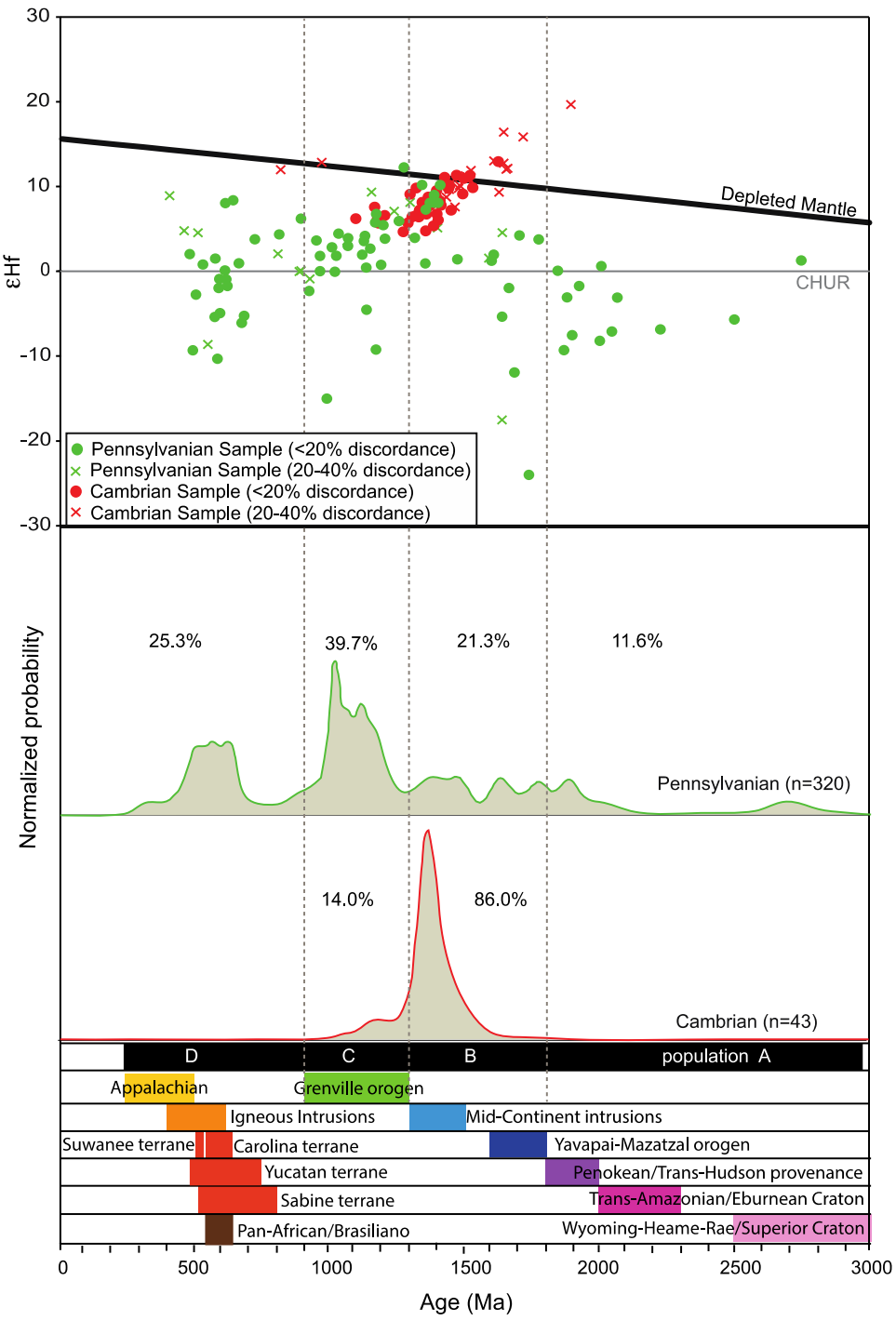

Figure 4-3 Detrital zircon εHf values and U-Pb ages of the two studied samples in the Midland Basin.

4. 5 RESULTS

The detrital zircon U-Pb ages range from Archean (2.932 Ga) to Pennsylvanian (330 Ma). The Cambrian sample has a different age distribution compared to the Pennsylvanian sample (Fig. 3). Based on known ages of major magmatic terranes in North America (e.g., Thomas et al., 2004; Dickinson and Gehrels, 2009; Soreghan et al., 2002; Gehrels et al., 2011) and the abundance of zircons from each terrane in my samples, a total of 363 dates are divided into four populations (Figure 4-3), including the Archean–Paleoproterozoic (2.739-1.825 Ga) grains of population A, late Paleoproterozoic–early Mesoproterozoic (1.825-1.300 Ga) grains of population B, middle Mesoproterozoic–early Neoproterozoic (1.300-0.900 Ga) grains of population C, and Neoproterozoic–Paleozoic (800-330 Ma) grains of population D. The Cambrian sample has 86.0% population B, and 14.0% population C grains. Grains of population B are mostly in the range of 1.533-1.300 Ga. The Pennsylvanian sample has 11.6% population A, 21.3% population B, 39.7% population C, and 25.3% population D. Only 6.6% of the grains are younger than 500 Ma. The remaining 2.2% of the grains are of 900 – 800 Ma age. Given their low abundance, a population is not assigned. Population C of the Pennsylvanian samples contains two peaks, including a larger one at ~1.02 Ga and a smaller one at ~1.15 Ga.

Grains of the Cambrian sample have εHf values between +5 and +20, overlapping the values of Paleoproterozoic–Mesoproterozoic igneous zircon grains in the Grenville and Granite-Rhyolite provinces (Thomas et al., 2018; Figure 4-3). Grains of the Pennsylvanian sample have εHf values ranging from -24 to +12.

4. 6 POTENTIAL ZIRCON SOURCES

4. 6.1 Laurentia Source

Laurentia craton

The North American craton has several distinct age provinces, including the: 1) Wyoming-Heame-Rae and Superior provenances (3.60-2.50 Ga), 2) Penokean-Trans-Hudson provenances (2.00-1.80 Ga), 3) Central Plains (~1.86-1.50 Ga), which mainly include the Yavapai-Mazatzal province

(1.83-1.60 Ga), 4) Granite-Rhyolite province (1.50-1.30 Ga), and 5) Grenville province (1.30-0.90 Ga) (Figure 4-4) (e.g., Hoffman, 1988; Frost et al., 2000; Mueller et al., 2002; Whitmeyer and Karlstrom, 2007). The Grenville orogeny includes the Shawinigan (1.16–1.19 Ga) and the Ottawan (0.98–1.09 Ga) orogenies (Heumann et al., 2006; Bartholomew and Hatcher, 2010; Chiarenzelli et al., 2010; McLelland et al., 2010; Rivers et al., 2012). Zircon grains from these provinces yield εHf values that range from –13 to +7 (Mueller et al., 2008; Bickford et al., 2010; Thomas et al., 2018).

Zircon grains with these ages have been documented in Proterozoic to Paleozoic strata of North America (e.g., Gleason et al., 2002; 2007; Eriksson et al., 2004; Sharrah, 2006; Dickinson and Gehrels, 2009; Park et al., 2010; Gehrels et al., 2011; Amato and Mack, 2012; Spencer et al., 2014; Alsalem et al., 2018; Xie et al., 2018; 2019). The high zircon fertility of the Grenville basement has led to abundant Grenvillian grains in Neoproterozoic to Paleozoic strata (Moecher and Samson, 2006), particularly in the Appalachian foreland basins (Erriksson et al., 2004; Becker et al., 2005; Moecher and Samson, 2006; Gleason et al., 2007; Thomas et al., 2018).

Neoproterozoic-early Paleozoic rift province

The breakup of Rodinia was associated with two magmatic events in southeastern Laurentia, including a failed rift event at 760-700 Ma and the opening of the Iapetus Ocean at 620-528 Ma (e.g., Hatcher, 1989; Walsh and Aleinikoff, 1999; Cawood and Nemchin, 2001; Thomas et al., 2016). The Iapetus synrift rocks are exposed along Appalachian external basement massifs (e.g., Thomas, 1991), in the southern Oklahoma aulacogen, New Mexico and southern Colorado (Johnson et al., 1988; Gilbert and Denison, 1993; Hogan and Gilbert, 1998; Cawood and Nemchin, 2001; Thomas et al., 2016). These rocks were exhumed during the Pennsylvanian-early Permian ARM Orogeny (King, 1948; Hull, 1957; Watson, 1979; Mazzullo et al., 1991). These rocks are potential sources of detrital grains with an age range of 760-528 Ma. Zircon grains derived from these rocks in the Arbuckle-Wichita uplifts yield strongly positive εHf values between +4.7 and +10, reflecting the juvenile magmas (Thomas et al., 2016).

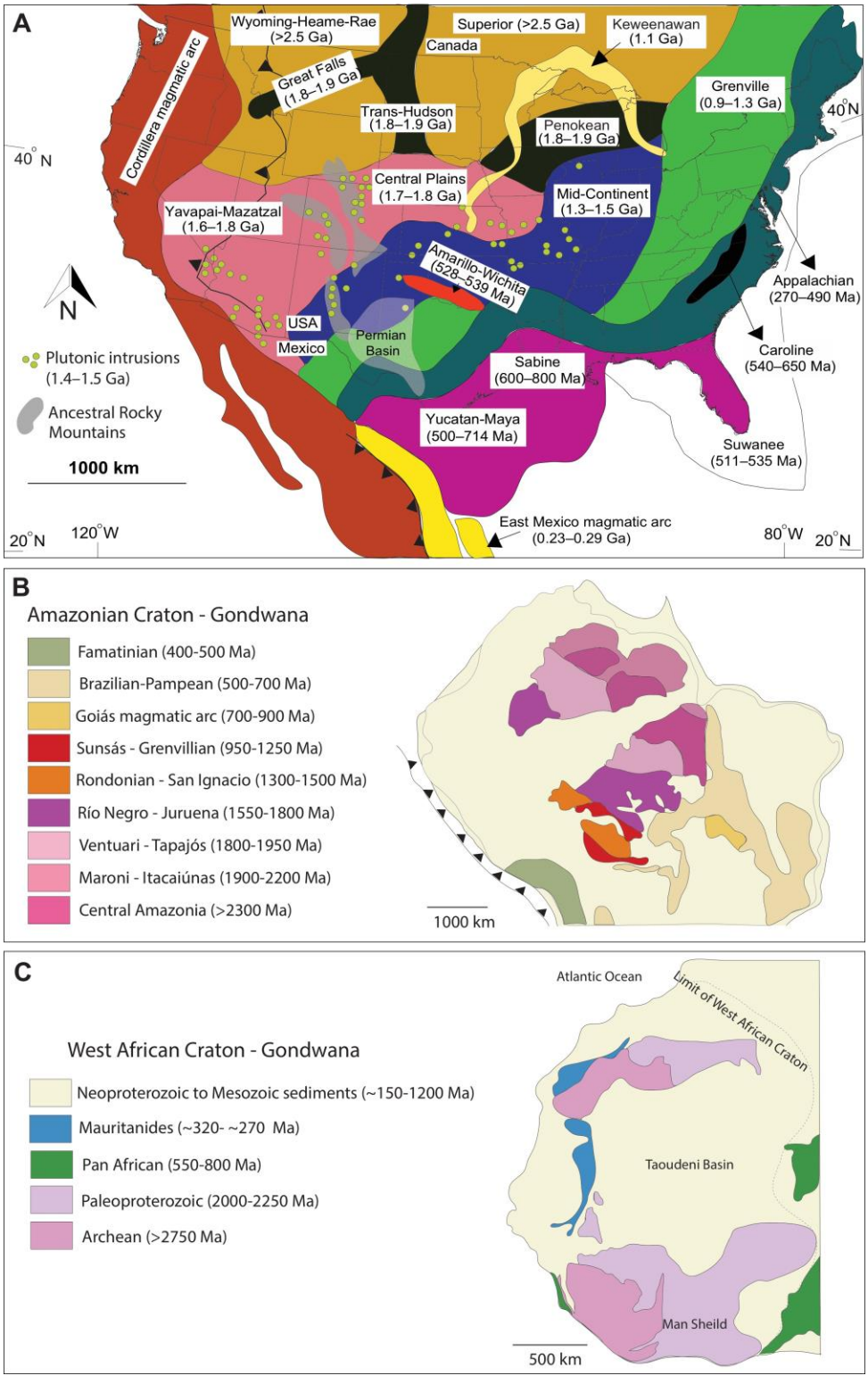
A
Wyoming-Heame-Rae (>2.5 Ga)
Superior (>2.5 Ga)
Keweenawan (1.1 Ga)
Canada
Great Falls (1.8–1.9 Ga)
Grenville (0.9–1.3 Ga)
Cordillera magmatic arc
Trans-Hudson (1.8–1.9 Ga)
Penokean (1.8–1.9 Ga)
40° N
40° N
Central Plains (1.7–1.8 Ga)
Mid-Continent (1.3–1.5 Ga)
Yavapai-Mazatzal (1.6–1.8 Ga)
Amarillo-Wichita (528–539 Ma)
Appalachian (270–490 Ma)
N
USA
Mexico
Permian Basin
Caroline (540–650 Ma)
Plutonic intrusions (1.4–1.5 Ga)
Sabine (600–800 Ma)
Ancestral Rocky Mountains
Yucatan-Maya (500–714 Ma)
Suwanee (511–535 Ma)
1000 km
East Mexico magmatic arc (0.23–0.29 Ga)
20° N
120° W
80° W
20° N
B
Amazonian Craton - Gondwana
Famatinian (400-500 Ma)
Brazilian-Pampean (500-700 Ma)
Goiás magmatic arc (700-900 Ma)
Sunsás - Grenvillian (950-1250 Ma)
Rondonian - San Ignacio (1300-1500 Ma)
Río Negro - Juruena (1550-1800 Ma)
Ventuari - Tapajós (1800-1950 Ma)
Maroni - Itacaiúnas (1900-2200 Ma)
Central Amazonia (>2300 Ma)
1000 km
C
West African Craton - Gondwana
Neoproterozoic to Mesozoic sediments (~150-1200 Ma)
Mauritanides (~320- ~270 Ma)
Pan African (550-800 Ma)
Paleoproterozoic (2000-2250 Ma)
Archean (>2750 Ma)
Atlantic Ocean
Limit of West African Craton
Taoudeni Basin
Man Sheild
500 km

Figure 4-4 (A) Map showing the main basement provinces and study area in North America. Permian Basin is shown in a stippled pattern. Modified after Alsalem et al. (2018). (B) Map showing the main basement provinces in the Amazonian Craton. Modified from Silva-Romo et al. (2015). (C) Map showing the main basement provinces in the West Africa Craton. Modified from Rollinson (2016).

Appalachian Province

The tectonomagmatic units of the Appalachian Orogeny occurred in eastern Laurentia include the Taconic (490-430 Ma), Acadian (420-350 Ma), and Alleghanian (330-270 Ma) orogenies (Hatcher, 1989; Miller et al., 2000). Zircon grains of this population have been documented in lower Paleozoic strata in the Appalachian foreland basins (Eriksson et al., 2004; Thomas et al., 2004; Park et al., 2010), Mississippian-lower Permian strata in the Grand Canyon region (Gehrels et al., 2011), Ordovician-Pennsylvanian strata in Oklahoma and Arkansas (Gleason et al., 2002; Sharrah, 2006; Xie at al., 2016; 2018), and Pennsylvanian-Permian strata in Texas (Alsalem et al., 2018; Xie et al., 2019). This group of zircon has highly variable εHf values between -12 and +6 (Mueller et al., 2008; Thomas et al., 2018). The Appalachian Orogeny exhumed Grenville basement, thus sedimentary rocks in the Appalachian foreland basins are characterized by abundant Grenvillian grains as well as newly formed Neoproterozoic grains (Thomas et al., 2018).

4. 6.2 Gondwana Source

Amazon Craton

The Amazon Craton (3.10-1.00 Ga) is the largest stable tectonic unit of South America, mainly in Brazil. The Craton contains the Archean province (3.10-2.76 Ga), Transamazonia Orogeny (~2.25-2.00 Ga), Tapajós-Parima Orogeny (2.10-1.87 Ga), central Amazonian province (~1.88-1.70 Ga), Rio Negro Collisional Belt (~1.56-1.52 Ga), Rondônia-Juruena Orogeny (~1.76-1.47 Ga), and Sunsas Orogeny (~1.33-0.99 Ga) (Santos et al., 2000; Henderson et al., 2016). Zircon grains derived from the Transamazonia Orogeny differentiate the Amazonia source from Laurentia source. Grains from

Amazonia have a broad εHf ranging between -25 and +15 (e.g., Reimann et al., 2010; Matteini et al., 2010; Ibanez-Mejia et al., 2015; McGee et al., 2015).

West African Province

The West African Craton contains three Archean and Palaeoproterozoic metamorphic and magmatic shields, formed by the Paleoarchean orogeny (~3.5-3.0 Ga), Liberiancy orogeny (2.95-2.75), and Eburnian orogeny (~2.2-1.75 Ga) (e.g., Kroner et al., 2001). The Craton did not have any magmatic activity during 1.7-1.0 Ga, which is the best fingerprint of the West African provenance (Linnemann et al., 2004). Grains from the West African province have a broad εHf range from -37 to +20 (e.g., Abati et al., 2012; Avigad et al., 201; Linnemann et al., 2014; Gärtner et al., 2014; Henderson et al., 2016).

Peri-Gondwana Terranes

During ~800-500 Ma, the Pan-African/Brasiliano orogeny occurred as a result of accretion and collision of many crustal blocks, including mainly South America and Africa, to form the late Neoproterozoic supercontinent Gondwana (Figure 4-4) (e.g., Pollock et al., 2010; Willner et al., 2013; Mueller et al., 2014; Henderson et al., 2016). The Goiás magmatic arc within the Brasiliano orogen can be as old as 900-750 Ma (Keppie et al., 2008). Blocks drifted away from Gondwana, called peri-Gondwana terranes, were accreted to Laurentia during the Alleghania-Ouachita-Marathon orogenies (Samson et al., 2001; Murphy et al., 2004; Mueller et al., 2014). Documented peri-Gondwana terranes include the Ganderia-Avalonian-Meguma (750–545 Ma) in the northern Appalachian Mountains (Hibbard et al., 2007; Hibbard and Karabinos, 2013); Carolinian-Uchee terranes (670-532 Ma) in the southern Appalachian Mountains (Samson et al. 1995; Wortman et al. 2000; Hibbard et al., 2002; Pollock at al., 2011); the Suwannee terrane (535-511 Ma) in the Florida subsurface (Opdyke et al., 1987; Mueller et al., 1994; Murphy et al., 2004; Martens et al., 2010); the Sabine terrane (800-600 Ma; Thomas, 2013) in eastern Texas and western Louisiana (Granata, 1963; Gleason et al., 2007; Nunn, 2012); and the Yucatan/Maya terrane (714-500 Ma) in southeastern Mexico (Rankin et al., 1989; Mueller et al., 1994; Thomas et al., 2004). Detrital zircon grains of the peri-Gondwana terranes are

characterized by a small 2.25-2.00 Ga age group formed by the Transamazonian-Eburian orogenies, and a prominent 800-500 Ma age group formed by the Pan-Africa Orogeny (Figure 4-7). The Grenville basement was redistributed to the Precordillera region in South America during the early Paleozoic (Thomas et al., 2002), therefore, peri-Gondwanan terranes also have Grenvillian zircon grains of 1.3-0.9 Ga. Precambrian grains from the peri-Gondwana terranes should have a broad εHf values between -20 and +15, because they were from both Amazonia and West Africa (Henderson et al., 2016; 2018).

4. 7 DISCUSSION

4. 7.1 Paleodrainage during the Cambrian

The Cambrian sample has 86.0% population B, almost all of the grains are in the granite-rhyolite population, suggesting that the paleoriver mainly drained the granite-rhyolite province that was exposed in the Texas Arch to the north of Midland Basin (Figure 4-6). The Texas Arch was a Cambro-Ordovician structural high located on the southeastern flank of the larger Transcontinental Arch (e.g., Adams, 1954; Wright, 1979; Billo, 1985), and may have remained as a positive topographic feature during the Early Mississippian (Ruppel, 1985). The subordinate amount of Grenvillian grains were most likely directly derived from the Grenville basement, as part of the exhumed region of the Texas Arch. These grains cannot be recycled because the sample does not have grains of other age populations. The εHf values support this interpretation. This interpretation is also consistent with that of the Cambrian sandstone in the southern side of the Fort Worth Basin in east Texas (Alsalem et al., 2018), which has similar detrital zircon age distribution as in the Midland Basin.

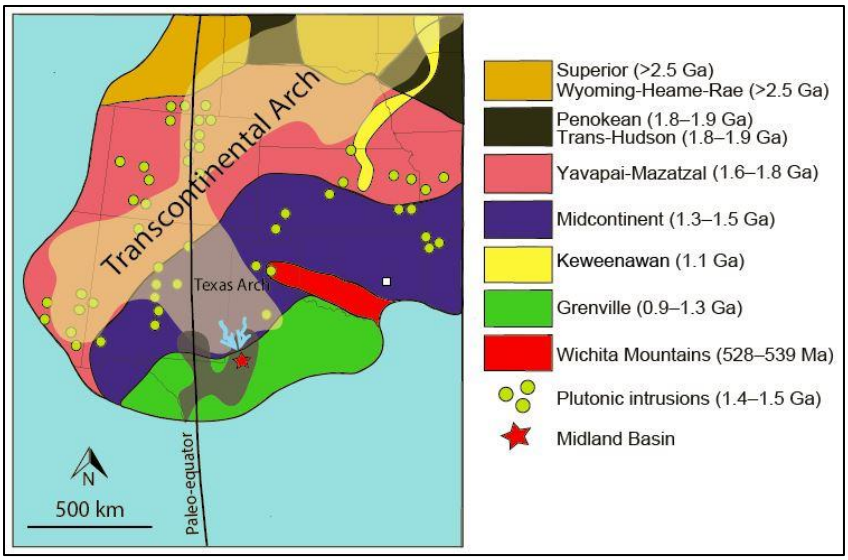

Figure 4-5 Paleogeographic map showing basement provinces in southern Laurentia and my inferred sediment dispersal (blue lines) from the Texas Arch to the Midland Basin area during the Late Cambrian. Modified after Alsalem et al. (2018).

4. 7.2 Sediment Provenance during the Late Pennsylvanian

The Pennsylvanian sample has grains from all the four populations. Grains of the Archean-Paleoproterozoic, the late Paleoproterozoic-early Mesoproterozoic and Grenvillian populations were either recycled from Neoproterozoic-Paleozoic sedimentary rocks on the southern margin of Laurentia or from the Peri-Gondwana terranes. Some grains of the late Paleoproterozoic-early Mesoproterozoic population may be directly derived from the ARM region located to the north and east of the basin. However, because of the low abundance of this group of zircons, ARM was not a major sediment source. The Grenvillian zircon grains could be directly derived from the Grenville basement, which was exhumed in the Appalachians during the late Paleozoic, or recycled from the Neoproterozoic-Paleozoic sedimentary rocks on the southern margin of Laurentia, or derived from the Peri-Gondwana terranes. The Grenvillian grains in the sample have two peaks, matching the ages of the Shawinigan (1.16–1.19 Ga) and the Ottawan (0.98–1.09 Ga) orogenies in the Appalachians (Heumann et al., 2006;

Bartholomew and Hatcher, 2010; Chiarenzelli et al., 2010; McLelland et al., 2010; Rivers et al., 2012). This pattern is also similar to that of the Paleozoic sedimentary rocks in the Appalachian foreland (Thomas et al., 2018) (Figure 4-6), suggesting that the Grenvillian grains were mainly from the Appalachians. This pattern is different from that of the Paleozoic strata in the midcontinent area (Konstantinou et al., 2014), lower Paleozoic strata in New Mexico (Amato and Mack, 2012), and Mesoproterozoic and Cambrian strata in West Texas (Spencer et al., 2014) (Figure 4-6), suggesting that the grains were not recycled. Thus, the grains were most likely directly derived from the Appalachians. The 2.2% of grains of 900-800 Ma and the Neoproterozoic-early Paleozoic population were derived mainly from the peri-Gondwana terranes (800-500 Ma) (Figure 4-6), which were incorporated in the Alleghania-Ouachita-Marathon orogenic belt. The Paleozoic grains younger than 500 Ma were ultimately from the Appalachians through direct erosion or recycling of grains in Paleozoic rocks. Therefore, sediments in the Late Pennsylvanian Canyon Group were derived from both the Appalachians on eastern Laurentia and peri-Gondwana terranes. The large variation of εHf values also support this interpretation (Figure 4-7). Detrital grains from the peri-Gondwana terranes in the Midland Basin were transported by regional rivers draining these terranes incorporated in the Ouachita orogeny (Figure 4-8). Direct input of detrital grains from the Appalachians into the Midland Basin requires one or more transcontinental rivers connecting the Midland Basin with the Appalachian foreland during the Pennsylvania (Figure 4-8).

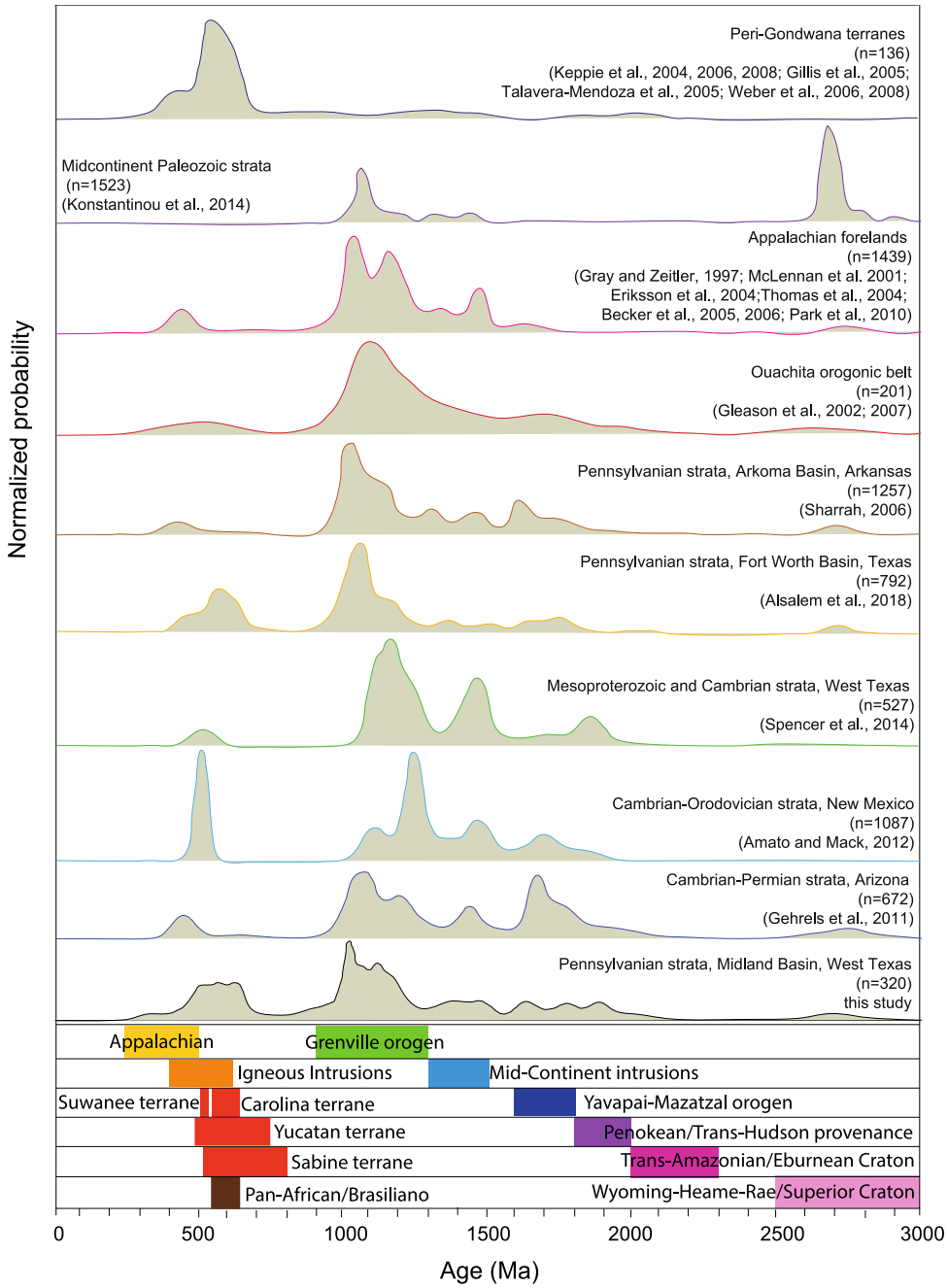

Figure 4-6 KDS plot of my Pennsylvanian sample is compared with Neoproterozoic and Paleozoic strata in peri-Gondwana terranes and other Laurentia geographic units.

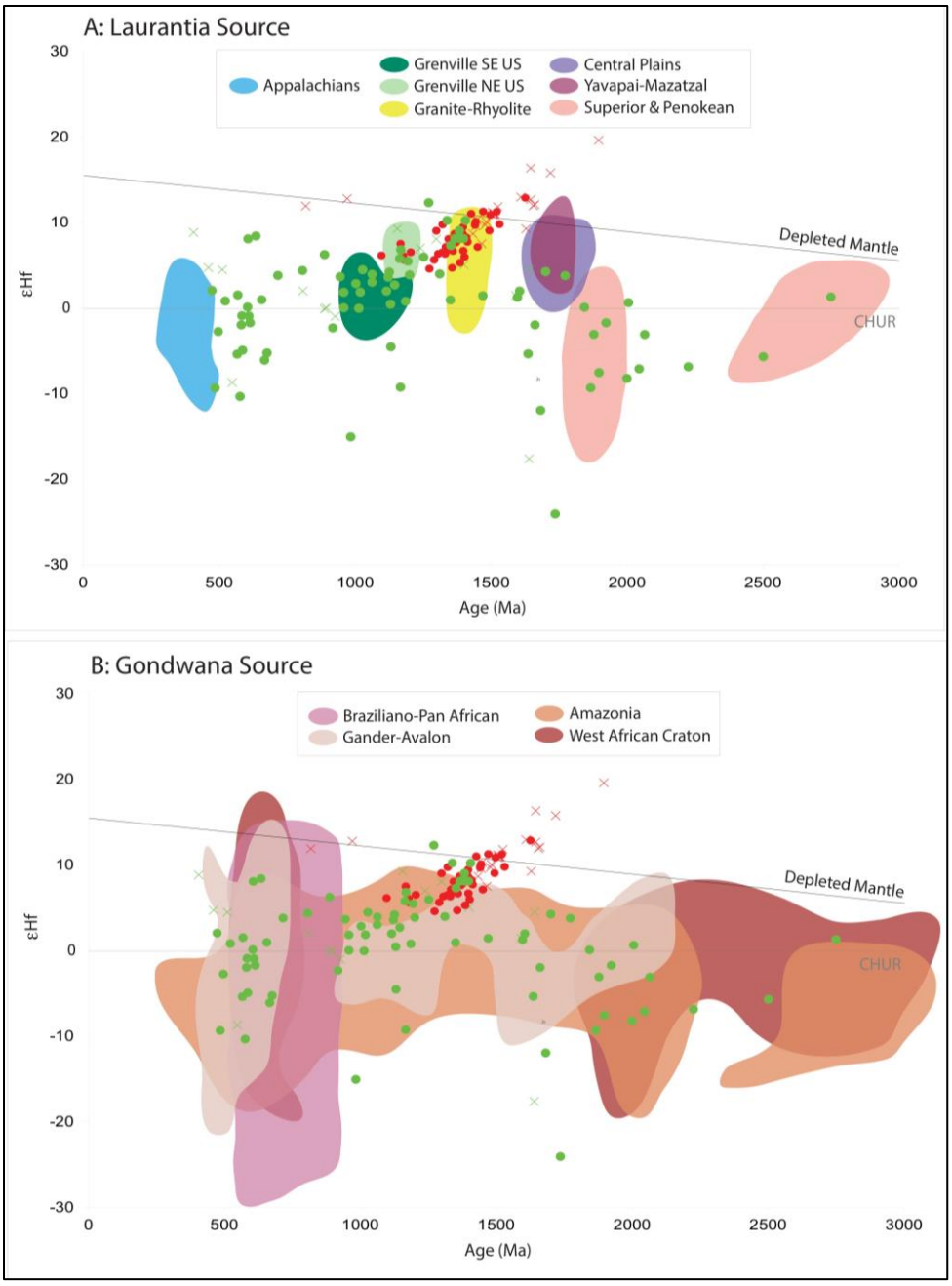

Figure 4-7 εHf values and U-Pb ages of the zircon grains of the two studied samples are compared with the values and ages of grains from the Laurentia sources (A) and Gondwana sources (B). Modified from Henderson et al. (2016); Oriolo et al. (2017); and Thomas et al. (2018).

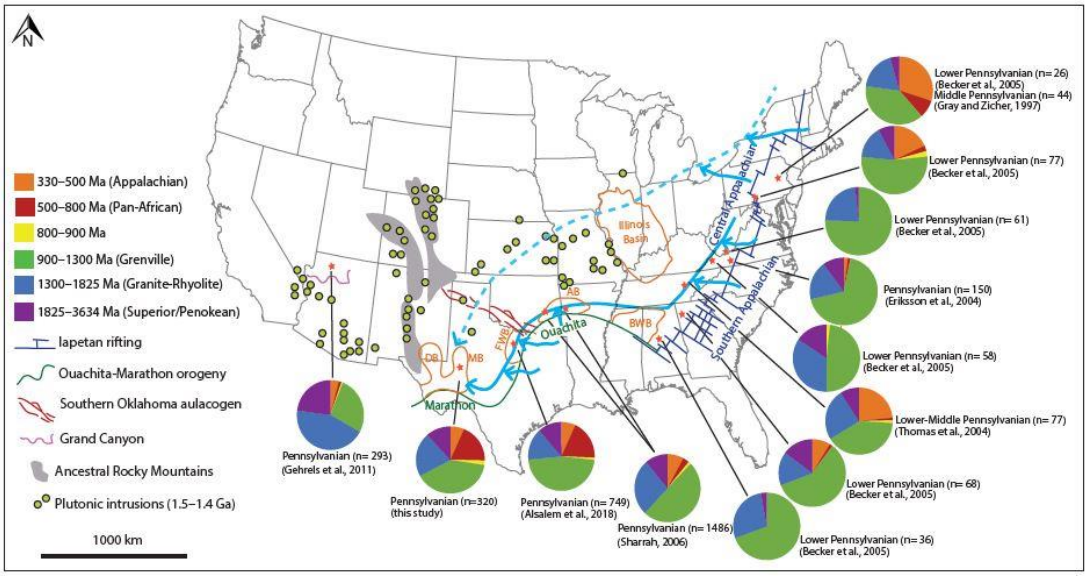

Figure 4-8 Relative abundance of zircon grains of populations A–E in southern and eastern Laurentia during the Pennsylvanian and the inferred paleodrainage of the rivers (blue lines) that brought sediments to the Midland Basin. The ages below the pie graphs represent the ages of the strata with detrital zircon studies. n is the total number of zircon data presented in each study. FWB—Fort Worth Basin; AB—Arkoma Basin; BWB—Black Warrior Basin. The long light blue arrow represents my inferred longitudinal river from the Appalachians, and the long blue dashed arrow represents the inferred river in Xie et al. (2019). See text for details. Modified after Alsalem et al. (2018).

4. 7.3 Late Pennsylvanian Transcontinental Rivers

The transcontinental river that delivered Appalachian detritus was likely developed in the Appalachian-Ouachita forelands. Graham et al. (1975) proposed that the Appalachian detritus were transported by a large longitudinal river flowed along the Appalachian and Ouachita foreland during the Pennsylvanian. A recent study has suggested that the river delivered sediments to the Fort Worth Basin in central Texas during the Pennsylvanian (Figure 4-6) (Alsalem et al., 2018). This river may have extended to West Texas during the Late Pennsylvanian. The deposition of deltaic Late Pennsylvanian siliciclastic rocks on the Eastern Shelf supports the interpretation of sediments derived generally from the east (Brown et al., 1990; Wright, 2011). The similarity of Pennsylvanian detrital

zircon signal between the Fort Worth and Midland Basins (Figure 4-7) suggest the connection of drainage between the two basins (Figure 4-8). The direct transport of sediments by the transcontinental river may be assisted by the progressive incorporation of synorogenic sediments within the orogen during the sequential closure of ocean basin as the collision proceeded (Figure 4-8) (Graham et al., 1975; Alsalem et al., 2018). This interpretation is further supported by the age population similarity between the Ouachita orogenic front and the Midland Basin (Gleason et al., 2002; 2007)

A different transcontinental river has been suggested to deliver Appalachian detritus into the Arkoma Basin during the Pennsylvanian (Sharrah, 2006; Xie et al., 2018). The detrital zircon age distribution of grains older than 900 Ma in the Arkoma Basin is very similar to that in the Appalachian basin (Figure 4-7). It was suggested that the river drained through the Illinois Basin before it entered the Ouachita foreland (Sharrah, 2006; Xie et al., 2018). A river of similar route was suggested to deliver Appalachian detritus to the Grand Canyon region as early as the Mississippian (Gehrels et al., 2011), and to the Delaware Basin during the middle Permian (Xie et al., 2019). Although a longitudinal river for sediment transport is my preferred provenance interpretation, other transcontinental river may exist in the midcontinent region to assist sediment dispersal into the Midland Basin during the Late Pennsylvanian (Figure 4-8). These rivers may emerge during marine lowstands and disappear during marine highstands.

4. 7.4 Implications for organic matter enrichment

In both the Fort Worth and Midland Basins, the Pennsylvanian strata contain shallow-water carbonate and shale and fluvial and deltaic sandstone of the Atoka, Strawn, Canyon and Cisco Groups (Brown et al., 1990; Wright, 2006; Wright, 2011). The carbonate and sandstone in both basins are conventional hydrocarbon reservoirs. The interbedded shale, for example, the Smithwick Formation, has an average TOC of 5-6% in parts of the Midland Basin (Wright, 2006) and 1.5% in the Fort Worth Basin in San Saba County (Hughes, 2011). These shales have been thought as the source rocks of the conventional reservoirs. They were not deposited in deep marine environment; thus, their high organic

matter contents are not likely related to deep marine anoxia environment in a similar way as the Mississippian Barnett Shale (Loucks and Ruppel, 2007). The high TOC in the Pennsylvanian shale may be related to change in sediment provenance. The organic matter in the Pennsylvanian strata are dominantly marine algal (Hughes, 2011), suggesting they are not directly from land. I propose that the erosion of silicate rocks in both the Appalachian and Ouachita orogens have brought abundant nutrients into the Fort Wort and Midland Basins, and led to high marine productivity.

Rivers carry large amounts of nutrients, including nitrogen, phosphorus and iron to ocean. River outflow is a well-known mechanism for coastal productivity. In coastal region, ~15% of the oceanic production, and most of the burial of organic carbon take place (Liu et al., 2000). Resuspension of nutrient in such regions by wind and tide can further increase coastal ocean primary production as well as open ocean production (Giraud et al., 2018). Collision between Laurentia and Gondwana formed the east-west oriented equatorial Central Pangea Mountains of ~1000 km wide and 5000-7000 km long during the Pennsylvanian (Ziegler et al., 1997). This Mountain belt has altered atmosphere circulation patterns and caused monsoon climate in western equatorial Pangea (Parrish, 1993; Tabor and Poulson, 2008). The orogenic events exhumed basement rocks of the Sabine terrane to the east of the Fort Worth Basin (Alsalem et al., 2018), as well as basement rocks in the Appalachians by the Alleghanian orogeny. Weathering of these silicate rocks may be enhanced by the monsoonal system. It is well documented that intense silicate weathering can alter ocean chemistry (Edmond, 1992). Intense silicate weathering also likely increases nutrient availability (Averbuch et al., 2005). Therefore, I suggest abundant nutrients transported by the Pennsylvanian rivers may have played an important control on marine productivity during the Pennsylvanian. The nutrients may have caused algal bloom and enhanced organic matter burial in the Midland and Fort Worth Basins.

4. 8 CONCLUSIONS

I study detrital zircon U-Pb ages and Hf isotope compositions to understand the sediment dispersal pathways into the Midland Basin before and during the Laurentia-Gondwana collision. Local

rivers draining the Texas arch to the north of the Midland Basin, which was part of the Paleozoic Transcontinental Arch, delivered Laurentia continental sediments to the southern Laurentia margin during the Cambrian. During the Late Pennsylvanian, sediments were dispersed to the Midland Basin located in the southwestern terminus of the Ouachita-Marathon belt by a transcontinental river in the Appalachian-Gondwana terranes in the Ouachita orogen. Sediment delivery during this time may be assisted by another transcontinental river connecting the Appalachian foreland with the northern Midland Basin through the midcontinent region. The Ancestral Rocky Mountains of the western U.S. were not a major source of the late Paleozoic sediments.

4. 9 REFERANCES CITED

Abati, J., Aghzer, A.M., Gerdes, A., and Ennih, N., 2012, Insights on the crustal evolution of the West African Craton from Hf isotopes in detrital zircons from the Anti-Atlas belt: Precambrian Res., v. 212-213, p. 263-274.

Adams, J.E., 1954, Mid-Paleozoic paleogeography of central Texas: San Angelo Geological Society Cambrian field trip, Llano area, March 19-20, p. 70-73.

Adams, J.E., 1965, Stratigraphic-tectonic development of Delaware Basin: American Association of Petroleum Geologists bulletin, v. 49, p. 2140-2148.

Alsalem, O.B., Fan, M., Zamora, J., Xie, X., and Griffin, W.R., 2018, Paleozoic sediment dispersal before and during the collision between Laurentia and Gondwana in the Fort Worth Basin, USA: Geosphere, v. 14, p. 325-342.

Amato, J.M., and Mack, G.H., 2012, Detrital zircon geochronology from the Cambrian-Ordovician Bliss Sandstone, New Mexico: Evidence for contrasting Grenville-age and Cambrian sources on opposite sides of the Transcontinental Arch: Geological Society of America Bulletin, v. 124, p. 1826-1840.

Averbuch, O., Tribovillard, N., Devleeschouwer, X., Riquier, L., Misiaen, B., and Vlie-Lance, B., 2005, Mountain building-enhanced continental weathering and organic carbon burial as major causes for climatic cooling at the Frasnian-Famennian boundary (c. 376 Ma)?: Terra Nova, v. 17, p. 25-34.

Avigad, D., Gerdes, A., Morag, N., and Bechstädt, T., 2012, Coupled U–Pb–Hf of detrital zircons of Cambrian sandstones from Morocco and Sardinia: implications for provenance and Precambrian crustal evolution of North Africa: Gondwana Res., v. 21, p. 690-703.

Ball, Mahlon, 1995, Permian Basin Province (044), in Gautier, D.L., Dolton, G.I., Takahashi, K.T., and Varnes, K.L., eds., 1995, National Assessment of United States Oil and Gas Resources—Results, Methodology, and Supporting Data: U.S. Geological Survey Digital Data Series DDS-30.

Bartholomew, M.J., and Hatcher, R.D., Jr., 2010, The Grenville orogenic cycle of southern Laurentia: Unraveling sutures, rifts, and shear zones as potential piercing points for Amazonia: Journal of South American Earth Sciences, v. 29, p. 4-20, doi:10.1016/j.jsames.2009.08.007.

Becker, T.P., Thomas, W.A., Samson, S.D., and Gehrels, G.E., 2005, Detrital zircon evidence of Laurentian crustal dominance in the lower Pennsylvanian deposits of the Alleghanian clastic wedge in eastern North America: Sedimentary Geology, v. 182, p. 59-86.

Berg, R.R., 1979, Reservoir sandstones of the Delaware Mountain Group, southeast New Mexico, in Sullivan, N.M., ed., Guadalupian Delaware Mountain Group of West Texas and New Mexico: SEPM, Permian Basin Section, Field Conference Guidebook, Publication 79-18, p. 75-95.

Blichert-Toft, J., 2008, The Hf isotopic composition of zircon reference material 91500: Chemical Geology, v. 253, p. 252-257.

Bickford, M.E., Soegaard, K., Nielsen, K.C., and McLelland, J.M., 2000, Geology and geochronology of Grenville-age rocks in the Van Horn and Franklin Mountains area, West Texas:

Implications for the tectonic evolution of Laurentia during the Grenville: Geological Society of America Bulletin, v. 112, p.1134-1148.

Billo, S.M., 1985, The Transcontinental Arch and its Relation to the Colorado oil and mineral belt: Journal of Petroleum Geology, v. 8, p. 343-352.

Black, L.P, Kamo, S.L., Allen, C.M., Davis, D.W., Aleinikoff, J.N., Valley, J.W., Mundil, R., Campbell, I.H., Korsch, R.J., Williams, I.S., and Foudoulis, C., 2004, Improved $^{206}Pb/^{238}U$ microprobe geochronology by the monitoring of a trace element-related matrix effect: SHRIMP, ID-TIMS, ELA-ICP-MS, and oxygen isotope documentation for a series of zircon standards: Chemical Geology, v. 2015, p. 115-140.

Bouvier, A., Vervoort, J.D., Patchett, P.J., 2008, The Lu–Hf and Sm–Nd isotopic composition of CHUR: constraints from unequilibrated chondrites and implications for the bulk composition of terrestrial planets: Earth and Planetary Science Letters, v. 273, p. 48-57.

Bozanich, R.G., 1979, The Bell Canyon and Cherry Canyon formations, eastern Delaware Basin, Texas; lithology, environments and mechanisms of deposition, in Sullivan, N.M., ed., Guadalupian Delaware Mountain Group of West Texas and Southeast New Mexico, Society of Economic Paleontologists and Mineralogists Permian Basin Section Publication 79-18, p. 121-141.

Broadhead, R.F., and King, W.E., 1988, Petroleum geology of Pennsylvanian and Lower Permian strata, Tucumcari Basin, east-central New Mexico: New Mexico Bureau of Mines and Mineral Resources Bulletin, v. 119, 75 p.

Broadhead, R.F., Raatz, W.D., Dutton, S.P., and Kim, E.M., 2004, Play analysis and digital portfolio of major oil reservoirs in the Permian Basin: New Mexico [abs.]: American Association of Petroleum Geologists Annual Meeting Expanded Abstracts, v. 13, p. 17.

Brown, L.F., JR., Iriarte, R.F.S., and Johns, D.A., 1990, Regional depositional systems tracts, paleogeography, and sequence stratigraphy, Upper Pennsylvanian and Lower Permian strata,

north-central Texas: The University of Texas at Austin, Bureau of Economic Geology, Reports of Investigations 197, 116 p., 27 plates.

Cawood, P.A., and Nemchin, A.A., 2001, Source regions for Laurentian margin sediments: Constraints from U/Pb dating of detrital zircon in the Newfoundland Appalachians: Geological Society of America Bulletin, v. 113, p. 1234-1246.

Chang, Z., Vervoort, J.D., McClelland, W.C. and Knaack, C., 2006, U–Pb dating of zircon by LA-ICP-MS: Geochemistry, Geophysics, Geosystems, v. 7, doi:10.1029/2005GC001100.

Chiarenzelli, J., Regan, S., Peck, W.H., Selleck, B.W., Cousens, B., Baird, G.B., and Shrady, C.H., 2010, Shawinigan arc magmatism in the Adirondack Lowlands as a consequence of closure of the Trans-Adirondack backarc basin: Geosphere, v. 6, p.900-916.

Dickinson, W.R., and Gehrels, G.E., 2009, U-Pb ages of detrital zircons in Jurassic eolian and associated sandstones of the Colorado Plateau: Evidence for transcontinental dispersal and intraregional recycling of sediment: Geological Society of America Bulletin, v. 121, p. 408-433.

Dickinson, W.R, and Lawton, T.F., 2003, Sequential intercontinental suturing as the ultimate control for Pennsylvanian Ancestral Rocky Mountains deformation: Geology, v. 31, p. 609-612.

Dutton, S.P., Holtz, M.H., Tremblay, T.A., and Zirzcy, H.H., 2000, Expansion of gas reserve database, Permian Basin, Texas, in DeMis, W.D., Nelis, M.K., and Trentham, R.C., eds., The Permian Basin: Proving ground for tomorrow's technologies: West Texas Geological Society, Publication no. 00-109, p. 197-204.

Dutton, S.P., Kim, E.M., Broadhead, R.F., Breton, C.L., Raatz, W.D., Ruppel, S.C., and Kerans, C., 2004, Play analysis and digital portfolio of major oil reservoirs in the Permian basin: Application and transfer of advanced geological and engineering technologies for incremental production opportunities: Bureau of Economic Geology and New Mexico Bureau of Geology and Mineral Resources, 428 p.

Dutton, S.P, Kim, E.M., Broadhead, R.F., Raatz, W.D., Breton, C.L., Ruppel, S.C, and Kerans, C., 2005, Play analysis and leading-edge oil-reservoir development methods in the Permian basin: Increased recovery through advanced technologies: American Association of Petroleum Geologists Bulletin, v. 89, p. 553-576.

Edmond, J. M., 1992, Himalayan tectonics, weathering processes and the strontium isotope record in marine limestones: Science, v. 258, p. 1594-1597.

Elebiju, O.O., Keller, G.R., and Marfurt, K.J., 2010, Case History: Investigation of links between Precambrian basement structure and Paleozoic strata in the Fort Worth basin, Texas, U.S.A., using high-resolution aeromagnetic, HRAM data and seismic attributes: Geophysics, v. 75, p. B157-B168.

Eriksson, K.A., Campbell, I.H., Palin, J.M., Allen, C.M., and Bock, B., 2004, Evidence for multiple recycling in Neoproterozoic through Pennsylvanian sedimentary rocks of the central Appalachian Basin: The Journal of Geology, v. 112, p. 261-276. doi:10.1086/382758.

Erlich, R. N., and J. L. Coleman, 2005, Drowning of the Upper Marble Falls Carbonate Platform (Pennsylvanian), central Texas: A case of conflicting 'signals?': Sedimentary Geology, v. 175, p. 479-499.

Fisher, C.M., Hanchar, J.M., Samson, S.D., Dhuime, B., Blichert-Toft, J., Vervoort, J.D., and Lam, R., 2011, Synthetic zircon doped with hafnium and rare earth elements: A reference material for in situ hafnium isotope analysis: Chemical Geology, v. 286, p. 32-47.

Fisher, C.M., Vervoort, J.D., and DuFrane, S.A., 2014a, Accurate Hf isotope determinations of complex zircons using the "laser ablation split stream" method: Geochemistry, Geophysics, Geosystems, v. 15, p. 121-139.

Fisher, C.M., Vervoort, J.D., and Hanchar, J.M., 2014b, Guidelines for reporting zircon Hf isotopic data by LA-MC-ICPMS and potential pitfalls in the interpretation of these data: Chemical Geology, v. 363, p. 125-133.

Frenzel, H. N., et al., 1988, The Permian Basin region, in Sloss, L. L., ed., Sedimentary Cover: North American Craton: Geological Society of America, The Geology of North America, v. D-2, p. 261-306.

Galley, J.E., 1958, Oil and Geology in the Permian Basin of Texas and New Mexico, in Weeks, L.G., ed., Habitat of Oil: The American Association of Petroleum Geologists Special Publication, p. 395-446.

Gärtner, A., Villeneuve, M., Linnemann, U., Gerdes, A., Youbi, N., Guillou, O., and Rjimati, E.-C., 2014, History of the West African Neoproterozoic Ocean: key to the geotectonic history of circum-Atlantic Peri-Gondwana (Adrar Souttouf Massif, Moroccan Sahara): Gondwana Res., v. 29, p. 220-233.

Gehrels, G.E., Blakey, R., Karlstrom, K.E., Timmons, J.M., Dickinson, W.R., and Pecha, M., 2011, Detrital zircon U-Pb geochronology of Paleozoic strata in the Grand Canyon, Arizona: Lithosphere, v. 3, p. 183-200.

Giraud, X., le Quéré, C., and da Cunha, L. C., 2008, Importance of coastal nutrient supply for global ocean biogeochemistry: Global Biogeochemical Cycles, v. 22, GB2025, doi:10.1029/2006GB002717.

Gilbert, M.C., and Denison, R.E., 1993, Late Proterozoic to Early Cambrian basement of Oklahoma, in Reed, J.C., Jr., Bickford, M.E., Houston, R.S., Link, P.K., Rankin, D.W., Sims, P.K., and Van Schmus, W.R., eds., Precambrian: Conterminous U.S.: Geological Society of America, The Geology of North America, v. C-2, p. 303-314.

Gleason, J.D., Patchett, P.J., Dickinson, W.R., and Ruiz, J., 1994, Nd isotopes link Ouachita turbidites to Appalachian sources: Geology, v. 22, p. 347-350.

Gleason, J.D., Patchett, P.J., Dickinson, W.R., and Ruiz, J., 1995, Nd isotopic constraints on sediment sources of the Ouachita-Marathon fold belt: Geological Society of America Bulletin, v. 107, p. 1192-1210.

Gleason, J.D., Finney, S.C., and Gehrels, G.E., 2002, Paleotectonic implications of a mid-to late-Ordovician provenance shift, as recorded in sedimentary strata of the Ouachita and southern Appalachian mountains: The Journal of geology, v. 110, p. 291-304.

Gleason, J.D., Gehrels, G.E., Dickinson, W.R., Patchett, P.J., and Kring, D.A., 2007, Laurentian sources for detrital zircon grains in turbidite and deltaic sandstones of the Pennsylvanian Haymond Formation, Marathon assemblage, West Texas, USA: Journal of Sedimentary Research, v. 77, p. 888-900.

Graham, S.A., Dickinson, W.R., and Ingersoll, R.V., 1975, Himalayan– Bengal model for flysch dispersal in the Appalachian–Ouachita system: Geological Society of America Bulletin, v. 86, p. 273-286.

Granata Jr, W.H., 1963, Cretaceous stratigraphy and structural development of the Sabine Uplift area, Texas and Louisiana, in Report on Selected North Louisiana and South Arkansas oil and gas fields and Regional Geology: Shreveport Geological Society Reference Report, v. 5, p. 50-95.

Hatcher, R.D. Jr. 1989, Tectonic synthesis of the U.S. Appalachians, in Hatcher, R.D., Jr., W.A. Thomas, and G.W. Viele, eds., The Appalachian-Ouachita Orogen in the United States: Geological Society of America Decade of North American Geology, v. F2, p. 29-41.

Henderson, B.J., Collins, W.J., Murphy, J.B., Gutierrez-Alonso, G., and Hand, M., 2016, Gondwanan basement terranes of the Variscan–Appalachian orogen: Baltican, Saharan and West African hafnium isotopic fingerprints in Avalonia, Iberia and the Armorican Terranes: Tectonophysics, v. 681, p. 278-304.

Henderson, B.J., Collins, W.J., Murphy, J.B., and Hand, M., 2018, A hafnium isotopic record of magmatic arcs and continental growth in the Iapetus Ocean: The contrasting evolution of Ganderia and the peri-Laurentian margin: Gondwana Research, v. 58, p. 141-160.

Heumann, M.J., Bickford, M.E., Hill, B.M., McLelland, J.M., Selleck, B.W., and Jercinovic, M.J., 2006, Timing of anatexis in metapelites from the Adirondack lowlands and southern

highlands: A manifestation of the Shawinigan orogeny and subsequent anorthosite-mangerite-charnockite-granite magmatism: Geological Society of America Bulletin, v. 118, p. 1283-1298.

Hibbard, J., and Karabinos, P., 2013, Disparate paths in the geologic evolution of the northern and southern Appalachians: A case for inherited contrasting crustal/lithospheric substrates: Geoscience Canada, v. 40, p. 303-317, doi:10.12789/geocanj.2013.40.021.

Hibbard, J.P., Stoddard, E.F., Secor, D.T., and Dennis, A.J., 2002, The Carolina Zone: overview of Neoproterozoic to early Paleozoic peri-Gondwanan terranes along the eastern flank of the southern Appalachians: Earth-Science Reviews, v. 57, p. 299-339, doi:10. 1016/S0012-8252(01)00079-4.

Hibbard, J.P., van Staal, C.R., and Miller, B.V., 2007, Links between Carolinia, Avalonia and Ganderia in the Appalachian periGondwanan realm, in Sears, J., Harms, T., and Evenchick C., eds., From Whence the Mountains?: Inquiries into the Evolution of Orogenic Systems: A Volume in Honor of Raymond A. Price, GSA Special Paper 433, p. 291-311.

Hogan, J.P., and Gilbert, M.C., 1998, The Southern Oklahoma aulacogen: A Cambrian analog for Mid-Proterozoic AMCG (anorthosite-mangerite-charnockite-granite) complexes?: Basement Tectonics 12, volume 6 of the series Proceedings of the International Conferences on Basement Tectonics, p. 39-78.

Horak, R. L., 1985, Tectonic and hydrocarbon maturation history in the Permian basin: Oil & Gas Journal, May 27, v. 83, p. 124-129.

Hughes, 2011, Chemostratigraphy And Paleoenvironment Of The Smithwick Formation, Fort Worth Basin, San Saba County, Texas [M.S. Thesis], The University of Texas at Arlington, TX, 93 p.

Hull Jr, J.P., 1957, Petrogenesis of Permian Delaware Mountain Sandstone, Texas and New Mexico: American Association of Petroleum Geologists Bulletin, v. 41, p. 278-307.

Ibanez-Mejia, M., Pullen, A., Arenstein, J., Gehrels, G.E., Valley, J., and Ducea, M.N., et al., 2015, Unraveling crustal growth and reworking processes in complex zircons from orogenic lower-crust: The Proterozoic Putumayo Orogen of Amazonia: Precambrian Res., v. 267, p. 285-310.

Johnson, K.S., Amsden, T.W., Denison, R.E., Dutton, S.P., Goldstein, A.G., Rascoe, B., Jr., Sutherland, P.K., and Thompson, D.M., 1988, Southern Midcontinent region, in Sloss, L.L., ed., Sedimentary Cover–North American Craton: U.S.: Geological Society of America, The Geology of North America, v. D-2, p. 307-359.

Jones, R.H., 2009, THE Middle-Upper Ordovician Simpson Group of the Permian Basin: Deposition, Diagenesis, and Reservoir Development: Texas, Bureau of Economic Geology, The University of Texas at Austin, 41 p.

Keppie, J.D., Dostal, J., Murphy, J.B., and Nance, R.D., 2008, Synthesis and tectonic interpretation of the westernmost Paleozoic Variscan orogen in southern Mexico: from rifted Rheic margin to active Pacific margin: Tectonophysics, v. 461, p. 277-290.

Keppie, J.D., Nance, R.D., Murphy, J.B., and Dostal, J., 2003, Tethyan, Mediterranean, and Pacific analogues for the Neoproterozoic–Paleozoic birth and development of peri-Gondwanan terranes and their transfer to Laurentia and Laurussia: Tectonophysics, v. 365, p. 195-219.

Kocurek, G., and Kirkland, B.L., 1998, Getting to the source; aeolian influx to the Permian Delaware Basin region: Sedimentary Geology, v. 117, p. 143-149. doi:10.1016/S0037-0738(98)00024-4.

Konstantinou, A., Wirth, K.R., Vervoort, J.D., Malone, D.H., Davidson, C., and Craddock, J.P., 2014, Provenance of quartz arenites of the early Paleozoic midcontinent region, USA: The Journal of Geology, v. 122, p. 201-216, doi:10.1086/675327.

King, P.B., 1948, Geology of the southern Guadalupe Mountains, Texas: US Government Printing Office Professional Paper 215.

Kröner, A., Ekwueme, B.N., and Pidgeon, R.T., 2001, The oldest rocks in West Africa: SHRIMP zircon age for early Archean migmatitic orthogneiss at Kaduna, northern Nigeria: The Journal of Geology, v. 109, p.399-406.

Leary, R.J., Umhoefer, P., Smith, M.E., and Riggs, N., 2017. A three-sided orogen: A new tectonic model for Ancestral Rocky Mountain uplift and basin development: Geology, v. 45, p. 735-738, doi:10.1130/G39041.1.

Linnemann, U., McNaughton, N.J., Romer, R.L., Gehmlich, M., Drost, K., and Tonk, C., 2004, West African provenance for Saxo–Thuringia (Bohemian Massif): did Armorica ever leave pre-Pangean Gondwana?–U/Pb-SHRIMP zircon evidence and the Nd-isotopic record: International Journal of Earth Science, v. 93, p. 683-705.

Linnemann, U., Gerdes, A., Hofmann, M., and Marko, L., 2014, The Cadomian Orogen: Neoproterozoic to Early Cambrian crustal growth and orogenic zoning along the periphery of the West African Craton — constraints from U–Pb zircon ages and Hf isotopes (Schwarzburg Antiform, Germany): Precambrian Research, v. 244, p. 236-278.

Liu, K. K., Iseki, K., and Chao, S.Y., 2000, Continental margin carbon fluxes, in Hanson, R. B., Ducklow, H. W., and Field, J.G., eds., The Changing Ocean Carbon Cycl, Cambridge University Press, New York, p. 187–239.

Loomis, J., Weaver, B., and Blatt, H., 1994, Geochemistry of Mississippian tuffs from the Ouachita Mountains, and Implications for the Tectonic of the Ouachita orogen, Oklahoma and Arkansas: Geological Society of America Bulletin, v.106, p. 1158-1171.

Loucks, R., 2010, Review of the Lower Ordovician Ellenburger Group of the Permian Basin, West Texas: Texas, Bureau of Economic Geology, The University of Texas at Austin, 92 p.

Loucks, R.G., and Ruppel, S.C., 2007, Mississippian Barnett Shale: Lithofacies and depositional setting of a deep-water shale-gas succession in the Fort Worth Basin, Texas: American Association of Petroleum Geologists Bulletin, v. 91, p. 579-601.

Ludwig, K.R., 2003, User's Manual for Isoplot/Ex, Version 3.0, A geochronological toolkit for Microsoft Excel: Berkeley Geochronology Center Special Publication, v. 4, Berkeley Geochronology Center, 2455 Ridge Road, Berkeley, CA 94709, USA.

Martens, U., Weber, B., and Valencia, V.A., 2010, U/Pb geochronology of Devonian and older Paleozoic beds in the southeastern Maya block, Central America: Its affinity with peri-Gondwanan terranes: Geological Society of America Bulletin, v. 122, p. 815-829.

Matteini, M., Junges, S.L., Dantas, E.L., Pimentel, M.M., and Bühn, B., 2010, In situ zircon U–Pb and Lu–Hf isotope systematic on magmatic rocks: Insights on the crustal evolution of the Neoproterozoic Goiás Magmatic Arc, Brasília belt, Central Brazil: Gondwana Res., v. 17, p. 1-12.

Mazzullo, J., Malicse, A., and Siegel, J., 1991, Facies and depositional environments of the Shattuck Sandstone on the northwestern shelf of the Permian Basin: Journal of Sedimentary Petrology, v. 61, p. 940-958. doi:10.1306/D4267811-2B26-11D7-8648000102C1865D.

McGee, B., Collins, A.S., Trindade, R.I., and Payne, J., 2015, Age and provenance of the Cryogenian to Cambrian passive margin to foreland basin sequence of the northern Paraguay Belt, Brazil: Geological Society of America Bulletin., v. 127, p. 76-86.

McLelland, J.M., Selleck, B.W., Bickford, M.E., Tollo, R.P., Bartholomew, M.J., Hibbard, J.P., and Karabinos, P.M., 2010, Review of the Proterozoic evolution of the Grenville Province, its Adirondack outlier, and the Mesoproterozoic inliers of the Appalachians: From Rodinia to Pangea: The Lithotectonic Record of the Appalachian Region: Geological Society of America Memoir, v. 206, p. 21-49.

Merrill, M.D., Slucher, E.R., Roberts-Ashby, T.L., Warwick, P.D., Blondes, M.S., Freeman, P.A., Cahan, S.M., DeVera, C.A., and Lohr, C.D., 2015, Geologic Framework for the National Assessment of Carbon Dioxide Storage Resources-Permian and Palo Duro Basins and Bend Arch–Fort Worth Basin, in Warwick P. D., and Corum, M. D., eds., Chapter K of Geologic

Framework for the National Assessment of Carbon Dioxide Storage Resources: US Geological Survey Open-File Report 2012-2014-K, 42 p.

Miall, A.D., 2008, The southern Midcontinent, Permian Basin, and Ouachitas, in Miall, A.D., and Hsu, K.J., eds., The Sedimentary Basins of the United States and Canada: Amsterdam, Elsevier, p. 297-328.

Moecher, D.P., and Samson, S.D., 2006, Differential zircon fertility of source terranes and natural bias in the detrital zircon record: Implications for sedimentary provenance analysis: Earth and Planetary Science Letters, v. 247, p. 252-266.

Montgomery, S.L., 1998, Thirtyone Formation, Permian Basin, Texas: Structural and Lithologic Heterogeneity in a Lower Devonian Chert Reservoir: American Association of Petroleum Geologists Bulletin, v. 82, p. 1-24, doi:10.1306/1D9BC381-172D-11D7-8645000102C1865D.

Mueller, P.A., Heatherington, A.L., Wooden, J.L., Shuster, R.D., Nutman, A.P., and Williams, I.S., 1994, Precambrian zircons from the Florida basement: A Gondwanan connection: Geology, v. 22, p. 119-122.

Mueller, P.A., Heatherington, A.L., Kelly, D.M., Wooden, J.L. and Mogk, D.W., 2002, Paleoproterozoic crust within the Great Falls tectonic zone: Implications for the assembly of southern Laurentia: Geology, v. 30, p. 127-130.

Mueller, P.A., Heatherington, A.L., Foster, D.A., Thomas, W.A., and Wooden, J.L., 2014, The Suwannee suture: Significance for Gondwana-Laurentia terrane transfer and formation of Pangaea: Gondwana Research, v. 26, p. 365-373.

Mueller, P.A., Kamenov, G.D., Heatherington, A.L., and Richards, J., 2008, Crustal evolution in the Southern Appalachian Orogen: evidence from Hf isotopes in detrital zircons: Journal of Geology, v. 116, p. 414-422.

Murphy, J.B., Eguiluz, L., and Zulauf G., 2002, Cadomian orogens, periGondwanan correlatives and Laurentia-Baltica connections: Tectonophys, v. 352, p. 1-9.

Murphy, J.B., Pisarevsky, S.A., Nance, R.D., and Keppie, J.D., 2004, Neoproterozoic—Early Paleozoic evolution of peri-Gondwanan terranes: implications for Laurentia-Gondwana connections: International Journal of Earth Sciences, v. 93, p. 659-682.

Murphy, J.B., Gutierrez-Alonso, G., Nance, R.D., Fernandez-Suarez, J., Keppie, J.D., Quesada, C., Strachan, R.A., and Dostal, J., 2006, Origin of the Rheic Ocean: Rifting along a Neoproterozoic suture?: Geology, v. 34, p. 325-328.

Murphy, R.J., 2015, Depositional systems interpretation of early Permian mixed siliciclastics and carbonates, Midland Basin, Texas [M.S. Thesis], Indiana University, 109 p.

Nance, R.D., and Linnemann, U., 2008, The Rheic Ocean: origin, evolution, and significance: Geological Society of America Today, v. 18, p. 4-12.

Nance, R.D., Murphy, J.B., and Keppie, J.D., 2002, A Cordilleran model for the evolution of Avalonia: Tectonophysics, v. 352, p. 11-31.

Nance, R.D., Gutiérrez-Alonso, G., Keppie, J.D., Linnemann, U., Murphy, J.B., Quesada, C., Strachan, R.A. and Woodcock, N.H., 2010, Evolution of the Rheic ocean: Gondwana Research, v. 17, p. 194-222.

Newell, N.D., Bradley, J.S., Whiteman, A.J., and Fischer, A.G., 1953, The Permian reef complex of the Guadalupe Mountains region, texas and New Mexico: A study in paleoecology: San Francisco, W.H. Freeman and Co., 236 p.

Nunn, J.A., 2012, Burial and thermal history of the Haynesville shale: Implications for overpressure, gas generation, and natural hydrofracture: Gulf Coast Association of Geological Societies, v. 1, p. 81-96.

Opdyke, N.D., Jones, D.S., MacFadden, B.J., Smith, D.L., Mueller, P.A., and Shuster, R.D., 1987, Florida as an exotic terrane: Paleomagnetic and geochronologic investigation of lower Paleozoic rocks from the subsurface of Florida: Geology, v. 15, p. 900-903.

Oriolo, S., Oyhantçabal, P., Wemmer, K., and Siegesmund, S., 2017, Contemporaneous assembly of Western Gondwana and final Rodinia break-up: Implications for the supercontinent cycle: Geoscience Frontiers, v. 8, p.1431-1445.

Paces, J.B., and Miller, J.D., 1993, Precise U-Pb Ages of the Duluth Complex and Related Mafic Intrusions, Northeastern Minnesota: Geochronological Insights to Physical, Petrogenetic, Paleomagnetic, and Tectonomagmatic Processes Associated With the 1.1 Ga Midcontinent Rift System: Journal of Geophysical Research, v. 98, p. 13,997-14,013.

Park, H., Barbeau Jr, D.L., Rickenbaker, A., Bachmann-Krug, D., and Gehrels, G., 2010, Application of foreland basin detrital-zircon geochronology to the reconstruction of the southern and central Appalachian orogen: The Journal of Geology, v.118, p. 23-44.

Parrish, J. T., 1993, Climate of the supercontinent Pangaea: The Journal of Geology, v. 101, p. 215-233.

Paton, C., Hellstrom, J., Paul, B., Woodhead, J., and Hergt, J., 2011, Iolite: Freeware for the visualisation and processing of mass spectrometric data: Journal of Analytical Atomic Spectrometry, v. 26, p. 2508-2518.

Payne, M.W., 1976, Basinal sandstone facies, Delaware Basin, West Texas and southeast New Mexico: American Association of Petroleum Geologists Bulletin, v. 60, p. 517-527.

Pollock, J. 2010, Middle Cambrian to Ordovician arc-backarc development on the leading edge of Ganderia, Newfoundland Appalachians, in Tollo, R. P., Bartholomew, M. J., Hibbard, J. P., and Karabinos P. M., eds., From Rodinia to Pangea: the Lithotectonic Record of the Appalachian Region, Geological Society of America Memoir 206, p. 367-396.

Pollock, J.C., Hibbard, J.P., and Sylvester, P.J., 2009, Early Ordovician rifting of Avalonia and birth of the Rheic Ocean: U–Pb detrital zircon constraints from Newfoundland: Journal of the Geological Society, v. 166, p. 501-515.

Poole, F.G., Perry, W.J., Madrid, R.J., and Martinez, R.A., 2005, Tectonic synthesis of the Ouachita-Marathon-Sonora orogenic margin of southern Laurentia: Stratigraphic and structural implications for timing of deformational events and plate-tectonic model: Geological Society of America Special Papers, v. 393, p. 543-596.

Pope, M.C., 2004, Cherty carbonate facies of the Montoya Group, southern New Mexico and western Texas and its regional correlatives: a record of Late Ordovician paleoceanography on southern Laurentia: Palaeogeography, Palaeoclimatology, Palaeoecology, v. 210, p. 367-384.

Rankin, D.W., Drake, A.A., Jr., Glover, L., III, Goldsmith, R., Hall, L.M., Murray, D.P., Ratcliffe, N.M., Read, J.F., Secor, D.T., Jr., and Stanley, R.S., 1989, Pre-orogenic terranes, in Hatcher, R.D., Jr., Thomas, W.A., and Viele, G.W., eds. The Appalachian-Ouachita Orogen in the United States: Geological Society of America, Geology of North America, v. F-2, p. 7-100.

Reimann, C., Bahlburg, H., Kooijman, E., Berndt, J., Gerdes, A., Carlotto, V., and Lopez, S., 2010, Geodynamic evolution of the early Paleozoic Western Gondwana margin 14–17 S reflected by the detritus of the Devonian and Ordovician basins of southern Peru and northern Bolivia: Gondwana Research, v. 18, p. 370-384.

Rivers, T., Culshaw, N., Hynes, A., Indares, A., Jamieson, R., and Martignole, J., 2012, The Grenville orogen—A post-LITHOPROBE perspective, in Percival, J.A., Cook, F.A., and Clowes, R.M., eds., Tectonic Styles in Canada: The LITHOPROBE Perspective: Geological Association of Canada Special Paper 49, p. 97-236.

Robinson, K., 1988, Petroleum Geology and Hydrocarbon Plays of the Permian Basin Petroleum Province West Texas and Southeast New Mexico: U.S. Geological Survey Open-File Report 1988-450Z.

Rollinson, H., 2016, Archaean crustal evolution in West Africa: A new synthesis of the Archaean geology in Sierra Leone, Liberia, Guinea and Ivory Coast: Precambrian Research, v. 281, p.1-12.

Ruppel, S.C., 1985, Stratigraphy and petroleum potential of pre-Pennsylvanian rocks, Palo Duro Basin, Texas Panhandle: University of Texas at Austin. Bureau of Economic Geology, Report of investigations No. 147, p. 71-73.

Ruppel, S.C., 2008, The Fusselman of the Permian Basin: Patterns in Depositional and Diagenetic Facies Development on a Stable Platform During the Late Ordovician-Early Silurian Icehouse: Bureau of Economic Geology, Jackson School of Geosciences, Permian Basin Geological Synthesis Project Report, p.1-13.

Samson, S.D., Secor, D.T., and Hamilton, M.A., 2001, Wandering Carolina: Tracking exotic terranes with detrital zircons [abs.]: Geological Society of America Abstracts with Programs, v. 33, p. 263.

Samson, S., Hibbard, J., and Wortman, G., 1995, Nd isotopic evidence for juvenile crust in the Carolina terrane, southern Appalachians: Contributions to Mineralogy and Petrology, v. 121, p. 171–184, doi:10.1007/s004100050097.

Santos, J.O.S., Hartmann, L.A., Gaudette, H.E., Groves, D.I., Mcnaughton, N.J., and Fletcher, I.R., 2000, A new understanding of the provinces of the Amazon Craton based on integration of field mapping and U-Pb and Sm-Nd geochronology: Gondwana Research, v. 3, p.453-488.

Sarg, J.F., Markello, J.R., and Weber, L.J., 1999, The second-order cycle, carbonate-platform growth, and reservoir, source, and trap prediction: Special publications of SEPM, no. 63, p. 11-34.

Scholle, P.A., Goldstein, R.H., and Ulmer-Scholle, D.S., 2007, Classic upper Paleozoic reefs and bioherms of West Texas and New Mexico, a field guide to the Guadalupe and Sacramento Mountains of West Texas and New Mexico: New Mexico Bureau of Geology and Mineral Resources Open-file Report 504, 174 p.

Sharrah, K.L., 2006, Comparative Study of the Sedimentology and Provenance of the Atoka Formation in the Frontal Ouachita Thrust Belt, Oklahoma [Ph.D. Dissertation], University of Tulsa, 268 p.

Silva-Romo, G., Mendoza-Rosales, C.C., Campos-Madrigal, E., Centeno-García, E., and Peralta-Salazar, R., 2015, Early Mesozoic Southern Mexico–Amazonian connection based on U–Pb ages from detrital zircons: the La Mora Paleo-River in the Mixteca Terrane and its paleogeographic and tectonic implications: Gondwana Research, v. 28, p.689-701.

Sláma, J., Košler, J., Condon, D.J., Crowley, J.L., Gerdes, A., Hanchar, J.M., Horstwood, M.S., Morris, G.A., Nasdala, L., Norberg, N., and Schaltegger, U., 2008, Plešovice zircon—a new natural reference material for U–Pb and Hf isotopic microanalysis: Chemical Geology, v. 249, p.1-35.

Soreghan, G.S., and Soreghan, M.J., 2013, Tracing clastic delivery to the Permian Delaware Basin, U.S.A.; implications for paleogeography and circulation in westernmost equatorial Pangea: Journal of Sedimentary Research, v. 83, p. 786–802. doi:10.2110/jsr.2013.63.

Soreghan, M.J., Soreghan, G.S., and Hamilton, M., 2002, Paleowinds inferred from detrital-zircon geochronology of upper Paleozoic loessite, western equatorial Pangea: Geology, v. 30, p. 695–698.

Spencer, C.J., Prave, A.R., Cawood, P.A., and Roberts, N.M., 2014, Detrital zircon geochronology of the Grenville/Llano foreland and basal Sauk Sequence in West Texas, USA: Geological Society of America Bulletin, v.126, p. 1117-1128.

Tabor, N. J., and Poulsen, C. J., 2008, Palaeoclimate across the Lae Pennsylvanaian-Early Permian tropical palaeolatitudes: a review of climate indicators, their distribution, and relation to palaeophysiographic climate factors: Palaeogeography, Palaeoclimtology, Palaeoecology, v. 268, p. 293-310.

Thomas, W.A., 1991, The Appalachian-Ouachita rifted margin of southeastern North America: Geological Society of America Bulletin, v. 103, p. 415-431.

Thomas, W.A., 2004, Genetic relationship of rift-stage crustal structure, terrane accretion, and foreland tectonics along the southern Appalachian-Ouachita orogen: Journal of Geodynamics, v. 37, p. 549-563.

Thomas, W.A., 2006, Tectonic inheritance at a continental margin: Geological Society of America today, v. 16, p. 4-11.

Thomas, W.A., 2013, The Sabine and Coahuila terranes at the southern margin of Laurentia [abs.]: Geological Society of America Abstracts with Programs, v. 45, p. 293.

Thomas, W.A., Astini, R.A., and Bayona, G., 2002, Ordovician collision of the Argentine Precordillera with Gondwana, independent of Laurentian Taconic orogeny: Tectonophysics, v. 345, p.131-152.

Thomas, W.A., Becker, T.P., Samson, S.D., and Hamilton, M.A., 2004, Detrital zircon evidence of a recycled orogenic foreland provenance for Alleghanian clastic-wedge sandstones: The Journal of Geology, v. 112, p. 23-37, doi:10.1086/379690.

Thomas, W.A., Gehrels, G.E., and Romero, M.C., 2016, Detrital zircons from crystalline rocks along the Southern Oklahoma fault system, Wichita and Arbuckle Mountains, USA: Geosphere, v. 12, p. 1224-1234, doi:10.1130/GES01316.1.

Thomas, W.A., Gehrels, G.E., Greb, S.F., Nadon, G.C., Satkoski, A.M., and Romero, M.C., 2017, Detrital zircons and sediment dispersal in the Appalachian foreland: Geosphere, v. 13, p. 2206-2230, doi:10.1130/GES01525.1.

Tyler, N., and Banta, N.J., 1989, Oil and gas resources remaining in the Permian Basin: targets for additional hydrocarbon recovery: The University of Texas at Austin, Bureau of Economic Geology Geological Circular 89-4, 20 p.

Van Staal, C.R., Whalen, J.B., Valverde-Vaquero, P., Zagorevski, A., and Rogers, N., 2009, Pre-Carboniferous, episodic accretion-related, orogenesis along the Laurentian margin of the northern Appalachians: Geological Society Special Publications [London], v. 327, p. 271-316.

Vermeesch, P., 2012, On the visualisation of detrital age distributions: Chemical Geology, v. 312, p. 190-194.

Vermeesch, P., Resentini, A. and Garzanti, E., 2016, An R package for statistical provenance analysis: Sedimentary Geology, v. 336, p. 14-25.

Vervoort, J.D., Patchett, P.J., Söderlund, U., and Baker, M., 2004, Isotopic composition of Yb and the determination of Lu concentrations and Lu/Hf ratios by isotope dilution using MC–ICPMS: Geochemistry, Geophysics, Geosystems, v. 5, doi:10.1029/2004GC000721.

Viele, G.W., and Thomas, W.A., 1989, Tectonic synthesis of the Ouachita orogenic belt, in Hatcher, R.D., Jr., Thomas, W.A., and Viele, G.W., eds., The Appalachian-Ouachita Orogen in the United States: Geological Society of America, The Geology of North America, v. F-2, p. 695-728.

Walsh, G.J., and Aleinikoff, J.N., 1999, U-Pb zircon age of metafelsite from the Pinney Hollow Formation; implications for the development of the Vermont Appalachians: American Journal of Science, v. 299, p.157-170.

Walper, J.L., 1982, Plate tectonic evolution of the Fort Worth Basin: in Martin, C.A., ed., Petroleum Geology of the Fort Worth Basin and Bend Arch Area: Dallas Geological Society, p. 237-251.

Ward, R.F., Kendall, C.G.S.C., and Harris, P.M., 1986, Upper Permian (Guadalupian) facies and their association with hydrocarbons; Permian Basin, West Texas and New Mexico: American Association of Petroleum Geologists Bulletin, v. 70, p. 239-262.

Watson, W.G., 1979, Inhomogeneities of the Ramsey Member of the Permian Bell Canyon Formation, Geraldine Ford Field, Culberson and Reeves counties: Texas, USA, in Sullivan, N.M., ed.,

Guadalupian Delaware Mountain Group of West Texas and Southeast New Mexico: SEPM, Permian Basin Section, Publication 79-18, p. 2-38.

Wiedenbeck, M., Alle, P., Corfu, F., Griffin, W.L., Meier, M., Oberli, F., von Quadt, A., Roddick, J.C., and Spiegel, W, 1995, Three natural zircon standards for U–Th–Pb, Lu–Hf, trace element and REE analyses: Geostandards Newsletter, v. 19, p. 1-23.

Williams, I. S., 1998, U–Th–Pb geochronology by ion microprobe, in McKibben, M.A., Shanks III, W.C., and Ridley, W.I., eds., Applications of Microanalytical Techniques to Understanding Mineralizing Processes: Reviews in Economic Geology, v. 7, p. 1-35.

Williamson, C. R., 1979, Deep-sea sedimentation and stratigraphic traps, Bell Canyon Formation (Permian), Delaware Basin, in Sullivan, N. M., ed., Guadalupian Delaware Mountain Group of West Texas and Southeast New Mexico: Midland, Society of Economic Paleontologists and Mineralogists Permian Basin Section Publication 79-18, p. 39-74.

Willner, A. P., Barr, S. M., Gerdes, A., Massonne, H. J., and White, C. E., 2013, Origin and evolution of Avalonia: Evidence from U–Pb and Lu–Hf isotopes in zircon from the Mira terrane, Canada, and the Stavelot–Venn Massif, Belgium: Journal of the Geological Society, v. 170, p. 769-784, doi:10.1144/jgs2012-152.

Wright, W. F., 1979, Petroleum geology of the Permian Basin: Midland, West Texas geological Society Special Publication, no. 79-71, 98 p.

Wright, W. R., 2006, Depositional History of the Atokan Succession (Lower Pennsylvanian) in the Permian basin: Bureau of Economic Geology, p.1-67.

Wright, W. R., 2011, Pennsylvanian paleodepositional evolution of the greater Permian Basin, Texas and New Mexico: Depositional systems and hydrocarbon reservoir analysis: American Association of Petroleum Geologists Bulletin, v. 95, p.1525-1555.

Wortman, G., Samson, S. D., and Hibbard, J. P., 2000, Precise U-Pb zircon constraints on the earliest magmatic history of the Carolina Terrane: The Journal of Geology, v. 108, p. 321-338, doi:10.1086/ 314401. PMID:10769159.

Woodhead, J. D., and Hergt, J. M., 2005, A preliminary appraisal of seven natural zircon reference materials for in situ Hf isotope determination: Geostandards and Geoanalytical Research, v. 29, p.183-195.

Xie, X., Anthony, J. M., and Busbey, A. B., 2019, Provenance of Permian Delaware Mountain Group, central and southern Delaware Basin, and implications of sediment dispersal pathway near the southwestern terminus of Pangea: International Geology Review, v. 61, p. 361-380, doi: 10.1080/00206814.2018.1425925.

Xie, X., Buratowski, G., Manger, W.L., and Zachry, D., 2018, U-Pb Detrital-zircon Geochronology of the Middle Bloyd Sandstone (morrowan) of Northern Arkansas (USA): Implications for Early Pennsylvanian Sediment Dispersal in the Laurentian Foreland: Journal of Sedimentary Research, v. 88, p. 795-810.

Xie, X., Cains, W., and Manger, W. L., 2016, U–Pb detrital zircon evidence of transcontinental sediment dispersal: Provenance of Late Mississippian Wedington Sandstone member, NW Arkansas: International Geology Review, v. 58, p. 1951–1966, doi:10.1080/ 00206814.2016.1193775.

Yang, K. M., and Dorobek, S. L., 1995, The Permian Basin of West Texas and New Mexico: Flexural modelling and evidence for lithospheric heterogeneity across the Marathon Foreland, in Dorobek, S.L., and Ross, G.M., eds., Stratigraphic Evolution of Foreland Basins: Society for Sedimentary Geology Special Publication 52, p. 149-174, doi:10.2110/pec.95.52.0149.

Ye, H., Royden, L., Burchfiel, C., and Schuepbach, M., 1996, Late Paleozoic deformation of interior North America: the greater Ancestral Rocky Mountains: American Association of Petroleum Geologists Bulletin, v. 80, p. 1397-1432.

Ziegler, A. M., Hulver, M. L., and Rowley, D. B., 1997, Permian world topography and climate, in Late Glacial and Post-Glacial Environmental Changes–Quaternary, Martini, I.P., Ed., Carboniferous–Permian and Proterozoic, Oxford University Press, Oxford, p. 111-146.

Chapter 5 CONCLUSIONS

This dissertation addresses the Paleozoic sediment dispersal patterns of the Fort Worth Basin and Midland Basin in the southern margin of Laurentia in order to test the two existing hypotheses that the siliciclastic grains of the upper Paleozoic basin fill were derived from local sources including the Ouachita orogen or distal source of the Appalachians highlands via a transcontinental river system routing along the Appalachian forelands. In Chapter 2, I utilized detrital zircon U-Pb geochronology to the Paleozoic basin-fill of the Fort Worth Basin in order to understand sediment dispersal and reconstruct paleogeography on the southern margin of Laurentia before and during the suturing of Laurentia and Gondwana. Results of the Cambrian strata suggest that sediments were dispersed by local rivers from the Texas arch. Zircons of the Pennsylvanian strata suggest that sediments were derived from local sources including the basin-bounding Ouachita orogen and Muenster uplift, and distal source of the Appalachian forelands. In Chapter 3, I used sandstone petrography and mudstone rare earth elements patterns to determine sediment provenance of the Paleozoic rocks in the Fort Worth Basin. The sandstone composition changes from the Cambrian ($Q_{91}F_6L_3$) to the Pennsylvanian ($Q_{91}F_4L_5$), suggesting more continental input from Laurentian craton during the Cambrian, but more recycled orogen input during the Pennsylvanian. The Paleozoic mudstone samples show enrichment of LREE, flat distributions of HREE, and negative Eu anomalies after normalized to Chondrite, consistent with the REE pattern of average upper crust. The Middle Pennsylvanian-earliest Permian samples are depleted with LREE and have larger Eu anomalies compared to the Cambrian-Early Pennsylvanian samples, reflecting influence of sediments transported by long distance, likely from the Appalachians, and sediments eroded from local peri-Gondwana terranes. This change confirms the interpretation of Appalachian-derived sediments based on detrital zircon geochronology, and further suggests that the Appalachians became an important sediment source as early as the Middle Pennsylvanian. In Chapter 4, I studied the detrital zircon U-Pb ages and Hf isotope compositions of two Cambrian and Late Pennsylvanian fluvial and deltaic sandstones in the Midland Basin to constrain sediment provenances.

The Cambrian sample contains predominantly grains derived from the Proterozoic midcontinent Granite-Rhyolite province and a small portion of Grenville grains. The εHf values of the Cambrian sample are between +5 and +20, suggesting that the paleoriver mainly drained the Proterozoic basement that was exposed in the Texas Arch to the north of the basin. The Pennsylvanian sample contain grains ranging from Archean to late Paleozoic age, and is characterized by a large Grenville and Neoproterozoic-early Paleozoic population. The εHf values range from -24 to +12. By comparing the detrital zircon signature with potential sources and Paleozoic clastic rocks in southern Laurentia, I suggest that the Late Pennsylvanian sediments were dispersed by a transcontinental river along the Appalachian-Ouachita foreland and regional rivers draining the peri-Gondwana terranes in the Ouachita thrust belt.

The large volume of siliciclastic sediments may have brought a rich amount of nutrients and promoted marine productivity in the basins during the Late Paleozoic. The high productivity and the anoxic ocean bottom may have caused organic matter richness in both basins. It is very likely that the change in sediment provenance was associated with the presence of organic-rich intervals.

Appendix A

Zircon U-Pb geochronological data for the Fort Worth Basin

						Isotope ratios					Apparent ages (Ma)								
Analysis	U	^{206}Pb	U/Th	^{206}Pb*	±	^{207}Pb*	±	^{206}Pb*	±	error	^{206}Pb*	±	^{207}Pb*	±	^{206}Pb*	±	Best age	±	Conc.
	(ppm)	^{204}Pb		^{207}Pb*	(%)	^{235}U*	(%)	^{238}U	(%)	corr.	^{238}U*	(Ma)	^{235}U	(Ma)	^{207}Pb*	(Ma)	(Ma)	(Ma)	(%)
Lower Hickory sandstone, sample 1 (Late Middle Cambrian)																			
LOWER HICKORY-8 <>	25	8966	1.1	13.5201	3.2	1.8621	3.4	0.1826	1.2	0.37	1081.1	12.4	1067.7	22.5	1040.5	64.0	1040.5	64.0	103.9
LOWER HICKORY-47 <>	59	41738	1.8	13.4102	3.2	1.8437	3.9	0.1793	2.3	0.58	1063.3	22.1	1061.2	25.7	1056.9	64.1	1056.9	64.1	100.6
LOWER HICKORY-58 <>	75	28609	0.8	13.3909	1.8	1.8502	3.1	0.1797	2.5	0.81	1065.3	24.9	1063.5	20.6	1059.9	36.9	1059.9	36.9	100.5
LOWER HICKORY-96 <>	99	40011	2.4	13.3121	1.0	1.9052	4.8	0.1839	4.7	0.98	1088.5	46.8	1082.9	31.9	1071.7	20.7	1071.7	20.7	101.6
LOWER HICKORY-52 <>	77	80561	2.5	13.2687	1.9	1.9378	5.1	0.1865	4.8	0.93	1102.3	48.3	1094.2	34.5	1078.3	38.8	1078.3	38.8	102.2
LOWER HICKORY-83 <>	145	82188	2.3	13.1910	0.9	1.9916	2.4	0.1905	2.3	0.93	1124.3	23.4	1112.6	16.5	1090.0	17.9	1090.0	17.9	103.1
LOWER HICKORY-109 <>	45	61813	1.3	13.1623	3.5	1.8248	3.7	0.1742	1.3	0.34	1035.2	12.1	1054.4	24.5	1094.4	70.3	1094.4	70.3	94.6
LOWER HICKORY-14 <>	155	49317	2.0	13.1316	0.9	1.8956	1.5	0.1805	1.3	0.83	1069.9	12.4	1079.5	10.1	1099.1	17.2	1099.1	17.2	97.3
LOWER HICKORY-11 <>	92	73961	1.3	13.0996	1.2	1.9702	2.1	0.1872	1.7	0.82	1106.1	17.6	1105.4	14.2	1104.0	24.2	1104.0	24.2	100.2
LOWER HICKORY-88 <>	189	5151	1.1	13.0942	3.4	1.8372	8.6	0.1745	7.9	0.92	1036.7	75.9	1058.9	56.8	1104.8	68.4	1104.8	68.4	93.8
LOWER HICKORY-26 <>	88	12030	2.2	13.0777	2.2	1.9348	2.4	0.1835	1.0	0.40	1086.1	9.8	1093.2	16.4	1107.3	44.8	1107.3	44.8	98.1
LOWER HICKORY-31 <>	197	42751	1.7	13.0475	1.6	1.9802	2.3	0.1874	1.6	0.72	1107.2	16.5	1108.8	15.3	1111.9	31.7	1111.9	31.7	99.6
LOWER HICKORY-61 <>	131	32346	2.2	13.0291	0.7	1.9079	2.7	0.1803	2.6	0.97	1068.6	25.5	1083.9	17.8	1114.7	13.0	1114.7	13.0	95.9
LOWER HICKORY-125 <>	46	23684	1.1	12.9829	2.9	2.0039	3.0	0.1887	0.7	0.23	1114.3	7.0	1116.8	20.3	1121.8	58.2	1121.8	58.2	99.3
LOWER HICKORY-119 <>	20	10158	0.8	12.8811	6.8	1.9105	7.4	0.1785	2.9	0.39	1058.7	28.3	1084.8	49.1	1137.5	134.6	1137.5	134.6	93.1
LOWER HICKORY-56 <>	61	15408	1.2	12.7430	2.5	2.0055	3.7	0.1853	2.7	0.72	1096.1	26.8	1117.4	24.9	1158.9	50.2	1158.9	50.2	94.6
LOWER HICKORY-93 <>	55	3482	2.0	12.7389	3.3	1.9586	3.6	0.1810	1.5	0.42	1072.2	15.2	1101.4	24.4	1159.5	65.1	1159.5	65.1	92.5
LOWER HICKORY-37 <>	47	47689	1.6	12.4494	1.3	2.1788	4.6	0.1967	4.4	0.96	1157.7	46.2	1174.3	31.7	1205.0	25.8	1205.0	25.8	96.1
LOWER HICKORY-35 <>	61	30795	1.2	12.2106	3.1	2.4088	3.5	0.2133	1.6	0.46	1246.5	18.2	1245.2	25.1	1243.0	60.7	1243.0	60.7	100.3
LOWER HICKORY-86 <>	85	52001	1.3	12.1638	1.8	2.3907	2.2	0.2109	1.3	0.59	1233.7	14.6	1239.8	15.8	1250.5	34.8	1250.5	34.8	98.6
LOWER HICKORY-67 <>	120	66265	1.6	12.1215	1.4	2.4155	2.0	0.2124	1.4	0.71	1241.4	15.8	1247.2	14.2	1257.4	27.4	1257.4	27.4	98.7
LOWER HICKORY-74 <>	97	90671	2.1	12.1096	0.8	2.5413	2.2	0.2232	2.1	0.94	1298.8	24.2	1284.0	15.9	1259.3	14.7	1259.3	14.7	103.1
LOWER HICKORY-57 <>	111	59262	1.3	12.0925	1.1	2.4759	2.9	0.2171	2.7	0.93	1266.8	31.0	1265.0	21.0	1262.0	21.0	1262.0	21.0	100.4
LOWER HICKORY-39 <>	103	65820	2.9	12.0562	1.3	2.5087	2.8	0.2194	2.5	0.89	1278.5	29.3	1274.5	20.6	1267.9	25.4	1267.9	25.4	100.8
LOWER HICKORY-11 <>	44	48332	1.2	11.8928	2.0	2.6304	3.5	0.2269	2.8	0.81	1318.2	33.6	1309.2	25.5	1294.5	39.2	1294.5	39.2	101.8

LOWER HICKORY-68 <>	90	11030	2.5	11.7066	1.1	2.2021	1.6	0.1870	1.1	0.71	1104.9	11.2	1181.7	10.9	1325.1	21.4	1325.1	21.4	83.4
LOWER HICKORY-18 <>	55	48205	1.3	11.6511	2.1	2.8633	3.0	0.2420	2.1	0.70	1396.9	26.8	1372.3	22.8	1334.3	41.6	1334.3	41.6	104.7
LOWER HICKORY-44 <>	195	73670	1.5	11.6203	0.6	2.6943	1.7	0.2271	1.6	0.93	1319.1	18.8	1326.9	12.5	1339.4	11.9	1339.4	11.9	98.5
LOWER HICKORY-20 <>	142	27012	1.7	11.5888	1.5	2.7357	2.8	0.2299	2.4	0.84	1334.2	28.3	1338.2	20.8	1344.7	29.3	1344.7	29.3	99.2
LOWER HICKORY-33 <>	96	24394	1.5	11.5816	0.8	2.7024	1.5	0.2270	1.3	0.84	1318.7	15.5	1329.1	11.4	1345.9	16.1	1345.9	16.1	98.0
LOWER HICKORY-16 <>	60	35179	1.8	11.5631	1.0	2.8448	1.7	0.2386	1.4	0.81	1379.3	17.5	1367.4	13.1	1349.0	19.9	1349.0	19.9	102.2
LOWER HICKORY-50 <>	142	83169	1.9	11.5551	0.8	2.8390	0.9	0.2379	0.5	0.52	1375.9	5.9	1365.9	6.8	1350.3	14.9	1350.3	14.9	101.9
LOWER HICKORY-5 <>	71	41471	2.0	11.5522	1.0	2.7332	3.3	0.2290	3.1	0.95	1329.3	37.3	1337.5	24.3	1350.8	19.7	1350.8	19.7	98.4
LOWER HICKORY-7 <>	49	17485	1.2	11.5455	2.4	2.7597	4.2	0.2311	3.5	0.83	1340.2	42.7	1344.7	31.6	1351.9	45.5	1351.9	45.5	99.1
LOWER HICKORY-38 <>	103	51483	1.4	11.5419	0.7	2.8206	2.0	0.2361	1.8	0.93	1366.5	22.5	1361.0	14.7	1352.5	13.9	1352.5	13.9	101.0
LOWER HICKORY 2	339	36175	2.1	11.5357	0.2	2.6880	1.7	0.2249	1.7	0.99	1307.7	20.2	1325.2	12.7	1353.5	3.7	1353.5	3.7	96.6
LOWER HICKORY-15 <>	76	34243	1.7	11.5287	1.1	2.8717	1.4	0.2401	0.9	0.66	1387.3	11.6	1374.5	10.6	1354.7	20.3	1354.7	20.3	102.4
LOWER HICKORY-76 <>	75	56799	1.3	11.5164	1.1	2.8476	2.0	0.2378	1.6	0.82	1375.5	19.8	1368.2	14.7	1356.8	21.5	1356.8	21.5	101.4
LOWER HICKORY-75 <>	193	120209	2.1	11.5096	0.4	2.8175	1.0	0.2352	0.9	0.90	1361.7	11.2	1360.2	7.6	1357.9	8.6	1357.9	8.6	100.3
LOWER HICKORY-30 <>	100	13155	1.6	11.5069	1.1	2.8419	1.6	0.2372	1.2	0.76	1372.0	15.4	1366.7	12.3	1358.4	20.4	1358.4	20.4	101.0
LOWER HICKORY-90 <>	174	10811	1.8	11.5069	1.3	2.7402	5.4	0.2287	5.2	0.97	1327.6	63.0	1339.4	40.2	1358.4	25.0	1358.4	25.0	97.7
LOWER HICKORY-120 <>	131	10320	1.3	11.4887	1.8	2.6117	3.0	0.2176	2.4	0.81	1269.3	28.0	1303.9	22.0	1361.4	33.8	1361.4	33.8	93.2
LOWER HICKORY-27 <>	71	50857	1.5	11.4867	2.2	2.8303	2.5	0.2358	1.1	0.43	1364.8	12.9	1363.6	18.6	1361.7	43.2	1361.7	43.2	100.2
LOWER HICKORY-110 <>	63	20786	1.6	11.4848	1.3	2.8164	2.9	0.2346	2.6	0.90	1358.5	32.0	1359.9	21.8	1362.1	24.6	1362.1	24.6	99.7
LOWER HICKORY-121 <>	36	52170	1.0	11.4827	2.0	2.8994	4.0	0.2415	3.4	0.87	1394.3	43.2	1381.8	30.0	1362.4	38.0	1362.4	38.0	102.3
LOWER HICKORY 3	44	55883	1.9	11.4787	2.1	2.8136	3.6	0.2342	2.9	0.81	1356.7	35.7	1359.2	27.1	1363.1	41.0	1363.1	41.0	99.5
LOWER HICKORY-79 <>	183	133760	1.7	11.4743	0.5	2.8449	0.7	0.2367	0.5	0.69	1369.8	6.3	1367.5	5.5	1363.8	10.2	1363.8	10.2	100.4
LOWER HICKORY-69 <>	139	28052	1.9	11.4726	0.8	2.7692	1.0	0.2304	0.6	0.58	1336.7	6.9	1347.3	7.4	1364.1	15.5	1364.1	15.5	98.0
LOWER HICKORY 1	104	76625	1.4	11.4588	0.8	2.8460	1.6	0.2365	1.5	0.89	1368.6	18.0	1367.8	12.3	1366.4	14.6	1366.4	14.6	100.2
LOWER HICKORY-107 <>	58	42755	1.8	11.4512	1.4	2.6824	1.9	0.2228	1.3	0.68	1296.6	15.1	1323.6	14.0	1367.7	26.9	1367.7	26.9	94.8
LOWER HICKORY-46 <>	108	32328	2.3	11.4476	1.2	2.8884	1.5	0.2398	1.0	0.63	1385.7	12.1	1378.9	11.5	1368.3	22.8	1368.3	22.8	101.3
LOWER HICKORY-28 <>	127	191729	1.6	11.4345	1.2	2.8700	1.8	0.2380	1.3	0.75	1376.3	16.7	1374.1	13.5	1370.5	23.0	1370.5	23.0	100.4
LOWER HICKORY-4 <>	76	18790	1.4	11.4213	1.6	2.3201	2.5	0.1922	2.0	0.77	1133.2	20.3	1218.4	18.0	1372.7	31.3	1372.7	31.3	82.6
LOWER HICKORY-21 <>	192	49752	1.8	11.4131	0.4	2.8107	5.5	0.2327	5.5	1.00	1348.4	67.0	1358.4	41.4	1374.1	7.6	1374.1	7.6	98.1
LOWER HICKORY-70 <>	94	42533	1.9	11.4092	1.4	2.8682	2.7	0.2373	2.3	0.86	1372.8	28.4	1373.6	20.1	1374.8	26.2	1374.8	26.2	99.9

LOWER HICKORY-101 <>	58	58847	1.9	11.4072	1.3	2.9029	1.5	0.2402	0.8	0.55	1387.6	10.6	1382.7	11.6	1375.1	24.8	1375.1	24.8	100.9
LOWER HICKORY-59 <>	206	108784	2.1	11.4003	0.3	2.8681	0.9	0.2371	0.9	0.95	1371.8	10.7	1373.6	6.9	1376.3	5.4	1376.3	5.4	99.7
LOWER HICKORY-82 <>	82	49208	1.7	11.3960	1.3	2.8762	2.0	0.2377	1.5	0.74	1374.8	18.2	1375.7	15.0	1377.0	25.9	1377.0	25.9	99.8
LOWER HICKORY-104 <>	65	33574	1.7	11.3940	1.8	2.8531	2.0	0.2358	0.7	0.36	1364.7	8.6	1369.6	14.8	1377.3	35.5	1377.3	35.5	99.1
LOWER HICKORY-40 <>	68	59740	1.1	11.3903	1.4	2.8817	1.6	0.2381	0.8	0.50	1376.6	9.7	1377.1	11.8	1378.0	26.1	1378.0	26.1	99.9
LOWER HICKORY-72 <>	72	74313	1.6	11.3862	1.1	2.9001	1.3	0.2395	0.7	0.57	1384.0	9.2	1381.9	9.7	1378.7	20.3	1378.7	20.3	100.4
LOWER HICKORY-51 <>	93	131931	1.5	11.3839	0.6	2.8842	1.2	0.2381	1.1	0.87	1377.0	13.1	1377.8	9.2	1379.1	11.6	1379.1	11.6	99.8
LOWER HICKORY-9 <>	131	45712	1.1	11.3820	0.9	2.7455	4.8	0.2266	4.7	0.98	1316.9	56.4	1340.9	35.9	1379.4	18.0	1379.4	18.0	95.5
LOWER HICKORY-114 <>	157	121637	1.6	11.3785	0.6	2.9249	1.6	0.2414	1.5	0.92	1393.8	18.2	1388.4	11.9	1380.0	11.5	1380.0	11.5	101.0
LOWER HICKORY-116 <>	34	42803	1.1	11.3779	2.6	2.8970	9.9	0.2391	9.6	0.96	1381.8	118.9	1381.1	74.9	1380.1	50.3	1380.1	50.3	100.1
LOWER HICKORY-89 <>	154	40474	2.9	11.3754	0.9	2.7699	1.9	0.2285	1.7	0.88	1326.7	19.8	1347.5	14.0	1380.5	17.3	1380.5	17.3	96.1
LOWER HICKORY-102 <>	226	17174	1.5	11.3723	0.8	2.7699	6.3	0.2285	6.2	0.99	1326.4	74.6	1347.5	46.8	1381.0	14.8	1381.0	14.8	96.0
LOWER HICKORY-85 <>	167	199254	1.8	11.3672	0.5	2.8862	2.0	0.2379	1.9	0.97	1376.0	24.1	1378.3	15.1	1381.9	9.5	1381.9	9.5	99.6
LOWER HICKORY-19 <>	195	98938	2.0	11.3644	0.4	2.8976	1.2	0.2388	1.2	0.95	1380.6	14.4	1381.3	9.2	1382.3	7.6	1382.3	7.6	99.9
LOWER HICKORY-36 <>	56	39978	1.0	11.3583	1.6	2.8499	1.8	0.2348	0.9	0.50	1359.5	11.2	1368.8	13.6	1383.4	30.1	1383.4	30.1	98.3
LOWER HICKORY-105 <>	57	13431	1.0	11.3583	2.1	2.9648	2.8	0.2442	1.9	0.68	1408.7	24.3	1398.6	21.6	1383.4	40.3	1383.4	40.3	101.8
LOWER HICKORY-98 <>	58	27192	1.2	11.3568	2.3	2.8612	4.8	0.2357	4.2	0.88	1364.1	52.1	1371.7	36.1	1383.6	43.3	1383.6	43.3	98.6
LOWER HICKORY-12 <>	124	110589	1.8	11.3515	0.5	2.8790	1.8	0.2370	1.7	0.96	1371.2	21.2	1376.4	13.5	1384.5	9.3	1384.5	9.3	99.0
LOWER HICKORY-43 <>	48	33053	1.9	11.3496	1.8	2.8272	2.9	0.2327	2.2	0.78	1348.7	27.2	1362.8	21.5	1384.8	34.5	1384.8	34.5	97.4
LOWER HICKORY-60 <>	44	21581	2.1	11.3373	2.3	2.8676	2.9	0.2358	1.8	0.62	1364.8	22.2	1373.5	21.8	1386.9	43.4	1386.9	43.4	98.4
LOWER HICKORY-81 <>	61	30168	1.3	11.3345	1.8	2.9379	1.9	0.2415	0.6	0.33	1394.6	7.7	1391.7	14.1	1387.4	33.8	1387.4	33.8	100.5
LOWER HICKORY-84 <>	92	93454	1.5	11.3333	0.9	2.8699	2.7	0.2359	2.5	0.94	1365.3	31.3	1374.0	20.3	1387.6	17.2	1387.6	17.2	98.4
LOWER HICKORY-92 <>	138	129126	2.0	11.3320	0.7	2.8952	1.8	0.2379	1.7	0.92	1376.0	21.0	1380.7	13.9	1387.8	13.8	1387.8	13.8	99.1
LOWER HICKORY-13 <>	223	7359	1.9	11.3247	0.8	2.6415	2.0	0.2170	1.8	0.91	1265.8	21.2	1312.3	15.0	1389.1	16.2	1389.1	16.2	91.1
LOWER HICKORY-94 <>	57	35823	1.4	11.3213	1.3	2.9033	2.8	0.2384	2.5	0.89	1378.3	30.7	1382.8	21.1	1389.6	24.6	1389.6	24.6	99.2
LOWER HICKORY-99 <>	136	70491	1.6	11.3191	1.1	2.8591	3.1	0.2347	2.9	0.94	1359.2	35.4	1371.2	23.2	1390.0	20.8	1390.0	20.8	97.8
LOWER HICKORY-124 <>	40	24727	2.0	11.3118	3.5	2.9159	3.7	0.2392	1.0	0.27	1382.7	12.1	1386.1	27.6	1391.3	67.6	1391.3	67.6	99.4
LOWER HICKORY-55 <>	75	24106	1.4	11.3072	1.5	2.9022	2.0	0.2380	1.3	0.66	1376.3	16.1	1382.5	15.0	1392.0	28.8	1392.0	28.8	98.9
LOWER HICKORY-66 <>	55	12685	1.7	11.2918	1.2	2.8954	2.4	0.2371	2.1	0.87	1371.7	26.1	1380.7	18.3	1394.6	22.9	1394.6	22.9	98.4
LOWER HICKORY-53 <>	72	123936	1.7	11.2829	2.5	2.8726	2.6	0.2351	0.8	0.30	1361.0	9.5	1374.7	19.5	1396.1	47.4	1396.1	47.4	97.5

LOWER HICKORY-29 <>	157	367135	1.6	11.2762	0.9	2.9636	1.5	0.2424	1.2	0.79	1399.0	14.9	1398.3	11.5	1397.3	17.9	1397.3	17.9	100.1
LOWER HICKORY-123 <>	68	36458	2.1	11.2742	0.8	2.9147	1.0	0.2383	0.5	0.54	1378.0	6.8	1385.7	7.6	1397.6	16.1	1397.6	16.1	98.6
LOWER HICKORY-23 <>	38	36099	1.8	11.2691	2.6	2.9281	4.7	0.2393	3.8	0.83	1383.1	47.9	1389.2	35.3	1398.5	50.5	1398.5	50.5	98.9
LOWER HICKORY-100 <>	52	19915	1.1	11.2678	1.7	2.9048	2.9	0.2374	2.4	0.82	1373.1	29.8	1383.2	22.2	1398.7	32.1	1398.7	32.1	98.2
LOWER HICKORY-103 <>	83	21324	0.7	11.2656	0.9	2.7671	1.1	0.2261	0.7	0.59	1314.0	7.9	1346.7	8.4	1399.1	17.4	1399.1	17.4	93.9
LOWER HICKORY-71 <>	184	37274	1.4	11.2639	0.7	2.9575	1.7	0.2416	1.5	0.90	1395.0	19.3	1396.8	12.9	1399.4	14.0	1399.4	14.0	99.7
LOWER HICKORY-118 <>	127	103773	1.1	11.2612	0.6	2.9868	0.9	0.2439	0.7	0.79	1407.2	9.4	1404.3	7.1	1399.8	11.1	1399.8	11.1	100.5
LOWER HICKORY-91 <>	45	34162	1.8	11.2556	2.5	2.8887	3.1	0.2358	2.0	0.63	1364.9	24.2	1379.0	23.7	1400.8	47.0	1400.8	47.0	97.4
LOWER HICKORY-24 <>	83	83247	1.4	11.2278	0.8	2.9606	1.4	0.2411	1.1	0.80	1392.4	13.7	1397.6	10.3	1405.5	15.6	1405.5	15.6	99.1
LOWER HICKORY-54 <>	112	55232	1.2	11.1995	0.7	2.9567	1.3	0.2402	1.1	0.85	1387.6	13.8	1396.6	9.8	1410.4	13.0	1410.4	13.0	98.4
LOWER HICKORY-77 <>	88	47362	1.8	11.1922	0.9	2.9777	1.4	0.2417	1.1	0.78	1395.6	13.3	1401.9	10.3	1411.6	16.3	1411.6	16.3	98.9
LOWER HICKORY-34 <>	55	4174	1.7	11.1337	5.5	2.9975	5.9	0.2420	2.0	0.34	1397.3	25.3	1407.0	44.9	1421.6	106.0	1421.6	106.0	98.3
LOWER HICKORY-42 <>	64	12370	1.3	11.1249	0.9	2.9842	1.4	0.2408	1.1	0.76	1390.8	13.6	1403.6	10.8	1423.1	17.6	1423.1	17.6	97.7
LOWER HICKORY-106 <>	109	12557	1.9	11.1216	1.1	2.9968	1.5	0.2417	1.0	0.68	1395.7	13.1	1406.8	11.8	1423.7	21.8	1423.7	21.8	98.0
LOWER HICKORY-95 <>	39	5892	1.1	11.0949	3.5	2.9944	3.8	0.2410	1.5	0.41	1391.6	19.3	1406.2	29.0	1428.3	66.4	1428.3	66.4	97.4
LOWER HICKORY-117 <>	41	57964	1.4	11.0832	2.9	3.0294	4.1	0.2435	2.9	0.70	1404.9	36.7	1415.1	31.6	1430.3	56.1	1430.3	56.1	98.2
LOWER HICKORY-87 <>	78	75785	2.6	11.0767	1.5	3.0772	3.0	0.2472	2.6	0.86	1424.1	32.9	1427.0	22.8	1431.4	28.7	1431.4	28.7	99.5
Upper Hickory sandstone, sample 2 (Late Cambrian)																			
UPPER HICKORY-36 <>	219	2495	1.1	16.8161	3.6	0.6728	4.1	0.0821	1.9	0.47	508.4	9.4	522.4	16.8	584.2	79.1	508.4	9.4	87.0
UPPER HICKORY-53 <>	215	29921	1.5	17.2405	2.0	0.6765	3.3	0.0846	2.7	0.81	523.5	13.4	524.7	13.6	529.9	43.0	523.5	13.4	98.8
UPPER HICKORY-38 <>	163	15941	1.3	16.7539	1.9	0.7092	2.4	0.0862	1.4	0.59	532.9	7.3	544.3	10.1	592.3	41.9	532.9	7.3	90.0
UPPER HICKORY-82 <>	279	48486	1.0	17.2390	2.2	0.6916	2.8	0.0865	1.7	0.61	534.6	8.8	533.8	11.7	530.1	48.9	534.6	8.8	100.9
UPPER HICKORY-110 <>	272	80830	0.9	17.2977	1.8	0.6897	2.1	0.0865	1.2	0.56	535.0	6.1	532.6	8.9	522.6	38.9	535.0	6.1	102.4
UPPER HICKORY-30 <>	102	45604	1.0	13.5213	1.7	1.8296	2.3	0.1794	1.6	0.69	1063.8	15.7	1056.1	15.1	1040.3	33.5	1040.3	33.5	102.3
UPPER HICKORY-49 <>	44	4884	0.8	13.0550	3.5	2.0382	3.6	0.1930	1.0	0.28	1137.5	10.5	1128.3	24.7	1110.8	69.6	1110.8	69.6	102.4
UPPER HICKORY-63 <>	58	31885	2.1	13.0242	2.7	2.0161	3.3	0.1904	1.9	0.57	1123.7	19.4	1120.9	22.6	1115.5	54.9	1115.5	54.9	100.7
UPPER HICKORY-113 <>	37	22365	1.5	13.0095	4.6	1.9945	5.6	0.1882	3.1	0.56	1111.6	32.0	1113.7	37.6	1117.8	91.7	1117.8	91.7	99.4
UPPER HICKORY-19 <>	27	20738	1.7	12.9777	3.9	2.0672	6.2	0.1946	4.8	0.78	1146.1	50.5	1138.0	42.3	1122.6	77.3	1122.6	77.3	102.1

UPPER HICKORY-54 <>	108	39111	2.1	12.9715	1.6	1.9877	3.4	0.1870	3.0	0.88	1105.1	30.0	1111.3	22.8	1123.6	32.5	1123.6	32.5	98.4
UPPER HICKORY-13 <>	62	28110	1.1	12.8968	2.1	1.9958	2.4	0.1867	1.2	0.49	1103.4	11.9	1114.1	16.3	1135.1	41.8	1135.1	41.8	97.2
UPPER HICKORY-92 <>	139	81215	1.9	12.8635	1.1	2.0139	1.2	0.1879	0.6	0.49	1109.9	6.3	1120.2	8.5	1140.2	21.5	1140.2	21.5	97.3
UPPER HICKORY-31 <>	47	48473	1.4	12.8306	4.4	2.0194	5.7	0.1879	3.7	0.65	1110.1	37.7	1122.0	38.8	1145.3	86.6	1145.3	86.6	96.9
UPPER HICKORY-114 <>	59	8140	1.6	12.8083	3.2	2.0142	3.8	0.1871	1.9	0.51	1105.7	19.6	1120.3	25.5	1148.8	64.2	1148.8	64.2	96.2
UPPER HICKORY-34 <>	94	58906	1.1	12.7437	1.3	2.0506	1.6	0.1895	0.8	0.52	1118.8	8.4	1132.5	10.7	1158.8	26.7	1158.8	26.7	96.6
UPPER HICKORY-97 <>	49	48390	2.4	12.6522	2.3	2.0709	2.8	0.1900	1.6	0.57	1121.5	16.2	1139.2	19.0	1173.1	45.2	1173.1	45.2	95.6
UPPER HICKORY-21 <>	37	23978	0.9	11.6420	3.5	2.8156	4.2	0.2377	2.2	0.52	1374.9	26.8	1359.7	31.1	1335.8	68.6	1335.8	68.6	102.9
UPPER HICKORY-67 <>	61	28065	1.5	11.6365	2.2	2.8290	4.5	0.2388	3.9	0.87	1380.2	48.9	1363.3	33.7	1336.7	42.2	1336.7	42.2	103.3
UPPER HICKORY-104 <>	94	63682	1.4	11.6330	2.0	2.7960	3.4	0.2359	2.8	0.82	1365.4	34.8	1354.5	25.7	1337.3	37.9	1337.3	37.9	102.1
UPPER HICKORY-115 <>	114	183788	2.3	11.6076	1.3	2.7550	4.8	0.2319	4.6	0.96	1344.6	55.7	1343.4	35.6	1341.5	24.9	1341.5	24.9	100.2
UPPER HICKORY-24 <>	43	24074	1.3	11.5953	2.6	2.8127	3.3	0.2365	1.9	0.59	1368.7	23.8	1358.9	24.4	1343.6	50.8	1343.6	50.8	101.9
UPPER HICKORY-87 <>	52	32871	0.6	11.5892	1.8	2.8414	2.4	0.2388	1.5	0.64	1380.6	18.8	1366.5	17.7	1344.6	34.7	1344.6	34.7	102.7
UPPER HICKORY-44 <>	77	198337	1.2	11.5721	1.7	2.8685	2.1	0.2408	1.2	0.58	1390.6	14.9	1373.7	15.5	1347.5	32.3	1347.5	32.3	103.2
UPPER HICKORY-79 <>	77	71568	1.5	11.5650	1.8	2.8515	2.0	0.2392	0.9	0.44	1382.4	11.2	1369.2	15.3	1348.6	35.1	1348.6	35.1	102.5
UPPER HICKORY-93 <>	107	27631	1.2	11.5471	1.3	2.7852	4.0	0.2333	3.8	0.95	1351.5	46.4	1351.6	30.0	1351.6	24.8	1351.6	24.8	100.0
UPPER HICKORY-81 <>	117	122924	1.3	11.5375	0.7	2.8703	1.5	0.2402	1.3	0.89	1387.6	16.5	1374.2	11.2	1353.2	13.0	1353.2	13.0	102.5
UPPER HICKORY-52 <>	79	15089	1.1	11.5341	1.2	2.6667	1.7	0.2231	1.2	0.69	1298.1	13.5	1319.3	12.4	1353.8	23.6	1353.8	23.6	95.9
UPPER HICKORY-78 <>	101	42467	1.7	11.4983	0.9	2.8993	2.6	0.2418	2.4	0.93	1396.0	29.9	1381.7	19.3	1359.8	17.9	1359.8	17.9	102.7
UPPER HICKORY-103 <>	79	29121	0.7	11.4941	1.7	2.8604	2.9	0.2384	2.3	0.80	1378.6	28.8	1371.5	21.8	1360.5	33.6	1360.5	33.6	101.3
UPPER HICKORY-95 <>	93	27111	1.0	11.4934	1.7	2.7780	4.1	0.2316	3.7	0.91	1342.7	45.4	1349.6	30.7	1360.6	32.4	1360.6	32.4	98.7
UPPER HICKORY-59 <>	79	20548	0.9	11.4869	0.7	2.8324	1.3	0.2360	1.1	0.83	1365.7	13.1	1364.2	9.6	1361.7	13.9	1361.7	13.9	100.3
UPPER HICKORY-106 <>	67	45668	0.6	11.4866	2.4	2.8443	3.3	0.2370	2.2	0.67	1370.8	27.4	1367.3	24.8	1361.8	47.1	1361.8	47.1	100.7
UPPER HICKORY-75 <>	97	55188	1.5	11.4848	0.7	2.8802	2.1	0.2399	1.9	0.93	1386.2	23.8	1376.7	15.5	1362.1	14.4	1362.1	14.4	101.8
UPPER HICKORY-48 <>	41	26467	1.0	11.4784	2.9	2.8532	3.8	0.2375	2.5	0.66	1373.8	31.3	1369.7	28.8	1363.1	55.3	1363.1	55.3	100.8
UPPER HICKORY-99 <>	165	34366	1.5	11.4694	0.9	2.7395	1.9	0.2279	1.7	0.89	1323.4	20.3	1339.2	14.1	1364.7	16.4	1364.7	16.4	97.0
UPPER HICKORY-62 <>	82	67924	1.6	11.4647	2.4	2.8516	4.4	0.2371	3.6	0.83	1371.7	44.7	1369.2	32.9	1365.4	47.2	1365.4	47.2	100.5
UPPER HICKORY-73 <>	94	48377	1.8	11.4551	1.2	2.9284	4.2	0.2433	4.1	0.96	1403.8	51.3	1389.3	32.0	1367.0	22.3	1367.0	22.3	102.7
UPPER HICKORY-112 <>	103	37866	0.9	11.4479	1.6	2.8493	2.0	0.2366	1.3	0.63	1368.8	15.8	1368.6	15.4	1368.3	30.7	1368.3	30.7	100.0
UPPER HICKORY-69 <>	116	80027	1.7	11.4478	0.7	2.8294	2.4	0.2349	2.3	0.96	1360.2	28.2	1363.4	18.0	1368.3	13.2	1368.3	13.2	99.4

UPPER HICKORY-80 <>	162	7926	1.2	11.4447	1.1	2.7252	8.6	0.2262	8.5	0.99	1314.6	101.4	1335.3	63.9	1368.8	20.4	1368.8	20.4	96.0
UPPER HICKORY-119 <>	88	36543	1.6	11.4368	2.0	2.8270	2.4	0.2345	1.4	0.57	1358.0	16.9	1362.7	18.2	1370.1	38.4	1370.1	38.4	99.1
UPPER HICKORY-32 <>	104	87991	1.6	11.4316	0.8	2.9329	1.4	0.2432	1.2	0.83	1403.1	14.6	1390.4	10.5	1371.0	14.7	1371.0	14.7	102.3
UPPER HICKORY-105 <>	94	46563	1.7	11.4291	1.1	2.8422	1.4	0.2356	0.9	0.66	1363.7	11.6	1366.7	10.8	1371.4	20.7	1371.4	20.7	99.4
UPPER HICKORY-18 <>	85	59979	1.0	11.4192	1.8	2.9194	2.7	0.2418	2.1	0.76	1396.0	26.0	1386.9	20.5	1373.1	33.7	1373.1	33.7	101.7
UPPER HICKORY-118 <>	154	53262	1.8	11.4122	0.8	2.9694	2.9	0.2458	2.8	0.96	1416.7	35.3	1399.8	22.0	1374.3	15.3	1374.3	15.3	103.1
UPPER HICKORY-72 <>	136	76324	0.7	11.4092	1.1	2.7753	2.6	0.2296	2.4	0.91	1332.7	28.7	1348.9	19.6	1374.8	21.1	1374.8	21.1	96.9
UPPER HICKORY-101 <>	32	25174	0.8	11.4088	5.1	2.8667	6.8	0.2372	4.4	0.66	1372.2	55.0	1373.2	51.0	1374.8	98.1	1374.8	98.1	99.8
UPPER HICKORY-65 <>	123	81970	0.8	11.4088	1.1	2.8934	2.4	0.2394	2.1	0.89	1383.6	26.7	1380.2	18.1	1374.8	20.8	1374.8	20.8	100.6
UPPER HICKORY-55 <>	160	49597	1.1	11.4084	0.8	2.9082	1.8	0.2406	1.6	0.89	1390.0	19.7	1384.1	13.3	1374.9	15.4	1374.9	15.4	101.1
UPPER HICKORY-27 <>	101	73506	1.8	11.4076	1.0	2.6564	1.6	0.2198	1.3	0.80	1280.7	15.2	1316.4	12.0	1375.0	18.6	1375.0	18.6	93.1
UPPER HICKORY-6 <>	127	28240	1.4	11.4035	1.1	2.8040	2.3	0.2319	2.1	0.88	1344.5	24.9	1356.6	17.4	1375.7	21.0	1375.7	21.0	97.7
UPPER HICKORY-17 <>	59	30551	1.4	11.4034	1.8	2.8765	3.8	0.2379	3.4	0.89	1375.8	42.4	1375.8	29.0	1375.8	33.7	1375.8	33.7	100.0
UPPER HICKORY-70 <>	49	50214	1.1	11.4030	1.9	2.8755	2.0	0.2378	0.8	0.40	1375.3	9.9	1375.5	15.2	1375.8	35.7	1375.8	35.7	100.0
UPPER HICKORY-64 <>	29	21222	1.4	11.3984	4.9	2.8458	6.1	0.2353	3.7	0.60	1362.0	45.0	1367.7	46.0	1376.6	94.4	1376.6	94.4	98.9
UPPER HICKORY-122 <>	108	56136	2.0	11.3958	1.0	2.8098	1.6	0.2322	1.3	0.79	1346.2	15.3	1358.2	12.0	1377.0	19.1	1377.0	19.1	97.8
UPPER HICKORY-26 <>	54	52572	1.0	11.3956	1.9	2.9004	4.6	0.2397	4.2	0.91	1385.2	52.0	1382.0	34.5	1377.1	36.1	1377.1	36.1	100.6
UPPER HICKORY-117 <>	65	22432	1.3	11.3775	1.2	2.8696	2.1	0.2368	1.8	0.83	1370.0	21.6	1374.0	15.9	1380.1	22.4	1380.1	22.4	99.3
UPPER HICKORY-8 <>	100	25864	0.5	11.3734	1.0	2.7102	3.0	0.2236	2.8	0.95	1300.6	33.2	1331.3	22.1	1380.8	18.7	1380.8	18.7	94.2
UPPER HICKORY-100 <>	113	81548	1.6	11.3730	1.0	2.8841	1.3	0.2379	0.8	0.60	1375.8	9.4	1377.8	9.5	1380.9	19.5	1380.9	19.5	99.6
UPPER HICKORY-56 <>	86	44939	1.3	11.3696	0.9	2.8061	1.3	0.2314	1.0	0.75	1341.8	12.2	1357.2	10.0	1381.5	17.0	1381.5	17.0	97.1
UPPER HICKORY-20 <>	38	17173	1.1	11.3626	2.1	2.9174	3.4	0.2404	2.6	0.78	1388.9	32.8	1386.4	25.6	1382.6	41.0	1382.6	41.0	100.5
UPPER HICKORY-77 <>	83	45547	1.9	11.3624	1.5	2.9657	3.5	0.2444	3.1	0.90	1409.5	39.3	1398.9	26.3	1382.7	29.3	1382.7	29.3	101.9
UPPER HICKORY-116 <>	93	45743	0.7	11.3589	1.7	2.8916	2.1	0.2382	1.2	0.58	1377.4	14.9	1379.7	15.6	1383.3	32.2	1383.3	32.2	99.6
UPPER HICKORY-85 <>	86	7399	1.0	11.3531	2.4	2.6970	3.1	0.2221	1.9	0.63	1292.8	22.7	1327.6	22.7	1384.2	45.7	1384.2	45.7	93.4
UPPER HICKORY-43 <>	101	44654	0.9	11.3494	1.6	2.8412	1.9	0.2339	1.0	0.53	1354.8	12.1	1366.5	14.1	1384.9	30.7	1384.9	30.7	97.8
UPPER HICKORY-123 <>	69	26393	0.7	11.3468	1.9	2.8570	4.8	0.2351	4.4	0.92	1361.3	53.9	1370.7	36.1	1385.3	37.0	1385.3	37.0	98.3
UPPER HICKORY-15 <>	66	64402	1.4	11.3467	1.0	2.8993	3.0	0.2386	2.8	0.94	1379.4	34.5	1381.7	22.4	1385.3	19.9	1385.3	19.9	99.6
UPPER HICKORY-96 <>	106	63058	1.5	11.3457	1.5	2.9673	4.5	0.2442	4.3	0.94	1408.3	54.3	1399.3	34.6	1385.5	29.1	1385.5	29.1	101.6
UPPER HICKORY-23 <>	80	15372	1.5	11.3454	2.1	2.7696	5.4	0.2279	5.0	0.92	1323.4	59.7	1347.4	40.4	1385.5	40.7	1385.5	40.7	95.5

UPPER HICKORY-60 <>	132	55393	1.8	11.3435	0.9	2.8263	1.4	0.2325	1.1	0.78	1347.7	13.0	1362.5	10.3	1385.9	16.4	1385.9	16.4	97.2
UPPER HICKORY-37 <>	119	10974	1.5	11.3422	1.2	2.9454	3.0	0.2423	2.8	0.91	1398.6	34.6	1393.7	22.8	1386.1	23.4	1386.1	23.4	100.9
UPPER HICKORY-45 <>	74	62246	2.0	11.3390	2.2	2.9283	2.6	0.2408	1.3	0.51	1391.0	16.7	1389.3	19.6	1386.6	42.7	1386.6	42.7	100.3
UPPER HICKORY-76 <>	65	6701	1.1	11.3335	1.9	2.6243	4.2	0.2157	3.8	0.89	1259.2	43.3	1307.5	31.2	1387.6	37.0	1387.6	37.0	90.7
UPPER HICKORY-39 <>	99	35619	0.6	11.3312	1.0	3.0049	2.6	0.2469	2.4	0.92	1422.7	30.7	1408.9	19.8	1388.0	19.3	1388.0	19.3	102.5
UPPER HICKORY-25 <>	135	78987	1.9	11.3233	0.9	2.9148	1.4	0.2394	1.1	0.79	1383.4	14.0	1385.8	10.8	1389.3	16.6	1389.3	16.6	99.6
UPPER HICKORY-40 <>	36	19994	0.7	11.3226	2.1	2.9282	3.4	0.2405	2.6	0.78	1389.1	33.0	1389.2	25.6	1389.4	40.5	1389.4	40.5	100.0
UPPER HICKORY-9 <>	88	38236	1.1	11.3188	1.5	2.8492	2.1	0.2339	1.4	0.67	1354.9	17.0	1368.6	15.7	1390.1	29.7	1390.1	29.7	97.5
UPPER HICKORY-121 <>	135	121058	1.2	11.3174	0.8	2.7661	1.0	0.2270	0.6	0.57	1319.0	6.8	1346.4	7.4	1390.3	15.7	1390.3	15.7	94.9
UPPER HICKORY-35 <>	198	124872	10.6	11.3162	0.5	2.8428	3.2	0.2333	3.2	0.99	1351.8	39.2	1366.9	24.4	1390.5	8.7	1390.5	8.7	97.2
UPPER HICKORY-33 <>	57	52365	0.9	11.3098	2.5	2.9403	4.4	0.2412	3.6	0.82	1392.8	45.6	1392.3	33.5	1391.6	48.2	1391.6	48.2	100.1
UPPER HICKORY-42 <>	46	18944	0.8	11.3055	1.8	2.8600	3.3	0.2345	2.8	0.84	1358.1	33.8	1371.5	24.7	1392.3	34.4	1392.3	34.4	97.5
UPPER HICKORY-102 <>	112	64414	0.9	11.2982	0.8	2.8448	1.8	0.2331	1.6	0.89	1350.8	19.5	1367.4	13.6	1393.5	16.1	1393.5	16.1	96.9
UPPER HICKORY-111 <>	78	44351	1.7	11.2907	1.6	2.8787	2.2	0.2357	1.5	0.67	1364.4	18.3	1376.3	16.7	1394.8	31.5	1394.8	31.5	97.8
UPPER HICKORY-12 <>	136	36740	1.7	11.2833	1.4	2.7760	3.0	0.2272	2.6	0.88	1319.6	31.6	1349.1	22.4	1396.1	26.9	1396.1	26.9	94.5
UPPER HICKORY-86 <>	73	58651	1.9	11.2816	1.4	2.9200	1.5	0.2389	0.6	0.39	1381.1	7.4	1387.1	11.5	1396.4	26.9	1396.4	26.9	98.9
UPPER HICKORY-88 <>	112	11715	1.7	11.2769	1.0	2.6712	2.7	0.2185	2.6	0.94	1273.8	29.8	1320.5	20.3	1397.2	18.5	1397.2	18.5	91.2
UPPER HICKORY-71 <>	52	22968	2.0	11.2729	3.1	2.9407	3.4	0.2404	1.5	0.42	1388.9	18.2	1392.5	26.1	1397.9	59.8	1397.9	59.8	99.4
UPPER HICKORY-98 <>	97	5681	1.0	11.2725	1.2	2.6711	3.1	0.2184	2.8	0.92	1273.3	32.7	1320.5	22.7	1397.9	22.8	1397.9	22.8	91.1
UPPER HICKORY-125 <>	77	48771	1.9	11.2637	1.4	2.8352	3.6	0.2316	3.4	0.93	1342.9	40.9	1364.9	27.3	1399.4	26.2	1399.4	26.2	96.0
UPPER HICKORY-50 <>	114	9848	1.1	11.2586	1.4	2.5729	2.4	0.2101	1.9	0.81	1229.3	21.8	1293.0	17.5	1400.3	26.7	1400.3	26.7	87.8
UPPER HICKORY-47 <>	155	18463	1.0	11.2579	1.8	3.0048	5.9	0.2453	5.6	0.95	1414.4	71.3	1408.8	44.9	1400.4	34.4	1400.4	34.4	101.0
UPPER HICKORY-109 <>	104	35106	0.9	11.2535	0.5	2.9577	2.3	0.2414	2.3	0.98	1394.0	28.5	1396.8	17.7	1401.2	9.8	1401.2	9.8	99.5
UPPER HICKORY-57 <>	64	8731	1.1	11.2531	1.3	2.8839	3.2	0.2354	2.9	0.91	1362.6	36.0	1377.7	24.2	1401.2	25.0	1401.2	25.0	97.2
UPPER HICKORY-29 <>	145	56271	2.2	11.2500	0.6	2.9394	1.4	0.2398	1.2	0.89	1385.8	15.3	1392.1	10.5	1401.7	12.2	1401.7	12.2	98.9
UPPER HICKORY-46 <>	125	36298	1.2	11.2342	0.7	2.8983	2.8	0.2362	2.8	0.97	1366.7	33.9	1381.5	21.4	1404.4	12.6	1404.4	12.6	97.3
UPPER HICKORY-2 <>	88	71600	0.8	11.2308	1.2	2.9332	2.9	0.2389	2.7	0.92	1381.1	33.0	1390.5	21.9	1405.0	22.2	1405.0	22.2	98.3
UPPER HICKORY-94 <>	34	19955	0.8	11.2225	1.9	2.9598	3.1	0.2409	2.5	0.79	1391.4	31.1	1397.4	23.9	1406.4	36.9	1406.4	36.9	98.9
UPPER HICKORY-66 <>	26	11708	0.9	11.1832	3.1	2.8563	6.1	0.2317	5.2	0.86	1343.2	63.6	1370.5	46.0	1413.2	60.1	1413.2	60.1	95.1
UPPER HICKORY-61 <>	113	83710	1.8	11.1693	1.0	3.0590	1.5	0.2478	1.2	0.77	1427.1	14.9	1422.5	11.6	1415.5	18.7	1415.5	18.7	100.8

UPPER HICKORY-108 <>	59	27306	1.1	11.1595	1.5	2.8712	4.2	0.2324	4.0	0.94	1347.0	48.1	1374.4	31.8	1417.2	27.9	1417.2	27.9	95.0
UPPER HICKORY-14 <>	164	117744	1.2	11.1508	0.3	3.0461	1.6	0.2463	1.6	0.98	1419.6	20.3	1419.3	12.4	1418.7	6.2	1418.7	6.2	100.1
UPPER HICKORY-1 <>	242	3434	1.0	11.0783	3.1	2.7725	6.9	0.2228	6.2	0.89	1296.5	72.3	1348.2	51.6	1431.2	59.8	1431.2	59.8	90.6
UPPER HICKORY-4 <>	58	26004	1.0	11.0564	3.3	2.9865	4.9	0.2395	3.7	0.74	1384.0	45.5	1404.2	37.6	1434.9	63.4	1434.9	63.4	96.5
UPPER HICKORY-91 <>	91	2019	0.7	11.0454	3.9	2.6577	8.1	0.2129	7.1	0.88	1244.3	80.7	1316.8	60.0	1436.8	74.3	1436.8	74.3	86.6
UPPER HICKORY-41 <>	106	22320	1.5	11.0395	1.0	2.7950	2.8	0.2238	2.6	0.93	1301.8	30.4	1354.2	20.7	1437.9	19.1	1437.9	19.1	90.5
UPPER HICKORY-5 <>	212	21726	1.0	10.9659	0.6	3.0702	1.6	0.2442	1.5	0.93	1408.4	18.6	1425.3	12.1	1450.6	10.8	1450.6	10.8	97.1
Big Saline sandstone, sample 3 (Middle Pennsylvanian)																			
PennSS-Spot 192	292	113498	1.6	18.6684	1.6	0.4165	2.7	0.0564	2.1	0.79	353.7	7.3	353.5	8.0	352.9	36.7	353.7	7.3	100.2
PennSS-Spot 232	485	66215	1.9	14.8913	2.7	0.5864	3.4	0.0633	2.2	0.63	395.9	8.3	468.6	12.9	842.5	55.8	395.9	8.3	46.9
PennSS-Spot 290	140	75636	1.8	17.9601	1.9	0.4906	2.7	0.0639	1.8	0.68	399.3	7.1	405.3	8.9	439.6	43.2	399.3	7.1	90.8
PennSS-Spot 131	165	129477	1.9	18.0567	2.0	0.5114	2.8	0.0670	2.0	0.71	417.9	8.0	419.4	9.6	427.6	43.8	417.9	8.0	97.7
PennSS-Spot 103	82	38976	2.1	18.1160	2.3	0.5126	2.9	0.0673	1.7	0.59	420.1	6.8	420.2	9.8	420.3	51.6	420.1	6.8	100.0
PennSS-Spot 247	409	72015	8.8	18.0695	1.5	0.5150	2.2	0.0675	1.6	0.74	421.0	6.6	421.8	7.5	426.0	32.5	421.0	6.6	98.8
PennSS-Spot 266	148	94028	1.2	18.1097	1.8	0.5139	2.5	0.0675	1.8	0.69	421.1	7.2	421.1	8.8	421.1	40.9	421.1	7.2	100.0
PennSS-Spot 267	175	85474	1.9	17.6297	2.2	0.5380	2.8	0.0688	1.8	0.65	428.8	7.6	437.1	10.1	480.7	47.8	428.8	7.6	89.2
PennSS-Spot 186	107	32440	1.7	17.2513	2.8	0.5523	3.2	0.0691	1.5	0.48	430.7	6.4	446.5	11.7	528.5	62.3	430.7	6.4	81.5
PennSS-Spot 140	134	36684	2.8	17.7191	1.7	0.5383	2.8	0.0692	2.2	0.79	431.2	9.3	437.3	10.1	469.6	38.4	431.2	9.3	91.8
PennSS-Spot 109	201	97587	1.5	18.0577	1.4	0.5391	2.5	0.0706	2.1	0.84	439.8	8.8	437.9	8.8	427.5	30.1	439.8	8.8	102.9
PennSS-Spot 168	232	26411	2.0	17.6344	1.6	0.5705	2.6	0.0730	2.0	0.78	454.0	8.9	458.4	9.6	480.1	36.0	454.0	8.9	94.6
PennSS-Spot 97	103	48365	1.5	17.4775	2.0	0.5760	3.0	0.0730	2.3	0.76	454.3	10.1	461.9	11.3	499.9	43.9	454.3	10.1	90.9
PennSS-Spot 104	192	57839	1.4	17.4382	2.0	0.5781	2.6	0.0731	1.7	0.64	454.9	7.3	463.3	9.6	504.8	43.9	454.9	7.3	90.1
PennSS-Spot 1	180	79126	1.9	17.9139	2.2	0.5671	3.1	0.0737	2.2	0.71	458.3	9.7	456.2	11.3	445.3	48.3	458.3	9.7	102.9
PennSS-Spot 233	284	163947	2.9	17.6378	1.6	0.5890	2.6	0.0753	2.0	0.79	468.3	9.1	470.2	9.6	479.7	34.8	468.3	9.1	97.6
PennSS-Spot 184	164	60671	1.2	17.7206	2.0	0.5929	3.0	0.0762	2.2	0.75	473.4	10.1	472.7	11.2	469.4	43.6	473.4	10.1	100.9
PennSS-Spot 145	194	30949	2.2	17.5406	1.5	0.6225	2.4	0.0792	1.9	0.77	491.3	8.8	491.4	9.4	492.0	33.8	491.3	8.8	99.9
PennSS-Spot 254	242	75627	0.4	17.5786	1.9	0.6294	2.8	0.0802	2.1	0.73	497.6	9.8	495.7	11.1	487.2	42.9	497.6	9.8	102.1
PennSS-Spot 111	48	32116	2.9	17.5474	2.7	0.6526	3.5	0.0830	2.2	0.62	514.3	10.7	510.0	14.0	491.1	60.4	514.3	10.7	104.7

PennSS-Spot 7	135	34807	4.4	17.2165	1.9	0.6662	2.8	0.0832	2.1	0.74	515.1	10.2	518.4	11.4	532.9	41.7	515.1	10.2	96.6
PennSS-Spot 45	118	130837	2.1	17.3368	2.1	0.6617	2.9	0.0832	2.1	0.70	515.2	10.2	515.7	11.9	517.6	45.9	515.2	10.2	99.5
PennSS-Spot 235	40	30374	3.1	17.2417	2.9	0.6702	3.7	0.0838	2.2	0.60	518.8	11.1	520.8	15.0	529.7	64.1	518.8	11.1	97.9
PennSS-Spot 218	494	148468	2.9	17.1548	1.6	0.6825	2.6	0.0849	2.1	0.80	525.4	10.7	528.3	10.9	540.8	34.7	525.4	10.7	97.2
PennSS-Spot 217	99	57698	2.7	17.0361	2.0	0.6979	2.8	0.0862	2.0	0.72	533.2	10.3	537.5	11.7	556.0	42.6	533.2	10.3	95.9
PennSS-Spot 282	382	232775	5.3	16.8103	1.4	0.7091	2.2	0.0865	1.7	0.78	534.5	8.9	544.2	9.4	585.0	30.5	534.5	8.9	91.4
PennSS-Spot 264	546	116217	17.0	16.7512	1.3	0.7229	2.4	0.0878	2.0	0.84	542.7	10.5	552.4	10.2	592.6	28.0	542.7	10.5	91.6
PennSS-Spot 147	340	152835	1.5	17.0616	1.4	0.7145	2.5	0.0884	2.0	0.82	546.1	10.7	547.4	10.6	552.7	31.6	546.1	10.7	98.8
PennSS-Spot 120	111	110219	1.8	16.9065	1.8	0.7218	2.5	0.0885	1.6	0.66	546.7	8.5	551.7	10.5	572.6	40.1	546.7	8.5	95.5
PennSS-Spot 277	82	216442	0.9	16.0469	2.7	0.7683	3.9	0.0894	2.8	0.71	552.1	14.7	578.8	17.2	685.0	58.4	552.1	14.7	80.6
PennSS-Spot 190	155	107602	0.6	16.8196	2.1	0.7344	2.9	0.0896	2.0	0.69	553.1	10.8	559.1	12.7	583.8	46.2	553.1	10.8	94.7
PennSS-Spot 135	108	43292	0.8	17.0831	2.0	0.7410	3.0	0.0918	2.3	0.75	566.3	12.4	563.0	13.1	549.9	43.6	566.3	12.4	103.0
PennSS-Spot 311	596	68860	5.8	16.9460	1.3	0.7480	2.0	0.0919	1.6	0.79	566.9	8.8	567.0	8.9	567.5	27.2	566.9	8.8	99.9
PennSS-Spot 151	247	45583	4.4	16.6809	1.5	0.7699	2.7	0.0931	2.2	0.83	574.1	12.3	579.7	11.9	601.7	32.1	574.1	12.3	95.4
PennSS-Spot 295	178	50287	2.7	16.8046	1.8	0.7796	2.9	0.0950	2.2	0.78	585.2	12.4	585.3	12.7	585.7	39.1	585.2	12.4	99.9
PennSS-Spot 198	812	240584	4.9	16.3883	1.3	0.8057	2.2	0.0958	1.8	0.82	589.5	10.3	600.0	10.1	639.9	27.5	589.5	10.3	92.1
PennSS-Spot 210	163	50170	2.3	16.6337	2.1	0.7947	3.1	0.0959	2.2	0.73	590.2	12.6	593.9	13.8	607.8	45.4	590.2	12.6	97.1
PennSS-Spot 209	163	75690	2.5	16.5805	1.7	0.8252	2.3	0.0992	1.6	0.70	609.9	9.4	611.0	10.6	614.8	36.0	609.9	9.4	99.2
PennSS-Spot 106	35	46166	1.0	16.3673	3.3	0.8365	3.9	0.0993	2.1	0.53	610.3	12.1	617.2	17.9	642.7	70.5	610.3	12.1	95.0
PennSS-Spot 121	188	55371	2.2	16.5684	1.7	0.8280	2.4	0.0995	1.6	0.70	611.5	9.6	612.5	10.9	616.3	36.7	611.5	9.6	99.2
PennSS-Spot 242	81	71270	1.2	16.2892	2.3	0.8454	3.2	0.0999	2.2	0.70	613.7	13.0	622.1	14.7	653.0	48.4	613.7	13.0	94.0
PennSS-Spot 164	199	127320	1.3	16.1810	1.6	0.8630	2.9	0.1013	2.4	0.83	621.9	14.2	631.8	13.6	667.2	34.5	621.9	14.2	93.2
PennSS-Spot 122	207	124155	3.6	16.4336	1.8	0.8513	2.3	0.1015	1.4	0.61	623.0	8.1	625.4	10.5	634.0	38.5	623.0	8.1	98.3
PennSS-Spot 180	86	121914	2.0	16.4498	1.6	0.8507	2.5	0.1015	1.9	0.77	623.2	11.5	625.1	11.7	631.9	34.5	623.2	11.5	98.6
PennSS-Spot 93	107	37679	1.3	16.2667	1.4	0.8669	2.3	0.1023	1.9	0.80	627.7	11.1	633.9	11.0	655.9	30.3	627.7	11.1	95.7
PennSS-Spot 283	205	173369	0.4	16.0542	1.6	0.8808	2.3	0.1026	1.6	0.69	629.4	9.5	641.4	10.8	684.1	35.0	629.4	9.5	92.0
PennSS-Spot 125	42	24413	2.0	16.4826	2.9	0.8856	3.6	0.1059	2.2	0.62	648.7	13.8	644.0	17.3	627.5	61.4	648.7	13.8	103.4
PennSS-Spot 159	300	158296	7.1	16.2692	1.5	0.9140	2.6	0.1078	2.2	0.83	660.2	13.6	659.2	12.7	655.6	31.8	660.2	13.6	100.7
PennSS-Spot 307	181	47375	0.9	15.6924	1.4	1.0206	2.3	0.1162	1.8	0.80	708.4	12.3	714.2	11.8	732.5	29.3	708.4	12.3	96.7
PennSS-Spot 189	120	121869	3.6	14.6708	2.2	1.1535	2.8	0.1227	1.8	0.63	746.3	12.3	778.9	15.2	873.5	44.9	746.3	12.3	85.4

PennSS-Spot 130	235	58932	5.8	15.6067	1.6	1.0994	2.9	0.1244	2.4	0.82	756.1	17.0	753.1	15.4	744.1	34.7	756.1	17.0	101.6
PennSS-Spot 158	205	444549	1.5	15.2059	1.4	1.1649	2.5	0.1285	2.1	0.83	779.1	15.4	784.3	13.7	798.9	29.1	779.1	15.4	97.5
PennSS-Spot 105	220	65181	1.3	15.2813	1.7	1.1849	2.4	0.1313	1.7	0.70	795.4	12.7	793.6	13.4	788.5	36.6	795.4	12.7	100.9
PennSS-Spot 187	18	31787	1.6	14.5840	2.7	1.4412	3.3	0.1524	1.9	0.57	914.6	16.1	906.2	19.9	885.8	56.6	885.8	56.6	103.3
PennSS-Spot 16	108	61399	2.8	14.5335	1.5	1.4420	2.3	0.1520	1.7	0.75	912.1	14.7	906.5	13.8	893.0	31.3	893.0	31.3	102.1
PennSS-Spot 251	51	43784	2.4	14.4381	2.5	1.4590	2.9	0.1528	1.5	0.51	916.5	12.7	913.6	17.6	906.5	51.6	906.5	51.6	101.1
PennSS-Spot 279	43	88735	3.2	14.3853	2.0	1.4317	2.9	0.1494	2.1	0.72	897.4	17.5	902.3	17.3	914.1	41.1	914.1	41.1	98.2
PennSS-Spot 177	100	38916	2.2	14.3814	1.8	1.4751	2.6	0.1539	1.9	0.72	922.6	15.9	920.2	15.6	914.6	36.8	914.6	36.8	100.9
PennSS-Spot 25	119	105584	2.9	14.3278	1.5	1.4622	2.5	0.1519	2.0	0.79	911.8	17.0	914.9	15.1	922.3	31.3	922.3	31.3	98.9
PennSS-Spot 117	144	73041	2.2	14.3021	2.0	1.4608	2.9	0.1515	2.1	0.73	909.5	17.8	914.3	17.4	926.0	40.5	926.0	40.5	98.2
PennSS-Spot 76	156	64902	3.7	14.2844	1.4	1.5270	2.4	0.1582	1.9	0.80	946.7	17.0	941.3	14.7	928.6	29.4	928.6	29.4	102.0
PennSS-Spot 47	150	217692	1.3	14.1487	1.8	1.5807	3.1	0.1622	2.5	0.82	969.0	22.9	962.6	19.2	948.1	36.0	948.1	36.0	102.2
PennSS-Spot 102	114	104965	2.0	14.1194	1.1	1.5103	2.3	0.1547	2.0	0.87	927.0	17.3	934.5	14.1	952.4	23.3	952.4	23.3	97.3
PennSS-Spot 31	216	106633	3.5	14.0682	1.0	1.6079	1.8	0.1641	1.5	0.83	979.3	13.9	973.3	11.5	959.8	21.2	959.8	21.2	102.0
PennSS-Spot 293	441	205219	3.8	13.9675	1.3	1.6023	2.3	0.1623	1.9	0.84	969.6	17.2	971.1	14.3	974.4	25.5	974.4	25.5	99.5
PennSS-Spot 194	25	28382	1.6	13.9381	2.0	1.5966	3.0	0.1614	2.3	0.75	964.6	20.4	968.9	18.9	978.7	40.4	978.7	40.4	98.6
PennSS-Spot 163	48	61496	0.8	13.9190	1.8	1.6127	2.8	0.1628	2.2	0.77	972.3	19.7	975.2	17.7	981.5	36.4	981.5	36.4	99.1
PennSS-Spot 157	104	30554	2.6	13.9034	1.5	1.5722	2.4	0.1585	1.9	0.79	948.7	16.9	959.3	14.9	983.8	29.8	983.8	29.8	96.4
PennSS-Spot 196	50	28683	3.3	13.8981	1.8	1.6072	2.6	0.1620	1.9	0.73	967.9	17.2	973.0	16.5	984.6	36.6	984.6	36.6	98.3
PennSS-Spot 84	33	109846	3.9	13.8868	2.2	1.5482	3.2	0.1559	2.3	0.72	934.1	20.1	949.8	19.7	986.2	44.9	986.2	44.9	94.7
PennSS-Spot 43	124	139132	3.4	13.8779	1.4	1.7012	2.8	0.1712	2.4	0.87	1018.9	22.6	1009.0	17.7	987.5	28.0	987.5	28.0	103.2
PennSS-Spot 182	76	46138	5.1	13.8584	1.9	1.6481	2.7	0.1657	1.8	0.70	988.1	16.9	988.8	16.8	990.4	38.8	990.4	38.8	99.8
PennSS-Spot 37	96	228137	3.6	13.8552	1.9	1.5807	2.7	0.1588	1.9	0.72	950.3	16.9	962.6	16.7	990.9	38.1	990.9	38.1	95.9
PennSS-Spot 23	113	113564	7.2	13.8401	1.7	1.6268	2.8	0.1633	2.2	0.78	975.0	19.6	980.6	17.5	993.1	35.4	993.1	35.4	98.2
PennSS-Spot 160	161	105871	6.1	13.8106	1.6	1.6651	2.6	0.1668	2.0	0.78	994.3	18.8	995.3	16.6	997.4	33.2	997.4	33.2	99.7
PennSS-Spot 174	76	81937	1.9	13.8086	1.3	1.5921	1.8	0.1594	1.2	0.68	953.7	10.8	967.1	11.2	997.7	26.9	997.7	26.9	95.6
PennSS-Spot 11	30	68314	0.4	13.7993	2.1	1.6659	3.2	0.1667	2.4	0.75	994.0	22.2	995.6	20.3	999.1	42.6	999.1	42.6	99.5
PennSS-Spot 123	21	52405	1.5	13.7837	2.9	1.6576	3.4	0.1657	1.7	0.51	988.4	15.9	992.5	21.5	1001.4	59.1	1001.4	59.1	98.7
PennSS-Spot 255	62	42554	1.9	13.7715	1.7	1.4991	2.4	0.1497	1.7	0.72	899.4	14.6	930.0	14.8	1003.2	34.5	1003.2	34.5	89.7
PennSS-Spot 100	42	35156	1.2	13.7668	2.3	1.6022	2.9	0.1600	1.8	0.62	956.6	16.1	971.1	18.1	1003.9	46.0	1003.9	46.0	95.3

PennSS-Spot 221	208	29428068	1.9	13.7611	1.7	1.6011	2.7	0.1598	2.0	0.76	955.7	17.9	970.7	16.6	1004.7	35.1	1004.7	35.1	95.1
PennSS-Spot 276	108	123437	4.0	13.7503	1.9	1.7597	2.9	0.1755	2.2	0.76	1042.3	21.0	1030.8	18.6	1006.3	37.8	1006.3	37.8	103.6
PennSS-Spot 72	24	13293	2.3	13.7459	2.6	1.6503	3.2	0.1645	1.8	0.57	981.9	16.5	989.7	20.0	1007.0	52.8	1007.0	52.8	97.5
PennSS-Spot 170	90	67621	1.8	13.7197	1.0	1.7407	1.9	0.1732	1.6	0.84	1029.7	15.0	1023.7	12.2	1010.8	20.9	1010.8	20.9	101.9
PennSS-Spot 52	117	99835	3.4	13.7095	1.4	1.7726	2.6	0.1762	2.2	0.84	1046.5	21.4	1035.5	17.2	1012.3	29.3	1012.3	29.3	103.4
PennSS-Spot 132	217	245736	3.3	13.7076	1.4	1.5152	2.2	0.1506	1.7	0.76	904.6	14.1	936.6	13.5	1012.6	29.0	1012.6	29.0	89.3
PennSS-Spot 61	130	155995	4.0	13.6995	1.4	1.6641	2.5	0.1653	2.0	0.82	986.4	18.6	995.0	15.8	1013.8	29.0	1013.8	29.0	97.3
PennSS-Spot 220	427	301772	5.8	13.6976	1.5	1.6790	2.5	0.1668	2.1	0.81	994.4	19.1	1000.6	16.2	1014.1	29.9	1014.1	29.9	98.1
PennSS-Spot 91	78	151035	2.0	13.6869	1.8	1.6150	2.8	0.1603	2.1	0.75	958.5	18.5	976.0	17.3	1015.7	36.8	1015.7	36.8	94.4
PennSS-Spot 226	122	90005	4.7	13.6831	1.6	1.6821	2.9	0.1669	2.4	0.84	995.2	22.3	1001.8	18.4	1016.2	31.8	1016.2	31.8	97.9
PennSS-Spot 243	175	105370	0.9	13.6759	1.4	1.6597	2.6	0.1646	2.2	0.85	982.4	20.2	993.3	16.6	1017.3	28.1	1017.3	28.1	96.6
PennSS-Spot 77	105	196554	2.8	13.6730	1.5	1.7110	2.5	0.1697	2.1	0.82	1010.3	19.4	1012.7	16.3	1017.7	29.6	1017.7	29.6	99.3
PennSS-Spot 40	166	114542	1.2	13.6650	1.6	1.7360	2.9	0.1721	2.5	0.84	1023.4	23.4	1022.0	18.9	1018.9	31.8	1018.9	31.8	100.4
PennSS-Spot 286	37	39743	2.1	13.6594	2.4	1.6947	3.2	0.1679	2.2	0.68	1000.5	20.4	1006.5	20.7	1019.7	48.4	1019.7	48.4	98.1
PennSS-Spot 146	67	37441	4.4	13.6560	2.1	1.6238	3.1	0.1608	2.3	0.75	961.4	20.8	979.5	19.5	1020.2	41.7	1020.2	41.7	94.2
PennSS-Spot 216	128	181636	3.0	13.6536	1.4	1.6277	2.6	0.1612	2.2	0.85	963.4	19.4	981.0	16.1	1020.6	27.5	1020.6	27.5	94.4
PennSS-Spot 229	96	79447	1.3	13.6323	1.7	1.6585	2.7	0.1640	2.1	0.77	978.8	18.7	992.8	16.9	1023.8	34.5	1023.8	34.5	95.6
PennSS-Spot 250	195	50851	10.7	13.6255	1.4	1.6424	2.2	0.1623	1.7	0.76	969.6	15.2	986.6	14.0	1024.8	28.9	1024.8	28.9	94.6
PennSS-Spot 89	180	562258	2.8	13.6203	1.5	1.7318	2.5	0.1711	2.0	0.80	1018.0	18.9	1020.4	16.3	1025.5	30.9	1025.5	30.9	99.3
PennSS-Spot 237	150	56748	3.1	13.6128	1.3	1.7349	2.4	0.1713	1.9	0.82	1019.2	18.3	1021.6	15.2	1026.7	27.3	1026.7	27.3	99.3
PennSS-Spot 241	86	42711	5.2	13.6093	1.9	1.7867	3.1	0.1764	2.4	0.79	1047.0	23.4	1040.6	20.1	1027.2	38.5	1027.2	38.5	101.9
PennSS-Spot 213	315	59879	4.4	13.5975	0.8	1.7716	1.9	0.1747	1.8	0.91	1038.0	17.0	1035.1	12.6	1028.9	16.2	1028.9	16.2	100.9
PennSS-Spot 59	417	113500	2.6	13.5876	1.1	1.7143	2.0	0.1689	1.6	0.82	1006.3	15.0	1013.9	12.6	1030.4	22.8	1030.4	22.8	97.7
PennSS-Spot 90	61	210673	3.6	13.5867	1.6	1.7200	2.5	0.1695	1.9	0.78	1009.3	18.1	1016.0	16.1	1030.5	31.9	1030.5	31.9	97.9
PennSS-Spot 69	55	193157	2.4	13.5727	1.6	1.6678	2.5	0.1642	1.9	0.76	980.0	17.3	996.4	15.9	1032.6	32.9	1032.6	32.9	94.9
PennSS-Spot 193	47	205453	1.2	13.5656	2.2	1.7873	3.2	0.1758	2.3	0.72	1044.2	22.6	1040.8	21.2	1033.7	45.5	1033.7	45.5	101.0
PennSS-Spot 137	92	50108	0.7	13.5346	1.5	1.7328	2.4	0.1701	1.9	0.78	1012.6	17.6	1020.8	15.5	1038.3	30.7	1038.3	30.7	97.5
PennSS-Spot 92	102	43164	7.1	13.5106	1.7	1.6781	2.5	0.1644	1.8	0.72	981.4	16.3	1000.3	15.7	1041.9	34.5	1041.9	34.5	94.2
PennSS-Spot 208	54	30761	2.8	13.5036	1.9	1.7685	3.0	0.1732	2.4	0.79	1029.7	22.7	1034.0	19.6	1042.9	37.5	1042.9	37.5	98.7
PennSS-Spot 83	211	178957	2.0	13.5005	1.2	1.7602	2.3	0.1724	1.9	0.84	1025.0	18.0	1030.9	14.7	1043.4	25.0	1043.4	25.0	98.2

PennSS-Spot 179	60	235390	1.2	13.5001	1.6	1.7187	2.7	0.1683	2.2	0.80	1002.6	20.3	1015.5	17.5	1043.4	32.8	1043.4	32.8	96.1
PennSS-Spot 230	96	89326	1.7	13.4950	1.5	1.8818	2.5	0.1842	2.0	0.80	1089.8	20.3	1074.7	16.7	1044.2	30.1	1044.2	30.1	104.4
PennSS-Spot 252	141	185157	3.8	13.4931	1.7	1.7698	2.7	0.1732	2.0	0.77	1029.7	19.4	1034.5	17.2	1044.5	34.1	1044.5	34.1	98.6
PennSS-Spot 51	99	215581	5.7	13.4846	2.0	1.8606	3.3	0.1820	2.6	0.79	1077.7	25.7	1067.2	21.6	1045.8	40.4	1045.8	40.4	103.1
PennSS-Spot 304	56	25569	2.5	13.4833	2.1	1.8044	2.8	0.1765	1.9	0.66	1047.6	18.1	1047.1	18.6	1046.0	43.1	1046.0	43.1	100.2
PennSS-Spot 27	265	74522	2.6	13.4693	1.5	1.8334	2.5	0.1791	2.0	0.80	1062.0	19.4	1057.5	16.2	1048.1	29.6	1048.1	29.6	101.3
PennSS-Spot 41	64	32125	3.1	13.4455	1.7	1.8095	2.8	0.1765	2.3	0.81	1047.6	21.9	1048.9	18.4	1051.7	33.4	1051.7	33.4	99.6
PennSS-Spot 10	110	95996	1.9	13.4423	1.6	1.7781	2.7	0.1734	2.2	0.80	1030.6	20.6	1037.5	17.5	1052.1	32.4	1052.1	32.4	97.9
PennSS-Spot 154	108	49725	1.6	13.4374	1.6	1.4865	2.4	0.1449	1.8	0.75	872.1	14.9	924.9	14.8	1052.9	32.6	1052.9	32.6	82.8
PennSS-Spot 166	1016	107417	15.3	13.4373	1.2	1.7877	2.1	0.1742	1.7	0.82	1035.3	16.7	1041.0	13.9	1052.9	24.7	1052.9	24.7	98.3
PennSS-Spot 303	29	45123	2.5	13.4319	2.8	1.5794	4.1	0.1539	3.0	0.73	922.6	26.0	962.1	25.6	1053.7	56.5	1053.7	56.5	87.6
PennSS-Spot 248	30	19691	1.3	13.4140	2.6	1.7893	3.2	0.1741	2.0	0.61	1034.5	18.6	1041.6	21.0	1056.4	51.5	1056.4	51.5	97.9
PennSS-Spot 148	490	77873	4.5	13.3945	1.5	1.7458	2.5	0.1696	1.9	0.78	1009.9	18.2	1025.6	16.0	1059.3	31.2	1059.3	31.2	95.3
PennSS-Spot 70	155	106000	3.0	13.3882	1.6	1.7572	2.4	0.1706	1.8	0.76	1015.6	17.0	1029.8	15.4	1060.3	31.2	1060.3	31.2	95.8
PennSS-Spot 112	62	28526	3.4	13.3630	1.8	1.8329	2.6	0.1776	1.9	0.73	1054.1	18.2	1057.3	16.9	1064.0	35.5	1064.0	35.5	99.1
PennSS-Spot 81	169	114156	3.8	13.3598	1.2	1.7584	2.3	0.1704	1.9	0.85	1014.2	18.1	1030.3	14.7	1064.5	24.3	1064.5	24.3	95.3
PennSS-Spot 48	216	94990	2.5	13.3553	1.3	1.7971	2.6	0.1741	2.3	0.87	1034.5	22.0	1044.4	17.2	1065.2	25.7	1065.2	25.7	97.1
PennSS-Spot 127	65	45519	1.2	13.3421	1.7	1.8303	2.5	0.1771	1.8	0.73	1051.2	17.9	1056.4	16.6	1067.2	34.8	1067.2	34.8	98.5
PennSS-Spot 82	82	145742	2.7	13.3396	1.6	1.8087	2.6	0.1750	2.0	0.78	1039.5	19.2	1048.6	16.8	1067.6	32.5	1067.6	32.5	97.4
PennSS-Spot 26	98	34335	1.1	13.3377	1.5	1.8441	2.7	0.1784	2.2	0.82	1058.2	21.8	1061.3	17.8	1067.9	30.9	1067.9	30.9	99.1
PennSS-Spot 238	49	47412	2.7	13.3356	2.0	1.7060	2.8	0.1650	2.0	0.70	984.5	18.1	1010.8	18.1	1068.2	40.5	1068.2	40.5	92.2
PennSS-Spot 149	119	55387	1.6	13.3089	1.4	1.9037	2.6	0.1838	2.2	0.85	1087.4	22.0	1082.4	17.3	1072.2	27.9	1072.2	27.9	101.4
PennSS-Spot 269	176	154417	2.5	13.2910	1.5	1.7981	2.3	0.1733	1.7	0.77	1030.4	16.6	1044.8	14.8	1074.9	29.3	1074.9	29.3	95.9
PennSS-Spot 253	151	74423	2.5	13.2837	1.4	1.7691	2.1	0.1704	1.6	0.76	1014.5	15.2	1034.2	13.9	1076.0	28.0	1076.0	28.0	94.3
PennSS-Spot 240	27	38128	1.1	13.2834	3.2	1.7713	3.9	0.1706	2.3	0.58	1015.7	21.4	1035.0	25.4	1076.1	63.8	1076.1	63.8	94.4
PennSS-Spot 183	108	214163	1.4	13.2793	1.5	1.7234	2.5	0.1660	2.0	0.80	989.9	18.6	1017.3	16.4	1076.7	30.9	1076.7	30.9	91.9
PennSS-Spot 6	109	147358	2.9	13.2743	1.8	1.9013	3.3	0.1830	2.8	0.85	1083.6	28.2	1081.5	22.2	1077.4	35.8	1077.4	35.8	100.6
PennSS-Spot 114	124	148930	3.0	13.2575	1.5	1.8092	2.6	0.1740	2.1	0.81	1033.9	20.2	1048.8	17.1	1079.9	30.9	1079.9	30.9	95.7
PennSS-Spot 297	440	331430	3.5	13.2567	1.2	1.8465	2.5	0.1775	2.2	0.88	1053.5	21.5	1062.2	16.6	1080.1	24.0	1080.1	24.0	97.5
PennSS-Spot 223	65	28069	3.0	13.2416	1.6	1.8369	2.6	0.1764	2.0	0.78	1047.3	19.5	1058.7	17.0	1082.3	32.5	1082.3	32.5	96.8

PennSS-Spot 263	172	68722	2.1	13.2337	1.2	1.9006	2.6	0.1824	2.3	0.88	1080.2	22.8	1081.3	17.3	1083.5	24.5	1083.5	24.5	99.7
PennSS-Spot 39	669	106912	2.7	13.2314	1.2	1.9017	2.6	0.1825	2.3	0.88	1080.6	23.2	1081.7	17.6	1083.9	24.9	1083.9	24.9	99.7
PennSS-Spot 126	160	116703	4.7	13.2229	1.5	1.8980	2.6	0.1820	2.2	0.82	1078.0	21.5	1080.4	17.5	1085.2	30.0	1085.2	30.0	99.3
PennSS-Spot 136	101	54208	2.1	13.2198	1.7	1.8721	2.8	0.1795	2.3	0.80	1064.2	22.2	1071.3	18.8	1085.7	34.1	1085.7	34.1	98.0
PennSS-Spot 288	129	104553	3.0	13.1986	1.6	1.7850	2.8	0.1709	2.3	0.82	1016.9	21.6	1040.0	18.1	1088.9	31.6	1088.9	31.6	93.4
PennSS-Spot 298	147	233702	1.4	13.1966	1.7	1.8760	2.7	0.1795	2.1	0.77	1064.5	20.1	1072.6	17.6	1089.2	33.8	1089.2	33.8	97.7
PennSS-Spot 108	48	45461	3.0	13.1947	1.8	1.8110	2.7	0.1733	2.0	0.75	1030.3	19.0	1049.5	17.4	1089.5	35.2	1089.5	35.2	94.6
PennSS-Spot 49	60	40557	2.4	13.1782	1.7	1.8772	2.9	0.1794	2.4	0.82	1063.8	23.7	1073.1	19.5	1092.0	33.6	1092.0	33.6	97.4
PennSS-Spot 150	137	129072	0.9	13.1767	1.8	1.7613	2.7	0.1683	2.1	0.76	1002.9	19.5	1031.3	17.8	1092.2	35.5	1092.2	35.5	91.8
PennSS-Spot 302	52	124296	3.7	13.1680	1.8	1.7479	2.8	0.1669	2.1	0.75	995.2	19.1	1026.4	17.9	1093.6	36.9	1093.6	36.9	91.0
PennSS-Spot 71	41	48630	2.3	13.1525	1.7	1.8330	2.8	0.1749	2.2	0.79	1038.8	21.2	1057.4	18.4	1095.9	34.7	1095.9	34.7	94.8
PennSS-Spot 234	52	35445	1.6	13.0891	2.4	1.7771	3.1	0.1687	2.0	0.64	1005.0	18.4	1037.1	20.0	1105.6	47.2	1105.6	47.2	90.9
PennSS-Spot 29	105	101919	2.9	13.0774	1.6	1.9839	2.5	0.1882	1.9	0.76	1111.4	19.4	1110.1	16.8	1107.4	32.3	1107.4	32.3	100.4
PennSS-Spot 257	120	144087	2.1	13.0664	1.2	1.8864	2.1	0.1788	1.7	0.80	1060.2	16.4	1076.3	13.9	1109.0	24.9	1109.0	24.9	95.6
PennSS-Spot 18	113	74538	2.7	13.0656	1.6	2.0569	3.0	0.1949	2.5	0.84	1147.9	26.8	1134.6	20.7	1109.1	32.5	1109.1	32.5	103.5
PennSS-Spot 32	229	59387	2.6	13.0357	1.3	1.9941	2.2	0.1885	1.8	0.81	1113.4	18.5	1113.5	15.1	1113.7	26.1	1113.7	26.1	100.0
PennSS-Spot 65	273	558528	1.9	12.9819	1.2	1.9692	1.7	0.1854	1.3	0.73	1096.5	12.8	1105.0	11.6	1122.0	23.4	1122.0	23.4	97.7
PennSS-Spot 15	354	65357	3.1	12.9812	1.3	2.0108	2.4	0.1893	2.1	0.85	1117.7	21.1	1119.2	16.5	1122.1	25.9	1122.1	25.9	99.6
PennSS-Spot 78	108	112885	2.7	12.9764	1.7	1.9590	2.5	0.1844	1.9	0.74	1090.8	18.6	1101.5	16.9	1122.8	33.8	1122.8	33.8	97.1
PennSS-Spot 88	319	128354	3.9	12.9398	1.6	2.0523	2.6	0.1926	2.1	0.79	1135.5	21.5	1133.0	17.9	1128.5	31.9	1128.5	31.9	100.6
PennSS-Spot 222	175	77280	7.1	12.9393	1.5	1.9102	2.3	0.1793	1.7	0.74	1063.0	16.7	1084.7	15.3	1128.6	30.8	1128.6	30.8	94.2
PennSS-Spot 162	150	47299	2.1	12.9214	1.7	2.0396	2.6	0.1911	1.9	0.75	1127.5	20.2	1128.8	17.6	1131.3	33.7	1131.3	33.7	99.7
PennSS-Spot 249	52	26405	2.8	12.8892	2.0	2.1217	2.8	0.1983	2.0	0.72	1166.4	21.6	1155.9	19.4	1136.3	39.0	1136.3	39.0	102.7
PennSS-Spot 5	65	40977	3.8	12.8815	1.7	2.0146	3.0	0.1882	2.5	0.83	1111.7	25.3	1120.4	20.3	1137.5	33.3	1137.5	33.3	97.7
PennSS-Spot 173	74	199077	2.6	12.8544	2.0	2.0233	3.0	0.1886	2.3	0.75	1114.0	23.3	1123.4	20.6	1141.6	39.6	1141.6	39.6	97.6
PennSS-Spot 301	101	74154	3.2	12.8436	1.4	1.9544	2.6	0.1821	2.1	0.83	1078.2	21.0	1100.0	17.2	1143.3	28.6	1143.3	28.6	94.3
PennSS-Spot 138	84	53066	3.8	12.8200	1.4	1.9879	2.3	0.1848	1.8	0.78	1093.3	18.0	1111.4	15.4	1147.0	28.1	1147.0	28.1	95.3
PennSS-Spot 33	80	77704	3.6	12.8169	1.6	1.9612	2.4	0.1823	1.8	0.74	1079.6	17.6	1102.3	16.0	1147.4	31.8	1147.4	31.8	94.1
PennSS-Spot 310	167	179376	1.3	12.8149	1.2	1.9979	2.3	0.1857	2.0	0.86	1098.0	19.7	1114.8	15.3	1147.7	22.9	1147.7	22.9	95.7
PennSS-Spot 305	213	56050	2.3	12.7896	1.4	2.0902	2.4	0.1939	1.9	0.80	1142.4	19.8	1145.6	16.2	1151.6	28.0	1151.6	28.0	99.2

PennSS-Spot 315	104	44164	2.3	12.7873	1.5	1.9508	2.5	0.1809	2.0	0.79	1072.0	19.4	1098.7	16.8	1152.0	30.6	1152.0	30.6	93.1
PennSS-Spot 300	118	66875	4.0	12.7788	1.8	2.0490	2.9	0.1899	2.3	0.80	1120.8	23.9	1132.0	19.9	1153.3	35.0	1153.3	35.0	97.2
PennSS-Spot 4	97	1741011	4.2	12.7537	1.0	2.0669	2.2	0.1912	2.0	0.89	1127.8	20.4	1137.9	15.2	1157.2	20.4	1157.2	20.4	97.5
PennSS-Spot 128	63	45716	4.0	12.7498	1.5	1.9633	2.4	0.1816	1.9	0.79	1075.4	19.0	1103.0	16.3	1157.8	29.2	1157.8	29.2	92.9
PennSS-Spot 191	131	65776	3.1	12.7454	1.4	2.0991	2.5	0.1940	2.1	0.82	1143.2	21.6	1148.5	17.2	1158.5	28.3	1158.5	28.3	98.7
PennSS-Spot 124	85	92547	3.3	12.7337	1.5	2.0570	2.4	0.1900	1.8	0.77	1121.2	18.9	1134.6	16.4	1160.3	30.5	1160.3	30.5	96.6
PennSS-Spot 207	242	151922	3.0	12.6217	1.2	2.1917	2.3	0.2006	2.0	0.85	1178.7	21.3	1178.4	16.1	1177.9	23.8	1177.9	23.8	100.1
PennSS-Spot 64	153	103838	1.8	12.6118	1.4	2.1162	2.2	0.1936	1.7	0.79	1140.7	18.0	1154.1	15.1	1179.4	26.8	1179.4	26.8	96.7
PennSS-Spot 19	55	26649	1.6	12.5942	1.8	2.2295	2.7	0.2036	2.0	0.74	1194.9	21.9	1190.4	19.1	1182.2	36.4	1182.2	36.4	101.1
PennSS-Spot 202	145	191504	5.1	12.5750	1.6	2.1841	2.6	0.1992	2.1	0.79	1171.0	22.3	1176.0	18.3	1185.2	31.9	1185.2	31.9	98.8
PennSS-Spot 181	237	168286	4.5	12.5502	1.5	2.1345	2.4	0.1943	1.9	0.80	1144.5	20.4	1160.0	16.9	1189.1	29.3	1189.1	29.3	96.3
PennSS-Spot 44	230	44660	3.2	12.5056	1.9	1.8721	2.9	0.1698	2.2	0.76	1011.0	20.5	1071.3	19.1	1196.1	36.8	1196.1	36.8	84.5
PennSS-Spot 256	46	43603	3.5	12.4478	1.9	2.2584	2.9	0.2039	2.3	0.77	1196.2	24.6	1199.4	20.7	1205.2	37.3	1205.2	37.3	99.3
PennSS-Spot 142	153	185409	2.3	12.3915	1.4	2.1218	2.5	0.1907	2.1	0.84	1125.1	21.6	1155.9	17.3	1214.1	27.0	1214.1	27.0	92.7
PennSS-Spot 296	829	107887	2.3	12.3050	1.8	2.3328	2.9	0.2082	2.2	0.78	1219.2	24.9	1222.3	20.5	1227.9	35.5	1227.9	35.5	99.3
PennSS-Spot 167	27	157526	5.0	12.2903	1.7	2.2586	2.6	0.2013	2.0	0.77	1182.4	21.8	1199.5	18.6	1230.3	33.3	1230.3	33.3	96.1
PennSS-Spot 306	243	163387	5.0	12.1973	1.3	2.3681	2.7	0.2095	2.3	0.87	1226.1	26.2	1233.0	19.3	1245.2	26.0	1245.2	26.0	98.5
PennSS-Spot 74	139	126406	1.9	12.0708	1.1	2.3528	2.2	0.2060	1.9	0.87	1207.3	21.0	1228.4	15.5	1265.5	20.7	1265.5	20.7	95.4
PennSS-Spot 55	189	41972	1.8	12.0569	1.5	2.1272	2.3	0.1860	1.8	0.77	1099.8	17.9	1157.7	15.9	1267.8	28.8	1267.8	28.8	86.7
PennSS-Spot 215	87	125156	1.9	11.9964	1.4	2.4582	2.4	0.2139	1.9	0.79	1249.4	21.1	1259.8	17.0	1277.6	28.0	1277.6	28.0	97.8
PennSS-Spot 30	26	40022	1.3	11.9247	2.1	2.5542	2.9	0.2209	2.0	0.70	1286.7	23.5	1287.6	21.1	1289.3	40.3	1289.3	40.3	99.8
PennSS-Spot 38	71	74618	2.7	11.7938	1.5	2.6068	2.4	0.2230	1.9	0.78	1297.6	22.4	1302.6	17.9	1310.7	29.5	1310.7	29.5	99.0
PennSS-Spot 205	149	215235	1.5	11.7542	1.4	2.5961	2.1	0.2213	1.6	0.76	1288.8	19.0	1299.6	15.7	1317.3	27.0	1317.3	27.0	97.8
PennSS-Spot 54	146	172373	3.3	11.6909	1.5	2.6679	2.7	0.2262	2.3	0.84	1314.6	27.5	1319.6	20.3	1327.7	28.6	1327.7	28.6	99.0
PennSS-Spot 22	35	83689	2.8	11.6793	2.3	2.7170	3.2	0.2301	2.3	0.71	1335.3	27.3	1333.1	23.7	1329.6	43.7	1329.6	43.7	100.4
PennSS-Spot 98	115	121810	1.6	11.6593	1.5	2.5114	2.5	0.2124	2.0	0.81	1241.4	23.0	1275.4	18.2	1333.0	28.4	1333.0	28.4	93.1
PennSS-Spot 299	49	91952	2.3	11.5961	2.2	2.5126	3.1	0.2113	2.2	0.72	1235.8	25.1	1275.7	22.6	1343.5	42.0	1343.5	42.0	92.0
PennSS-Spot 309	90	111656	1.8	11.4165	1.3	2.7695	2.6	0.2293	2.2	0.85	1330.9	26.5	1347.4	19.3	1373.5	25.8	1373.5	25.8	96.9
PennSS-Spot 14	32	83874	2.1	11.3779	1.5	2.7342	2.8	0.2256	2.4	0.85	1311.5	28.4	1337.8	20.9	1380.1	28.1	1380.1	28.1	95.0
PennSS-Spot 8	433	246857	2.6	11.3638	1.2	2.8331	2.5	0.2335	2.2	0.88	1352.8	26.8	1364.3	18.7	1382.4	22.9	1382.4	22.9	97.9

PennSS-Spot 101	150	62692	3.3	11.3611	1.7	2.7999	2.9	0.2307	2.4	0.81	1338.2	28.5	1355.5	21.9	1382.9	33.4	1382.9	33.4	96.8
PennSS-Spot 53	84	151091	2.5	11.3416	1.4	2.9091	2.1	0.2393	1.6	0.76	1383.0	20.4	1384.3	16.2	1386.2	26.7	1386.2	26.7	99.8
PennSS-Spot 287	52	107981	2.2	11.2633	1.7	2.7085	2.7	0.2213	2.1	0.78	1288.5	24.7	1330.8	20.1	1399.5	32.4	1399.5	32.4	92.1
PennSS-Spot 3	148	173641	1.9	11.1672	1.2	2.8879	2.6	0.2339	2.3	0.89	1354.9	27.8	1378.8	19.3	1415.9	22.6	1415.9	22.6	95.7
PennSS-Spot 85	50	74867	3.3	11.1651	1.4	2.9375	2.1	0.2379	1.6	0.75	1375.6	19.9	1391.6	16.2	1416.3	26.9	1416.3	26.9	97.1
PennSS-Spot 153	467	58341	3.1	11.1363	1.4	2.9607	2.1	0.2391	1.6	0.75	1382.2	19.8	1397.6	16.1	1421.2	26.9	1421.2	26.9	97.3
PennSS-Spot 58	246	134190	6.5	10.9960	1.4	3.1354	2.1	0.2500	1.5	0.74	1438.7	19.7	1441.4	15.9	1445.4	26.6	1445.4	26.6	99.5
PennSS-Spot 17	118	229643	2.1	10.8157	1.1	3.2653	2.1	0.2561	1.8	0.86	1470.1	23.9	1472.8	16.4	1476.8	20.6	1476.8	20.6	99.5
PennSS-Spot 258	366	238808	2.6	10.8134	1.5	3.1983	2.3	0.2508	1.8	0.77	1442.7	23.4	1456.7	18.1	1477.2	28.2	1477.2	28.2	97.7
PennSS-Spot 60	1006	156336	11.7	10.8091	1.4	3.0384	2.6	0.2382	2.2	0.86	1377.3	27.8	1417.3	20.0	1478.0	25.6	1478.0	25.6	93.2
PennSS-Spot 271	440	236236	2.0	10.7756	1.3	3.3507	2.5	0.2619	2.1	0.86	1499.4	28.5	1492.9	19.5	1483.8	24.3	1483.8	24.3	101.0
PennSS-Spot 139	92	220417	3.0	10.7319	1.1	3.1470	2.2	0.2449	1.9	0.86	1412.4	24.1	1444.3	16.9	1491.5	20.9	1491.5	20.9	94.7
PennSS-Spot 203	283	120229	3.5	10.6402	1.2	3.3286	1.8	0.2569	1.4	0.77	1473.8	18.8	1487.8	14.4	1507.8	22.2	1507.8	22.2	97.7
PennSS-Spot 68	163	138986	1.7	10.6142	1.4	3.3390	2.0	0.2570	1.3	0.69	1474.7	17.7	1490.2	15.3	1512.4	26.8	1512.4	26.8	97.5
PennSS-Spot 228	97	99429	2.8	10.5660	1.3	3.3600	2.4	0.2575	2.0	0.83	1476.9	26.2	1495.1	18.7	1521.0	25.3	1521.0	25.3	97.1
PennSS-Spot 63	69	31440	1.4	10.5472	1.4	3.4940	2.5	0.2673	2.1	0.83	1526.9	28.2	1525.8	19.7	1524.3	26.4	1524.3	26.4	100.2
PennSS-Spot 225	31	67085	1.4	10.5017	2.1	3.3515	3.1	0.2553	2.2	0.72	1465.6	29.4	1493.1	24.3	1532.5	40.4	1532.5	40.4	95.6
PennSS-Spot 274	81	152288	3.2	10.2771	1.5	3.5567	2.7	0.2651	2.3	0.84	1515.9	30.8	1539.9	21.4	1573.0	27.3	1573.0	27.3	96.4
PennSS-Spot 156	166	121145	2.5	10.1810	1.4	3.8199	2.7	0.2821	2.4	0.86	1601.7	33.5	1597.0	22.0	1590.6	25.9	1590.6	25.9	100.7
PennSS-Spot 265	159	60051	1.7	10.1660	1.5	3.3094	2.6	0.2440	2.1	0.81	1407.5	26.4	1483.3	20.2	1593.4	28.5	1593.4	28.5	88.3
PennSS-Spot 99	104	182287	1.8	10.1577	1.4	3.4870	2.6	0.2569	2.1	0.83	1473.9	27.8	1524.3	20.2	1594.9	27.0	1594.9	27.0	92.4
PennSS-Spot 133	183	226379	2.1	10.0702	1.1	3.7819	2.4	0.2762	2.1	0.88	1572.3	29.0	1588.9	19.1	1611.0	21.2	1611.0	21.2	97.6
PennSS-Spot 129	265	77532	3.0	10.0443	1.2	3.6115	2.9	0.2631	2.6	0.90	1505.6	34.6	1552.1	22.7	1615.8	23.2	1615.8	23.2	93.2
PennSS-Spot 20	31	50014	3.3	9.9559	1.8	4.0542	2.8	0.2927	2.2	0.78	1655.2	32.4	1645.1	23.2	1632.3	33.0	1632.3	33.0	101.4
PennSS-Spot 169	146	208278	1.5	9.9433	1.4	3.8880	2.4	0.2804	1.9	0.82	1593.3	27.1	1611.2	19.0	1634.6	25.2	1634.6	25.2	97.5
PennSS-Spot 275	79	55672	1.0	9.9068	1.4	3.9656	2.2	0.2849	1.7	0.76	1616.2	24.0	1627.2	17.9	1641.5	26.5	1641.5	26.5	98.5
PennSS-Spot 110	111	96580	1.4	9.9012	1.5	3.9870	3.1	0.2863	2.7	0.87	1623.1	38.0	1631.6	24.8	1642.5	28.2	1642.5	28.2	98.8
PennSS-Spot 200	51	29345	1.5	9.8470	1.6	3.2384	2.9	0.2313	2.4	0.83	1341.2	29.4	1466.4	22.5	1652.7	29.6	1652.7	29.6	81.2
PennSS-Spot 185	653	59047	1.1	9.8215	1.2	4.0417	2.2	0.2879	1.9	0.86	1631.0	27.8	1642.6	18.3	1657.5	21.3	1657.5	21.3	98.4
PennSS-Spot 115	125	70737	2.2	9.8051	1.4	3.9713	2.6	0.2824	2.1	0.83	1603.5	30.5	1628.3	20.9	1660.6	26.5	1660.6	26.5	96.6

PennSS-Spot 80	248	124227	3.3	9.7757	1.4	3.8613	2.4	0.2738	1.9	0.81	1559.9	26.9	1605.6	19.3	1666.1	26.0	1666.1	26.0	93.6
PennSS-Spot 50	230	192471	1.4	9.7607	1.5	3.9673	2.6	0.2809	2.2	0.83	1595.7	31.2	1627.5	21.4	1669.0	26.9	1669.0	26.9	95.6
PennSS-Spot 314	75	47918	2.2	9.7330	1.5	4.0272	2.6	0.2843	2.1	0.81	1612.9	30.0	1639.7	21.1	1674.2	28.1	1674.2	28.1	96.3
PennSS-Spot 259	100	100432	1.8	9.7256	1.3	4.1404	2.3	0.2921	1.9	0.84	1651.8	28.1	1662.3	18.9	1675.7	23.3	1675.7	23.3	98.6
PennSS-Spot 143	207	166839	1.7	9.6958	1.2	4.1246	2.3	0.2900	2.0	0.85	1641.7	28.4	1659.2	18.9	1681.3	22.5	1681.3	22.5	97.6
PennSS-Spot 42	297	1250692	5.7	9.6848	1.3	4.2295	2.2	0.2971	1.8	0.83	1676.8	27.1	1679.8	18.3	1683.4	23.1	1683.4	23.1	99.6
PennSS-Spot 278	196	148559	3.5	9.6816	1.1	4.0387	2.0	0.2836	1.7	0.84	1609.4	23.8	1642.0	16.1	1684.0	19.5	1684.0	19.5	95.6
PennSS-Spot 28	175	106995	3.2	9.5362	1.1	4.1958	1.9	0.2902	1.5	0.81	1642.5	22.0	1673.2	15.4	1711.9	20.5	1711.9	20.5	95.9
PennSS-Spot 292	88	42898	0.9	9.4807	1.4	4.3237	2.6	0.2973	2.2	0.85	1677.9	33.0	1697.9	21.7	1722.6	25.4	1722.6	25.4	97.4
PennSS-Spot 36	327	78449	1.9	9.4398	1.2	4.4869	2.4	0.3072	2.1	0.87	1726.9	31.4	1728.6	19.8	1730.6	21.4	1730.6	21.4	99.8
PennSS-Spot 291	57	88976	1.2	9.3993	1.4	4.3964	2.4	0.2997	1.9	0.81	1689.8	29.0	1711.7	20.0	1738.5	26.1	1738.5	26.1	97.2
PennSS-Spot 56	219	847061	1.3	9.3983	1.5	4.5919	2.9	0.3130	2.5	0.86	1755.4	37.9	1747.8	24.0	1738.7	27.1	1738.7	27.1	101.0
PennSS-Spot 227	98	76472	1.9	9.3954	1.1	4.2303	2.1	0.2883	1.7	0.84	1632.8	25.2	1679.9	17.2	1739.2	21.0	1739.2	21.0	93.9
PennSS-Spot 313	57	46384	1.1	9.3864	1.4	4.2343	2.1	0.2883	1.6	0.75	1632.8	22.5	1680.7	17.0	1741.0	25.0	1741.0	25.0	93.8
PennSS-Spot 141	571	514599	2.9	9.3853	1.3	4.5317	1.9	0.3085	1.5	0.75	1733.2	22.2	1736.8	16.2	1741.2	23.6	1741.2	23.6	99.5
PennSS-Spot 294	136	242406	1.5	9.3682	1.4	4.4729	2.4	0.3039	2.0	0.82	1710.7	29.7	1726.0	20.0	1744.5	25.5	1744.5	25.5	98.1
PennSS-Spot 219	116	53759	5.1	9.3350	1.4	4.5754	2.7	0.3098	2.3	0.86	1739.6	35.3	1744.8	22.4	1751.0	25.2	1751.0	25.2	99.3
PennSS-Spot 176	341	177931	1.2	9.2185	1.6	4.4560	2.8	0.2979	2.3	0.82	1681.0	33.8	1722.8	23.2	1774.0	29.5	1774.0	29.5	94.8
PennSS-Spot 285	545	49623	3.1	9.2099	1.7	3.8314	2.4	0.2559	1.7	0.72	1469.0	22.8	1599.4	19.4	1775.7	30.5	1775.7	30.5	82.7
PennSS-Spot 211	186	63387	1.5	9.1899	1.4	4.5972	2.4	0.3064	1.9	0.81	1723.0	29.1	1748.8	19.9	1779.7	25.7	1779.7	25.7	96.8
PennSS-Spot 62	223	68824	2.3	9.1701	1.0	4.7291	1.9	0.3145	1.6	0.84	1762.9	24.6	1772.4	16.0	1783.6	19.1	1783.6	19.1	98.8
PennSS-Spot 21	158	328751	2.1	9.1575	1.2	4.7106	2.6	0.3129	2.3	0.88	1754.8	35.5	1769.1	21.9	1786.1	22.3	1786.1	22.3	98.2
PennSS-Spot 204	224	115778	0.7	9.1141	1.3	4.2830	2.3	0.2831	1.9	0.81	1607.0	26.4	1690.1	18.8	1794.7	24.2	1794.7	24.2	89.5
PennSS-Spot 116	396	1295538	1.4	9.0992	1.1	4.5997	2.1	0.3035	1.8	0.85	1708.9	26.6	1749.2	17.4	1797.7	20.0	1797.7	20.0	95.1
PennSS-Spot 9	223	183955	1.6	9.0573	1.5	5.0187	2.3	0.3297	1.8	0.77	1836.8	28.1	1822.5	19.4	1806.1	26.6	1806.1	26.6	101.7
PennSS-Spot 284	213	168404	1.9	9.0247	0.9	4.9723	1.8	0.3255	1.6	0.88	1816.3	25.5	1814.6	15.5	1812.7	15.9	1812.7	15.9	100.2
PennSS-Spot 171	162	402381	8.1	8.7378	1.1	5.2864	2.2	0.3350	1.9	0.86	1862.6	30.1	1866.7	18.5	1871.2	19.8	1871.2	19.8	99.5
PennSS-Spot 214	20	35470	0.9	8.6690	1.6	5.2581	2.6	0.3306	2.0	0.77	1841.3	32.0	1862.1	22.0	1885.4	29.4	1885.4	29.4	97.7
PennSS-Spot 272	153	207898	1.0	8.3514	1.2	5.8861	2.2	0.3565	1.8	0.84	1965.7	31.2	1959.2	18.9	1952.3	20.9	1952.3	20.9	100.7
PennSS-Spot 312	423	807108	2.5	8.2900	1.4	5.5001	2.4	0.3307	2.0	0.83	1841.7	32.3	1900.6	21.0	1965.5	24.5	1965.5	24.5	93.7

PennSS-Spot 35	135	131760	2.8	8.2752	1.0	5.5406	2.2	0.3325	1.9	0.89	1850.7	31.3	1906.9	18.9	1968.7	18.0	1968.7	18.0	94.0
PennSS-Spot 224	618	1352564	4.0	8.2555	1.5	5.7890	2.5	0.3466	2.0	0.81	1918.4	33.2	1944.8	21.5	1972.9	26.2	1972.9	26.2	97.2
PennSS-Spot 172	172	135273	1.6	8.1851	1.3	5.6810	2.4	0.3372	2.0	0.85	1873.4	33.1	1928.5	20.7	1988.2	22.6	1988.2	22.6	94.2
PennSS-Spot 86	334	101987	9.1	8.1527	1.1	5.8305	2.5	0.3448	2.2	0.89	1909.5	36.3	1951.0	21.4	1995.2	19.9	1995.2	19.9	95.7
PennSS-Spot 260	314	100244	3.3	8.1360	1.3	5.2334	2.1	0.3088	1.7	0.80	1734.8	25.5	1858.1	17.9	1998.9	22.4	1998.9	22.4	86.8
PennSS-Spot 308	319	67416	11.0	7.8803	1.1	5.8194	2.5	0.3326	2.2	0.89	1851.0	35.2	1949.3	21.4	2055.4	20.2	2055.4	20.2	90.1
PennSS-Spot 201	204	50100	2.2	7.3050	1.1	7.5838	2.1	0.4018	1.8	0.86	2177.3	33.2	2182.9	18.8	2188.2	18.9	2188.2	18.9	99.5
PennSS-Spot 67	130	163857	2.1	6.3068	1.3	10.6236	2.7	0.4859	2.3	0.87	2553.0	48.9	2490.8	24.8	2440.4	22.2	2440.4	22.2	104.6
PennSS-Spot 34	66	84716	3.8	6.2913	1.0	9.3253	2.1	0.4255	1.8	0.87	2285.4	35.5	2370.5	19.5	2444.5	17.8	2444.5	17.8	93.5
PennSS-Spot 262	102	58790	1.8	5.7542	1.3	10.4286	2.2	0.4352	1.8	0.80	2329.2	34.6	2473.6	20.6	2594.4	22.4	2594.4	22.4	89.8
PennSS-Spot 270	97	121031	1.3	5.6416	1.2	11.1668	2.2	0.4569	1.8	0.83	2425.9	37.1	2537.1	20.5	2627.3	20.3	2627.3	20.3	92.3
PennSS-Spot 244	144	86916	1.2	5.6249	1.2	12.0293	2.1	0.4907	1.8	0.82	2573.9	37.2	2606.7	20.0	2632.3	20.3	2632.3	20.3	97.8
PennSS-Spot 246	245	193686	3.3	5.5341	1.1	12.0356	2.0	0.4831	1.6	0.83	2540.7	34.1	2607.2	18.4	2659.3	18.2	2659.3	18.2	95.5
PennSS-Spot 107	169	166632	3.2	5.4579	1.1	12.8765	1.9	0.5097	1.6	0.82	2655.4	33.9	2670.7	17.9	2682.2	18.0	2682.2	18.0	99.0
PennSS-Spot 281	74	5355417	1.8	5.4503	1.2	11.7245	2.2	0.4635	1.8	0.82	2454.8	36.3	2582.7	20.3	2684.5	20.6	2684.5	20.6	91.4
PennSS-Spot 94	107	70771	1.1	5.3906	1.2	12.9213	2.2	0.5052	1.8	0.84	2636.0	39.8	2673.9	20.7	2702.7	19.7	2702.7	19.7	97.5
PennSS-Spot 239	507	106184	7.3	5.3836	1.2	10.9966	2.0	0.4294	1.7	0.82	2302.9	32.3	2522.8	19.0	2704.9	19.3	2704.9	19.3	85.1
PennSS-Spot 13	55	207503	2.2	5.3032	1.3	13.3596	2.4	0.5138	2.1	0.86	2673.0	45.6	2705.4	23.0	2729.7	20.8	2729.7	20.8	97.9
PennSS-Spot 134	93	77360	0.9	5.2538	1.0	13.6007	2.1	0.5182	1.9	0.87	2691.7	40.8	2722.3	20.0	2745.1	16.9	2745.1	16.9	98.1
PennSS-Spot 212	23	43554	1.0	5.2127	1.5	12.7323	2.7	0.4814	2.3	0.83	2533.2	47.7	2660.1	25.7	2758.0	24.9	2758.0	24.9	91.8
PennSS-Spot 79	103	191616	2.3	5.0779	1.2	14.3633	2.2	0.5290	1.9	0.85	2737.1	42.6	2774.0	21.3	2800.9	19.2	2800.9	19.2	97.7
PennSS-Spot 12	121	54072	3.4	4.6280	1.5	15.7067	2.6	0.5272	2.1	0.81	2729.7	47.5	2859.1	25.1	2951.7	24.9	2951.7	24.9	92.5
PennSS-Spot 197	64	120635	4.4	3.8750	1.3	22.2417	2.3	0.6251	1.9	0.83	3130.1	47.7	3194.3	22.6	3234.9	20.7	3234.9	20.7	96.8
Dobbs Valley sandstone, sample 4 (Middle Pennsylvanian)																			
DOBB'S-80 <>	95	11710	1.1	17.8162	6.1	0.5537	6.8	0.0715	2.8	0.42	445.4	12.2	447.4	24.4	457.5	136.0	445.4	12.2	97.4
DOBB'S-84 <>	128	31301	1.8	16.9999	3.1	0.6358	3.5	0.0784	1.5	0.44	486.5	7.1	499.7	13.8	560.6	68.6	486.5	7.1	86.8
DOBB'S-38 <>	127	26884	1.1	17.6028	3.1	0.6311	3.6	0.0806	1.9	0.53	499.5	9.3	496.8	14.3	484.1	68.3	499.5	9.3	103.2
DOBB'S-65 <>	141	40948	3.5	17.3640	4.5	0.6506	5.7	0.0819	3.5	0.61	507.7	17.0	508.8	22.8	514.2	98.8	507.7	17.0	98.7

DOBB'S-83 <>	103	23493	0.7	17.0657	5.1	0.6702	5.9	0.0830	3.0	0.50	513.7	14.7	520.9	24.0	552.1	111.0	513.7	14.7	93.0
DOBB'S-105 <>	111	49669	0.8	17.1233	4.1	0.6691	4.6	0.0831	2.1	0.45	514.6	10.3	520.2	18.7	544.8	89.6	514.6	10.3	94.5
DOBB'S-121 <>	107	31136	1.6	17.1180	3.6	0.7030	3.8	0.0873	1.4	0.37	539.4	7.2	540.6	16.0	545.5	77.8	539.4	7.2	98.9
DOBB'S-31 <>	119	19760	1.8	18.1349	5.1	0.6696	5.9	0.0881	2.8	0.49	544.1	14.9	520.4	23.9	418.0	114.6	544.1	14.9	130.2
DOBB'S-120 <>	133	30530	2.3	17.2333	3.4	0.7102	4.5	0.0888	2.9	0.64	548.2	15.1	544.8	18.9	530.8	75.4	548.2	15.1	103.3
DOBB'S-124 <>	60	11594	3.5	17.8446	6.9	0.6887	7.9	0.0891	3.8	0.48	550.4	19.8	532.0	32.7	454.0	154.3	550.4	19.8	121.2
DOBB'S-61 <>	31	9434	0.6	18.2561	11.6	0.6805	12.0	0.0901	2.9	0.24	556.1	15.2	527.1	49.2	403.1	260.7	556.1	15.2	138.0
DOBB'S-101 <>	70	42839	1.2	16.1636	5.8	0.7769	6.4	0.0911	2.6	0.41	561.9	14.2	583.7	28.5	669.5	125.2	561.9	14.2	83.9
DOBB'S-32 <>	74	26432	1.7	19.4424	6.5	0.6541	6.6	0.0922	1.2	0.18	568.7	6.6	511.0	26.6	260.4	149.6	568.7	6.6	218.4
DOBB'S-123 <>	62	11412	1.5	17.7706	7.4	0.7209	8.0	0.0929	2.8	0.35	572.8	15.4	551.2	33.9	463.2	165.2	572.8	15.4	123.7
DOBB'S-115 <>	59	11590	0.7	16.9349	6.6	0.7599	7.0	0.0933	2.3	0.33	575.3	12.8	574.0	30.7	569.0	143.8	575.3	12.8	101.1
DOBB'S-64 <>	65	4115	0.6	16.1299	4.3	0.8297	7.0	0.0971	5.5	0.79	597.2	31.4	613.5	32.3	674.0	92.8	597.2	31.4	88.6
DOBB'S-107 <>	53	17147	1.0	17.2973	8.0	0.7755	8.2	0.0973	2.1	0.26	598.5	12.1	582.9	36.6	522.6	175.1	598.5	12.1	114.5
DOBB'S-81 <>	40	16104	6.2	15.8245	3.9	0.8715	4.2	0.1000	1.5	0.36	614.5	8.8	636.4	19.8	714.7	82.9	614.5	8.8	86.0
DOBB'S-82 <>	80	25937	1.1	16.3480	6.0	0.8466	6.1	0.1004	1.1	0.18	616.7	6.4	622.8	28.6	645.2	129.8	616.7	6.4	95.6
DOBB'S-69 <>	239	114985	6.1	16.3519	1.0	0.8524	1.5	0.1011	1.1	0.75	620.8	6.5	626.0	6.9	644.7	21.1	620.8	6.5	96.3
DOBB'S-44 <>	323	23633	1.1	16.2893	1.5	0.8978	3.8	0.1061	3.5	0.92	649.9	21.4	650.5	18.1	652.9	32.1	649.9	21.4	99.5
DOBB'S-108 <>	135	54610	2.2	14.4330	1.3	1.4757	4.3	0.1545	4.0	0.95	926.0	34.8	920.5	25.7	907.2	27.6	907.2	27.6	102.1
DOBB'S-95 <>	102	56137	1.5	14.3441	3.0	1.4645	3.5	0.1524	1.7	0.50	914.1	14.8	915.8	21.1	920.0	62.2	920.0	62.2	99.4
DOBB'S-72 <>	158	12142	1.3	14.0877	4.1	1.4785	4.1	0.1511	0.6	0.15	906.9	5.4	921.6	25.1	956.9	83.8	956.9	83.8	94.8
DOBB'S-19 <>	63	46487	69.0	13.9762	3.8	1.6410	4.5	0.1663	2.5	0.55	991.9	22.7	986.1	28.3	973.2	76.5	973.2	76.5	101.9
DOBB'S-34 <>	80	41336	2.6	13.9734	2.6	1.6777	3.4	0.1700	2.1	0.63	1012.2	19.9	1000.1	21.3	973.6	52.9	973.6	52.9	104.0
DOBB'S-33 <>	545	73627	2.0	13.9688	0.4	1.5996	1.2	0.1621	1.1	0.93	968.2	10.1	970.0	7.5	974.3	8.9	974.3	8.9	99.4
DOBB'S-66 <>	101	20853	0.7	13.9606	1.8	1.6941	3.1	0.1715	2.5	0.81	1020.6	23.8	1006.3	19.9	975.4	37.2	975.4	37.2	104.6
DOBB'S-24 <>	356	113680	2.2	13.8610	0.5	1.6847	1.9	0.1694	1.9	0.96	1008.6	17.5	1002.8	12.4	990.0	10.7	990.0	10.7	101.9
DOBB'S-52 <>	42	16386	0.6	13.8531	4.4	1.6457	4.9	0.1653	2.2	0.44	986.4	20.1	987.9	31.2	991.2	90.1	991.2	90.1	99.5
DOBB'S-118 <>	22	21249	2.1	13.6911	6.3	1.7479	7.1	0.1736	3.1	0.44	1031.7	29.9	1026.4	45.7	1015.0	128.6	1015.0	128.6	101.6
DOBB'S-68 <>	60	17658	1.3	13.6907	2.6	1.7218	5.8	0.1710	5.2	0.90	1017.4	48.7	1016.7	37.0	1015.1	51.7	1015.1	51.7	100.2
DOBB'S-13 <>	58	16030	2.9	13.6886	3.0	1.7253	3.7	0.1713	2.2	0.59	1019.2	21.0	1018.0	24.1	1015.4	61.1	1015.4	61.1	100.4
DOBB'S-111 <>	198	297098	1.9	13.6766	1.2	1.7180	1.2	0.1704	0.3	0.24	1014.4	2.7	1015.3	7.6	1017.2	23.3	1017.2	23.3	99.7

DOBB'S-3 <>	268	115207	3.1	13.6013	0.7	1.7603	0.9	0.1736	0.5	0.57	1032.1	4.9	1030.9	5.7	1028.4	14.7	1028.4	14.7	100.4
DOBB'S-77 <>	189	116208	1.2	13.5154	0.8	1.7809	1.1	0.1746	0.7	0.69	1037.2	7.1	1038.5	7.0	1041.2	15.7	1041.2	15.7	99.6
DOBB'S-94 <>	46	39126	1.1	13.4888	4.8	1.8509	5.1	0.1811	1.8	0.35	1072.8	17.6	1063.8	33.6	1045.2	96.4	1045.2	96.4	102.6
DOBB'S-93 <>	123	142477	1.5	13.4798	1.6	1.7639	3.1	0.1725	2.7	0.86	1025.6	25.5	1032.3	20.3	1046.5	32.3	1046.5	32.3	98.0
DOBB'S-75 <>	28	14517	0.5	13.4789	6.5	1.6228	7.6	0.1586	4.0	0.52	949.2	35.0	979.1	47.8	1046.7	131.1	1046.7	131.1	90.7
DOBB'S-9 <>	178	82054	1.5	13.4476	1.1	1.7960	2.1	0.1752	1.8	0.85	1040.5	17.0	1044.0	13.6	1051.3	22.2	1051.3	22.2	99.0
DOBB'S-70 <>	69	39620	1.7	13.4217	3.0	1.7633	4.1	0.1716	2.8	0.68	1021.1	26.1	1032.0	26.5	1055.2	60.7	1055.2	60.7	96.8
DOBB'S-35 <>	180	97460	4.1	13.3669	0.9	1.8325	2.4	0.1777	2.3	0.92	1054.2	22.0	1057.2	16.1	1063.5	18.8	1063.5	18.8	99.1
DOBB'S-73 <>	146	49316	4.5	13.3459	1.4	1.8293	3.2	0.1771	2.8	0.89	1050.9	27.3	1056.0	20.7	1066.6	28.7	1066.6	28.7	98.5
DOBB'S-1 <>	139	109202	1.4	13.3150	1.3	1.8906	2.2	0.1826	1.7	0.80	1081.0	17.3	1077.8	14.4	1071.3	26.1	1071.3	26.1	100.9
DOBB'S-11 <>	230	141662	1.8	13.2974	0.8	1.8138	2.0	0.1749	1.9	0.93	1039.2	18.2	1050.4	13.4	1073.9	15.3	1073.9	15.3	96.8
DOBB'S-12 <>	147	54439	2.2	13.2258	1.2	1.8352	3.2	0.1760	3.0	0.93	1045.3	28.8	1058.1	21.1	1084.8	24.0	1084.8	24.0	96.4
DOBB'S-112 <>	80	57042	1.4	13.1886	2.0	1.8993	2.1	0.1817	0.8	0.38	1076.1	8.0	1080.8	14.2	1090.4	39.5	1090.4	39.5	98.7
DOBB'S-56 <>	44	31376	0.7	13.1262	2.5	1.9679	4.0	0.1873	3.2	0.79	1107.0	32.4	1104.6	27.1	1099.9	49.3	1099.9	49.3	100.6
DOBB'S-78 <>	89	41188	1.6	13.1130	1.2	1.9377	1.6	0.1843	1.1	0.66	1090.3	10.9	1094.2	11.0	1101.9	24.6	1101.9	24.6	98.9
DOBB'S-85 <>	284	104136	2.4	12.8367	0.4	2.0695	0.6	0.1927	0.5	0.77	1135.8	5.0	1138.8	4.3	1144.4	8.0	1144.4	8.0	99.3
DOBB'S-50 <>	111	56273	1.7	12.8352	1.0	2.1374	1.8	0.1990	1.4	0.81	1169.8	15.3	1161.0	12.1	1144.6	20.2	1144.6	20.2	102.2
DOBB'S-7 <>	167	16779	2.2	12.6671	1.6	2.0773	3.7	0.1908	3.3	0.90	1126.0	34.4	1141.4	25.4	1170.8	32.4	1170.8	32.4	96.2
DOBB'S-15 <>	98	84356	2.0	12.6652	1.2	2.0766	2.5	0.1908	2.3	0.88	1125.5	23.2	1141.1	17.5	1171.1	23.7	1171.1	23.7	96.1
DOBB'S-25 <>	70	45081	1.9	12.6412	2.3	2.1341	2.8	0.1957	1.6	0.57	1152.0	16.9	1159.9	19.4	1174.8	45.6	1174.8	45.6	98.1
DOBB'S-100 <>	127	84549	2.4	12.6227	1.3	2.1953	2.7	0.2010	2.3	0.87	1180.6	25.0	1179.5	18.7	1177.7	26.4	1177.7	26.4	100.2
DOBB'S-55 <>	207	213771	1.4	12.3491	0.8	2.3173	1.8	0.2075	1.6	0.90	1215.7	18.1	1217.6	12.9	1220.9	15.8	1220.9	15.8	99.6
DOBB'S-91 <>	104	30717	1.9	12.2749	1.5	2.3334	2.3	0.2077	1.7	0.74	1216.7	18.4	1222.5	16.1	1232.8	30.1	1232.8	30.1	98.7
DOBB'S-47 <>	116	72356	1.9	12.2615	1.1	2.4674	1.4	0.2194	0.9	0.65	1278.8	10.6	1262.5	10.2	1234.9	21.2	1234.9	21.2	103.6
DOBB'S-10 <>	31	16671	1.3	12.0803	3.8	2.2758	4.0	0.1994	1.3	0.33	1172.1	14.1	1204.8	28.3	1264.0	73.9	1264.0	73.9	92.7
DOBB'S-63 <>	42	35010	1.1	11.8890	2.4	2.6390	2.9	0.2276	1.6	0.54	1321.7	18.7	1311.6	21.4	1295.1	47.5	1295.1	47.5	102.1
DOBB'S-98 <>	78	31414	2.5	11.8024	2.3	2.5197	3.1	0.2157	2.1	0.67	1259.0	23.9	1277.7	22.6	1309.3	44.7	1309.3	44.7	96.2
DOBB'S-4 <>	37	18123	1.3	11.6589	2.5	2.6614	4.6	0.2250	3.9	0.84	1308.5	46.0	1317.8	34.2	1333.0	48.8	1333.0	48.8	98.2
DOBB'S-122 <>	104	36942	1.5	11.6313	1.0	2.7527	1.2	0.2322	0.6	0.53	1346.1	7.7	1342.8	8.9	1337.6	19.6	1337.6	19.6	100.6
DOBB'S-88 <>	129	67157	1.2	11.5042	1.0	2.7713	4.1	0.2312	4.0	0.97	1340.9	48.5	1347.8	30.8	1358.8	19.5	1358.8	19.5	98.7

DOBB'S-117 <>	44	27665	0.9	11.5041	1.3	2.7603	1.9	0.2303	1.3	0.72	1336.1	16.2	1344.9	14.0	1358.8	25.3	1358.8	25.3	98.3
DOBB'S-54 <>	51	34194	1.7	11.4718	2.1	2.7934	3.1	0.2324	2.3	0.73	1347.1	27.8	1353.8	23.5	1364.2	41.4	1364.2	41.4	98.7
DOBB'S-114 <>	18	45394	1.2	11.4389	5.8	2.7939	6.2	0.2318	2.1	0.34	1343.9	25.8	1353.9	46.3	1369.8	111.8	1369.8	111.8	98.1
DOBB'S-57 <>	84	76568	1.1	11.4388	0.9	2.8896	1.6	0.2397	1.3	0.84	1385.3	16.8	1379.2	12.0	1369.8	16.6	1369.8	16.6	101.1
DOBB'S-79 <>	28	12521	2.0	11.0984	2.9	2.9508	3.3	0.2375	1.5	0.45	1373.8	18.2	1395.0	24.8	1427.7	55.8	1427.7	55.8	96.2
DOBB'S-87 <>	82	39086	1.3	10.9528	1.3	3.1140	3.5	0.2474	3.2	0.92	1424.9	41.1	1436.1	26.8	1452.9	25.6	1452.9	25.6	98.1
DOBB'S-60 <>	64	51825	1.5	10.6762	2.1	3.4056	2.6	0.2637	1.6	0.60	1508.7	21.4	1505.7	20.8	1501.4	39.9	1501.4	39.9	100.5
DOBB'S-42 <>	89	91506	1.9	10.6256	0.8	3.4693	2.4	0.2674	2.2	0.94	1527.4	30.4	1520.3	18.7	1510.4	14.8	1510.4	14.8	101.1
DOBB'S-49 <>	187	225314	1.4	10.3069	0.4	3.6814	1.1	0.2752	1.0	0.91	1567.1	13.5	1567.3	8.5	1567.6	8.3	1567.6	8.3	100.0
DOBB'S-96 <>	38	38921	0.6	10.1310	1.7	3.8887	2.8	0.2857	2.2	0.80	1620.1	32.0	1611.3	22.4	1599.8	30.8	1599.8	30.8	101.3
DOBB'S-41 <>	206	84145	1.8	9.9199	0.5	4.0045	1.2	0.2881	1.1	0.90	1632.1	15.7	1635.1	9.9	1639.0	10.0	1639.0	10.0	99.6
DOBB'S-27 <>	15	8644	2.1	9.7203	4.9	4.3012	5.5	0.3032	2.6	0.47	1707.3	38.8	1693.6	45.5	1676.6	90.1	1676.6	90.1	101.8
DOBB'S-90 <>	33	38299	1.5	9.7026	3.4	4.2003	4.3	0.2956	2.6	0.61	1669.3	38.4	1674.1	35.1	1680.0	62.6	1680.0	62.6	99.4
DOBB'S-58 <>	203	82998	4.3	9.4001	0.4	4.6384	0.7	0.3162	0.6	0.79	1771.3	8.6	1756.2	5.9	1738.3	8.0	1738.3	8.0	101.9
DOBB'S-2 <>	64	53302	1.3	9.3821	1.2	4.5714	1.4	0.3111	0.8	0.55	1745.9	11.8	1744.1	11.8	1741.8	21.7	1741.8	21.7	100.2
DOBB'S-119 <>	139	99929	1.2	9.3506	0.6	4.7238	3.9	0.3204	3.9	0.99	1791.5	60.8	1771.5	33.0	1748.0	11.3	1748.0	11.3	102.5
DOBB'S-48 <>	176	122259	2.6	9.3127	0.4	4.6511	1.9	0.3141	1.8	0.98	1761.1	28.5	1758.5	15.7	1755.4	6.8	1755.4	6.8	100.3
DOBB'S-28 <>	98	70869	1.2	9.2877	0.7	4.2596	4.4	0.2869	4.4	0.99	1626.2	62.6	1685.6	36.3	1760.3	13.0	1760.3	13.0	92.4
DOBB'S-45 <>	136	103593	1.2	9.2864	0.4	4.5895	2.5	0.3091	2.5	0.99	1736.3	38.2	1747.4	21.2	1760.6	7.7	1760.6	7.7	98.6
DOBB'S-26 <>	211	72451	2.7	9.1494	0.4	4.9181	0.9	0.3264	0.8	0.87	1820.7	12.6	1805.4	7.7	1787.7	8.2	1787.7	8.2	101.8
DOBB'S-59 <>	102	108609	2.1	8.8451	0.6	5.1896	1.9	0.3329	1.8	0.94	1852.5	29.2	1850.9	16.4	1849.1	11.5	1849.1	11.5	100.2
DOBB'S-102 <>	62	65828	0.6	8.7346	0.9	5.3492	2.3	0.3389	2.1	0.91	1881.2	34.4	1876.8	19.8	1871.8	17.0	1871.8	17.0	100.5
DOBB'S-89 <>	83	98739	0.9	8.5375	0.6	5.5456	3.1	0.3434	3.1	0.98	1902.9	50.8	1907.7	27.0	1912.9	10.6	1912.9	10.6	99.5
DOBB'S-17 <>	72	56110	0.9	8.1974	0.8	5.9563	3.2	0.3541	3.1	0.97	1954.2	52.1	1969.5	27.8	1985.5	14.6	1985.5	14.6	98.4
DOBB'S-20 <>	126	144224	0.7	8.1817	0.6	5.9772	3.3	0.3547	3.3	0.98	1956.9	55.1	1972.5	28.9	1988.9	11.3	1988.9	11.3	98.4
DOBB'S-110 <>	100	96228	0.9	7.9603	0.4	6.2893	1.3	0.3631	1.3	0.96	1996.9	22.1	2017.0	11.8	2037.6	6.9	2037.6	6.9	98.0
DOBB'S-53 <>	174	64355	0.9	7.7260	0.4	6.7526	3.0	0.3784	3.0	0.99	2068.7	52.7	2079.5	26.6	2090.3	7.1	2090.3	7.1	99.0
DOBB'S-67 <>	110	144245	1.0	7.5497	0.3	7.1525	1.6	0.3916	1.6	0.99	2130.4	29.1	2130.6	14.5	2130.8	4.9	2130.8	4.9	100.0
DOBB'S-40 <>	32	37737	0.7	5.5137	0.7	12.8587	3.8	0.5142	3.7	0.98	2674.6	80.9	2669.4	35.4	2665.4	11.4	2665.4	11.4	100.3
DOBB'S-113 <>	216	67480	1.4	5.3492	0.2	13.5211	2.1	0.5246	2.1	0.99	2718.5	47.2	2716.8	20.3	2715.4	3.7	2715.4	3.7	100.1

DOBB'S-86 <>	38	68495	1.0	5.3393	0.6	13.5018	1.1	0.5228	1.0	0.85	2711.2	21.8	2715.4	10.9	2718.5	9.8	2718.5	9.8	99.7
DOBB'S-5 <>	57	76925	0.4	5.3082	0.6	13.8752	0.8	0.5342	0.6	0.70	2759.0	12.6	2741.2	7.6	2728.1	9.4	2728.1	9.4	101.1
DOBB'S-99 <>	16	29432	1.7	5.1966	1.4	13.1162	4.4	0.4943	4.2	0.95	2589.4	89.0	2688.0	41.6	2763.1	23.3	2763.1	23.3	93.7
DOBB'S-8 <>	69	103366	1.8	5.1095	0.4	14.5456	1.1	0.5390	1.0	0.93	2779.4	23.6	2786.0	10.7	2790.8	6.8	2790.8	6.8	99.6
DOBB'S-62 <>	44	54634	0.6	5.1067	0.3	14.8745	1.5	0.5509	1.4	0.98	2829.0	33.0	2807.2	14.1	2791.7	5.2	2791.7	5.2	101.3
DOBB'S-30 <>	19	26114	2.4	4.9253	1.7	15.7448	2.1	0.5624	1.2	0.58	2876.6	28.6	2861.4	20.3	2850.7	28.2	2850.7	28.2	100.9
DOBB'S-46 <>	15	24737	1.4	4.8305	1.1	16.1244	1.7	0.5649	1.4	0.78	2886.9	31.5	2884.2	16.6	2882.3	17.8	2882.3	17.8	100.2
DOBB'S-103 <>	13	18735	2.2	4.5016	1.2	17.7460	2.2	0.5794	1.9	0.83	2946.2	44.2	2976.1	21.6	2996.3	20.1	2996.3	20.1	98.3
DOBB'S-43 <>	170	88520	1.8	4.4130	0.1	18.2189	6.0	0.5831	6.0	1.00	2961.4	142.1	3001.4	57.7	3028.2	2.4	3028.2	2.4	97.8
DOBB'S-92 <>	48	85366	0.9	4.2104	0.3	20.0870	1.3	0.6134	1.3	0.97	3083.5	32.0	3095.6	13.0	3103.3	5.0	3103.3	5.0	99.4
Brazos River sandstone, sample 5 (Middle Pennsylvanian)																			
BRAZOS RIVER-65 <>	315	42259	1.3	19.3468	2.0	0.3711	2.2	0.0521	1.0	0.45	327.2	3.2	320.5	6.1	271.6	45.6	327.2	3.2	120.0
BRAZOS RIVER-18 <>	322	3951	1.1	17.4789	13.1	0.4130	13.1	0.0524	1.0	0.08	329.0	3.2	351.1	38.9	499.7	289.1	329.0	3.2	65.0
BRAZOS RIVER-55 <>	433	82783	2.7	18.4151	1.7	0.4194	1.8	0.0560	0.7	0.36	351.3	2.3	355.6	5.5	383.6	38.3	351.3	2.3	91.6
BRAZOS RIVER-77 <>	729	4923	2.8	16.5929	0.9	0.5247	2.8	0.0631	2.6	0.95	394.7	10.1	428.3	9.7	613.1	18.9	394.7	10.1	64.4
BRAZOS RIVER-2 <>	107	9120	0.4	18.2393	5.5	0.4811	6.2	0.0636	2.9	0.46	397.8	11.0	398.9	20.4	405.1	123.0	397.8	11.0	98.2
BRAZOS RIVER-90 <>	85	10156	1.5	18.6519	8.6	0.4825	8.9	0.0653	2.0	0.23	407.6	8.0	399.8	29.3	354.9	195.5	407.6	8.0	114.9
BRAZOS RIVER-35 <>	121	20878	1.7	18.6335	4.0	0.4970	5.4	0.0672	3.6	0.67	419.0	14.7	409.7	18.2	357.1	90.4	419.0	14.7	117.4
BRAZOS RIVER-87 <>	633	3127	3.1	15.5859	1.4	0.5963	3.3	0.0674	3.0	0.90	420.5	12.3	474.9	12.7	746.9	30.5	420.5	12.3	56.3
BRAZOS RIVER-74 <>	310	38820	6.5	17.3074	2.1	0.5600	2.4	0.0703	1.3	0.52	438.0	5.3	451.6	8.8	521.4	45.3	438.0	5.3	84.0
BRAZOS RIVER-118 <>	253	14475	0.8	17.7849	2.5	0.5583	2.9	0.0720	1.4	0.50	448.3	6.2	450.4	10.5	461.3	55.4	448.3	6.2	97.2
BRAZOS RIVER-51 <>	159	29338	1.0	17.3798	2.3	0.5789	4.0	0.0730	3.2	0.81	454.0	14.2	463.7	14.9	512.2	51.5	454.0	14.2	88.6
BRAZOS RIVER-8 <>	110	19169	1.3	17.1790	7.0	0.6100	7.1	0.0760	1.4	0.20	472.2	6.6	483.5	27.4	537.7	153.0	472.2	6.6	87.8
BRAZOS RIVER-114 <>	281	110680	1.5	17.5932	1.2	0.6220	1.3	0.0794	0.7	0.50	492.3	3.2	491.1	5.2	485.3	25.6	492.3	3.2	101.4
BRAZOS RIVER-81 <>	99	16564	1.5	18.2047	5.8	0.6337	6.0	0.0837	1.5	0.25	518.0	7.4	498.4	23.7	409.4	130.5	518.0	7.4	126.5
BRAZOS RIVER-104 <>	106	38781	1.4	18.7091	2.7	0.6212	3.8	0.0843	2.6	0.69	521.7	13.1	490.6	14.8	347.9	62.1	521.7	13.1	149.9
BRAZOS RIVER-56 <>	150	53590	1.0	17.9229	3.4	0.6716	3.9	0.0873	1.9	0.49	539.5	9.8	521.7	15.8	444.2	75.1	539.5	9.8	121.5
BRAZOS RIVER-48 <>	323	118552	2.5	17.0501	1.5	0.7156	1.6	0.0885	0.7	0.42	546.6	3.5	548.0	6.8	554.2	31.7	546.6	3.5	98.6

BRAZOS RIVER-3 <>	21	9321	2.2	19.4392	27.6	0.6505	28.2	0.0917	6.2	0.22	565.7	33.7	508.8	113.5	260.7	643.6	565.7	33.7	217.0
BRAZOS RIVER-32 <>	21	4094	0.4	21.6412	21.8	0.5920	22.0	0.0929	3.2	0.14	572.8	17.4	472.1	83.3	8.5	529.4	572.8	17.4	6760.6
BRAZOS RIVER-22 <>	160	12828	0.5	16.7526	1.7	0.7717	3.2	0.0938	2.8	0.85	577.7	15.2	580.7	14.3	592.4	36.3	577.7	15.2	97.5
BRAZOS RIVER-44 <>	202	11065	0.4	16.5251	2.4	0.7884	2.5	0.0945	1.0	0.39	582.0	5.5	590.2	11.4	622.0	50.7	582.0	5.5	93.6
BRAZOS RIVER-102 <>	343	125162	5.4	16.6001	1.8	0.7940	4.6	0.0956	4.2	0.92	588.5	23.7	593.4	20.6	612.2	38.5	588.5	23.7	96.1
BRAZOS RIVER-83 <>	167	16801	1.5	16.6138	2.8	0.7967	3.1	0.0960	1.3	0.42	590.9	7.3	594.9	13.8	610.4	59.9	590.9	7.3	96.8
BRAZOS RIVER-38 <>	126	65286	0.9	16.5602	3.5	0.8107	4.0	0.0974	2.0	0.50	599.0	11.6	602.8	18.4	617.4	75.5	599.0	11.6	97.0
BRAZOS RIVER-110 <>	297	11004	3.5	15.6201	3.7	0.8832	4.4	0.1001	2.3	0.53	614.7	13.5	642.7	20.8	742.3	78.7	614.7	13.5	82.8
BRAZOS RIVER-59 <>	241	34121	2.3	16.5042	1.7	0.8361	1.9	0.1001	0.8	0.45	614.9	5.0	617.0	8.7	624.7	36.4	614.9	5.0	98.4
BRAZOS RIVER-105 <>	172	46850	1.4	16.6268	1.8	0.8363	2.2	0.1008	1.3	0.57	619.4	7.5	617.1	10.4	608.7	39.9	619.4	7.5	101.7
BRAZOS RIVER-46 <>	297	64474	1.0	16.4884	1.4	0.8509	1.8	0.1018	1.2	0.65	624.7	7.0	625.1	8.4	626.8	29.4	624.7	7.0	99.7
BRAZOS RIVER-89 <>	81	72407	2.4	15.5672	5.3	0.9102	5.4	0.1028	0.8	0.16	630.6	5.1	657.2	26.1	749.4	112.7	630.6	5.1	84.1
BRAZOS RIVER-29 <>	283	11574	1.0	16.4809	2.2	0.8738	3.3	0.1044	2.4	0.73	640.4	14.5	637.6	15.5	627.8	48.4	640.4	14.5	102.0
BRAZOS RIVER-53 <>	87	11343	1.1	15.3107	4.3	0.9502	5.3	0.1055	3.2	0.60	646.7	19.5	678.2	26.3	784.4	89.7	646.7	19.5	82.4
BRAZOS RIVER-21 <>	97	22215	0.6	16.4611	3.0	0.8841	4.1	0.1055	2.7	0.67	646.8	16.8	643.2	19.5	630.4	65.5	646.8	16.8	102.6
BRAZOS RIVER-99 <>	162	55424	1.2	16.2859	2.1	0.8966	2.4	0.1059	1.1	0.45	648.9	6.5	649.9	11.3	653.4	45.3	648.9	6.5	99.3
BRAZOS RIVER-36 <>	189	16702	2.6	15.7690	4.3	0.9825	5.7	0.1124	3.7	0.66	686.5	24.4	694.9	28.8	722.2	91.8	686.5	24.4	95.1
BRAZOS RIVER-30 <>	134	49362	1.4	15.3901	1.9	1.0402	3.9	0.1161	3.5	0.88	708.1	23.2	724.0	20.4	773.6	39.1	708.1	23.2	91.5
BRAZOS RIVER-14 <>	57	21143	1.5	13.8202	5.1	1.6892	5.7	0.1693	2.6	0.46	1008.3	24.4	1004.4	36.5	996.0	103.5	996.0	103.5	101.2
BRAZOS RIVER-80 <>	40	24859	2.3	13.8023	3.8	1.7566	5.2	0.1758	3.5	0.68	1044.2	34.1	1029.6	33.6	998.6	77.3	998.6	77.3	104.6
BRAZOS RIVER-71 <>	143	33799	1.0	13.7910	1.1	1.6980	1.2	0.1698	0.6	0.47	1011.2	5.4	1007.8	7.9	1000.3	22.3	1000.3	22.3	101.1
BRAZOS RIVER-4 <>	114	88313	1.9	13.7772	2.8	1.6657	3.1	0.1664	1.5	0.46	992.5	13.4	995.6	19.9	1002.3	56.4	1002.3	56.4	99.0
BRAZOS RIVER-78 <>	153	90113	2.3	13.7364	1.2	1.6487	1.3	0.1643	0.5	0.37	980.4	4.4	989.1	8.3	1008.3	24.8	1008.3	24.8	97.2
BRAZOS RIVER-112 <>	24	12257	1.0	13.6591	5.4	1.8219	6.4	0.1805	3.4	0.53	1069.6	33.9	1053.4	42.2	1019.8	110.3	1019.8	110.3	104.9
BRAZOS RIVER-94 <>	174	66615	3.4	13.5806	1.1	1.7630	1.8	0.1736	1.4	0.77	1032.2	13.1	1032.0	11.6	1031.4	22.9	1031.4	22.9	100.1
BRAZOS RIVER-39 <>	131	91024	1.9	13.5740	1.7	1.7334	1.9	0.1706	0.7	0.36	1015.7	6.2	1021.0	11.9	1032.4	35.0	1032.4	35.0	98.4
BRAZOS RIVER-113 <>	217	107758	2.4	13.5642	0.6	1.7538	0.9	0.1725	0.6	0.73	1026.0	6.1	1028.6	5.7	1033.9	12.1	1033.9	12.1	99.2
BRAZOS RIVER-64 <>	114	97252	2.1	13.5613	3.2	1.5986	4.2	0.1572	2.8	0.66	941.4	24.6	969.7	26.5	1034.3	64.0	1034.3	64.0	91.0
BRAZOS RIVER-41 <>	124	7868	1.7	13.5611	1.4	1.5458	3.4	0.1520	3.1	0.91	912.4	26.6	948.8	21.1	1034.3	27.9	1034.3	27.9	88.2
BRAZOS RIVER-95 <>	132	23791	1.2	13.4141	1.6	1.8551	1.8	0.1805	0.9	0.51	1069.6	9.3	1065.2	12.1	1056.4	31.6	1056.4	31.6	101.3

BRAZOS RIVER-31 <>	56	17545	1.7	13.4095	2.8	1.8118	4.4	0.1762	3.3	0.76	1046.2	32.1	1049.7	28.5	1057.1	56.9	1057.1	56.9	99.0
BRAZOS RIVER-26 <>	276	15070	1.1	13.4022	0.8	1.8295	2.5	0.1778	2.4	0.95	1055.1	22.9	1056.1	16.2	1058.2	15.1	1058.2	15.1	99.7
BRAZOS RIVER-15 <>	114	21245	1.5	13.3626	3.4	1.8898	6.3	0.1831	5.3	0.84	1084.2	52.8	1077.5	41.9	1064.1	68.8	1064.1	68.8	101.9
BRAZOS RIVER-54 <>	167	102320	2.5	13.3592	1.0	1.8730	3.5	0.1815	3.3	0.95	1075.0	32.6	1071.6	22.9	1064.6	20.8	1064.6	20.8	101.0
BRAZOS RIVER-86 <>	119	55691	1.1	13.3159	1.2	1.8998	2.5	0.1835	2.3	0.89	1085.9	22.6	1081.0	16.9	1071.1	23.5	1071.1	23.5	101.4
BRAZOS RIVER-62 <>	110	79641	1.2	13.2743	1.4	1.9128	3.5	0.1842	3.3	0.92	1089.6	32.9	1085.6	23.7	1077.4	27.1	1077.4	27.1	101.1
BRAZOS RIVER-50 <>	100	89729	2.7	13.2743	1.4	1.9648	1.6	0.1892	0.8	0.48	1116.8	7.8	1103.5	10.5	1077.4	27.5	1077.4	27.5	103.7
BRAZOS RIVER-109 <>	84	70449	0.7	13.2432	1.8	1.8070	2.0	0.1736	0.9	0.46	1031.7	8.7	1048.0	12.9	1082.1	35.2	1082.1	35.2	95.3
BRAZOS RIVER-24 <>	22	14596	0.9	13.0543	9.3	2.0355	9.8	0.1927	2.9	0.30	1136.1	30.2	1127.5	66.6	1110.9	186.6	1110.9	186.6	102.3
BRAZOS RIVER-1 <>	75	29775	1.3	12.9792	2.0	2.1223	2.5	0.1998	1.5	0.59	1174.1	15.6	1156.1	17.0	1122.4	39.5	1122.4	39.5	104.6
BRAZOS RIVER-120 <>	77	111678	2.4	12.9384	1.9	2.0744	2.2	0.1947	1.1	0.49	1146.5	11.2	1140.4	14.9	1128.7	37.8	1128.7	37.8	101.6
BRAZOS RIVER-101 <>	206	19386	1.6	12.9220	1.3	1.9027	2.8	0.1783	2.5	0.89	1057.8	24.7	1082.0	18.9	1131.2	25.6	1131.2	25.6	93.5
BRAZOS RIVER-93 <>	71	48513	2.0	12.8006	2.7	2.1014	3.2	0.1951	1.7	0.54	1148.9	18.1	1149.3	21.8	1150.0	52.9	1150.0	52.9	99.9
BRAZOS RIVER-33 <>	70	59835	1.5	12.5615	1.9	2.2034	2.2	0.2007	1.1	0.48	1179.3	11.5	1182.1	15.5	1187.3	38.3	1187.3	38.3	99.3
BRAZOS RIVER-125 <>	187	122674	1.8	12.4824	0.9	2.2871	1.3	0.2071	0.9	0.70	1213.1	10.2	1208.3	9.3	1199.8	18.4	1199.8	18.4	101.1
BRAZOS RIVER-124 <>	170	11751	2.0	12.3297	0.9	2.1300	2.1	0.1905	2.0	0.91	1123.9	20.2	1158.6	14.8	1224.0	17.0	1224.0	17.0	91.8
BRAZOS RIVER-20 <>	204	36864	2.4	11.8731	0.9	2.5494	2.1	0.2195	2.0	0.91	1279.4	22.8	1286.3	15.7	1297.7	17.0	1297.7	17.0	98.6
BRAZOS RIVER-96 <>	99	13730	2.6	11.7213	1.4	2.4958	2.4	0.2122	1.9	0.80	1240.4	21.3	1270.8	17.1	1322.7	27.3	1322.7	27.3	93.8
BRAZOS RIVER-76 <>	128	59927	1.5	11.6836	0.6	2.6783	1.0	0.2270	0.8	0.81	1318.5	9.9	1322.5	7.6	1328.9	11.5	1328.9	11.5	99.2
BRAZOS RIVER-6 <>	47	14441	0.7	11.6214	2.1	2.8057	3.3	0.2365	2.5	0.76	1368.4	31.2	1357.1	24.8	1339.2	41.3	1339.2	41.3	102.2
BRAZOS RIVER-121 <>	121	53480	1.6	11.4935	1.0	2.6854	1.2	0.2238	0.6	0.54	1302.2	7.4	1324.4	8.7	1360.6	19.1	1360.6	19.1	95.7
BRAZOS RIVER-84 <>	473	5417	1.0	11.4421	0.5	2.5009	1.3	0.2075	1.2	0.92	1215.7	13.4	1272.3	9.6	1369.2	10.2	1369.2	10.2	88.8
BRAZOS RIVER-73 <>	79	11704	1.0	11.3643	2.9	2.5078	3.0	0.2067	0.8	0.25	1211.2	8.4	1274.3	21.7	1382.4	55.5	1382.4	55.5	87.6
BRAZOS RIVER-117 <>	39	21973	1.7	10.9292	3.9	3.1310	6.0	0.2482	4.5	0.76	1429.1	58.0	1440.3	45.9	1457.0	73.8	1457.0	73.8	98.1
BRAZOS RIVER-11 <>	101	105842	2.3	10.5753	1.2	3.5119	1.8	0.2694	1.4	0.77	1537.5	19.3	1529.9	14.5	1519.3	22.1	1519.3	22.1	101.2
BRAZOS RIVER-23 <>	56	18182	1.1	10.4561	1.7	3.0997	2.7	0.2351	2.1	0.79	1361.0	25.7	1432.6	20.5	1540.7	31.1	1540.7	31.1	88.3
BRAZOS RIVER-52 <>	56	33196	1.5	10.2433	1.8	3.6497	2.2	0.2711	1.3	0.57	1546.6	17.7	1560.4	17.9	1579.2	34.4	1579.2	34.4	97.9
BRAZOS RIVER-19 <>	61	50329	1.4	10.1789	1.7	3.7121	2.0	0.2740	1.1	0.53	1561.3	14.6	1574.0	15.8	1591.0	31.2	1591.0	31.2	98.1
BRAZOS RIVER-25 <>	129	76115	1.8	9.8908	0.7	3.8867	0.9	0.2788	0.6	0.65	1585.4	8.2	1610.9	7.2	1644.5	12.5	1644.5	12.5	96.4
BRAZOS RIVER-100 <>	91	42725	0.9	9.8756	1.0	4.0779	1.4	0.2921	1.0	0.72	1651.9	14.5	1649.9	11.3	1647.3	17.9	1647.3	17.9	100.3

BRAZOS RIVER-7 <>	218	90936	2.4	9.8686	0.3	4.0935	1.4	0.2930	1.4	0.98	1656.4	20.4	1653.0	11.6	1648.6	5.6	1648.6	5.6	100.5
BRAZOS RIVER-40 <>	34	47499	2.0	9.7602	1.9	4.1708	2.4	0.2952	1.3	0.57	1667.7	19.8	1668.3	19.3	1669.1	35.8	1669.1	35.8	99.9
BRAZOS RIVER-97 <>	224	291476	4.7	9.3706	0.4	4.6140	2.2	0.3136	2.2	0.98	1758.3	33.3	1751.8	18.4	1744.1	7.9	1744.1	7.9	100.8
BRAZOS RIVER-47 <>	351	113435	1.4	9.2853	0.3	4.2479	1.8	0.2861	1.7	0.99	1621.8	25.0	1683.3	14.5	1760.8	5.2	1760.8	5.2	92.1
BRAZOS RIVER-5 <>	87	92244	1.8	9.2235	0.5	4.8807	2.2	0.3265	2.1	0.98	1821.4	34.0	1798.9	18.5	1773.0	8.3	1773.0	8.3	102.7
BRAZOS RIVER-107 <>	178	45892	2.0	8.7006	0.4	5.2803	3.2	0.3332	3.2	0.99	1853.9	51.6	1865.7	27.6	1878.8	6.9	1878.8	6.9	98.7
BRAZOS RIVER-68 <>	165	38463	1.5	7.8806	0.5	6.6862	0.7	0.3822	0.5	0.73	2086.3	9.0	2070.8	6.1	2055.4	8.4	2055.4	8.4	101.5
BRAZOS RIVER-72 <>	176	54583	1.7	7.7905	0.4	6.6037	0.6	0.3731	0.5	0.84	2044.1	9.5	2059.8	5.7	2075.6	6.2	2075.6	6.2	98.5
BRAZOS RIVER-43 <>	101	65963	1.6	7.7788	0.7	6.5206	2.3	0.3679	2.1	0.94	2019.4	36.9	2048.7	19.8	2078.3	13.0	2078.3	13.0	97.2
BRAZOS RIVER-91 <>	308	269074	8.3	6.2353	0.2	9.9795	2.2	0.4513	2.2	0.99	2401.0	44.5	2432.9	20.6	2459.6	4.0	2459.6	4.0	97.6
BRAZOS RIVER-34 <>	45	35260	0.9	5.4059	0.5	11.9625	1.4	0.4690	1.3	0.94	2479.2	27.4	2601.5	13.2	2698.1	7.9	2698.1	7.9	91.9
BRAZOS RIVER-92 <>	215	218673	1.2	5.2082	0.2	12.3160	0.8	0.4652	0.8	0.97	2462.6	16.0	2628.8	7.6	2759.4	3.5	2759.4	3.5	89.2
BRAZOS RIVER-60 <>	45	110926	1.0	5.1322	0.7	14.2839	1.2	0.5317	1.0	0.81	2748.5	21.3	2768.7	11.1	2783.5	11.3	2783.5	11.3	98.7
BRAZOS RIVER-66 <>	73	82780	0.6	5.0213	0.4	15.1587	1.5	0.5520	1.5	0.97	2833.7	34.2	2825.3	14.6	2819.2	5.9	2819.2	5.9	100.5
BRAZOS RIVER-49 <>	453	444996	10.5	4.7996	0.2	16.1692	2.8	0.5629	2.8	1.00	2878.4	64.2	2886.9	26.6	2892.7	3.7	2892.7	3.7	99.5
Lake Pinto sandstone, sample 6 (Middle Pennsylvanian)																			
LAKE PINTO-108 <>	210	134515	3.7	17.8120	1.8	0.5163	2.2	0.0667	1.2	0.54	416.2	4.7	422.7	7.5	458.0	40.2	416.2	4.7	90.9
LAKE PINTO-111 <>	13	4402	1.4	28.4773	89.0	0.3276	89.5	0.0677	9.3	0.10	422.0	38.1	287.7	228.1	-699.4	3273.5	422.0	38.1	NA
LAKE PINTO-14 <>	155	32002	5.8	17.6031	4.2	0.5519	4.8	0.0705	2.3	0.48	438.9	9.8	446.2	17.2	484.1	92.1	438.9	9.8	90.7
LAKE PINTO-121 <>	264	36332	2.6	17.7211	2.4	0.5814	2.9	0.0747	1.7	0.58	464.6	7.6	465.4	11.0	469.3	53.1	464.6	7.6	99.0
LAKE PINTO-104 <>	134	43976	1.8	17.6187	4.3	0.5956	4.8	0.0761	2.1	0.44	472.9	9.7	474.5	18.2	482.2	94.9	472.9	9.7	98.1
LAKE PINTO-79 <>	162	85862	1.0	17.2638	1.3	0.6337	2.7	0.0794	2.3	0.86	492.2	10.9	498.4	10.5	526.9	29.2	492.2	10.9	93.4
LAKE PINTO-12 <>	157	95156	2.2	17.1352	2.1	0.6473	5.7	0.0804	5.3	0.93	498.8	25.4	506.8	22.7	543.3	46.1	498.8	25.4	91.8
LAKE PINTO-34 <>	78	69545	0.6	18.7816	6.1	0.5996	6.4	0.0817	1.9	0.30	506.1	9.4	477.0	24.3	339.2	137.9	506.1	9.4	149.2
LAKE PINTO-53 <>	28	24849	1.3	16.0832	11.3	0.7133	11.7	0.0832	3.1	0.26	515.2	15.1	546.7	49.4	680.2	241.5	515.2	15.1	75.8
LAKE PINTO-60 <>	278	76935	1.5	17.1376	1.8	0.6928	2.0	0.0861	1.0	0.48	532.5	5.0	534.5	8.5	543.0	39.2	532.5	5.0	98.1
LAKE PINTO-58 <>	198	73621	2.1	17.4739	1.8	0.6876	5.1	0.0871	4.7	0.93	538.6	24.3	531.3	20.9	500.4	40.4	538.6	24.3	107.6
LAKE PINTO-41 <>	29	16080	1.3	17.6266	21.0	0.6817	21.4	0.0872	4.0	0.19	538.7	20.6	527.8	88.2	481.1	468.8	538.7	20.6	112.0

LAKE PINTO-46 <>	136	14630	4.4	16.7818	2.2	0.7169	3.2	0.0873	2.3	0.71	539.3	11.8	548.8	13.6	588.7	48.8	539.3	11.8	91.6
LAKE PINTO-119 <>	297	124077	4.0	17.2231	1.2	0.7052	3.1	0.0881	2.9	0.92	544.3	14.9	541.9	13.0	532.1	27.0	544.3	14.9	102.3
LAKE PINTO-83 <>	95	38748	2.2	17.0036	4.1	0.7170	5.4	0.0884	3.6	0.66	546.2	18.9	548.9	23.0	560.1	88.6	546.2	18.9	97.5
LAKE PINTO-61 <>	317	107025	1.9	17.0913	1.2	0.7157	1.8	0.0887	1.3	0.73	548.0	7.0	548.1	7.7	548.9	26.9	548.0	7.0	99.8
LAKE PINTO-25 <>	92	94798	2.4	16.5134	4.0	0.7472	4.2	0.0895	1.4	0.34	552.5	7.5	566.6	18.3	623.5	85.7	552.5	7.5	88.6
LAKE PINTO-80 <>	253	16091	3.2	16.6128	3.2	0.7451	3.5	0.0898	1.5	0.43	554.2	8.0	565.4	15.2	610.6	68.4	554.2	8.0	90.8
LAKE PINTO-89 <>	107	68974	0.3	17.7084	3.0	0.7017	3.7	0.0901	2.0	0.56	556.3	10.9	539.8	15.3	470.9	67.1	556.3	10.9	118.1
LAKE PINTO-48 <>	223	73406	2.5	16.9153	1.9	0.7434	2.9	0.0912	2.2	0.76	562.7	11.8	564.4	12.5	571.4	41.0	562.7	11.8	98.5
LAKE PINTO-100 <>	87	60526	1.0	16.5985	3.4	0.7584	4.2	0.0913	2.4	0.57	563.2	12.9	573.1	18.4	612.4	74.5	563.2	12.9	92.0
LAKE PINTO-65 <>	106	83714	0.6	16.8473	3.7	0.7630	3.9	0.0932	1.2	0.31	574.6	6.7	575.7	17.3	580.2	81.2	574.6	6.7	99.0
LAKE PINTO-42 <>	162	89436	1.7	17.1685	3.0	0.7551	3.5	0.0940	1.8	0.52	579.3	10.0	571.2	15.2	539.0	64.9	579.3	10.0	107.5
LAKE PINTO-93 <>	134	42028	6.0	15.9838	1.9	0.8555	4.1	0.0992	3.7	0.89	609.6	21.4	627.7	19.4	693.4	40.5	609.6	21.4	87.9
LAKE PINTO-116 <>	386	161599	6.7	16.5556	0.7	0.8354	1.4	0.1003	1.2	0.87	616.2	7.3	616.6	6.6	618.0	15.2	616.2	7.3	99.7
LAKE PINTO-82 <>	455	37779	2.6	16.3155	0.9	0.8483	1.4	0.1004	1.1	0.76	616.6	6.3	623.7	6.5	649.5	19.3	616.6	6.3	94.9
LAKE PINTO-57 <>	41	54566	1.1	15.4605	7.0	0.9003	7.9	0.1009	3.7	0.47	619.9	22.0	651.9	38.1	764.0	147.6	619.9	22.0	81.1
LAKE PINTO-49 <>	89	43840	0.8	16.2858	2.5	0.8705	2.9	0.1028	1.4	0.48	630.9	8.4	635.9	13.6	653.4	54.2	630.9	8.4	96.6
LAKE PINTO-67 <>	290	36459	1.5	16.0899	1.2	0.8879	4.7	0.1036	4.6	0.96	635.5	27.5	645.2	22.5	679.3	26.7	635.5	27.5	93.6
LAKE PINTO-87 <>	98	41072	1.8	16.1963	3.0	0.8914	3.4	0.1047	1.7	0.51	641.9	10.7	647.1	16.5	665.2	63.6	641.9	10.7	96.5
LAKE PINTO-1 <>	405	324617	7.1	16.4027	0.9	0.8973	1.3	0.1067	0.9	0.68	653.8	5.3	650.3	6.1	638.0	20.1	653.8	5.3	102.5
LAKE PINTO-113 <>	188	326566	1.4	16.3057	1.0	0.9235	2.5	0.1092	2.3	0.92	668.1	14.6	664.2	12.3	650.8	21.8	668.1	14.6	102.7
LAKE PINTO-47 <>	33	22951	1.6	15.1544	6.3	1.0639	7.4	0.1169	3.9	0.53	712.9	26.5	735.7	38.7	806.0	131.3	712.9	26.5	88.4
LAKE PINTO-120 <>	90	44194	1.1	15.7952	3.4	1.0470	5.5	0.1199	4.3	0.78	730.2	29.8	727.4	28.6	718.7	72.6	730.2	29.8	101.6
LAKE PINTO-3 <>	372	213379	1.9	15.8348	0.7	1.0474	1.3	0.1203	1.1	0.86	732.2	7.9	727.6	6.9	713.4	14.5	732.2	7.9	102.6
LAKE PINTO-26 <>	172	87083	2.3	14.7544	1.0	1.1545	4.0	0.1235	3.9	0.97	750.9	27.3	779.4	21.7	861.7	21.0	750.9	27.3	87.1
LAKE PINTO-102 <>	69	33812	1.4	14.3611	3.5	1.2626	3.9	0.1315	1.8	0.46	796.5	13.5	829.1	22.1	917.6	71.0	796.5	13.5	86.8
LAKE PINTO-115 <>	209	135500	2.8	15.3043	0.8	1.1869	1.7	0.1317	1.5	0.87	797.8	11.0	794.5	9.2	785.3	17.3	797.8	11.0	101.6
LAKE PINTO-94 <>	122	55263	1.4	14.5920	1.7	1.2946	3.5	0.1370	3.1	0.88	827.7	24.1	843.3	20.2	884.6	34.2	827.7	24.1	93.6
LAKE PINTO-77 <>	40	67447	2.1	14.4542	5.5	1.4679	5.9	0.1539	2.1	0.37	922.7	18.5	917.3	35.5	904.2	112.7	904.2	112.7	102.0
LAKE PINTO-95 <>	291	147043	6.6	14.3826	1.3	1.4779	2.2	0.1542	1.7	0.79	924.3	14.9	921.4	13.2	914.5	27.5	914.5	27.5	101.1
LAKE PINTO-54 <>	46	33776	1.1	14.1955	3.3	1.4589	3.8	0.1502	1.9	0.49	902.1	15.8	913.6	22.8	941.4	67.3	941.4	67.3	95.8

LAKE PINTO-17 <>	174	216725	2.8	14.0159	1.0	1.4729	3.3	0.1497	3.2	0.96	899.4	26.8	919.3	20.2	967.4	19.6	967.4	19.6	93.0
LAKE PINTO-75 <>	42	39467	2.1	13.9219	3.5	1.5594	4.9	0.1575	3.4	0.70	942.6	30.0	954.2	30.4	981.1	71.8	981.1	71.8	96.1
LAKE PINTO-45 <>	52	43773	3.2	13.8889	3.4	1.5803	5.9	0.1592	4.8	0.81	952.2	42.1	962.5	36.4	986.0	69.5	986.0	69.5	96.6
LAKE PINTO-23 <>	60	40286	0.5	13.8750	3.6	1.7346	4.2	0.1746	2.2	0.53	1037.1	21.2	1021.4	27.1	988.0	72.7	988.0	72.7	105.0
LAKE PINTO-8 <>	65	73276	1.9	13.8676	1.8	1.6960	3.8	0.1706	3.4	0.88	1015.3	31.6	1007.0	24.4	989.0	36.6	989.0	36.6	102.7
LAKE PINTO-105 <>	215	128102	1.0	13.7663	1.3	1.5231	3.0	0.1521	2.7	0.90	912.6	23.0	939.7	18.5	1003.9	27.1	1003.9	27.1	90.9
LAKE PINTO-9 <>	90	63318	1.9	13.7465	1.9	1.7524	8.0	0.1747	7.8	0.97	1038.0	74.4	1028.0	51.6	1006.9	37.6	1006.9	37.6	103.1
LAKE PINTO-106 <>	97	93437	3.3	13.6114	1.5	1.7125	2.1	0.1691	1.5	0.72	1006.9	14.0	1013.2	13.5	1026.9	29.8	1026.9	29.8	98.1
LAKE PINTO-114 <>	255	273700	2.6	13.5533	0.7	1.7237	1.8	0.1694	1.7	0.92	1009.0	15.7	1017.4	11.7	1035.5	14.4	1035.5	14.4	97.4
LAKE PINTO-29 <>	97	109726	1.3	13.5387	2.1	1.7472	2.5	0.1716	1.3	0.54	1020.7	12.6	1026.1	16.1	1037.7	42.4	1037.7	42.4	98.4
LAKE PINTO-44 <>	240	206527	3.9	13.5207	0.6	1.7841	3.4	0.1750	3.3	0.98	1039.3	31.7	1039.7	21.9	1040.4	12.7	1040.4	12.7	99.9
LAKE PINTO-6 <>	174	222336	2.6	13.5022	1.3	1.7770	2.7	0.1740	2.4	0.88	1034.2	22.9	1037.1	17.7	1043.1	26.3	1043.1	26.3	99.1
LAKE PINTO-97 <>	163	166055	2.1	13.4877	0.8	1.8132	1.3	0.1774	1.1	0.81	1052.6	10.5	1050.2	8.7	1045.3	15.6	1045.3	15.6	100.7
LAKE PINTO-31 <>	85	82554	0.7	13.4805	1.5	1.8883	3.4	0.1846	3.0	0.90	1092.2	30.3	1077.0	22.3	1046.4	30.1	1046.4	30.1	104.4
LAKE PINTO-30 <>	143	251344	2.0	13.4426	1.1	1.7844	2.2	0.1740	1.9	0.87	1034.0	18.0	1039.8	14.1	1052.1	21.6	1052.1	21.6	98.3
LAKE PINTO-99 <>	176	144893	1.4	13.4290	0.9	1.8198	2.9	0.1772	2.7	0.95	1051.9	26.4	1052.6	18.8	1054.1	17.9	1054.1	17.9	99.8
LAKE PINTO-69 <>	178	284410	1.4	13.4146	0.3	1.8459	0.7	0.1796	0.6	0.90	1064.7	6.2	1062.0	4.6	1056.3	6.1	1056.3	6.1	100.8
LAKE PINTO-13 <>	40	40588	1.0	13.3849	3.9	1.7564	5.5	0.1705	3.8	0.70	1014.9	35.9	1029.5	35.5	1060.8	79.1	1060.8	79.1	95.7
LAKE PINTO-117 <>	198	153019	1.2	13.3774	0.8	1.8637	2.5	0.1808	2.4	0.95	1071.5	23.7	1068.3	16.6	1061.9	15.1	1061.9	15.1	100.9
LAKE PINTO-124 <>	198	227752	2.2	13.2794	0.7	1.8703	1.6	0.1801	1.5	0.90	1067.7	14.3	1070.6	10.7	1076.7	14.3	1076.7	14.3	99.2
LAKE PINTO-84 <>	96	99688	2.1	13.2582	2.3	1.8888	3.4	0.1816	2.5	0.75	1075.9	25.2	1077.2	22.7	1079.8	45.6	1079.8	45.6	99.6
LAKE PINTO-5 <>	155	49277	2.0	13.2566	0.9	1.8459	1.8	0.1775	1.6	0.86	1053.2	15.4	1062.0	12.0	1080.1	18.5	1080.1	18.5	97.5
LAKE PINTO-27 <>	62	46030	3.0	12.9326	1.9	2.0519	3.4	0.1925	2.8	0.82	1134.7	28.7	1132.9	22.9	1129.5	38.0	1129.5	38.0	100.5
LAKE PINTO-103 <>	47	35058	2.0	12.9157	3.2	2.0534	4.3	0.1924	2.9	0.67	1134.1	30.1	1133.4	29.5	1132.2	63.9	1132.2	63.9	100.2
LAKE PINTO-16 <>	45	139168	0.9	12.8925	3.7	2.1629	5.2	0.2022	3.7	0.71	1187.3	40.1	1169.2	36.3	1135.7	73.5	1135.7	73.5	104.5
LAKE PINTO-125 <>	75	78045	1.2	12.7630	1.6	2.1249	2.4	0.1967	1.7	0.73	1157.6	18.1	1156.9	16.3	1155.8	32.2	1155.8	32.2	100.2
LAKE PINTO-123 <>	30	24287	1.4	12.7080	3.6	2.2221	4.0	0.2048	1.8	0.45	1201.1	19.7	1188.0	28.0	1164.3	70.9	1164.3	70.9	103.2
LAKE PINTO-11 <>	149	176235	2.5	12.6888	1.1	2.1585	1.8	0.1986	1.4	0.79	1168.0	15.4	1167.8	12.7	1167.3	22.4	1167.3	22.4	100.1
LAKE PINTO-40 <>	65	6658	2.5	12.6731	2.9	2.2729	3.1	0.2089	1.1	0.35	1223.0	11.9	1203.9	21.7	1169.8	57.0	1169.8	57.0	104.5
LAKE PINTO-91 <>	65	107182	1.1	12.5859	3.3	2.1349	3.4	0.1949	0.8	0.25	1147.7	8.7	1160.2	23.3	1183.5	64.5	1183.5	64.5	97.0

LAKE PINTO-66 <>	100	21028	1.5	12.5404	2.8	2.1346	9.0	0.1941	8.5	0.95	1143.8	89.5	1160.1	62.3	1190.6	56.1	1190.6	56.1	96.1
LAKE PINTO-55 <>	115	46050	2.2	12.5081	1.0	2.2079	2.8	0.2003	2.6	0.93	1176.9	27.6	1183.5	19.3	1195.7	20.4	1195.7	20.4	98.4
LAKE PINTO-39 <>	56	32425	1.6	12.4360	1.9	2.2330	2.2	0.2014	1.0	0.47	1182.9	10.9	1191.5	15.1	1207.1	37.5	1207.1	37.5	98.0
LAKE PINTO-92 <>	14	11256	0.8	12.2786	5.9	2.3397	6.1	0.2084	1.7	0.27	1220.1	18.4	1224.4	43.4	1232.2	115.1	1232.2	115.1	99.0
LAKE PINTO-73 <>	120	101517	2.2	12.2476	1.1	2.3407	1.7	0.2079	1.3	0.75	1217.7	14.0	1224.7	11.9	1237.1	21.6	1237.1	21.6	98.4
LAKE PINTO-35 <>	86	131377	2.6	11.8049	1.2	2.6242	3.2	0.2247	2.9	0.92	1306.6	34.4	1307.5	23.2	1308.9	24.2	1308.9	24.2	99.8
LAKE PINTO-21 <>	331	22361	3.1	11.4639	2.1	2.5064	6.3	0.2084	5.9	0.94	1220.2	66.1	1273.9	45.8	1365.6	40.7	1365.6	40.7	89.4
LAKE PINTO-68 <>	122	81409	3.3	11.1494	1.1	2.9708	3.2	0.2402	3.0	0.94	1387.9	38.0	1400.2	24.6	1418.9	21.1	1418.9	21.1	97.8
LAKE PINTO-71 <>	132	252280	1.9	10.9902	0.6	3.1530	0.8	0.2513	0.6	0.69	1445.3	7.2	1445.7	6.2	1446.4	11.0	1446.4	11.0	99.9
LAKE PINTO-33 <>	33	34297	1.8	10.9884	1.8	2.9483	3.2	0.2350	2.7	0.83	1360.5	32.6	1394.4	24.3	1446.7	34.2	1446.7	34.2	94.0
LAKE PINTO-22 <>	47	54598	1.9	10.9404	2.5	3.1572	3.7	0.2505	2.7	0.73	1441.1	34.8	1446.8	28.6	1455.0	48.5	1455.0	48.5	99.0
LAKE PINTO-78 <>	94	91947	0.9	10.5674	1.0	3.5055	3.0	0.2687	2.8	0.94	1534.0	38.9	1528.5	23.9	1520.7	19.3	1520.7	19.3	100.9
LAKE PINTO-101 <>	92	102037	0.9	10.5450	0.9	3.5087	1.3	0.2683	0.9	0.69	1532.4	12.4	1529.2	10.4	1524.7	17.9	1524.7	17.9	100.5
LAKE PINTO-59 <>	242	13342	1.5	10.3699	0.3	3.3107	1.8	0.2490	1.8	0.98	1433.3	22.9	1483.6	14.2	1556.2	6.6	1556.2	6.6	92.1
LAKE PINTO-118 <>	62	99628	1.4	9.9596	1.8	4.1442	4.6	0.2993	4.3	0.92	1688.1	63.3	1663.1	38.0	1631.6	34.2	1631.6	34.2	103.5
LAKE PINTO-43 <>	440	30398	2.1	9.9239	2.4	3.8475	3.3	0.2769	2.2	0.67	1575.8	30.7	1602.7	26.3	1638.3	44.7	1638.3	44.7	96.2
LAKE PINTO-50 <>	266	25911	3.1	9.9132	0.7	3.5988	3.8	0.2587	3.7	0.98	1483.4	49.2	1549.3	30.1	1640.3	13.8	1640.3	13.8	90.4
LAKE PINTO-28 <>	132	217382	1.3	9.4986	0.4	4.5433	0.9	0.3130	0.8	0.89	1755.4	12.8	1738.9	7.8	1719.2	8.0	1719.2	8.0	102.1
LAKE PINTO-81 <>	40	5753	0.8	9.4956	2.2	4.2569	3.4	0.2932	2.5	0.75	1657.3	37.2	1685.1	27.9	1719.8	41.1	1719.8	41.1	96.4
LAKE PINTO-15 <>	362	9732	0.9	9.4753	2.5	4.4291	7.9	0.3044	7.4	0.95	1712.9	112.0	1717.8	65.2	1723.7	46.1	1723.7	46.1	99.4
LAKE PINTO-96 <>	130	137833	2.6	9.3223	0.8	4.5912	4.1	0.3104	4.0	0.98	1742.8	61.7	1747.7	34.3	1753.5	14.6	1753.5	14.6	99.4
LAKE PINTO-112 <>	31	10379	1.2	9.1136	2.1	4.5284	2.9	0.2993	2.0	0.69	1687.9	29.4	1736.2	23.9	1794.8	38.0	1794.8	38.0	94.0
LAKE PINTO-51 <>	46	65352	2.6	9.0068	1.7	4.9696	2.1	0.3246	1.3	0.61	1812.3	20.3	1814.2	17.8	1816.3	30.2	1816.3	30.2	99.8
LAKE PINTO-20 <>	140	42801	2.3	8.9001	0.4	4.8808	0.9	0.3151	0.8	0.88	1765.5	12.1	1799.0	7.5	1837.9	7.5	1837.9	7.5	96.1
LAKE PINTO-2 <>	101	215426	1.8	8.6342	0.7	5.5359	2.6	0.3467	2.5	0.96	1918.6	41.5	1906.2	22.4	1892.6	13.4	1892.6	13.4	101.4
LAKE PINTO-88 <>	55	173451	1.1	8.1929	1.1	6.0042	2.0	0.3568	1.6	0.83	1966.8	27.4	1976.4	17.0	1986.5	19.4	1986.5	19.4	99.0
LAKE PINTO-110 <>	207	873536	1.4	7.7450	0.3	6.9131	0.7	0.3883	0.6	0.90	2115.0	11.3	2100.3	6.2	2086.0	5.5	2086.0	5.5	101.4
LAKE PINTO-52 <>	110	235879	2.1	7.3071	0.5	7.6884	1.1	0.4075	1.0	0.90	2203.3	18.5	2195.2	9.9	2187.7	8.5	2187.7	8.5	100.7
LAKE PINTO-90 <>	19	62766	1.6	5.4032	1.2	13.0510	3.1	0.5114	2.9	0.93	2662.8	62.9	2683.3	29.4	2698.9	19.4	2698.9	19.4	98.7
LAKE PINTO-18 <>	70	228017	1.3	5.3440	0.4	13.5769	2.4	0.5262	2.4	0.99	2725.5	52.7	2720.7	22.7	2717.0	6.1	2717.0	6.1	100.3

LAKE PINTO-7 <>	198	702781	1.5	5.3368	0.3	13.7101	2.2	0.5307	2.2	0.99	2744.2	49.0	2729.9	20.9	2719.3	4.2	2719.3	4.2	100.9
LAKE PINTO-85 <>	221	176671	2.6	5.2719	0.2	13.0034	1.7	0.4972	1.7	1.00	2601.7	37.1	2679.9	16.4	2739.4	2.6	2739.4	2.6	95.0
LAKE PINTO-63 <>	226	83494	1.4	5.1398	0.1	14.3021	1.8	0.5331	1.8	1.00	2754.7	39.4	2770.0	16.7	2781.1	1.8	2781.1	1.8	99.0
LAKE PINTO-122 <>	162	810676	2.1	4.9775	0.2	15.4755	1.7	0.5587	1.7	1.00	2861.2	39.2	2845.0	16.2	2833.5	2.7	2833.5	2.7	101.0
LAKE PINTO-19 <>	200	673285	2.1	3.4482	1.0	24.6675	2.4	0.6169	2.2	0.90	3097.6	53.1	3295.1	23.3	3417.6	15.9	3417.6	15.9	90.6
Turkey Creek sandstone, sample 7 (Late Pennsylvanian)																			
TURKEY CREEK-35 <>	642	17693	1.8	17.5624	1.8	0.5885	10.6	0.0750	10.4	0.99	466.0	46.9	469.9	39.8	489.2	39.7	466.0	46.9	95.3
TURKEY CREEK-6 <>	113	22554	1.5	18.2808	4.1	0.5714	4.8	0.0758	2.4	0.50	470.8	10.8	458.9	17.6	400.1	92.6	470.8	10.8	117.7
TURKEY CREEK-88 <>	18	3097	1.2	18.5546	25.6	0.5901	26.3	0.0794	6.0	0.23	492.6	28.4	470.9	99.3	366.6	585.1	492.6	28.4	134.4
TURKEY CREEK-125 <>	41	12155	0.9	17.5159	9.7	0.6653	10.9	0.0845	5.1	0.47	523.0	25.8	517.8	44.4	495.1	213.6	523.0	25.8	105.6
TURKEY CREEK-97 <>	46	15092	1.8	16.7512	7.1	0.7267	7.6	0.0883	2.8	0.37	545.4	14.8	554.6	32.7	592.6	154.1	545.4	14.8	92.0
TURKEY CREEK-84 <>	64	12767	1.1	17.0983	4.8	0.7241	5.3	0.0898	2.4	0.44	554.3	12.6	553.1	22.8	548.0	104.5	554.3	12.6	101.2
TURKEY CREEK-109 <>	200	44038	1.6	17.0387	3.6	0.7299	4.1	0.0902	2.0	0.49	556.7	10.8	556.5	17.6	555.6	77.9	556.7	10.8	100.2
TURKEY CREEK-99 <>	40	18098	1.3	16.1249	8.7	0.7824	10.6	0.0915	6.0	0.57	564.4	32.4	586.8	47.3	674.6	187.3	564.4	32.4	83.7
TURKEY CREEK-5 <>	240	58640	6.4	16.9209	2.5	0.7523	3.6	0.0923	2.6	0.72	569.2	13.9	569.5	15.5	570.7	54.0	569.2	13.9	99.7
TURKEY CREEK-103 <>	85	16254	0.9	16.7587	5.2	0.7685	5.5	0.0934	1.8	0.32	575.7	9.7	578.9	24.1	591.6	112.1	575.7	9.7	97.3
TURKEY CREEK-62 <>	43	12718	1.8	16.7336	8.2	0.7715	10.3	0.0936	6.1	0.60	577.0	33.9	580.6	45.5	594.9	178.9	577.0	33.9	97.0
TURKEY CREEK-85 <>	385	198012	4.3	16.9068	1.2	0.7676	2.9	0.0941	2.7	0.92	579.9	14.8	578.4	12.8	572.5	25.0	579.9	14.8	101.3
TURKEY CREEK-16 <>	64	16491	0.3	17.7042	5.1	0.7346	6.1	0.0943	3.2	0.53	581.1	17.9	559.2	26.1	471.4	114.0	581.1	17.9	123.3
TURKEY CREEK-116 <>	70	11247	0.4	16.3756	4.1	0.7988	4.3	0.0949	1.5	0.34	584.3	8.1	596.1	19.4	641.6	87.4	584.3	8.1	91.1
TURKEY CREEK-7 <>	114	30394	1.1	16.4530	3.6	0.7984	4.3	0.0953	2.3	0.54	586.6	13.0	595.9	19.5	631.5	78.5	586.6	13.0	92.9
TURKEY CREEK-61 <>	62	23737	1.6	17.1606	7.1	0.7755	9.7	0.0965	6.6	0.68	594.0	37.3	582.9	43.0	540.1	155.8	594.0	37.3	110.0
TURKEY CREEK-2 <>	193	89951	16.4	16.6616	2.1	0.8147	3.6	0.0984	2.9	0.82	605.3	16.9	605.1	16.3	604.2	44.4	605.3	16.9	100.2
TURKEY CREEK-74 <>	340	84608	0.8	16.5516	1.4	0.8334	3.4	0.1000	3.1	0.91	614.7	18.3	615.5	15.8	618.5	29.8	614.7	18.3	99.4
TURKEY CREEK-22 <>	108	39812	3.4	16.0870	4.6	0.8593	5.0	0.1003	1.9	0.38	615.9	11.3	629.7	23.6	679.7	99.3	615.9	11.3	90.6
TURKEY CREEK-87 <>	374	47686	1.8	16.4208	1.7	0.8771	2.1	0.1045	1.3	0.62	640.5	7.9	639.4	10.0	635.7	35.8	640.5	7.9	100.8
TURKEY CREEK-24 <>	55	4319	0.7	16.1352	7.7	0.9381	9.3	0.1098	5.2	0.56	671.5	33.1	671.9	45.6	673.3	164.4	671.5	33.1	99.7
TURKEY CREEK-90 <>	28	23495	0.3	15.4907	9.7	1.0659	10.3	0.1198	3.4	0.33	729.1	23.6	736.7	54.2	759.8	206.0	729.1	23.6	96.0

TURKEY CREEK-58 <>	25	1347	1.6	15.0377	10.2	1.1723	11.7	0.1279	5.6	0.48	775.6	41.0	787.7	63.9	822.2	213.8	775.6	41.0	94.3
TURKEY CREEK-106 <>	111	35223	1.0	14.6081	2.2	1.2777	2.8	0.1354	1.8	0.62	818.4	13.5	835.8	16.1	882.4	45.8	818.4	13.5	92.8
TURKEY CREEK-124 <>	57	18218	1.4	14.6893	6.0	1.3821	9.5	0.1472	7.4	0.78	885.5	61.0	881.3	56.0	870.9	124.1	885.5	61.0	101.7
TURKEY CREEK-60 <>	49	25557	1.7	14.3252	4.6	1.5037	5.3	0.1562	2.6	0.48	935.8	22.3	931.9	32.3	922.7	95.4	922.7	95.4	101.4
TURKEY CREEK-76 <>	93	17982	1.2	14.2302	3.5	1.4620	4.4	0.1509	2.7	0.61	905.9	22.8	914.8	26.7	936.3	71.8	936.3	71.8	96.8
TURKEY CREEK-69 <>	186	76155	3.1	14.1569	0.8	1.6165	2.0	0.1660	1.9	0.92	989.9	17.3	976.6	12.8	946.9	16.4	946.9	16.4	104.5
TURKEY CREEK-43 <>	75	33161	1.6	14.0916	3.0	1.5523	3.4	0.1586	1.5	0.45	949.3	13.4	951.4	20.7	956.4	61.2	956.4	61.2	99.3
TURKEY CREEK-10 <>	137	5843	1.4	14.0750	2.0	1.5847	3.2	0.1618	2.5	0.78	966.6	22.8	964.2	20.2	958.8	41.4	958.8	41.4	100.8
TURKEY CREEK-59 <>	55	12504	0.9	14.0221	4.3	1.6479	5.4	0.1676	3.2	0.59	998.8	29.5	988.7	33.9	966.5	88.3	966.5	88.3	103.3
TURKEY CREEK-65 <>	134	74834	2.8	13.9498	1.5	1.6880	6.0	0.1708	5.8	0.97	1016.4	54.8	1004.0	38.4	977.0	30.5	977.0	30.5	104.0
TURKEY CREEK-44 <>	42	13529	2.1	13.9117	5.3	1.6264	9.7	0.1641	8.1	0.83	979.5	73.5	980.4	61.0	982.6	109.0	982.6	109.0	99.7
TURKEY CREEK-75 <>	65	35615	2.5	13.8875	2.9	1.7008	3.5	0.1713	1.8	0.53	1019.3	17.3	1008.8	22.1	986.1	59.8	986.1	59.8	103.4
TURKEY CREEK-9 <>	50	13565	1.0	13.8703	2.5	1.6895	4.6	0.1700	3.8	0.83	1011.9	35.8	1004.6	29.3	988.7	51.6	988.7	51.6	102.4
TURKEY CREEK-77 <>	40	23065	1.3	13.8252	4.4	1.5762	5.2	0.1580	2.7	0.52	945.9	23.8	960.9	32.2	995.3	89.8	995.3	89.8	95.0
TURKEY CREEK-70 <>	172	44839	3.1	13.7275	1.0	1.7048	3.0	0.1697	2.8	0.94	1010.6	26.6	1010.3	19.4	1009.7	20.7	1009.7	20.7	100.1
TURKEY CREEK-50 <>	116	7637	2.9	13.6889	1.5	1.7370	2.8	0.1725	2.4	0.85	1025.6	22.9	1022.4	18.3	1015.4	30.0	1015.4	30.0	101.0
TURKEY CREEK-107 <>	239	131895	2.5	13.6586	0.6	1.7711	1.6	0.1754	1.4	0.92	1042.0	13.8	1034.9	10.1	1019.9	12.3	1019.9	12.3	102.2
TURKEY CREEK-32 <>	184	141912	3.1	13.6011	0.7	1.7156	3.8	0.1692	3.7	0.98	1007.9	34.5	1014.4	24.1	1028.4	14.0	1028.4	14.0	98.0
TURKEY CREEK-92 <>	217	42961	1.1	13.5740	0.7	1.7600	2.7	0.1733	2.6	0.96	1030.1	24.4	1030.9	17.2	1032.4	14.5	1032.4	14.5	99.8
TURKEY CREEK-3 <>	89	29152	2.2	13.5384	2.1	1.7541	2.7	0.1722	1.7	0.63	1024.4	15.8	1028.7	17.2	1037.7	41.7	1037.7	41.7	98.7
TURKEY CREEK-86 <>	30	11711	1.0	13.5379	7.5	1.5918	8.4	0.1563	3.9	0.46	936.1	33.6	967.0	52.7	1037.8	152.0	1037.8	152.0	90.2
TURKEY CREEK-56 <>	206	129240	2.7	13.5123	0.8	1.8168	2.2	0.1780	2.1	0.94	1056.3	20.0	1051.5	14.4	1041.6	15.7	1041.6	15.7	101.4
TURKEY CREEK-89 <>	157	105985	3.7	13.4800	1.2	1.8229	1.9	0.1782	1.5	0.79	1057.2	14.9	1053.7	12.7	1046.5	23.9	1046.5	23.9	101.0
TURKEY CREEK-71 <>	640	218132	3.8	13.4646	0.2	1.8509	3.3	0.1808	3.3	1.00	1071.1	32.4	1063.8	21.6	1048.8	3.7	1048.8	3.7	102.1
TURKEY CREEK-115 <>	89	40875	1.6	13.4512	2.0	1.8497	2.7	0.1805	1.9	0.68	1069.5	18.5	1063.3	18.1	1050.8	40.6	1050.8	40.6	101.8
TURKEY CREEK-8 <>	150	92637	2.5	13.4167	1.1	1.8236	3.0	0.1774	2.8	0.93	1053.0	26.8	1054.0	19.4	1056.0	21.6	1056.0	21.6	99.7
TURKEY CREEK-13 <>	131	23529	1.4	13.3968	1.2	1.8457	2.9	0.1793	2.6	0.90	1063.4	25.4	1061.9	18.9	1059.0	24.9	1059.0	24.9	100.4
TURKEY CREEK-53 <>	65	28935	1.1	13.3921	2.3	1.8794	4.7	0.1825	4.1	0.87	1080.9	41.2	1073.8	31.5	1059.7	46.8	1059.7	46.8	102.0
TURKEY CREEK-93 <>	48	30554	0.8	13.3802	1.6	1.7571	2.8	0.1705	2.3	0.81	1015.0	21.6	1029.8	18.3	1061.5	33.0	1061.5	33.0	95.6
TURKEY CREEK-100 <>	77	34876	2.1	13.3419	2.4	1.8490	7.8	0.1789	7.4	0.95	1061.0	72.6	1063.1	51.5	1067.2	48.4	1067.2	48.4	99.4

TURKEY CREEK-122 <>	279	135494	1.4	13.3274	0.6	1.8970	1.2	0.1834	1.0	0.87	1085.3	10.4	1080.0	7.9	1069.4	11.6	1069.4	11.6	101.5
TURKEY CREEK-111 <>	169	34908	1.8	13.3105	0.8	1.7987	3.2	0.1736	3.1	0.97	1032.2	29.9	1045.0	21.0	1072.0	15.1	1072.0	15.1	96.3
TURKEY CREEK-15 <>	37	16697	0.8	13.3038	4.0	1.8660	4.5	0.1800	2.0	0.45	1067.2	19.9	1069.1	29.5	1073.0	80.0	1073.0	80.0	99.5
TURKEY CREEK-118 <>	55	17660	1.3	13.2638	4.7	1.8780	9.0	0.1807	7.7	0.85	1070.6	76.1	1073.4	60.0	1079.0	94.7	1079.0	94.7	99.2
TURKEY CREEK-20 <>	52	35081	1.2	13.2236	3.2	1.8446	3.7	0.1769	1.9	0.51	1050.1	18.1	1061.5	24.3	1085.1	63.7	1085.1	63.7	96.8
TURKEY CREEK-47 <>	75	8606	1.5	13.2197	2.9	1.6865	4.3	0.1617	3.2	0.74	966.2	28.6	1003.5	27.5	1085.7	58.2	1085.7	58.2	89.0
TURKEY CREEK-117 <>	71	36521	1.1	13.2169	3.6	1.8927	4.7	0.1814	3.0	0.64	1074.8	29.7	1078.5	31.1	1086.1	72.0	1086.1	72.0	99.0
TURKEY CREEK-27 <>	39	59043	3.1	13.1643	3.5	1.9462	3.6	0.1858	0.8	0.22	1098.7	7.8	1097.1	23.8	1094.1	69.5	1094.1	69.5	100.4
TURKEY CREEK-33 <>	118	49556	0.9	13.1615	1.5	1.9444	3.1	0.1856	2.7	0.87	1097.5	27.6	1096.5	21.0	1094.5	30.3	1094.5	30.3	100.3
TURKEY CREEK-72 <>	112	66212	1.6	13.0749	1.5	2.0059	2.1	0.1902	1.4	0.70	1122.6	14.7	1117.5	13.9	1107.7	29.5	1107.7	29.5	101.3
TURKEY CREEK-95 <>	76	80527	3.5	13.0189	1.6	2.0662	2.8	0.1951	2.3	0.81	1148.9	23.7	1137.7	19.0	1116.3	32.7	1116.3	32.7	102.9
TURKEY CREEK-54 <>	72	36227	2.7	13.0158	3.3	1.9086	4.6	0.1802	3.2	0.69	1067.9	31.3	1084.1	30.5	1116.8	65.9	1116.8	65.9	95.6
TURKEY CREEK-57 <>	81	49201	1.3	13.0045	2.7	2.0496	3.0	0.1933	1.3	0.42	1139.3	13.1	1132.2	20.4	1118.5	54.1	1118.5	54.1	101.9
TURKEY CREEK-29 <>	228	116347	2.4	12.9813	0.5	2.0448	1.6	0.1925	1.5	0.95	1135.0	15.3	1130.6	10.6	1122.1	9.8	1122.1	9.8	101.2
TURKEY CREEK-120 <>	100	46942	2.0	12.9682	1.2	2.0004	4.5	0.1881	4.4	0.96	1111.3	44.4	1115.6	30.7	1124.1	24.9	1124.1	24.9	98.9
TURKEY CREEK-102 <>	33	22148	1.3	12.9105	5.8	1.8208	7.0	0.1705	3.9	0.56	1014.8	37.0	1053.0	46.2	1133.0	116.4	1133.0	116.4	89.6
TURKEY CREEK-42 <>	297	104631	2.8	12.8768	0.5	2.0049	2.2	0.1872	2.2	0.97	1106.4	21.9	1117.2	15.0	1138.2	9.9	1138.2	9.9	97.2
TURKEY CREEK-18 <>	66	20842	2.1	12.6906	4.6	1.9017	5.2	0.1750	2.6	0.49	1039.8	24.8	1081.7	34.9	1167.1	90.4	1167.1	90.4	89.1
TURKEY CREEK-51 <>	162	165299	3.3	12.6193	0.7	2.2476	2.6	0.2057	2.5	0.97	1205.9	28.0	1196.0	18.5	1178.2	13.1	1178.2	13.1	102.4
TURKEY CREEK-48 <>	61	26957	1.4	12.5645	1.7	2.0572	5.2	0.1875	4.9	0.95	1107.6	49.9	1134.7	35.4	1186.8	33.1	1186.8	33.1	93.3
TURKEY CREEK-23 <>	57	21957	2.0	12.5586	2.6	2.2090	3.3	0.2012	2.1	0.63	1181.8	22.3	1183.9	23.1	1187.8	50.9	1187.8	50.9	99.5
TURKEY CREEK-114 <>	41	18405	2.1	12.5115	3.3	2.2840	4.4	0.2073	3.0	0.67	1214.2	33.2	1207.3	31.4	1195.2	64.7	1195.2	64.7	101.6
TURKEY CREEK-30 <>	56	53231	1.8	12.3366	2.0	2.2014	2.3	0.1970	1.1	0.49	1159.0	12.0	1181.5	16.0	1222.9	39.3	1222.9	39.3	94.8
TURKEY CREEK-38 <>	1061	4826	2.3	12.2752	0.5	1.0881	6.8	0.0969	6.8	1.00	596.0	38.5	747.6	35.9	1232.7	9.3	1232.7	9.3	48.4
TURKEY CREEK-81 <>	24	11837	1.3	12.0355	4.3	2.6087	5.8	0.2277	3.9	0.68	1322.5	47.2	1303.1	42.9	1271.3	84.0	1271.3	84.0	104.0
TURKEY CREEK-28 <>	49	53500	1.1	12.0128	1.7	2.5495	2.1	0.2221	1.3	0.62	1293.1	15.3	1286.3	15.4	1274.9	32.2	1274.9	32.2	101.4
TURKEY CREEK-110 <>	114	128864	4.5	11.9803	1.2	2.5590	2.3	0.2223	1.9	0.83	1294.3	22.0	1289.0	16.5	1280.2	24.3	1280.2	24.3	101.1
TURKEY CREEK-25 <>	99	88651	1.7	11.5580	1.4	2.8248	2.1	0.2368	1.6	0.76	1370.0	19.9	1362.2	15.9	1349.8	26.7	1349.8	26.7	101.5
TURKEY CREEK-82 <>	28	24176	2.5	10.6752	4.8	2.9820	5.3	0.2309	2.3	0.43	1339.1	27.6	1403.0	40.4	1501.6	90.7	1501.6	90.7	89.2
TURKEY CREEK-46 <>	183	271846	1.2	10.5315	1.0	3.1013	9.6	0.2369	9.5	0.99	1370.5	117.3	1433.0	73.5	1527.1	19.1	1527.1	19.1	89.7

TURKEY CREEK-78 <>	204	52012	2.0	10.4799	0.7	3.4083	1.6	0.2591	1.4	0.91	1485.0	19.0	1506.3	12.4	1536.4	12.3	1536.4	12.3	96.7
TURKEY CREEK-104 <>	31	21125	0.8	10.2137	3.1	3.7093	4.0	0.2748	2.5	0.61	1565.0	34.1	1573.4	31.9	1584.6	58.9	1584.6	58.9	98.8
TURKEY CREEK-39 <>	84	65162	3.8	9.9718	0.8	4.0197	1.8	0.2907	1.6	0.89	1645.1	23.5	1638.2	14.8	1629.3	15.6	1629.3	15.6	101.0
TURKEY CREEK-79 <>	106	69957	1.0	9.8295	1.0	4.0577	2.8	0.2893	2.6	0.94	1637.9	37.8	1645.8	22.7	1656.0	18.0	1656.0	18.0	98.9
TURKEY CREEK-26 <>	67	17027	0.9	9.7990	1.8	3.9411	3.6	0.2801	3.1	0.87	1591.8	43.9	1622.2	29.1	1661.7	33.3	1661.7	33.3	95.8
TURKEY CREEK-91	19	12562	0.9	9.7703	4.5	4.0249	6.3	0.2852	4.5	0.70	1617.5	63.8	1639.2	51.6	1667.2	83.3	1667.2	83.3	97.0
TURKEY CREEK-37 <>	97	65522	1.0	9.5544	0.6	4.2744	2.2	0.2962	2.1	0.96	1672.4	31.7	1688.4	18.4	1708.4	10.9	1708.4	10.9	97.9
TURKEY CREEK-21 <>	50	41903	3.5	9.4537	1.7	4.6012	3.8	0.3155	3.4	0.90	1767.6	52.2	1749.5	31.4	1727.9	30.7	1727.9	30.7	102.3
TURKEY CREEK-66 <>	112	126851	1.7	9.3991	1.0	4.5060	1.8	0.3072	1.5	0.84	1726.7	23.3	1732.1	15.2	1738.5	17.9	1738.5	17.9	99.3
TURKEY CREEK-4 <>	298	153199	1.4	9.3899	0.3	4.5693	2.0	0.3112	2.0	0.99	1746.5	30.0	1743.7	16.5	1740.3	5.1	1740.3	5.1	100.4
TURKEY CREEK-68 <>	422	280992	2.7	9.1459	0.2	4.8211	1.7	0.3198	1.7	0.99	1788.7	26.0	1788.6	14.1	1788.4	3.8	1788.4	3.8	100.0
TURKEY CREEK-19 <>	242	239105	1.7	9.0979	0.4	4.9580	2.2	0.3271	2.2	0.98	1824.6	34.8	1812.2	18.9	1798.0	7.5	1798.0	7.5	101.5
TURKEY CREEK-108 <>	27	24935	0.6	8.8784	3.3	4.9822	3.9	0.3208	2.2	0.56	1793.7	34.2	1816.3	33.2	1842.3	59.1	1842.3	59.1	97.4
TURKEY CREEK-36 <>	346	502710	1.5	8.8572	0.2	5.2126	1.9	0.3348	1.9	0.99	1861.8	30.4	1854.7	16.1	1846.6	4.2	1846.6	4.2	100.8
TURKEY CREEK-119 <>	98	152239	0.8	8.6181	0.5	5.3724	2.9	0.3358	2.9	0.98	1866.4	47.0	1880.5	25.2	1896.0	9.3	1896.0	9.3	98.4
TURKEY CREEK-123 <>	30	34347	0.5	8.6139	1.8	5.4379	2.8	0.3397	2.1	0.76	1885.4	34.4	1890.8	23.7	1896.9	32.2	1896.9	32.2	99.4
TURKEY CREEK-112 <>	288	272948	5.6	7.9706	0.7	6.2157	1.7	0.3593	1.5	0.92	1978.9	25.7	2006.7	14.4	2035.3	11.8	2035.3	11.8	97.2
TURKEY CREEK-105 <>	223	143548	2.0	7.8323	5.3	5.2979	10.2	0.3009	8.7	0.85	1696.0	130.4	1868.5	87.6	2066.2	93.8	2066.2	93.8	82.1
TURKEY CREEK-17 <>	23	33321	0.5	7.5851	1.9	6.9928	4.2	0.3847	3.8	0.90	2098.2	67.9	2110.5	37.6	2122.6	32.8	2122.6	32.8	98.9
TURKEY CREEK-12 <>	33	5176	0.4	6.1103	1.5	10.5389	5.2	0.4670	5.0	0.96	2470.6	102.9	2483.3	48.6	2493.8	25.4	2493.8	25.4	99.1
TURKEY CREEK-40 <>	317	331624	2.2	5.4411	0.1	13.4515	1.8	0.5308	1.8	1.00	2745.0	40.5	2711.9	17.2	2687.3	2.2	2687.3	2.2	102.1
TURKEY CREEK-80 <>	9	5439	0.7	5.3249	4.1	10.8193	6.1	0.4178	4.5	0.74	2250.7	86.4	2507.7	56.9	2722.9	67.4	2722.9	67.4	82.7
TURKEY CREEK-73 <>	44	81887	0.5	5.2918	0.4	13.7814	2.0	0.5289	1.9	0.98	2736.9	43.0	2734.8	18.7	2733.2	7.2	2733.2	7.2	100.1
TURKEY CREEK-34 <>	98	157238	1.0	2.9956	0.2	28.2791	2.4	0.6144	2.3	0.99	3087.6	57.4	3428.8	23.1	3634.7	3.8	3634.7	3.8	84.9
Colony Creek sandstone, sample 8 (Late Pennsylvanian)																			
COLONY CREEK-107 <>	355	31629	1.4	18.3960	2.1	0.3788	3.8	0.0505	3.2	0.83	317.9	9.8	326.2	10.6	386.0	47.5	317.9	9.8	82.3
COLONY CREEK-27 <>	82	2022	1.7	17.6894	7.1	0.4153	7.7	0.0533	3.0	0.39	334.6	9.7	352.7	22.9	473.3	156.6	334.6	9.7	70.7
COLONY CREEK-85 <>	204	32337	1.8	18.8404	2.9	0.4426	4.3	0.0605	3.2	0.73	378.6	11.7	372.1	13.5	332.1	66.9	378.6	11.7	113.9

COLONY CREEK-103 <>	72	4693	1.1	16.1018	12.3	0.5692	12.7	0.0665	3.2	0.25	414.9	12.7	457.5	46.9	677.7	264.6	414.9	12.7	61.2
COLONY CREEK-99 <>	123	21451	0.6	18.7956	5.0	0.5094	8.5	0.0694	6.9	0.81	432.8	28.8	418.1	29.1	337.5	112.9	432.8	28.8	128.2
COLONY CREEK-75 <>	459	11363	1.1	17.5469	3.7	0.5647	4.3	0.0719	2.2	0.51	447.4	9.6	454.6	15.8	491.1	81.8	447.4	9.6	91.1
COLONY CREEK-21 <>	64	14001	0.5	18.1287	8.5	0.5547	9.3	0.0729	3.8	0.41	453.8	16.6	448.1	33.8	418.7	190.5	453.8	16.6	108.4
COLONY CREEK-39 <>	486	76201	0.5	17.7670	1.0	0.5922	2.5	0.0763	2.3	0.91	474.1	10.4	472.3	9.4	463.6	22.7	474.1	10.4	102.3
COLONY CREEK-70 <>	41	5155	0.3	18.6954	11.4	0.5909	12.0	0.0801	3.7	0.31	496.8	17.9	471.4	45.4	349.6	259.0	496.8	17.9	142.1
COLONY CREEK-19 <>	64	26206	0.4	17.3108	5.4	0.6422	6.0	0.0806	2.6	0.43	499.8	12.3	503.6	23.8	520.9	118.9	499.8	12.3	96.0
COLONY CREEK-30 <>	69	20399	1.2	17.7925	4.3	0.6297	4.6	0.0813	1.6	0.34	503.6	7.5	495.9	18.1	460.4	96.1	503.6	7.5	109.4
COLONY CREEK-24 <>	98	74552	1.9	17.1443	2.4	0.6558	3.8	0.0815	2.9	0.77	505.4	14.3	512.1	15.4	542.1	53.0	505.4	14.3	93.2
COLONY CREEK-64 <>	229	57217	1.6	17.3648	1.3	0.6725	3.2	0.0847	2.9	0.92	524.1	14.8	522.2	13.1	514.1	28.2	524.1	14.8	101.9
COLONY CREEK-116 <>	100	7100	2.3	17.2073	3.1	0.6787	3.3	0.0847	1.1	0.33	524.1	5.6	526.0	13.7	534.1	68.8	524.1	5.6	98.1
COLONY CREEK-44 <>	121	18222	1.0	17.1918	3.3	0.6840	3.9	0.0853	2.1	0.53	527.6	10.5	529.2	16.2	536.0	73.2	527.6	10.5	98.4
COLONY CREEK-16 <>	222	41877	3.2	17.1995	1.6	0.6948	5.1	0.0867	4.8	0.95	535.8	24.9	535.7	21.3	535.1	35.5	535.8	24.9	100.1
COLONY CREEK-31 <>	44	8597	1.2	18.4887	15.1	0.6549	15.3	0.0878	2.6	0.17	542.6	13.7	511.5	61.6	374.7	341.3	542.6	13.7	144.8
COLONY CREEK-56 <>	48	16168	3.5	17.6742	6.2	0.6908	6.4	0.0885	1.9	0.29	546.9	9.9	533.3	26.7	475.2	136.2	546.9	9.9	115.1
COLONY CREEK-26 <>	132	24674	1.8	17.4325	2.8	0.7174	3.3	0.0907	1.8	0.55	559.7	9.7	549.1	14.0	505.6	60.6	559.7	9.7	110.7
COLONY CREEK-67 <>	56	13434	1.8	18.4454	4.9	0.6837	5.2	0.0915	1.8	0.35	564.2	9.7	529.0	21.5	379.9	109.9	564.2	9.7	148.5
COLONY CREEK-120 <>	66	22387	2.3	16.6532	5.0	0.7577	5.6	0.0915	2.4	0.43	564.5	13.1	572.7	24.5	605.3	109.0	564.5	13.1	93.3
COLONY CREEK-12 <>	110	17198	1.5	17.2600	4.7	0.7508	6.7	0.0940	4.8	0.72	579.1	26.5	568.7	29.2	527.4	102.5	579.1	26.5	109.8
COLONY CREEK-1 <>	189	47253	0.7	17.0605	2.5	0.7645	2.9	0.0946	1.5	0.52	582.6	8.4	576.6	12.8	552.8	54.2	582.6	8.4	105.4
COLONY CREEK-92 <>	57	23708	0.9	14.9666	7.7	0.8886	7.8	0.0965	1.4	0.17	593.6	7.7	645.6	37.2	832.0	159.9	593.6	7.7	71.3
COLONY CREEK-79 <>	36	15797	1.7	16.8823	7.6	0.7981	8.5	0.0977	4.0	0.46	601.1	22.7	595.8	38.5	575.7	164.7	601.1	22.7	104.4
COLONY CREEK-48 <>	95	22936	0.8	16.2149	3.4	0.8340	4.1	0.0981	2.4	0.57	603.1	13.7	615.8	19.1	662.7	72.6	603.1	13.7	91.0
COLONY CREEK-98 <>	127	40030	0.8	16.5226	2.1	0.8639	2.3	0.1035	0.9	0.39	635.0	5.3	632.2	10.7	622.3	45.1	635.0	5.3	102.0
COLONY CREEK-102 <>	253	57598	1.9	16.6209	1.4	0.8613	1.9	0.1038	1.3	0.68	636.8	7.8	630.8	8.9	609.5	29.7	636.8	7.8	104.5
COLONY CREEK-87 <>	138	16022	0.7	16.2643	1.9	0.9075	2.1	0.1071	1.0	0.45	655.6	5.9	655.7	10.3	656.2	40.7	655.6	5.9	99.9
COLONY CREEK-121 <>	313	148414	1.4	15.7728	1.5	0.9874	1.9	0.1130	1.1	0.56	689.9	6.9	697.4	9.5	721.7	32.8	689.9	6.9	95.6
COLONY CREEK-93 <>	443	81770	2.9	16.1633	0.7	0.9751	1.6	0.1143	1.4	0.89	697.7	9.2	691.1	7.9	669.6	15.5	697.7	9.2	104.2
COLONY CREEK-110 <>	56	15450	0.9	15.7761	5.4	1.0790	5.8	0.1235	1.9	0.33	750.4	13.6	743.1	30.4	721.2	115.4	750.4	13.6	104.0
COLONY CREEK-62 <>	102	16282	2.4	14.7494	2.8	1.2081	4.3	0.1292	3.3	0.77	783.5	24.5	804.3	24.1	862.4	57.8	783.5	24.5	90.8

COLONY CREEK-9 <>	92	27443	1.2	14.9651	2.0	1.2202	2.8	0.1324	1.9	0.69	801.8	14.7	809.9	15.7	832.3	42.3	801.8	14.7	96.3
COLONY CREEK-106 <>	67	25774	1.3	14.3638	2.5	1.3436	4.2	0.1400	3.4	0.81	844.5	26.8	864.8	24.5	917.2	51.3	844.5	26.8	92.1
COLONY CREEK-34 <>	176	145986	1.7	14.5116	1.1	1.4906	1.8	0.1569	1.4	0.80	939.4	12.4	926.5	10.7	896.1	21.7	896.1	21.7	104.8
COLONY CREEK-124 <>	50	33413	2.1	14.4905	4.0	1.4358	4.4	0.1509	1.9	0.43	906.0	16.0	904.0	26.6	899.0	83.0	899.0	83.0	100.8
COLONY CREEK-65 <>	177	185838	2.2	14.3249	1.8	1.4734	3.2	0.1531	2.6	0.82	918.2	22.5	919.5	19.4	922.7	37.6	922.7	37.6	99.5
COLONY CREEK-6 <>	92	23340	1.1	14.3141	2.5	1.5084	3.2	0.1566	2.0	0.62	937.8	17.2	933.8	19.4	924.3	51.3	924.3	51.3	101.5
COLONY CREEK-2 <>	76	27414	2.2	14.2771	2.3	1.4493	5.0	0.1501	4.5	0.89	901.4	37.5	909.6	30.0	929.6	46.2	929.6	46.2	97.0
COLONY CREEK-4 <>	45	19293	2.0	14.2008	5.4	1.4873	6.6	0.1532	3.8	0.57	918.8	32.2	925.2	40.2	940.6	111.7	940.6	111.7	97.7
COLONY CREEK-17 <>	50	30702	1.4	14.1034	4.9	1.5475	5.5	0.1583	2.4	0.45	947.3	21.6	949.5	33.9	954.7	100.7	954.7	100.7	99.2
COLONY CREEK-81 <>	31	14274	2.2	14.0055	5.3	1.6804	6.3	0.1707	3.3	0.52	1015.9	30.9	1001.1	39.9	968.9	108.9	968.9	108.9	104.9
COLONY CREEK-125 <>	151	81007	0.9	14.0042	1.5	1.5999	2.0	0.1625	1.4	0.69	970.7	12.4	970.2	12.5	969.1	29.8	969.1	29.8	100.2
COLONY CREEK-123 <>	22	10716	0.4	13.9408	6.5	1.6437	6.7	0.1662	1.4	0.21	991.1	12.9	987.1	42.3	978.3	133.5	978.3	133.5	101.3
COLONY CREEK-63 <>	121	78964	2.2	13.9032	2.0	1.6570	2.7	0.1671	1.8	0.67	996.0	16.8	992.2	17.1	983.8	40.8	983.8	40.8	101.2
COLONY CREEK-80 <>	75	23094	1.9	13.8784	2.3	1.6541	3.0	0.1665	1.8	0.62	992.8	16.9	991.1	18.8	987.5	47.7	987.5	47.7	100.5
COLONY CREEK-54 <>	91	55189	1.8	13.8278	0.5	1.6737	2.1	0.1679	2.1	0.97	1000.3	19.2	998.6	13.6	994.9	10.2	994.9	10.2	100.5
COLONY CREEK-108 <>	96	94109	0.7	13.7365	1.9	1.6506	2.7	0.1644	1.9	0.70	981.4	17.0	989.8	16.9	1008.3	38.6	1008.3	38.6	97.3
COLONY CREEK-74 <>	186	93367	0.7	13.6862	1.0	1.6935	1.6	0.1681	1.2	0.75	1001.6	11.0	1006.1	10.0	1015.8	21.0	1015.8	21.0	98.6
COLONY CREEK-3 <>	99	75154	2.1	13.6546	1.6	1.7323	5.0	0.1716	4.7	0.95	1020.7	44.7	1020.6	32.2	1020.5	32.2	1020.5	32.2	100.0
COLONY CREEK-73 <>	66	37790	1.4	13.6476	2.7	1.7910	7.5	0.1773	7.0	0.93	1052.1	67.6	1042.2	48.7	1021.5	54.8	1021.5	54.8	103.0
COLONY CREEK-69 <>	64	25530	2.4	13.6254	1.2	1.7270	4.0	0.1707	3.8	0.96	1015.8	35.6	1018.6	25.5	1024.8	23.4	1024.8	23.4	99.1
COLONY CREEK-53 <>	135	72404	2.4	13.6172	1.6	1.7723	2.1	0.1750	1.3	0.62	1039.8	12.4	1035.4	13.4	1026.0	32.7	1026.0	32.7	101.3
COLONY CREEK-104 <>	38	41320	1.7	13.5751	3.4	1.8091	4.2	0.1781	2.5	0.58	1056.7	24.0	1048.8	27.6	1032.3	69.2	1032.3	69.2	102.4
COLONY CREEK-57 <>	27	4475	1.7	13.5084	9.0	1.5665	10.0	0.1535	4.5	0.45	920.4	38.9	957.0	62.3	1042.2	181.1	1042.2	181.1	88.3
COLONY CREEK-61 <>	56	33318	2.1	13.5057	3.2	1.6257	5.6	0.1592	4.6	0.82	952.6	40.6	980.2	35.1	1042.6	63.9	1042.6	63.9	91.4
COLONY CREEK-91 <>	119	60364	2.1	13.4508	1.9	1.7794	3.3	0.1736	2.7	0.82	1031.8	25.3	1038.0	21.2	1050.9	37.8	1050.9	37.8	98.2
COLONY CREEK-84 <>	281	170179	3.1	13.4368	0.7	1.8540	2.8	0.1807	2.7	0.97	1070.7	26.6	1064.9	18.3	1053.0	13.9	1053.0	13.9	101.7
COLONY CREEK-88 <>	210	107921	1.4	13.4353	1.0	1.8079	2.9	0.1762	2.7	0.94	1046.0	26.5	1048.3	19.1	1053.2	20.6	1053.2	20.6	99.3
COLONY CREEK-58 <>	233	13906	3.0	13.4327	1.1	1.7198	2.1	0.1675	1.7	0.83	998.6	15.9	1016.0	13.3	1053.6	23.1	1053.6	23.1	94.8
COLONY CREEK-14 <>	56	13226	1.9	13.4175	3.5	1.8805	6.3	0.1830	5.2	0.83	1083.3	52.2	1074.3	42.0	1055.9	71.5	1055.9	71.5	102.6
COLONY CREEK-15 <>	18	7997	0.7	13.3145	3.6	1.8908	4.4	0.1826	2.6	0.59	1081.1	26.0	1077.9	29.3	1071.4	71.5	1071.4	71.5	100.9

COLONY CREEK-68 <>	274	119825	2.2	13.2811	0.5	1.9313	1.3	0.1860	1.2	0.92	1099.8	11.9	1092.0	8.6	1076.4	10.3	1076.4	10.3	102.2
COLONY CREEK-105 <>	233	33543	3.7	13.2292	0.6	1.8037	2.3	0.1731	2.2	0.97	1029.0	20.7	1046.8	14.7	1084.3	11.8	1084.3	11.8	94.9
COLONY CREEK-60 <>	396	33264	2.3	13.1632	0.4	1.8839	2.6	0.1799	2.5	0.99	1066.2	24.9	1075.4	17.0	1094.3	7.3	1094.3	7.3	97.4
COLONY CREEK-49 <>	58	16120	1.7	13.0522	2.1	1.9766	3.4	0.1871	2.6	0.79	1105.7	26.9	1107.6	22.7	1111.2	41.3	1111.2	41.3	99.5
COLONY CREEK-43 <>	319	16470	1.9	13.0177	0.5	1.8685	2.1	0.1764	2.0	0.97	1047.3	19.5	1070.0	13.8	1116.5	10.5	1116.5	10.5	93.8
COLONY CREEK-83 <>	39	17663	2.7	12.9950	2.4	2.1169	5.5	0.1995	4.9	0.89	1172.7	52.3	1154.3	37.6	1120.0	48.8	1120.0	48.8	104.7
COLONY CREEK-34 <>	128	42506	2.5	12.6802	1.1	2.2338	2.6	0.2054	2.4	0.90	1204.4	26.0	1191.7	18.4	1168.7	22.3	1168.7	22.3	103.1
COLONY CREEK-51 <>	24	13036	1.0	12.6508	4.5	2.2186	5.9	0.2036	3.8	0.65	1194.5	42.0	1186.9	41.5	1173.3	89.3	1173.3	89.3	101.8
COLONY CREEK-114 <>	365	280918	2.1	12.6244	0.5	2.1779	2.7	0.1994	2.6	0.98	1172.1	28.2	1174.0	18.7	1177.5	10.3	1177.5	10.3	99.5
COLONY CREEK-41 <>	182	194988	1.4	12.6237	1.0	2.1220	3.1	0.1943	2.9	0.95	1144.5	30.8	1156.0	21.3	1177.6	19.2	1177.6	19.2	97.2
COLONY CREEK-95 <>	25	13657	2.7	12.5538	5.7	2.2455	8.8	0.2044	6.6	0.76	1199.2	72.4	1195.4	61.6	1188.5	113.3	1188.5	113.3	100.9
COLONY CREEK-119 <>	56	28473	2.1	12.5428	2.6	2.2944	3.7	0.2087	2.7	0.72	1222.0	29.6	1210.6	26.1	1190.3	50.5	1190.3	50.5	102.7
COLONY CREEK-86 <>	119	63288	3.1	12.4787	0.7	2.2645	2.3	0.2049	2.2	0.95	1201.9	23.6	1201.3	15.9	1200.4	13.6	1200.4	13.6	100.1
COLONY CREEK-72 <>	573	455444	2.5	12.4566	0.5	2.2018	2.6	0.1989	2.5	0.98	1169.5	27.0	1181.6	18.0	1203.8	10.1	1203.8	10.1	97.1
COLONY CREEK-59 <>	56	35725	1.6	12.3211	2.6	2.3872	3.5	0.2133	2.4	0.68	1246.5	27.1	1238.8	25.3	1225.3	51.1	1225.3	51.1	101.7
COLONY CREEK-96	81	14879	1.9	12.1181	1.4	2.5217	1.9	0.2216	1.3	0.68	1290.5	14.7	1278.3	13.6	1257.9	26.9	1257.9	26.9	102.6
COLONY CREEK-36 <>	59	23421	2.1	12.0737	1.5	2.5033	5.1	0.2192	4.9	0.96	1277.7	56.7	1273.0	37.2	1265.1	29.3	1265.1	29.3	101.0
COLONY CREEK-101 <>	57	34924	1.8	12.0287	1.9	2.6227	3.5	0.2288	2.9	0.83	1328.2	34.9	1307.0	25.8	1272.4	38.0	1272.4	38.0	104.4
COLONY CREEK-40 <>	86	71873	1.7	11.4651	1.0	2.8404	3.8	0.2362	3.7	0.97	1366.9	45.1	1366.3	28.5	1365.4	18.5	1365.4	18.5	100.1
COLONY CREEK-117 <>	48	32750	2.5	11.4437	3.8	2.4410	4.6	0.2026	2.6	0.57	1189.3	28.6	1254.8	33.5	1369.0	73.7	1369.0	73.7	86.9
COLONY CREEK-112 <>	42	37685	1.7	11.4013	2.8	2.7597	3.8	0.2282	2.6	0.68	1325.1	30.8	1344.7	28.1	1376.1	52.9	1376.1	52.9	96.3
COLONY CREEK-78 <>	84	43245	1.6	11.2583	1.1	3.0487	3.2	0.2489	3.0	0.94	1433.0	38.3	1419.9	24.2	1400.3	20.4	1400.3	20.4	102.3
COLONY CREEK-28 <>	105	111580	1.5	10.8156	1.3	3.3063	2.9	0.2594	2.5	0.88	1486.5	33.9	1482.5	22.5	1476.8	25.6	1476.8	25.6	100.7
COLONY CREEK-29 <>	124	101125	1.3	10.7311	0.5	3.2141	2.5	0.2502	2.5	0.98	1439.3	31.7	1460.6	19.5	1491.7	10.2	1491.7	10.2	96.5
COLONY CREEK-76 <>	265	219471	1.4	10.6664	0.4	3.3996	2.8	0.2630	2.7	0.99	1505.2	36.7	1504.3	21.6	1503.1	6.7	1503.1	6.7	100.1
COLONY CREEK-111 <>	51	37606	1.8	10.3481	1.6	3.4913	3.1	0.2620	2.6	0.85	1500.2	35.1	1525.2	24.4	1560.2	30.7	1560.2	30.7	96.2
COLONY CREEK-11 <>	37	45323	0.9	9.7217	2.3	4.3350	3.0	0.3057	1.8	0.61	1719.3	27.0	1700.0	24.3	1676.4	43.3	1676.4	43.3	102.6
COLONY CREEK-66 <>	243	206816	1.1	9.3722	0.5	4.5786	2.0	0.3112	2.0	0.97	1746.7	30.3	1745.4	17.0	1743.8	8.8	1743.8	8.8	100.2
COLONY CREEK-118 <>	31	24176	2.5	8.2185	1.9	5.9519	2.9	0.3548	2.3	0.77	1957.3	38.2	1968.8	25.6	1980.9	33.7	1980.9	33.7	98.8
COLONY CREEK-97 <>	132	215634	1.3	7.8313	0.2	6.3862	3.9	0.3627	3.9	1.00	1995.1	66.5	2030.4	34.1	2066.4	3.9	2066.4	3.9	96.5

COLONY CREEK-25 <>	171	323156	1.5	7.8055	0.2	6.7580	1.0	0.3826	1.0	0.98	2088.3	18.3	2080.2	9.3	2072.2	3.7	2072.2	3.7	100.8
COLONY CREEK-77 <>	47	23861	1.3	7.3966	0.6	7.4824	3.9	0.4014	3.8	0.99	2175.5	70.5	2170.9	34.6	2166.5	10.8	2166.5	10.8	100.4
COLONY CREEK-47 <>	164	76154	1.3	7.0540	1.0	7.5069	4.9	0.3841	4.8	0.98	2095.2	85.3	2173.8	43.6	2248.9	16.7	2248.9	16.7	93.2
COLONY CREEK-38 <>	99	151279	1.1	6.0770	0.5	10.0700	3.1	0.4438	3.1	0.98	2367.8	61.4	2441.2	29.1	2503.0	9.1	2503.0	9.1	94.6
COLONY CREEK-90 <>	100	168458	4.3	5.6954	0.5	11.4549	1.2	0.4732	1.2	0.93	2497.4	24.0	2560.9	11.6	2611.5	7.5	2611.5	7.5	95.6
COLONY CREEK-52 <>	32	39919	1.1	5.4379	0.6	12.9668	4.4	0.5114	4.4	0.99	2662.6	96.1	2677.2	41.9	2688.3	9.5	2688.3	9.5	99.0
COLONY CREEK-8 <>	196	23607	1.8	4.9227	0.4	14.2300	2.2	0.5080	2.2	0.98	2648.3	46.7	2765.2	20.8	2851.6	6.7	2851.6	6.7	92.9
COLONY CREEK-46 <>	62	101328	1.7	4.3731	0.5	18.7843	2.4	0.5958	2.3	0.98	3012.8	56.4	3030.8	23.2	3042.7	8.5	3042.7	8.5	99.0

Appendix B

Zircon U-Pb geochronological data for the Midland Basin

						Isotope ratios					Apparent ages (Ma)								
Analysis	U	^{206}Pb	U/Th	$^{206}Pb^*$	±	$^{207}Pb^*$	±	$^{206}Pb^*$	±	error	$^{206}Pb^*$	±	$^{207}Pb^*$	±	$^{206}Pb^*$	±	Best age	±	Conc.
	(ppm)	^{204}Pb		$^{207}Pb^*$	(%)	$^{235}U^*$	(%)	^{238}U	(%)	corr.	$^{238}U^*$	(Ma)	^{235}U	(Ma)	$^{207}Pb^*$	(Ma)	(Ma)	(Ma)	(%)
Cambrian sandstone, sample 1 (Late Middle Cambrian)																			
CORE_1_1	71	-2508	0.5	0.0912	0.0027	3.1590	0.110	0.2504	0.0045	0.264	1441.0	23.0	1437.0	27.0	1416.0	57.0	1416.0	57.0	101.8
CORE_1_3	190	799	0.5	0.0897	0.0027	2.6410	0.097	0.2143	0.0043	0.484	1251.0	23.0	1310.0	28.0	1399.0	60.0	1399.0	60.0	89.4
CORE_1_5	112	1947	0.8	0.0866	0.0024	2.1900	0.069	0.1846	0.0035	0.242	1091.0	19.0	1173.0	22.0	1324.0	56.0	1324.0	56.0	82.4
CORE_1_11	193	6182	0.5	0.0964	0.0032	2.9730	0.120	0.2232	0.0047	0.500	1298.0	25.0	1391.0	30.0	1523.0	61.0	1523.0	61.0	85.2
CORE_1_12	41	-307	1.2	0.0967	0.0044	2.8900	0.140	0.2178	0.0057	0.174	1268.0	30.0	1365.0	35.0	1496.0	91.0	1496.0	91.0	84.8
CORE_1_13	66	-790	0.5	0.0873	0.0024	2.8340	0.088	0.2353	0.0042	0.189	1361.0	22.0	1357.0	23.0	1333.0	53.0	1333.0	53.0	102.1
CORE_1_14	159	-13575	0.5	0.0878	0.0028	2.5550	0.098	0.2134	0.0051	0.512	1246.0	27.0	1285.0	27.0	1368.0	59.0	1368.0	59.0	91.1
CORE_1_15	73	-13985	0.4	0.0910	0.0025	2.7400	0.091	0.2183	0.0041	0.428	1272.0	22.0	1331.0	24.0	1429.0	52.0	1429.0	52.0	89.0
CORE_1_18	129	1082	0.8	0.0926	0.0039	2.5120	0.110	0.1980	0.0055	0.363	1163.0	29.0	1273.0	30.0	1453.0	81.0	1453.0	81.0	80.0
CORE_1_19	259	-5078	0.5	0.0885	0.0026	2.6600	0.090	0.2187	0.0051	0.397	1274.0	27.0	1318.0	26.0	1379.0	57.0	1379.0	57.0	92.4
CORE_1_20	100	12600	0.5	0.0900	0.0030	2.8430	0.110	0.2286	0.0051	0.344	1326.0	27.0	1359.0	29.0	1399.0	67.0	1399.0	67.0	94.8
CORE_1_21	138	3053	1.0	0.0903	0.0023	2.3800	0.077	0.1911	0.0037	0.511	1127.0	20.0	1231.0	23.0	1412.0	51.0	1412.0	51.0	79.8
CORE_1_23	48	576	0.5	0.0864	0.0039	2.6800	0.140	0.2254	0.0056	0.324	1309.0	29.0	1307.0	37.0	1276.0	94.0	1276.0	94.0	102.6
CORE_1_26	104	1902	0.4	0.0776	0.0028	2.0030	0.079	0.1870	0.0038	0.253	1105.0	21.0	1112.0	27.0	1100.0	74.0	1100.0	74.0	100.5
CORE_1_27	115	3891	0.3	0.0968	0.0034	3.0990	0.120	0.2316	0.0051	0.294	1342.0	26.0	1425.0	29.0	1533.0	64.0	1533.0	64.0	87.5
CORE_1_28	140	-5210	0.7	0.0900	0.0027	2.7900	0.095	0.2254	0.0046	0.359	1310.0	24.0	1350.0	26.0	1400.0	58.0	1400.0	58.0	93.6
CORE_1_31	90	36400	0.5	0.0873	0.0023	2.7940	0.086	0.2312	0.0041	0.232	1340.0	22.0	1348.0	23.0	1346.0	52.0	1346.0	52.0	99.6
CORE_1_33	59	1237	0.3	0.0895	0.0026	3.0490	0.100	0.2455	0.0044	0.331	1414.0	23.0	1410.0	26.0	1387.0	56.0	1387.0	56.0	101.9
CORE_1_36	160	-1767	0.5	0.0884	0.0021	2.8110	0.081	0.2302	0.0039	0.516	1335.0	20.0	1354.0	22.0	1373.0	47.0	1373.0	47.0	97.2
CORE_1_44	184	-2268	1.0	0.0893	0.0025	2.8390	0.090	0.2310	0.0044	0.280	1339.0	23.0	1363.0	24.0	1388.0	54.0	1388.0	54.0	96.5
CORE_1_45	269	1009	0.5	0.0917	0.0029	2.6430	0.087	0.2095	0.0045	0.263	1225.0	24.0	1309.0	24.0	1446.0	56.0	1446.0	56.0	84.7
CORE_1_48	317	1013	0.5	0.0933	0.0040	2.6800	0.130	0.2067	0.0061	0.531	1210.0	33.0	1318.0	37.0	1473.0	81.0	1473.0	81.0	82.1
CORE_1_50	115	1185	0.5	0.0892	0.0027	2.8970	0.100	0.2359	0.0045	0.401	1368.0	25.0	1377.0	27.0	1377.0	59.0	1377.0	59.0	99.3
CORE_1_51	324	723	0.8	0.1018	0.0030	3.1610	0.110	0.2249	0.0047	0.438	1309.0	24.0	1439.0	27.0	1628.0	55.0	1628.0	55.0	80.4

CORE_1_52	201	-2747	0.6	0.0897	0.0027	3.0090	0.110	0.2434	0.0053	0.370	1403.0	27.0	1405.0	27.0	1405.0	57.0	1405.0	57.0	99.9
CORE_1_53	206	1858	0.8	0.0914	0.0025	2.5210	0.082	0.1995	0.0040	0.418	1172.0	22.0	1273.0	24.0	1443.0	54.0	1443.0	54.0	81.2
CORE_1_54	128	1435	0.4	0.0890	0.0029	2.8690	0.100	0.2351	0.0048	0.234	1360.0	25.0	1367.0	27.0	1362.0	63.0	1362.0	63.0	99.9
CORE_1_55	105	1052	0.5	0.0884	0.0025	2.8270	0.092	0.2337	0.0046	0.353	1353.0	24.0	1362.0	25.0	1371.0	54.0	1371.0	54.0	98.7
CORE_1_57	88	717	0.5	0.0816	0.0033	1.9520	0.084	0.1743	0.0042	0.283	1037.0	22.0	1088.0	29.0	1170.0	80.0	1170.0	80.0	88.6
CORE_1_58	921	11879	0.4	0.0863	0.0019	2.7700	0.078	0.2313	0.0041	0.528	1341.0	21.0	1345.0	21.0	1346.0	43.0	1346.0	43.0	99.6
CORE_1_59	107	-4456	0.4	0.0878	0.0023	3.0070	0.095	0.2480	0.0046	0.388	1427.0	24.0	1403.0	24.0	1348.0	52.0	1348.0	52.0	105.9
CORE_1_60	128	-8420	0.3	0.0857	0.0022	2.6870	0.082	0.2260	0.0039	0.326	1312.0	21.0	1319.0	23.0	1308.0	50.0	1308.0	50.0	100.3
CORE_1_62	131	-4056	0.5	0.0877	0.0034	2.5970	0.110	0.2137	0.0057	0.338	1247.0	30.0	1294.0	31.0	1350.0	75.0	1350.0	75.0	92.4
CORE_1_64	204	6900	0.8	0.0948	0.0029	2.6600	0.099	0.2049	0.0053	0.545	1200.0	28.0	1316.0	28.0	1500.0	58.0	1500.0	58.0	80.0
CORE_1_65	78	-1091	0.5	0.0811	0.0023	2.4040	0.079	0.2145	0.0038	0.226	1252.0	20.0	1238.0	23.0	1184.0	57.0	1184.0	57.0	105.7
CORE_1_68	120	-1719	0.5	0.0815	0.0024	2.4610	0.084	0.2181	0.0041	0.266	1271.0	21.0	1256.0	25.0	1207.0	60.0	1207.0	60.0	105.3
CORE_1_69	237	2110	0.7	0.0853	0.0033	2.3310	0.097	0.1990	0.0045	0.343	1169.0	24.0	1217.0	29.0	1293.0	75.0	1293.0	75.0	90.4
CORE_1_70	117	2574	0.5	0.0867	0.0026	2.6960	0.092	0.2259	0.0049	0.360	1314.0	25.0	1321.0	25.0	1336.0	58.0	1336.0	58.0	98.4
CORE_1_71	41	975	0.8	0.0890	0.0030	2.9480	0.110	0.2401	0.0049	0.234	1385.0	25.0	1386.0	28.0	1359.0	67.0	1359.0	67.0	101.9
CORE_1_72	308	8227	0.3	0.0849	0.0023	2.3630	0.076	0.2015	0.0040	0.393	1183.0	21.0	1228.0	23.0	1301.0	52.0	1301.0	52.0	90.9
CORE_1_73	82	-2885	0.5	0.0884	0.0025	2.8190	0.091	0.2303	0.0041	0.206	1335.0	21.0	1354.0	25.0	1364.0	54.0	1364.0	54.0	97.9
CORE_1_74	240	1613	0.5	0.0916	0.0024	3.0020	0.094	0.2377	0.0046	0.354	1374.0	24.0	1403.0	24.0	1444.0	53.0	1444.0	53.0	95.2
CORE_1_76	244	-7443	0.4	0.0876	0.0020	2.7420	0.078	0.2265	0.0039	0.489	1315.0	20.0	1337.0	21.0	1363.0	42.0	1363.0	42.0	96.5
Pennsylvanian sandstone, sample 2 (Late Pennsylvanian)																			
CORE_3_1	738	-14250	0.1	0.0603	0.0014	0.7840	0.016	0.0943	0.0018	0.368	581.0	11.0	587.3	8.9	591.0	51.0	581.0	11.0	98.3
CORE_3_2	388	6083	0.2	0.0778	0.0020	1.8650	0.049	0.1743	0.0039	0.490	1035.0	21.0	1065.0	17.0	1122.0	52.0	1122.0	52.0	92.2
CORE_3_4	149	2290	0.3	0.0787	0.0025	1.9660	0.060	0.1809	0.0036	0.225	1071.0	20.0	1095.0	20.0	1126.0	65.0	1126.0	65.0	95.1
CORE_3_5	573	-14407	0.5	0.1231	0.0026	5.7600	0.120	0.3409	0.0070	0.595	1890.0	33.0	1939.0	17.0	1994.0	38.0	1994.0	38.0	94.8
CORE_3_6	285	-10331	0.5	0.1643	0.0036	9.5100	0.210	0.4180	0.0089	0.594	2250.0	41.0	2383.0	21.0	2492.0	36.0	2492.0	36.0	90.3
CORE_3_7	379	-4810	0.6	0.0897	0.0018	2.7710	0.052	0.2234	0.0045	0.570	1299.0	24.0	1343.0	14.0	1404.0	38.0	1404.0	38.0	92.5
CORE_3_8	237	-6125	0.4	0.0879	0.0035	2.2180	0.092	0.1840	0.0062	0.494	1087.0	34.0	1181.0	31.0	1337.0	78.0	1337.0	78.0	81.3
CORE_3_9	186	52850	0.8	0.1908	0.0040	11.6000	0.220	0.4361	0.0090	0.488	2334.0	41.0	2567.0	18.0	2739.0	35.0	2739.0	35.0	85.2
CORE_3_11	213	-4618	0.6	0.1145	0.0022	4.7810	0.078	0.2995	0.0053	0.485	1688.0	26.0	1776.0	14.0	1862.0	35.0	1862.0	35.0	90.7

CORE_3_13	547	-25700	0.1	0.1161	0.0021	4.8150	0.068	0.2979	0.0055	0.500	1680.0	27.0	1787.0	11.0	1892.0	33.0	1892.0	33.0	88.8
CORE_3_14	590	-3392	0.1	0.0784	0.0018	1.9180	0.038	0.1771	0.0036	0.428	1053.0	20.0	1087.0	14.0	1146.0	48.0	1146.0	48.0	91.9
CORE_3_16	777	-6060	0.3	0.0733	0.0017	1.6610	0.036	0.1636	0.0032	0.452	977.0	18.0	992.0	14.0	1004.0	48.0	1004.0	48.0	97.3
CORE_3_17	607	25800	0.3	0.0791	0.0018	1.9410	0.039	0.1765	0.0034	0.398	1047.0	19.0	1093.0	13.0	1168.0	44.0	1168.0	44.0	89.6
CORE_3_19	341	-3556	0.2	0.0923	0.0021	2.9920	0.067	0.2332	0.0050	0.616	1350.0	26.0	1403.0	17.0	1468.0	40.0	1468.0	40.0	92.0
CORE_3_21	217	-4280	0.2	0.0991	0.0029	3.4900	0.110	0.2546	0.0071	0.560	1460.0	36.0	1517.0	25.0	1594.0	54.0	1594.0	54.0	91.6
CORE_3_22	109	2223	0.3	0.0725	0.0021	1.5790	0.044	0.1567	0.0032	0.357	939.0	18.0	955.0	18.0	960.0	60.0	960.0	60.0	97.8
CORE_3_23	951	-4522	1.1	0.0615	0.0012	0.8490	0.013	0.0993	0.0017	0.496	610.2	10.0	623.1	7.5	642.0	41.0	610.2	10.0	95.0
CORE_3_24	158	-814	0.6	0.0729	0.0022	1.5130	0.044	0.1513	0.0032	0.397	908.0	18.0	930.0	18.0	960.0	63.0	960.0	63.0	94.6
CORE_3_25	745	-18080	0.3	0.0597	0.0012	0.7690	0.012	0.0930	0.0016	0.378	573.3	9.5	577.5	7.1	571.0	43.0	573.3	9.5	100.4
CORE_3_26	139	-1494	0.7	0.1073	0.0026	3.9310	0.100	0.2657	0.0063	0.629	1516.0	32.0	1618.0	21.0	1732.0	45.0	1732.0	45.0	87.5
CORE_3_27	477	-18407	0.5	0.0624	0.0021	0.8180	0.030	0.0955	0.0025	0.479	588.0	14.0	604.0	17.0	653.0	73.0	588.0	14.0	90.0
CORE_3_29	1498	3333	0.2	0.0578	0.0013	0.6270	0.014	0.0789	0.0016	0.561	489.7	9.4	493.2	8.4	504.0	49.0	489.7	9.4	97.2
CORE_3_31	657	71867	1.2	0.0994	0.0021	3.5490	0.073	0.2605	0.0050	0.530	1492.0	25.0	1534.0	16.0	1602.0	41.0	1602.0	41.0	93.1
CORE_3_32	574	3483	0.3	0.0874	0.0028	2.3920	0.082	0.2001	0.0048	0.526	1179.0	27.0	1235.0	24.0	1351.0	61.0	1351.0	61.0	87.3
CORE_3_34	469	2468	0.3	0.0652	0.0022	0.9300	0.030	0.1042	0.0027	0.365	639.0	16.0	664.0	16.0	752.0	73.0	639.0	16.0	85.0
CORE_3_36	194	10820	0.4	0.0799	0.0027	1.8900	0.062	0.1747	0.0044	0.434	1037.0	24.0	1075.0	23.0	1164.0	69.0	1164.0	69.0	89.1
CORE_3_37	214	-4121	0.3	0.0676	0.0026	1.0890	0.042	0.1191	0.0027	0.249	725.0	16.0	742.0	20.0	809.0	86.0	752.0	16.0	89.6
CORE_3_38	177	-1406	0.4	0.0755	0.0017	1.8870	0.039	0.1829	0.0036	0.486	1082.0	19.0	1072.0	14.0	1064.0	44.0	1064.0	44.0	101.7
CORE_3_39	238	-3580	0.4	0.0640	0.0017	0.9570	0.025	0.1097	0.0020	0.557	670.7	12.0	676.0	12.0	693.0	56.0	670.7	12.0	96.8
CORE_3_40	497	-3544	0.4	0.0593	0.0015	0.6580	0.016	0.0810	0.0018	0.498	501.5	11.0	511.4	9.6	555.0	54.0	501.5	11.0	90.4
CORE_3_42	191	-6667	0.4	0.0857	0.0020	2.4410	0.057	0.2080	0.0043	0.538	1217.0	23.0	1250.0	17.0	1310.0	46.0	1310.0	46.0	92.9
CORE_3_44	567	-11684	0.6	0.1035	0.0020	4.1140	0.070	0.2923	0.0056	0.471	1652.0	28.0	1655.0	14.0	1679.0	37.0	1679.0	37.0	98.4
CORE_3_47	359	-7300	0.2	0.0772	0.0020	1.7410	0.046	0.1645	0.0035	0.479	981.0	19.0	1022.0	17.0	1116.0	52.0	1116.0	52.0	87.9
CORE_3_48	168	-983	0.4	0.0720	0.0026	1.4740	0.056	0.1498	0.0041	0.454	899.0	23.0	912.0	23.0	947.0	77.0	947.0	77.0	94.9
CORE_3_49	128	914	0.3	0.0752	0.0032	1.6140	0.072	0.1556	0.0037	0.336	932.0	21.0	966.0	28.0	1029.0	90.0	1029.0	90.0	90.6
CORE_3_50	195	549	1.0	0.0586	0.0024	0.6170	0.025	0.0771	0.0018	0.288	478.4	11.0	481.0	15.0	461.0	86.0	478.4	11.0	103.8
CORE_3_51	265	5108	0.5	0.0727	0.0018	1.6240	0.035	0.1620	0.0029	0.153	967.9	16.0	976.0	14.0	985.0	52.0	985.0	52.0	98.3
CORE_3_52	78	3976	0.6	0.0807	0.0034	2.0150	0.080	0.1822	0.0045	0.213	1078.0	24.0	1107.0	27.0	1132.0	89.0	1132.0	89.0	95.2
CORE_3_53	206	7217	0.5	0.0836	0.0017	2.4990	0.043	0.2157	0.0038	0.382	1259.0	20.0	1267.0	12.0	1270.0	39.0	1270.0	39.0	99.1

CORE_3_54	128	-1279	0.5	0.0884	0.0029	2.5110	0.073	0.2065	0.0043	0.207	1209.0	23.0	1269.0	22.0	1349.0	64.0	1349.0	64.0	89.6
CORE_3_55	221	1840	0.2	0.0657	0.0021	1.0710	0.029	0.1181	0.0024	0.192	719.4	14.0	735.0	15.0	751.0	68.0	719.4	14.0	95.8
CORE_3_56	244	7467	0.5	0.0806	0.0025	2.2230	0.070	0.1995	0.0046	0.428	1172.0	25.0	1181.0	23.0	1186.0	62.0	1186.0	62.0	98.8
CORE_3_57	241	13322	0.3	0.1262	0.0026	6.2500	0.120	0.3579	0.0069	0.494	1971.0	33.0	2009.0	17.0	2039.0	36.0	2039.0	36.0	96.7
CORE_3_58	616	-19850	0.3	0.0736	0.0017	1.8090	0.036	0.1764	0.0033	0.333	1047.0	18.0	1046.0	13.0	1015.0	47.0	1015.0	47.0	103.2
CORE_3_60	62	1515	0.5	0.0828	0.0030	2.1690	0.076	0.1898	0.0045	0.334	1119.0	24.0	1160.0	25.0	1200.0	74.0	1200.0	74.0	93.3
CORE_3_62	129	1103	0.9	0.0647	0.0032	0.9010	0.049	0.0999	0.0034	0.515	613.0	20.0	640.0	27.0	670.0	110.0	613.0	20.0	91.5
CORE_3_63	491	3271	0.2	0.0628	0.0015	0.8340	0.020	0.0952	0.0018	0.519	585.9	10.0	613.0	11.0	674.0	52.0	585.9	10.0	86.9
CORE_3_64	347	2517	0.3	0.1177	0.0026	5.1100	0.110	0.3112	0.0066	0.505	1745.0	32.0	1836.0	19.0	1918.0	42.0	1918.0	42.0	91.0
CORE_3_67	175	4262	0.7	0.1017	0.0040	3.1220	0.098	0.2253	0.0086	0.267	1308.0	45.0	1434.0	25.0	1633.0	70.0	1633.0	70.0	80.1
CORE_3_70	76	-2050	0.5	0.0902	0.0027	2.7190	0.082	0.2189	0.0049	0.299	1274.0	26.0	1317.0	22.0	1366.0	59.0	1366.0	59.0	93.3
CORE_3_72	334	-1354	0.4	0.0632	0.0019	0.8520	0.024	0.0990	0.0019	0.309	608.5	11.0	622.0	13.0	674.0	63.0	608.5	11.0	90.3
CORE_3_73	236	2263	0.3	0.1026	0.0022	3.3420	0.074	0.2383	0.0050	0.606	1377.0	26.0	1485.0	17.0	1658.0	40.0	1658.0	40.0	83.1
CORE_3_74	72	-1422	0.4	0.0893	0.0025	2.7970	0.072	0.2323	0.0050	0.404	1345.0	26.0	1348.0	20.0	1383.0	53.0	1383.0	53.0	97.3
CORE_3_75	254	-7178	0.3	0.0808	0.0023	1.8100	0.049	0.1682	0.0035	0.323	1002.0	19.0	1045.0	18.0	1194.0	59.0	1194.0	59.0	83.9
CORE_3_76	52	-861	0.4	0.0769	0.0037	1.6990	0.082	0.1664	0.0040	0.309	991.0	22.0	992.0	32.0	1020.0	110.0	1020.0	110.0	97.2
CORE_3_77	343	4300	0.5	0.0754	0.0019	1.6280	0.039	0.1632	0.0032	0.386	974.0	17.0	979.0	15.0	1063.0	53.0	1063.0	53.0	91.6
CORE_3_78	95	-3124	0.7	0.1135	0.0027	4.9700	0.130	0.3310	0.0074	0.630	1841.0	36.0	1808.0	22.0	1839.0	44.0	1839.0	44.0	100.1
CORE_3_79	412	-5264	0.2	0.0633	0.0019	0.7680	0.022	0.0926	0.0019	0.307	570.6	11.0	576.0	12.0	698.0	63.0	570.6	11.0	81.7
CORE_3_80	273	2114	0.3	0.0778	0.0017	1.8460	0.034	0.1815	0.0034	0.431	1075.0	19.0	1061.0	12.0	1131.0	42.0	1131.0	42.0	95.0
CORE_3_81	308	27150	0.3	0.0883	0.0020	2.6840	0.066	0.2342	0.0051	0.663	1356.0	27.0	1323.0	18.0	1382.0	44.0	1382.0	44.0	98.1
CORE_3_1	357	977	0.3	0.0831	0.0024	2.1200	0.071	0.1869	0.0035	0.342	1104.0	19.0	1153.0	24.0	1252.0	56.0	1252.0	56.0	88.2
CORE_3_2	466	3294	0.7	0.0646	0.0022	0.8530	0.035	0.0959	0.0023	0.396	590.0	13.0	626.0	19.0	729.0	78.0	590.0	13.0	80.9
CORE_3_5	548	27550	0.7	0.1275	0.0032	5.7900	0.190	0.3300	0.0070	0.641	1837.0	34.0	1943.0	27.0	2059.0	42.0	2059.0	42.0	89.2
CORE_3_6	131	13693	1.5	0.1052	0.0034	3.6900	0.140	0.2557	0.0063	0.396	1466.0	32.0	1564.0	30.0	1697.0	61.0	1697.0	61.0	86.4
CORE_3_8	141	1132	0.7	0.1403	0.0035	6.4100	0.190	0.3327	0.0072	0.485	1849.0	35.0	2027.0	27.0	2218.0	43.0	2218.0	43.0	83.4
CORE_3_9	123	54690	0.6	0.1237	0.0033	5.5600	0.180	0.3256	0.0066	0.464	1818.0	33.0	1904.0	28.0	2000.0	46.0	2000.0	46.0	90.9
CORE_3_10	180	2139	0.8	0.0799	0.0026	1.8700	0.069	0.1710	0.0037	0.361	1017.0	21.0	1069.0	25.0	1167.0	67.0	1167.0	67.0	87.1
CORE_3_11	33	315	0.7	0.0793	0.0047	1.5890	0.097	0.1486	0.0041	0.283	891.0	23.0	930.0	40.0	920.0	130.0	920.0	130.0	96.8
CORE_3_12	214	12230	0.5	0.0897	0.0024	2.8110	0.090	0.2283	0.0046	0.359	1324.0	24.0	1353.0	24.0	1397.0	53.0	1397.0	53.0	94.8

CORE_3_13	346	4194	1.5	0.0696	0.0017	1.4220	0.043	0.1480	0.0025	0.311	889.5	14.0	894.0	18.0	889.0	51.0	894.0	18.0	100.1
CORE_3_14	823	-28636	0.4	0.1087	0.0025	4.6190	0.140	0.3088	0.0063	0.655	1733.0	31.0	1749.0	25.0	1768.0	42.0	1768.0	42.0	98.0
CORE_3_15	189	-7580	0.4	0.1153	0.0029	5.0300	0.170	0.3179	0.0075	0.708	1776.0	37.0	1819.0	29.0	1873.0	44.0	1873.0	44.0	94.8
CORE3_1	536	71600	3.5	0.0628	0.0014	0.8134	0.022	0.0940	0.0024	0.635	579.0	14.4	604.7	12.0	683.0	47.0	579.0	14.4	84.8
CORE3_2	90	19955	2.9	0.0816	0.0025	2.1260	0.062	0.1918	0.0039	0.346	1130.0	21.0	1151.0	20.0	1195.0	62.0	1130.0	21.0	94.6
CORE3_3	99	11708	1.9	0.0743	0.0020	1.5970	0.044	0.1592	0.0035	0.446	954.0	20.0	966.0	17.0	1017.0	56.0	954.0	20.0	93.8
CORE3_4	381	83710	0.8	0.0605	0.0014	0.6720	0.019	0.0816	0.0020	0.608	505.0	12.0	520.0	11.0	596.0	51.0	505.0	12.0	84.7
CORE3_5	331	27306	1.3	0.0771	0.0013	1.9040	0.043	0.1817	0.0039	0.706	1075.0	21.0	1077.0	15.0	1112.0	34.0	1075.0	21.0	96.7
CORE3_6	231	117744	1.5	0.0934	0.0020	3.4270	0.084	0.2723	0.0062	0.560	1551.0	31.0	1507.0	19.0	1491.0	40.0	1491.0	40.0	104.0
CORE3_7	108	3434	0.7	0.1849	0.0040	12.5600	0.340	0.4970	0.0140	0.706	2596.0	59.0	2641.0	25.0	2687.0	36.0	2687.0	36.0	96.6
CORE3_8	636	26004	7.6	0.0619	0.0011	0.8750	0.017	0.1043	0.0018	0.464	639.0	10.0	637.4	9.2	655.0	40.0	639.0	10.0	97.6
CORE3_10	253	22320	0.5	0.1087	0.0017	5.0030	0.091	0.3353	0.0062	0.611	1862.0	30.0	1816.0	16.0	1772.0	30.0	1772.0	30.0	105.1
CORE3_11	466	21726	2.0	0.1281	0.0017	6.5200	0.110	0.3724	0.0065	0.711	2037.0	31.0	2044.0	15.0	2066.0	24.0	2066.0	24.0	98.6
CORE3_12	469	71600	1.0	0.0578	0.0013	0.5650	0.014	0.0717	0.0014	0.538	446.3	8.5	453.3	9.3	494.0	49.0	446.3	8.5	90.3
CORE3_13	292	19955	3.7	0.0617	0.0014	0.8630	0.019	0.1033	0.0018	0.420	634.0	11.0	630.0	10.0	628.0	48.0	634.0	11.0	101.0
CORE3_15	75	83710	1.2	0.0780	0.0018	1.9610	0.051	0.1850	0.0033	0.468	1093.0	18.0	1096.0	17.0	1119.0	47.0	1093.0	18.0	97.7
CORE3_16	155	27306	0.6	0.1165	0.0017	5.4650	0.098	0.3429	0.0058	0.608	1898.0	28.0	1890.0	15.0	1896.0	26.0	1896.0	26.0	100.1
CORE3_17	283	117744	1.0	0.0748	0.0013	1.7810	0.035	0.1734	0.0031	0.602	1030.0	17.0	1035.0	13.0	1045.0	35.0	1030.0	17.0	98.6
CORE3_18	78	3434	1.7	0.0900	0.0022	3.1970	0.088	0.2599	0.0051	0.461	1487.0	26.0	1447.0	21.0	1422.0	50.0	1422.0	50.0	104.6
CORE3_19	78	26004	1.5	0.1110	0.0022	4.9900	0.100	0.3287	0.0060	0.537	1830.0	29.0	1815.0	17.0	1799.0	36.0	1799.0	36.0	101.7
CORE3_20	97	2019	0.6	0.1809	0.0029	12.8100	0.260	0.5140	0.0120	0.694	2669.0	49.0	2662.0	19.0	2655.0	27.0	2655.0	27.0	100.5
CORE3_21	105	22320	1.2	0.1817	0.0028	12.5400	0.210	0.5034	0.0086	0.605	2624.0	37.0	2641.0	16.0	2660.0	25.0	2660.0	25.0	98.6
CORE3_22	343	21726	4.5	0.0767	0.0011	1.9990	0.034	0.1900	0.0031	0.596	1120.0	17.0	1112.0	11.0	1106.0	30.0	1120.0	17.0	101.3
CORE3_23	264	71600	0.9	0.0547	0.0018	0.3970	0.014	0.0530	0.0009	0.323	332.8	5.3	338.0	10.0	363.0	74.0	332.8	5.3	91.7
CORE3_24	399	19955	1.3	0.0637	0.0013	1.0280	0.023	0.1175	0.0021	0.527	717.0	13.0	717.0	12.0	711.0	44.0	717.0	13.0	100.8
CORE3_25	142	11708	1.0	0.0616	0.0026	0.6490	0.029	0.0774	0.0019	0.397	480.0	11.0	504.0	18.0	594.0	93.0	480.0	11.0	80.8
CORE3_26	254	83710	2.5	0.0783	0.0015	2.1510	0.044	0.2006	0.0033	0.461	1178.0	18.0	1162.0	14.0	1135.0	39.0	1178.0	18.0	103.8
CORE3_27	82	27306	0.9	0.0870	0.0017	2.8810	0.066	0.2395	0.0043	0.506	1382.0	23.0	1372.0	18.0	1350.0	40.0	1350.0	40.0	102.4
CORE3_28	353	117744	1.5	0.0743	0.0014	1.8540	0.041	0.1798	0.0039	0.703	1065.0	21.0	1062.0	14.0	1035.0	37.0	1065.0	21.0	102.9
CORE3_29	182	3434	1.4	0.0766	0.0015	2.0120	0.045	0.1903	0.0033	0.560	1124.0	18.0	1116.0	15.0	1087.0	40.0	1124.0	18.0	103.4

CORE3_30	436	26004	2.0	0.0756	0.0013	1.9470	0.038	0.1868	0.0040	0.672	1105.0	22.0	1094.0	13.0	1074.0	33.0	1105.0	22.0	102.9
CORE3_31	499	2019	10.2	0.0630	0.0014	1.0100	0.027	0.1167	0.0022	0.623	711.0	13.0	706.0	13.0	691.0	49.0	711.0	13.0	102.9
CORE3_33	50	21726	1.1	0.0745	0.0028	1.7650	0.069	0.1722	0.0037	0.332	1023.0	20.0	1021.0	26.0	981.0	80.0	1023.0	20.0	104.3
CORE3_34	347	71600	1.8	0.0741	0.0013	1.8590	0.041	0.1823	0.0040	0.687	1078.0	22.0	1062.0	15.0	1024.0	36.0	1078.0	22.0	105.3
CORE3_35	124	19955	1.3	0.0662	0.0025	0.9720	0.042	0.1074	0.0026	0.527	657.0	15.0	685.0	22.0	779.0	75.0	657.0	15.0	84.3
CORE3_36	249	11708	1.9	0.0783	0.0015	2.1290	0.048	0.1981	0.0046	0.693	1164.0	25.0	1157.0	16.0	1138.0	39.0	1164.0	25.0	102.3
CORE3_37	225	83710	1.2	0.1097	0.0019	5.1800	0.120	0.3387	0.0079	0.703	1879.0	38.0	1847.0	19.0	1788.0	32.0	1788.0	32.0	105.1
CORE3_38	237	27306	0.4	0.0605	0.0021	0.6730	0.027	0.0798	0.0024	0.542	495.0	14.0	520.0	16.0	595.0	78.0	495.0	14.0	83.2
CORE3_39	416	117744	1.2	0.0750	0.0017	1.6070	0.045	0.1535	0.0036	0.617	920.0	20.0	969.0	17.0	1059.0	46.0	920.0	20.0	86.9
CORE3_40	229	3434	2.0	0.0745	0.0016	1.7620	0.036	0.1729	0.0031	0.439	1027.0	17.0	1028.0	13.0	1038.0	41.0	1027.0	17.0	98.9
CORE3_41	1297	26004	5.8	0.0794	0.0015	2.2880	0.050	0.2086	0.0045	0.652	1220.0	24.0	1206.0	15.0	1170.0	38.0	1220.0	24.0	104.3
CORE3_42	478	2019	1.0	0.0622	0.0012	0.9240	0.018	0.1075	0.0017	0.482	658.0	10.0	662.6	9.5	657.0	40.0	658.0	10.0	100.2
CORE3_43	221	22320	1.0	0.1005	0.0016	3.9580	0.071	0.2839	0.0049	0.653	1609.0	24.0	1622.0	15.0	1622.0	29.0	1622.0	29.0	99.2
CORE3_45	352	71600	4.6	0.0770	0.0013	2.1140	0.044	0.1981	0.0040	0.654	1164.0	21.0	1151.0	15.0	1109.0	34.0	1164.0	21.0	105.0
CORE3_46	288	19955	2.1	0.0760	0.0016	1.9820	0.050	0.1899	0.0044	0.604	1120.0	24.0	1105.0	17.0	1077.0	43.0	1120.0	24.0	104.0
CORE3_47	345	11708	1.3	0.0586	0.0016	0.6450	0.019	0.0795	0.0018	0.495	494.0	11.0	504.0	12.0	514.0	58.0	494.0	11.0	96.1
CORE3_49	91	27306	1.3	0.0814	0.0021	2.4030	0.063	0.2144	0.0039	0.425	1251.0	21.0	1240.0	20.0	1192.0	51.0	1192.0	51.0	104.9
CORE3_50	1309	117744	1.9	0.0596	0.0010	0.6970	0.013	0.0851	0.0015	0.594	527.7	9.2	536.7	8.2	572.0	37.0	527.7	9.2	92.3
CORE3_51	638	3434	1.3	0.0600	0.0013	0.7560	0.015	0.0915	0.0016	0.316	563.8	9.2	570.2	8.8	575.0	45.0	563.8	9.2	98.1
CORE3_52	454	26004	5.0	0.0779	0.0011	2.1290	0.036	0.1973	0.0031	0.579	1162.0	17.0	1156.0	12.0	1137.0	29.0	1162.0	17.0	102.2
CORE3_53	374	2019	1.2	0.0570	0.0014	0.5940	0.016	0.0751	0.0016	0.489	466.6	9.5	471.0	10.0	458.0	54.0	466.6	9.5	101.9
CORE3_54	635	22320	5.3	0.0957	0.0012	3.6220	0.064	0.2730	0.0054	0.729	1557.0	27.0	1552.0	14.0	1533.0	25.0	1533.0	25.0	101.6
CORE3_55	369	21726	2.5	0.0786	0.0013	2.1240	0.035	0.1959	0.0030	0.556	1152.0	16.0	1155.0	12.0	1149.0	32.0	1152.0	16.0	100.3
CORE3_56	43	71600	0.7	0.0949	0.0032	3.1200	0.100	0.2392	0.0049	0.318	1384.0	26.0	1431.0	26.0	1481.0	64.0	1481.0	64.0	93.5
CORE3_57	1028	19955	2.0	0.0736	0.0008	1.7870	0.027	0.1752	0.0026	0.715	1040.0	14.0	1038.6	9.8	1027.0	22.0	1040.0	14.0	101.3
CORE3_58	347	11708	0.9	0.0732	0.0012	1.7120	0.029	0.1691	0.0024	0.467	1006.0	13.0	1011.0	11.0	1005.0	33.0	1006.0	13.0	100.1
CORE3_59	494	83710	2.2	0.0790	0.0011	2.2230	0.036	0.2022	0.0030	0.571	1186.0	16.0	1187.0	11.0	1167.0	30.0	1186.0	16.0	101.6
CORE3_60	250	27306	0.7	0.0593	0.0016	0.6800	0.018	0.0831	0.0013	0.233	514.6	7.6	526.0	11.0	556.0	57.0	514.6	7.6	92.6
CORE3_61	331	117744	1.0	0.0587	0.0012	0.6820	0.015	0.0840	0.0011	0.418	519.9	6.6	525.9	9.4	543.0	49.0	519.9	6.6	95.7
CORE3_62	88	3434	2.0	0.2067	0.0027	15.8900	0.250	0.5540	0.0087	0.642	2837.0	36.0	2867.0	15.0	2875.0	21.0	2875.0	21.0	98.7

CORE3_64	63	2019	1.8	0.0636	0.0031	0.8880	0.043	0.1010	0.0019	0.154	620.0	11.0	641.0	24.0	640.0	110.0	620.0	11.0	96.9
CORE3_65	61	22320	0.8	0.0743	0.0027	1.7930	0.062	0.1747	0.0032	0.177	1037.0	17.0	1036.0	22.0	993.0	76.0	1037.0	17.0	104.4
CORE3_66	190	21726	2.3	0.0747	0.0022	1.4820	0.045	0.1440	0.0024	0.315	867.0	14.0	919.0	18.0	1031.0	60.0	867.0	14.0	84.1
CORE3_68	309	19955	4.8	0.0742	0.0020	1.3820	0.046	0.1376	0.0036	0.723	830.0	20.0	879.0	19.0	1023.0	52.0	830.0	20.0	81.1
CORE3_69	465	11708	1.3	0.1175	0.0024	5.5100	0.130	0.3450	0.0100	0.756	1908.0	49.0	1903.0	22.0	1910.0	36.0	1910.0	36.0	99.9
CORE3_70	178	83710	0.7	0.0631	0.0023	0.8050	0.032	0.0914	0.0017	0.418	564.0	10.0	595.0	18.0	661.0	77.0	564.0	10.0	85.3
CORE3_71	419	27306	1.9	0.0788	0.0016	2.2470	0.054	0.2061	0.0059	0.672	1206.0	31.0	1193.0	17.0	1162.0	38.0	1206.0	31.0	103.8
CORE3_72	273	117744	1.0	0.2142	0.0023	17.3000	0.270	0.5816	0.0087	0.754	2955.0	36.0	2947.0	15.0	2932.0	17.0	2932.0	17.0	100.8
CORE3_73	94	3434	0.5	0.1939	0.0025	15.0200	0.220	0.5592	0.0078	0.578	2863.0	33.0	2813.0	14.0	2768.0	22.0	2768.0	22.0	103.4
CORE3_74	76	26004	3.7	0.0903	0.0024	3.1170	0.080	0.2493	0.0043	0.349	1433.0	22.0	1431.0	20.0	1406.0	50.0	1406.0	50.0	101.9
CORE3_75	413	2019	5.2	0.1186	0.0014	6.0110	0.071	0.3660	0.0046	0.576	2009.0	22.0	1976.0	10.0	1928.0	21.0	1928.0	21.0	104.2
CORE3_76	295	22320	2.7	0.1847	0.0023	12.8100	0.200	0.5038	0.0090	0.740	2626.0	39.0	2662.0	15.0	2692.0	21.0	2692.0	21.0	97.5
CORE3_77	111	21726	0.6	0.1125	0.0027	4.6800	0.120	0.3029	0.0057	0.483	1704.0	28.0	1760.0	22.0	1823.0	43.0	1823.0	43.0	93.5
CORE3_78	426	71600	6.0	0.0757	0.0011	1.8950	0.030	0.1810	0.0022	0.502	1072.0	12.0	1078.0	11.0	1077.0	30.0	1072.0	12.0	99.5
CORE3_79	350	19955	1.0	0.1166	0.0023	5.4100	0.130	0.3383	0.0069	0.638	1877.0	33.0	1883.0	20.0	1895.0	35.0	1895.0	35.0	99.1
CORE3_80	146	11708	0.5	0.0605	0.0026	0.7230	0.032	0.0855	0.0016	0.299	528.8	9.7	547.0	19.0	564.0	95.0	528.8	9.7	93.8
CORE3_81	69	83710	1.6	0.1022	0.0019	4.1160	0.083	0.2934	0.0039	0.422	1659.0	20.0	1657.0	17.0	1645.0	36.0	1645.0	36.0	100.9
CORE3_83	784	117744	3.3	0.0610	0.0012	0.7530	0.016	0.0893	0.0014	0.421	551.1	8.6	570.0	9.6	633.0	45.0	551.1	8.6	87.1
CORE3_85	313	26004	1.2	0.0582	0.0019	0.5260	0.017	0.0655	0.0014	0.308	408.6	8.7	427.0	11.0	492.0	71.0	408.6	8.7	83.0
CORE3_86	127	2019	1.1	0.1011	0.0017	4.0880	0.077	0.2927	0.0045	0.518	1656.0	23.0	1646.0	15.0	1627.0	33.0	1627.0	33.0	101.8
CORE3_88	198	21726	1.3	0.0791	0.0021	2.0470	0.073	0.1876	0.0041	0.595	1107.0	22.0	1124.0	24.0	1152.0	53.0	1107.0	22.0	96.1
CORE3_89	199	83710	1.2	0.0794	0.0015	2.1980	0.057	0.2001	0.0042	0.682	1174.0	22.0	1173.0	18.0	1165.0	37.0	1174.0	22.0	100.8
CORE3_90	151	27306	1.0	0.0614	0.0027	0.7100	0.033	0.0830	0.0017	0.340	513.7	9.9	540.0	20.0	586.0	96.0	513.7	9.9	87.7
CORE3_91	137	117744	2.1	0.0757	0.0020	1.7600	0.044	0.1687	0.0030	0.283	1004.0	17.0	1028.0	17.0	1052.0	54.0	1004.0	17.0	95.4
CORE3_92	324	3434	1.0	0.0621	0.0021	0.7910	0.029	0.0925	0.0022	0.444	570.0	13.0	589.0	16.0	636.0	71.0	570.0	13.0	89.6
CORE3_93	512	26004	0.6	0.1041	0.0016	4.4780	0.092	0.3104	0.0067	0.722	1741.0	33.0	1726.0	18.0	1691.0	29.0	1691.0	29.0	103.0
CORE3_94	598	2019	2.9	0.0596	0.0011	0.7900	0.017	0.0959	0.0014	0.459	590.4	8.1	589.9	9.6	573.0	41.0	590.4	8.1	103.0
CORE3_95	449	22320	1.1	0.0616	0.0014	0.8790	0.021	0.1049	0.0021	0.487	643.0	12.0	640.0	12.0	631.0	49.0	643.0	12.0	101.9
CORE3_96	305	21726	1.3	0.0957	0.0016	3.5500	0.071	0.2682	0.0042	0.588	1530.0	21.0	1533.0	16.0	1529.0	31.0	1529.0	31.0	100.1
CORE3_97	246	71600	3.3	0.0610	0.0015	0.8880	0.024	0.1047	0.0021	0.452	642.0	12.0	644.0	13.0	624.0	55.0	642.0	12.0	102.9

CORE3_98	565	19955	1.5	0.0886	0.0016	2.9500	0.058	0.2429	0.0041	0.440	1400.0	21.0	1393.0	15.0	1381.0	33.0	1381.0	33.0	101.4
CORE3_100	726	83710	2.2	0.0723	0.0011	1.7110	0.028	0.1713	0.0032	0.618	1018.0	17.0	1011.0	10.0	986.0	31.0	1018.0	17.0	103.2
CORE3_101	218	27306	0.9	0.1170	0.0019	4.8500	0.100	0.3016	0.0063	0.709	1697.0	31.0	1791.0	18.0	1906.0	30.0	1906.0	30.0	89.0
CORE3_102	1550	117744	2.5	0.0765	0.0010	1.8270	0.037	0.1728	0.0032	0.770	1027.0	17.0	1054.0	13.0	1104.0	26.0	1027.0	17.0	93.0
CORE3_103	517	3434	2.8	0.0622	0.0012	0.8850	0.016	0.1035	0.0017	0.425	634.8	9.9	641.9	8.8	655.0	41.0	634.8	9.9	96.9
CORE3_104	255	26004	1.3	0.1019	0.0015	4.3230	0.080	0.3062	0.0059	0.687	1720.0	29.0	1696.0	15.0	1655.0	27.0	1655.0	27.0	103.9
CORE3_105	164	2019	1.1	0.0824	0.0018	2.4270	0.056	0.2139	0.0044	0.468	1248.0	23.0	1247.0	16.0	1240.0	44.0	1240.0	44.0	100.6
CORE3_106	184	22320	1.5	0.0697	0.0027	1.2520	0.049	0.1314	0.0032	0.302	795.0	18.0	818.0	22.0	873.0	82.0	795.0	18.0	91.1
CORE3_109	301	19955	3.1	0.0893	0.0017	2.8860	0.069	0.2314	0.0051	0.613	1341.0	26.0	1374.0	18.0	1400.0	36.0	1400.0	36.0	95.8
CORE3_111	1150	83710	2.0	0.0740	0.0010	1.8800	0.033	0.1834	0.0033	0.689	1085.0	18.0	1072.0	11.0	1037.0	28.0	1085.0	18.0	104.6
CORE3_112	1247	27306	1.9	0.0575	0.0009	0.6360	0.013	0.0800	0.0015	0.717	496.0	8.9	499.6	8.1	499.0	34.0	496.0	8.9	99.4
CORE3_114	140	3434	1.2	0.0602	0.0027	0.5780	0.026	0.0701	0.0012	0.280	436.8	7.1	459.0	16.0	532.0	94.0	436.8	7.1	82.1
CORE3_115	495	26004	4.2	0.0859	0.0012	2.7030	0.041	0.2300	0.0038	0.625	1333.0	20.0	1328.0	12.0	1324.0	27.0	1324.0	27.0	100.7
CORE3_116	602	2019	1.0	0.0767	0.0011	2.0080	0.044	0.1903	0.0041	0.753	1121.0	22.0	1113.0	15.0	1101.0	30.0	1121.0	22.0	101.8
CORE3_118	41	21726	0.3	0.0861	0.0032	2.2050	0.091	0.1845	0.0046	0.464	1090.0	25.0	1174.0	28.0	1305.0	73.0	1090.0	25.0	83.5
CORE3_121	379	11708	1.2	0.0824	0.0016	2.4600	0.071	0.2159	0.0047	0.675	1259.0	25.0	1252.0	21.0	1242.0	36.0	1242.0	36.0	101.4
CORE3_123	255	27306	1.5	0.0860	0.0014	2.7360	0.047	0.2315	0.0037	0.496	1341.0	19.0	1335.0	13.0	1322.0	31.0	1322.0	31.0	101.4
CORE3_124	92	117744	0.5	0.1162	0.0023	5.5000	0.120	0.3457	0.0060	0.446	1911.0	29.0	1896.0	19.0	1878.0	36.0	1878.0	36.0	101.8
CORE3_127	184	26004	1.6	0.0620	0.0018	0.8560	0.024	0.1012	0.0019	0.284	621.0	11.0	626.0	13.0	633.0	62.0	621.0	11.0	98.1
CORE3_128	103	2019	1.8	0.0795	0.0020	2.1100	0.058	0.1937	0.0037	0.451	1140.0	20.0	1147.0	20.0	1171.0	47.0	1140.0	20.0	97.4
CORE3_129	339	22320	1.3	0.0601	0.0015	0.6510	0.017	0.0794	0.0014	0.401	492.6	8.3	507.0	10.0	573.0	53.0	492.6	8.3	86.0
CORE3_130	111	21726	1.8	0.0610	0.0021	0.7350	0.027	0.0878	0.0019	0.320	542.0	12.0	555.0	15.0	589.0	77.0	542.0	12.0	92.0
CORE3_131	188	71600	0.8	0.0753	0.0017	1.7650	0.043	0.1715	0.0031	0.449	1019.0	17.0	1027.0	16.0	1048.0	47.0	1019.0	17.0	97.2
CORE3_132	383	19955	1.6	0.0782	0.0016	1.8720	0.046	0.1751	0.0041	0.634	1039.0	23.0	1067.0	16.0	1140.0	42.0	1039.0	23.0	91.1
CORE3_134	273	83710	2.8	0.0794	0.0015	2.1430	0.045	0.1987	0.0041	0.576	1167.0	22.0	1159.0	15.0	1163.0	37.0	1167.0	22.0	100.3
CORE3_135	588	27306	2.6	0.0782	0.0011	2.1100	0.037	0.1958	0.0031	0.648	1152.0	17.0	1149.0	12.0	1144.0	27.0	1152.0	17.0	100.7
CORE3_136	217	117744	2.7	0.0745	0.0015	1.7180	0.033	0.1708	0.0030	0.411	1016.0	16.0	1013.0	13.0	1029.0	42.0	1016.0	16.0	98.7
CORE3_137	223	3434	1.8	0.0770	0.0015	1.9740	0.042	0.1874	0.0032	0.481	1106.0	17.0	1103.0	14.0	1109.0	39.0	1106.0	17.0	99.7
CORE3_138	392	26004	3.2	0.0736	0.0011	1.7370	0.028	0.1739	0.0029	0.530	1032.0	16.0	1021.0	11.0	1017.0	31.0	1032.0	16.0	101.5
CORE3_139	66	2019	0.9	0.0822	0.0033	2.0780	0.075	0.1874	0.0047	0.219	1106.0	25.0	1135.0	25.0	1203.0	79.0	1106.0	25.0	91.9

CORE3_140	551	22320	1.4	0.0580	0.0012	0.6830	0.015	0.0864	0.0017	0.496	534.0	10.0	527.9	9.4	514.0	47.0	534.0	10.0	103.9
CORE3_141	478	21726	0.8	0.0613	0.0014	0.8370	0.017	0.1005	0.0019	0.375	617.0	11.0	615.8	9.6	625.0	48.0	617.0	11.0	98.7
CORE3_142	250	71600	1.1	0.0926	0.0013	3.3850	0.055	0.2679	0.0042	0.573	1528.0	21.0	1498.0	13.0	1476.0	26.0	1476.0	26.0	103.5
CORE3_143	1551	19955	18.7	0.0736	0.0008	1.7010	0.027	0.1694	0.0027	0.783	1008.0	15.0	1008.0	10.0	1025.0	22.0	1008.0	15.0	98.3
CORE3_145	400	83710	2.1	0.0732	0.0012	1.6860	0.029	0.1689	0.0030	0.579	1009.0	17.0	1000.0	11.0	1002.0	34.0	1009.0	17.0	100.7
CORE3_146	320	27306	0.8	0.1782	0.0027	11.7200	0.200	0.4840	0.0100	0.711	2541.0	43.0	2578.0	16.0	2628.0	25.0	2628.0	25.0	96.7
CORE3_147	323	117744	1.9	0.0816	0.0015	2.2670	0.046	0.2039	0.0036	0.507	1197.0	19.0	1197.0	14.0	1216.0	36.0	1216.0	36.0	98.4
CORE3_148	269	3434	1.5	0.0728	0.0014	1.5980	0.031	0.1622	0.0027	0.523	968.0	15.0	966.0	12.0	988.0	37.0	968.0	15.0	98.0
CORE3_149	117	26004	0.7	0.0788	0.0022	1.9950	0.054	0.1879	0.0036	0.336	1109.0	20.0	1106.0	18.0	1132.0	57.0	1109.0	20.0	98.0
CORE3_150	259	2019	0.7	0.1051	0.0018	3.9000	0.130	0.2722	0.0085	0.852	1548.0	43.0	1607.0	28.0	1709.0	31.0	1709.0	31.0	90.6
CORE3_151	405	22320	1.8	0.0737	0.0016	1.8260	0.043	0.1800	0.0044	0.614	1066.0	24.0	1051.0	16.0	1014.0	45.0	1066.0	24.0	105.1
CORE3_153	527	71600	1.0	0.1061	0.0017	4.5050	0.082	0.3124	0.0058	0.633	1754.0	30.0	1730.0	16.0	1726.0	29.0	1726.0	29.0	101.6
CORE3_154	341	19955	1.4	0.1991	0.0028	15.1000	0.280	0.5550	0.0120	0.774	2847.0	50.0	2819.0	18.0	2812.0	23.0	2812.0	23.0	101.2
CORE3_155	538	11708	3.8	0.0759	0.0013	1.7070	0.033	0.1658	0.0037	0.694	990.0	21.0	1009.0	13.0	1076.0	34.0	990.0	21.0	92.0
CORE3_156	69	83710	2.4	0.0829	0.0022	2.4270	0.071	0.2140	0.0041	0.416	1248.0	22.0	1244.0	21.0	1238.0	53.0	1238.0	53.0	100.8
CORE3_157	336	27306	1.4	0.0759	0.0014	1.7910	0.037	0.1734	0.0033	0.610	1030.0	18.0	1039.0	13.0	1073.0	38.0	1030.0	18.0	96.0
CORE3_158	625	117744	2.8	0.0746	0.0011	1.8380	0.035	0.1808	0.0034	0.685	1070.0	18.0	1056.0	13.0	1047.0	31.0	1070.0	18.0	102.2
CORE3_159	179	3434	0.7	0.1212	0.0021	6.0500	0.150	0.3664	0.0090	0.737	2006.0	42.0	1975.0	22.0	1962.0	31.0	1962.0	31.0	102.2
CORE3_160	208	26004	2.0	0.0754	0.0019	1.8750	0.049	0.1827	0.0040	0.518	1081.0	22.0	1068.0	17.0	1056.0	51.0	1081.0	22.0	102.4
CORE3_161	678	2019	6.5	0.0758	0.0012	1.9180	0.037	0.1854	0.0039	0.708	1095.0	21.0	1086.0	13.0	1086.0	30.0	1095.0	21.0	100.8
CORE3_162	134	22320	1.3	0.1023	0.0024	4.3500	0.130	0.3069	0.0080	0.574	1729.0	41.0	1696.0	23.0	1652.0	44.0	1652.0	44.0	104.7
CORE3_163	85	21726	2.9	0.0633	0.0029	0.7530	0.036	0.0873	0.0020	0.230	539.0	12.0	562.0	21.0	639.0	96.0	539.0	12.0	84.4
CORE3_164	972	83710	9.5	0.0784	0.0011	2.0940	0.045	0.1949	0.0040	0.744	1146.0	21.0	1142.0	15.0	1147.0	27.0	1146.0	21.0	99.9
CORE3_165	369	27306	1.7	0.0760	0.0013	1.8540	0.034	0.1791	0.0033	0.613	1061.0	18.0	1062.0	12.0	1084.0	34.0	1061.0	18.0	97.9
CORE3_166	165	117744	1.4	0.0730	0.0017	1.6570	0.041	0.1663	0.0030	0.381	991.0	16.0	989.0	16.0	983.0	50.0	991.0	16.0	100.8
CORE3_167	310	3434	1.8	0.1224	0.0018	6.0000	0.110	0.3608	0.0066	0.651	1982.0	31.0	1973.0	16.0	1982.0	27.0	1982.0	27.0	100.0
CORE3_168	760	26004	3.5	0.1079	0.0016	4.7100	0.091	0.3211	0.0078	0.774	1792.0	38.0	1768.0	15.0	1760.0	27.0	1760.0	27.0	101.8
CORE3_170	140	22320	2.6	0.0726	0.0020	1.5800	0.044	0.1613	0.0032	0.463	963.0	18.0	959.0	18.0	963.0	55.0	963.0	18.0	100.0
CORE3_171	205	21726	1.7	0.0824	0.0021	2.3800	0.065	0.2144	0.0049	0.509	1251.0	26.0	1235.0	20.0	1235.0	51.0	1235.0	51.0	101.3
CORE3_172	440	71600	1.0	0.0766	0.0012	1.9680	0.038	0.1877	0.0035	0.701	1110.0	20.0	1101.0	13.0	1095.0	31.0	1110.0	20.0	101.4

CORE3_173	48	19955	0.8	0.0948	0.0030	3.4300	0.140	0.2627	0.0079	0.596	1499.0	40.0	1496.0	32.0	1507.0	60.0	1507.0	60.0	99.5
CORE3_174	63	11708	1.6	0.0786	0.0026	1.8650	0.065	0.1728	0.0035	0.374	1027.0	19.0	1065.0	22.0	1132.0	63.0	1027.0	19.0	90.7
CORE3_175	148	83710	1.2	0.0786	0.0017	2.0590	0.053	0.1911	0.0045	0.631	1125.0	24.0	1129.0	18.0	1153.0	41.0	1125.0	24.0	97.6
CORE3_178	323	117744	1.8	0.0815	0.0013	2.3740	0.053	0.2126	0.0046	0.731	1243.0	25.0	1229.0	16.0	1224.0	32.0	1224.0	32.0	101.6
CORE3_180	279	26004	3.0	0.0804	0.0012	2.3620	0.043	0.2134	0.0036	0.609	1246.0	19.0	1227.0	13.0	1203.0	31.0	1203.0	31.0	103.6
CORE3_181	130	2019	1.4	0.0764	0.0020	1.8840	0.053	0.1785	0.0031	0.358	1058.0	17.0	1069.0	18.0	1073.0	55.0	1058.0	17.0	98.6
CORE3_182	244	22320	1.6	0.0757	0.0013	1.8600	0.039	0.1783	0.0033	0.656	1056.0	18.0	1063.0	14.0	1069.0	34.0	1056.0	18.0	98.8
CORE3_183	408	21726	0.7	0.0764	0.0012	2.0740	0.043	0.1966	0.0039	0.690	1156.0	21.0	1137.0	14.0	1101.0	31.0	1156.0	21.0	105.0
CORE3_184	213	71600	1.2	0.0954	0.0017	3.5930	0.076	0.2765	0.0051	0.623	1572.0	26.0	1543.0	17.0	1525.0	33.0	1525.0	33.0	103.1
CORE3_185	380	19955	0.8	0.0912	0.0017	3.1900	0.100	0.2543	0.0073	0.802	1457.0	37.0	1445.0	25.0	1447.0	38.0	1447.0	38.0	100.7
CORE3_188	138	11708	1.0	0.0578	0.0024	0.5640	0.024	0.0711	0.0015	0.393	442.6	9.3	455.0	17.0	482.0	87.0	442.6	9.3	91.8
CORE3_189	284	83710	2.4	0.1247	0.0020	6.0100	0.110	0.3513	0.0075	0.668	1938.0	36.0	1975.0	16.0	2014.0	29.0	2014.0	29.0	96.2
CORE3_190	46	27306	0.4	0.1168	0.0025	5.5300	0.130	0.3450	0.0063	0.468	1908.0	30.0	1902.0	21.0	1884.0	38.0	1884.0	38.0	101.3
CORE3_191	140	117744	1.0	0.0631	0.0018	0.9170	0.028	0.1050	0.0020	0.364	643.0	12.0	657.0	14.0	676.0	64.0	643.0	12.0	95.1
CORE3_192	288	3434	1.3	0.0649	0.0015	0.9270	0.023	0.1042	0.0021	0.494	638.0	12.0	664.0	12.0	747.0	48.0	638.0	12.0	85.4
CORE3_193	126	26004	1.7	0.1104	0.0031	5.0200	0.160	0.3300	0.0100	0.667	1834.0	49.0	1816.0	28.0	1791.0	51.0	1791.0	51.0	102.4
CORE3_195	98	2019	1.1	0.1090	0.0018	4.9300	0.110	0.3270	0.0061	0.678	1821.0	30.0	1799.0	19.0	1772.0	30.0	1772.0	30.0	102.8
CORE3_196	167	22320	2.4	0.1012	0.0016	3.9300	0.071	0.2830	0.0051	0.628	1604.0	25.0	1616.0	15.0	1633.0	30.0	1633.0	30.0	98.2
CORE3_197	82	21726	0.8	0.0896	0.0032	2.6460	0.099	0.2171	0.0063	0.496	1265.0	33.0	1308.0	27.0	1392.0	68.0	1392.0	68.0	90.9
CORE3_198	97	71600	1.3	0.1880	0.0023	13.4800	0.300	0.5220	0.0120	0.850	2699.0	50.0	2707.0	21.0	2719.0	20.0	2719.0	20.0	99.3
CORE3_199	649	19955	6.9	0.0944	0.0018	3.5120	0.091	0.2702	0.0069	0.723	1540.0	35.0	1525.0	20.0	1511.0	36.0	1511.0	36.0	101.9
CORE3_200	114	11708	0.7	0.0769	0.0021	1.6000	0.054	0.1507	0.0041	0.644	904.0	23.0	964.0	21.0	1090.0	56.0	904.0	23.0	82.9
CORE3_201	49	83710	1.8	0.0741	0.0024	1.7380	0.059	0.1700	0.0029	0.368	1013.0	16.0	1014.0	22.0	987.0	68.0	1013.0	16.0	102.6
CORE3_202	158	27306	1.9	0.0631	0.0017	0.9050	0.027	0.1030	0.0020	0.505	631.0	12.0	651.0	14.0	678.0	56.0	631.0	12.0	93.1
CORE3_204	36	3434	0.8	0.0776	0.0028	2.0370	0.079	0.1899	0.0035	0.372	1119.0	19.0	1118.0	26.0	1088.0	73.0	1119.0	19.0	102.8
CORE3_205	104	26004	0.8	0.0734	0.0027	1.7340	0.067	0.1698	0.0041	0.444	1010.0	23.0	1016.0	25.0	992.0	75.0	1010.0	23.0	101.8
CORE3_206	107	2019	2.5	0.0746	0.0017	1.7690	0.041	0.1714	0.0027	0.403	1019.0	15.0	1033.0	15.0	1038.0	44.0	1019.0	15.0	98.2
CORE3_207	132	22320	2.1	0.0593	0.0018	0.7210	0.022	0.0887	0.0015	0.346	548.8	8.7	550.0	13.0	527.0	65.0	548.8	8.7	104.1
CORE3_208	128	21726	2.8	0.0756	0.0017	1.8580	0.041	0.1781	0.0027	0.327	1057.0	15.0	1062.0	15.0	1055.0	46.0	1057.0	15.0	100.2
CORE3_209	97	71600	2.1	0.0811	0.0021	2.1550	0.060	0.1924	0.0041	0.363	1133.0	22.0	1163.0	19.0	1217.0	56.0	1133.0	22.0	93.1

CORE3_210	327	19955	1.5	0.0738	0.0011	1.8350	0.034	0.1802	0.0028	0.622	1069.0	16.0	1055.0	12.0	1022.0	31.0	1069.0	16.0	104.6
CORE3_211	99	11708	1.5	0.0908	0.0019	2.9770	0.058	0.2376	0.0033	0.281	1373.0	17.0	1399.0	15.0	1422.0	40.0	1422.0	40.0	96.6
CORE3_212	218	83710	1.2	0.0671	0.0016	1.2190	0.031	0.1323	0.0024	0.507	800.0	14.0	805.0	14.0	816.0	48.0	800.0	14.0	98.0
CORE3_214	79	117744	2.1	0.0708	0.0022	1.4650	0.049	0.1495	0.0027	0.414	897.0	15.0	907.0	20.0	903.0	66.0	897.0	15.0	99.3
CORE3_215	496	3434	1.7	0.0590	0.0019	0.7210	0.025	0.0894	0.0019	0.397	552.0	11.0	549.0	15.0	541.0	69.0	552.0	11.0	102.0
CORE3_216	467	26004	2.2	0.0733	0.0011	1.6310	0.027	0.1612	0.0026	0.518	963.0	14.0	980.0	10.0	1008.0	31.0	963.0	14.0	95.5
CORE3_217	131	2019	2.2	0.0745	0.0016	1.7580	0.041	0.1715	0.0029	0.422	1019.0	16.0	1025.0	15.0	1035.0	42.0	1019.0	16.0	98.5
CORE3_218	197	22320	1.2	0.1898	0.0021	14.0500	0.210	0.5376	0.0082	0.703	2769.0	34.0	2748.0	14.0	2734.0	18.0	2734.0	18.0	101.3
CORE3_219	77	21726	1.7	0.0618	0.0025	0.7150	0.028	0.0840	0.0017	0.182	520.0	10.0	544.0	17.0	610.0	90.0	520.0	10.0	85.2
CORE3_220	201	71600	1.1	0.1144	0.0016	5.4720	0.084	0.3459	0.0051	0.591	1916.0	25.0	1892.0	13.0	1859.0	25.0	1859.0	25.0	103.1
CORE3_221	429	19955	1.8	0.0604	0.0012	0.7900	0.017	0.0946	0.0016	0.480	582.6	9.3	589.3	9.5	597.0	43.0	582.6	9.3	97.6
CORE3_222	166	11708	2.3	0.1004	0.0014	4.0710	0.069	0.2934	0.0043	0.623	1657.0	22.0	1644.0	14.0	1622.0	25.0	1622.0	25.0	102.2
CORE3_223	121	83710	2.2	0.1011	0.0017	4.1080	0.077	0.2947	0.0043	0.493	1663.0	21.0	1652.0	15.0	1631.0	31.0	1631.0	31.0	102.0
CORE3_224	54	27306	0.9	0.0922	0.0025	3.2030	0.087	0.2517	0.0047	0.386	1446.0	24.0	1452.0	21.0	1447.0	51.0	1447.0	51.0	99.9
CORE3_226	137	117744	2.3	0.0859	0.0017	2.6420	0.057	0.2255	0.0044	0.586	1312.0	23.0	1308.0	16.0	1316.0	39.0	1316.0	39.0	99.7
CORE3_227	244	3434	0.8	0.0572	0.0020	0.4650	0.017	0.0591	0.0012	0.267	369.9	7.5	386.0	11.0	454.0	77.0	369.9	7.5	81.5
CORE3_231	659	21726	0.6	0.0614	0.0011	0.8700	0.020	0.1027	0.0020	0.648	630.0	12.0	633.0	11.0	638.0	40.0	630.0	12.0	98.7
CORE3_232	144	71600	2.5	0.0631	0.0017	0.9470	0.027	0.1094	0.0018	0.305	669.0	10.0	672.0	14.0	690.0	61.0	669.0	10.0	97.0
CORE3_234	32	11708	0.8	0.0957	0.0033	3.2600	0.110	0.2507	0.0057	0.339	1439.0	29.0	1458.0	27.0	1491.0	68.0	1491.0	68.0	96.5
CORE3_235	107	83710	1.8	0.0935	0.0019	3.3820	0.074	0.2645	0.0049	0.564	1511.0	25.0	1495.0	17.0	1484.0	38.0	1484.0	38.0	101.8
CORE3_236	51	27306	1.2	0.0931	0.0027	3.3900	0.120	0.2663	0.0056	0.511	1520.0	29.0	1497.0	30.0	1470.0	61.0	1470.0	61.0	103.4
CORE3_237	169	117744	1.0	0.0618	0.0017	0.7850	0.026	0.0928	0.0022	0.609	571.0	13.0	585.0	14.0	635.0	59.0	571.0	13.0	89.9
CORE3_238	52	3434	0.8	0.1016	0.0034	3.7400	0.160	0.2680	0.0077	0.666	1533.0	40.0	1568.0	35.0	1614.0	64.0	1614.0	64.0	95.0
CORE3_239	260	26004	0.6	0.1172	0.0021	5.3000	0.150	0.3336	0.0083	0.806	1860.0	42.0	1867.0	24.0	1906.0	31.0	1906.0	31.0	97.6
CORE3_240	489	2019	1.0	0.0569	0.0015	0.5550	0.017	0.0713	0.0018	0.597	444.0	11.0	447.0	11.0	468.0	58.0	444.0	11.0	94.9
CORE3_241	497	22320	5.7	0.0680	0.0013	1.3440	0.056	0.1434	0.0050	0.889	862.0	28.0	853.0	25.0	848.0	39.0	862.0	28.0	101.7
CORE3_242	43	21726	1.8	0.0826	0.0030	2.4310	0.080	0.2157	0.0049	0.201	1258.0	26.0	1243.0	24.0	1207.0	72.0	1207.0	72.0	104.2
CORE3_243	412	83710	1.2	0.0597	0.0012	0.7130	0.014	0.0877	0.0014	0.454	541.4	8.5	544.8	8.3	567.0	41.0	541.4	8.5	95.5
CORE3_245	30	27306	1.6	0.0947	0.0029	3.4500	0.110	0.2673	0.0053	0.343	1525.0	27.0	1507.0	24.0	1479.0	61.0	1479.0	61.0	103.1
CORE3_246	480	117744	1.4	0.0578	0.0012	0.5650	0.014	0.0721	0.0015	0.517	448.2	8.7	452.8	8.9	501.0	48.0	448.2	8.7	89.5

CORE3_247	1406	3434	21.5	0.0652	0.0016	1.0900	0.057	0.1240	0.0063	0.883	752.0	36.0	742.0	28.0	765.0	51.0	752.0	36.0	98.3
CORE3_248	120	26004	0.3	0.0623	0.0021	0.7820	0.027	0.0921	0.0018	0.371	567.0	11.0	582.0	15.0	624.0	73.0	567.0	11.0	90.9
CORE3_250	116	2019	0.8	0.1105	0.0041	4.8200	0.210	0.3203	0.0063	0.469	1788.0	31.0	1778.0	33.0	1771.0	57.0	1771.0	57.0	101.0
CORE3_252	434	21726	0.7	0.1089	0.0015	4.8700	0.088	0.3288	0.0063	0.736	1829.0	30.0	1795.0	15.0	1771.0	25.0	1771.0	25.0	103.3
CORE3_255	141	19955	1.2	0.1051	0.0017	4.2860	0.077	0.3021	0.0059	0.652	1702.0	30.0	1689.0	15.0	1704.0	31.0	1704.0	31.0	99.9
CORE3_259	166	27306	1.4	0.0807	0.0016	2.1600	0.049	0.1965	0.0039	0.565	1155.0	21.0	1164.0	16.0	1204.0	39.0	1155.0	21.0	95.9
CORE3_261	48	3434	0.9	0.0770	0.0026	1.8500	0.064	0.1765	0.0038	0.320	1047.0	21.0	1055.0	23.0	1094.0	72.0	1047.0	21.0	95.7
CORE3_262	148	26004	0.7	0.0761	0.0017	1.8720	0.046	0.1818	0.0035	0.495	1076.0	19.0	1066.0	16.0	1077.0	45.0	1076.0	19.0	99.9
CORE3_263	227	2019	0.6	0.0618	0.0017	0.8260	0.028	0.0983	0.0022	0.577	604.0	13.0	607.0	15.0	627.0	60.0	604.0	13.0	96.3
CORE3_264	88	22320	1.1	0.0914	0.0020	3.1690	0.077	0.2589	0.0060	0.614	1481.0	30.0	1442.0	18.0	1438.0	41.0	1438.0	41.0	103.0
CORE3_265	136	21726	1.9	0.0777	0.0020	1.8700	0.049	0.1793	0.0035	0.392	1062.0	19.0	1064.0	17.0	1116.0	52.0	1062.0	19.0	95.2
CORE3_266	203	71600	1.3	0.0708	0.0016	1.4100	0.034	0.1473	0.0026	0.420	885.0	15.0	888.0	14.0	931.0	46.0	885.0	15.0	95.1
CORE3_267	752	19955	0.9	0.0713	0.0013	1.3950	0.027	0.1464	0.0032	0.659	880.0	18.0	886.0	11.0	955.0	36.0	880.0	18.0	92.1
CORE3_268	194	11708	2.4	0.0750	0.0015	1.7490	0.046	0.1726	0.0038	0.625	1025.0	21.0	1020.0	17.0	1047.0	40.0	1025.0	21.0	97.9
CORE3_269	465	83710	1.3	0.1105	0.0021	4.4800	0.110	0.3033	0.0075	0.648	1705.0	37.0	1722.0	20.0	1801.0	34.0	1801.0	34.0	94.7
CORE3_270	40	27306	1.0	0.0864	0.0029	2.3570	0.074	0.2035	0.0043	0.258	1193.0	23.0	1222.0	23.0	1290.0	66.0	1290.0	66.0	92.5
CORE3_271	591	117744	1.8	0.0804	0.0011	2.1800	0.038	0.2009	0.0035	0.622	1181.0	19.0	1171.0	12.0	1195.0	28.0	1181.0	19.0	98.8
CORE3_272	118	3434	0.8	0.0748	0.0019	1.7380	0.045	0.1741	0.0034	0.272	1033.0	19.0	1017.0	16.0	1022.0	52.0	1033.0	19.0	101.1
CORE3_273	149	26004	1.2	0.0780	0.0017	1.7920	0.044	0.1709	0.0036	0.533	1016.0	20.0	1038.0	16.0	1120.0	44.0	1016.0	20.0	90.7
CORE3_275	210	22320	0.8	0.0596	0.0017	0.6260	0.020	0.0771	0.0016	0.470	479.9	9.6	491.0	12.0	558.0	63.0	479.9	9.6	86.0
CORE3_276	189	21726	2.2	0.0764	0.0015	1.8140	0.038	0.1763	0.0030	0.444	1046.0	16.0	1048.0	13.0	1086.0	41.0	1046.0	16.0	96.3
CORE3_277	138	71600	1.2	0.0833	0.0018	2.3750	0.060	0.2120	0.0042	0.566	1238.0	22.0	1230.0	18.0	1264.0	42.0	1264.0	42.0	97.9
CORE3_278	707	19955	9.6	0.0534	0.0012	0.3878	0.009	0.0541	0.0012	0.551	339.7	7.4	332.0	6.7	330.0	48.0	339.7	7.4	102.9
CORE3_280	364	83710	0.7	0.0591	0.0013	0.6500	0.018	0.0817	0.0018	0.454	506.0	11.0	506.0	11.0	543.0	45.0	506.0	11.0	93.2
CORE3_281	60	27306	2.2	0.0805	0.0020	2.1080	0.058	0.1928	0.0041	0.531	1135.0	22.0	1147.0	19.0	1181.0	51.0	1135.0	22.0	96.1
CORE3_282	203	117744	1.5	0.0753	0.0014	1.8760	0.044	0.1845	0.0037	0.641	1090.0	20.0	1068.0	15.0	1057.0	37.0	1090.0	20.0	103.1
CORE3_284	182	26004	1.9	0.0770	0.0015	1.9040	0.042	0.1824	0.0031	0.383	1079.0	17.0	1079.0	14.0	1110.0	40.0	1079.0	17.0	97.2
CORE3_286	79	22320	1.1	0.0754	0.0018	1.8980	0.052	0.1870	0.0045	0.592	1103.0	24.0	1074.0	18.0	1048.0	48.0	1103.0	24.0	105.2
CORE3_287	81	21726	2.7	0.0914	0.0018	3.0620	0.073	0.2488	0.0057	0.640	1429.0	29.0	1422.0	19.0	1437.0	37.0	1437.0	37.0	99.4
CORE3_288	12	71600	1.2	0.0818	0.0045	1.9100	0.110	0.1719	0.0049	0.297	1021.0	27.0	1067.0	39.0	1140.0	120.0	1021.0	27.0	89.6

CORE3_289	125	19955	1.4	0.0794	0.0014	2.2110	0.048	0.2062	0.0038	0.643	1207.0	20.0	1181.0	15.0	1169.0	34.0	1207.0	20.0	103.3
CORE3_290	277	11708	1.1	0.0560	0.0015	0.4290	0.012	0.0574	0.0011	0.425	359.9	6.9	361.2	8.2	407.0	58.0	359.9	6.9	88.4
CORE3_291	292	83710	2.6	0.1126	0.0018	5.1200	0.110	0.3343	0.0081	0.765	1856.0	39.0	1836.0	19.0	1833.0	29.0	1833.0	29.0	101.3
CORE3_292	113	27306	1.5	0.0858	0.0019	2.7620	0.065	0.2349	0.0054	0.545	1358.0	28.0	1341.0	18.0	1323.0	45.0	1323.0	45.0	102.6
CORE3_293	285	117744	1.0	0.0631	0.0013	0.9020	0.018	0.1059	0.0023	0.577	648.0	13.0	651.2	9.7	694.0	44.0	648.0	13.0	93.4
CORE3_294	366	3434	1.8	0.0777	0.0015	2.1300	0.050	0.2020	0.0054	0.729	1185.0	29.0	1156.0	16.0	1127.0	38.0	1185.0	29.0	105.1
CORE3_295	895	26004	7.8	0.0537	0.0010	0.3861	0.008	0.0535	0.0010	0.570	336.0	6.4	331.4	5.7	339.0	40.0	336.0	6.4	99.1
CORE3_296	181	2019	0.9	0.0609	0.0014	0.6900	0.018	0.0834	0.0016	0.566	516.0	9.7	530.0	11.0	608.0	50.0	516.0	9.7	84.9
CORE3_298	67	22320	0.4	0.0745	0.0020	1.7450	0.047	0.1729	0.0037	0.344	1027.0	20.0	1019.0	17.0	1027.0	58.0	1027.0	20.0	100.0
CORE3_299	35	21726	1.7	0.0818	0.0028	1.8680	0.071	0.1680	0.0038	0.418	1000.0	21.0	1057.0	25.0	1188.0	72.0	1000.0	21.0	84.2
CORE3_300	450	71600	0.8	0.0554	0.0013	0.3980	0.012	0.0525	0.0012	0.623	329.7	7.3	338.5	8.8	402.0	50.0	329.7	7.3	82.0

Appendix C

Zircon εHf data for the Midland Basin

					Measured					Calculated			
Analysis	^{176}Hf	^{176}Hf	^{177}Hf	^{177}Hf	^{176}Hf	^{176}Hf	^{176}Lu	^{176}Lu	Zircon age	^{176}Hf	εHf_0	εHf_i	$CHUR_i$
		Int2SE		Int2SE	^{177}Hf	^{177}Hf	^{177}Hf	^{177}Hf	(Ma)	^{177}Hfi			
					Corrected	Corrected	Corrected	Corrected					
						Int2SE		Int2SE					
Cambrian sandstone, sample 1 (Late Middle Cambrian)													
CORE_1_1	0.935	0.031	3.07	0.11	0.28213	0.000023	0.000741	0.000028	1416.0	0.2821101	-23.34	7.81	0.28189
CORE_1_2	0.77	0.069	2.42	0.24	0.282158	0.000053	0.001187	0.000098	825.0	0.2821396	-22.35	-4.57	0.28227
CORE_1_3	1.561	0.08	5.08	0.24	0.282166	0.000035	0.000718	0.000026	1399.0	0.282147	-22.07	8.73	0.2819
CORE_1_4	1.01	0.055	3.05	0.17	0.282077	0.000036	0.001435	0.00003	723.4	0.2820575	-25.21	-9.76	0.28233
CORE_1_5	1.185	0.086	3.74	0.26	0.282253	0.000021	0.000999	0.000025	1324.0	0.282228	-18.99	9.89	0.28195
CORE_1_6	1.306	0.071	4.05	0.22	0.282182	0.000024	0.001135	0.000056	1717.0	0.282145	-21.50	15.96	0.2817
CORE_1_7	1.238	0.099	3.86	0.35	0.282171	0.000023	0.00122	0.00019	1515.0	0.282136	-21.89	11.00	0.28183
CORE_1_8	1.446	0.072	4.47	0.23	0.282175	0.000025	0.001151	0.000046	1444.0	0.2821435	-21.75	9.64	0.28187
CORE_1_9	1.24	0.17	3.55	0.51	0.282078	0.000028	0.00203	0.00016	1628.0	0.2820154	-25.18	9.31	0.28175
CORE_1_10	1.46	0.084	4.67	0.28	0.282174	0.000023	0.000968	0.000056	1894.0	0.2821392	-21.78	19.84	0.28158
CORE_1_11	1.39	0.19	4.55	0.61	0.282163	0.000026	0.000708	0.000032	1523.0	0.2821426	-22.17	11.41	0.28182
CORE_1_12	1.176	0.086	3.32	0.25	0.282153	0.000028	0.001989	0.000067	1496.0	0.2820967	-22.53	9.17	0.28184
CORE_1_13	1.101	0.076	3.65	0.24	0.282138	0.00002	0.000585	0.000016	1333.0	0.2821233	-23.06	6.38	0.28194
CORE_1_14	1.561	0.089	5.08	0.28	0.282187	0.000028	0.000712	7.2E-06	1368.0	0.2821686	-21.32	8.79	0.28192
CORE_1_15	0.783	0.06	2.58	0.2	0.282214	0.000024	0.000647	0.000031	1429.0	0.2821965	-20.37	11.17	0.28188
CORE_1_16	1.02	0.12	2.94	0.26	0.282262	0.000028	0.00174	0.00015	1645.0	0.2822077	-18.67	16.53	0.28174
CORE_1_17	0.979	0.069	2.89	0.2	0.282114	0.000034	0.001549	0.000032	1465.0	0.282071	-23.90	7.55	0.28186
CORE_1_18	1.285	0.087	3.66	0.23	0.282122	0.000039	0.001928	0.00004	1453.0	0.282069	-23.62	7.20	0.28187
CORE_1_19	1.684	0.085	5.42	0.28	0.282169	0.000026	0.000844	0.000027	1379.0	0.282147	-21.96	8.28	0.28191
CORE_1_20	1.28	0.12	4.12	0.4	0.282193	0.000028	0.000832	0.000021	1399.0	0.282171	-21.11	9.58	0.2819
CORE_1_21	1.235	0.078	3.78	0.23	0.282164	0.000023	0.001369	0.00002	1412.0	0.2821274	-22.14	8.34	0.28189
CORE_1_22	1.273	0.069	4.15	0.22	0.282154	0.000032	0.000763	0.0000053	1322.0	0.2821349	-22.49	6.55	0.28195
CORE_1_23	1.032	0.055	3.35	0.17	0.282129	0.000027	0.000791	0.0000067	1276.0	0.2821099	-23.37	4.61	0.28198
CORE_1_24	1.343	0.084	4.27	0.27	0.282189	0.000031	0.000994	0.00006	1448.0	0.2821618	-21.25	10.38	0.28187

CORE_1_25	1.15	0.2	3.5	0.61	0.282197	0.000054	0.0014	0.00011	850.0	0.2821746	-20.97	-2.76	0.28225
CORE_1_26	1.38	0.1	4.52	0.33	0.282282	0.000022	0.000684	0.0000082	1100.0	0.2822678	-17.96	6.20	0.28209
CORE_1_27	1.206	0.083	4.21	0.3	0.2821	0.000023	0.000198	0.000026	1533.0	0.2820943	-24.40	9.93	0.28181
CORE_1_28	1.41	0.11	4.33	0.32	0.282124	0.000017	0.00127	0.000091	1400.0	0.2820904	-23.55	6.75	0.2819
CORE_1_29	1.27	0.12	3.73	0.33	0.282173	0.000019	0.001786	0.000058	1433.0	0.2821246	-21.82	8.71	0.28188
CORE_1_30	1.622	0.045	5.13	0.12	0.282153	0.000024	0.000973	0.000024	1478.0	0.2821258	-22.53	9.79	0.28185
CORE_1_31	1.184	0.095	3.82	0.31	0.282187	0.000018	0.000867	0.000045	1346.0	0.2821649	-21.32	8.16	0.28193
CORE_1_32	0.92	0.047	2.95	0.15	0.282234	0.000029	0.000874	0.000021	1180.0	0.2822145	-19.66	6.13	0.28204
CORE_1_33	1.07	0.051	3.65	0.18	0.282169	0.000019	0.00037	0.0000095	1387.0	0.2821593	-21.96	8.89	0.28191
CORE_1_34	1.18	0.18	3.71	0.63	0.282173	0.000027	0.0012	0.00022	1511.0	0.2821387	-21.82	11.00	0.28183
CORE_1_35	0.95	0.19	2.85	0.6	0.282212	0.000049	0.00193	0.00022	1524.0	0.2821563	-20.44	11.92	0.28182
CORE_1_36	1.175	0.069	3.83	0.23	0.282155	0.000017	0.000753	0.000022	1373.0	0.2821354	-22.45	7.73	0.28192
CORE_1_37	2.01	0.13	5.48	0.37	0.282157	0.000023	0.001918	0.000042	1764.0	0.2820928	-22.38	15.19	0.28166
CORE_1_38	1.236	0.095	4	0.3	0.282102	0.000027	0.000776	0.000057	1842.0	0.2820748	-24.33	16.35	0.28161
CORE_1_39	0.86	0.16	2.61	0.5	0.282192	0.000023	0.001382	0.000097	1978.0	0.28214	-21.15	21.81	0.28153
CORE_1_40	0.95	0.15	2.93	0.47	0.282208	0.000046	0.001262	0.000078	1632.0	0.282169	-20.58	14.85	0.28175
CORE_1_41	1.4	0.11	4.55	0.37	0.282164	0.000025	0.00071	0.00003	1511.0	0.2821437	-22.14	11.18	0.28183
CORE_1_42	0.795	0.074	2.59	0.24	0.282102	0.000037	0.000819	0.000023	1654.0	0.2820763	-24.33	12.07	0.28174
CORE_1_43	0.73	0.12	2.38	0.39	0.282161	0.000039	0.000894	0.000044	1609.0	0.2821337	-22.24	13.07	0.28177
CORE_1_44	1.208	0.065	3.5	0.22	0.282108	0.000028	0.00191	0.00012	1388.0	0.2820579	-24.12	5.32	0.28191
CORE_1_45	1.639	0.098	5.28	0.3	0.282181	0.000024	0.000796	0.000017	1446.0	0.2821592	-21.54	10.24	0.28187
CORE_1_46	1.4	0.14	3.99	0.34	0.282572	0.000035	0.00181	0.00013	972.0	0.2825389	-7.71	12.91	0.28217
CORE_1_47	0.878	0.028	2.91	0.1	0.282098	0.000035	0.000629	0.000048	2524.0	0.2820677	-24.47	31.97	0.28117
CORE_1_48	1.77	0.095	5.6	0.3	0.2822	0.000036	0.000881	0.00001	1473.0	0.2821754	-20.86	11.43	0.28185
CORE_1_49	0.78	0.16	2.48	0.51	0.282138	0.000036	0.001136	0.000071	1645.0	0.2821026	-23.06	12.80	0.28174
CORE_1_50	1.215	0.045	3.96	0.16	0.282157	0.000022	0.000763	0.000066	1377.0	0.2821371	-22.38	7.88	0.28191
CORE_1_51	1.396	0.075	4.13	0.19	0.28217	0.000026	0.00157	0.000079	1628.0	0.2821215	-21.92	13.08	0.28175
CORE_1_52	1.431	0.069	4.56	0.23	0.282093	0.00002	0.000986	0.000032	1405.0	0.2820668	-24.65	6.02	0.2819
CORE_1_53	1.289	0.067	3.97	0.21	0.282183	0.000021	0.001237	0.000024	1443.0	0.2821492	-21.46	9.82	0.28187
CORE_1_54	1.46	0.11	4.76	0.36	0.282133	0.00002	0.000722	0.000027	1362.0	0.2821144	-23.23	6.73	0.28192

CORE_1_55	1.243	0.096	3.84	0.28	0.282183	0.000026	0.0012	0.00012	1371.0	0.2821519	-21.46	8.27	0.28192
CORE_1_56	1.276	0.098	4.08	0.31	0.282623	0.00002	0.000805	0.000017	820.0	0.2826106	-5.91	12.01	0.28227
CORE_1_57	1.32	0.12	4.43	0.4	0.282271	0.000023	0.000401	0.000026	1170.0	0.2822621	-18.35	7.59	0.28205
CORE_1_58	1.92	0.15	6.32	0.48	0.282145	0.000023	0.000636	0.000016	1346.0	0.2821288	-22.81	6.88	0.28193
CORE_1_59	1.13	0.053	3.64	0.17	0.282156	0.000018	0.000868	0.000019	1348.0	0.2821339	-22.42	7.10	0.28193
CORE_1_60	1.31	0.13	4.34	0.43	0.282155	0.000018	0.000635	0.000061	1308.0	0.2821393	-22.45	6.38	0.28196
CORE_1_61	1.415	0.048	4.34	0.15	0.282118	0.000032	0.001345	0.000041	1660.0	0.2820757	-23.76	12.19	0.28173
CORE_1_62	1.599	0.099	5.15	0.29	0.282156	0.000021	0.000808	0.00003	1350.0	0.2821354	-22.42	7.20	0.28193
CORE_1_63	1.77	0.17	5.61	0.52	0.282164	0.000029	0.000856	0.00002	1506.0	0.2821396	-22.14	10.92	0.28183
CORE_1_64	1.59	0.23	4.52	0.6	0.282202	0.000028	0.00195	0.00015	1500.0	0.2821466	-20.79	11.03	0.28184
CORE_1_65	1.131	0.091	3.57	0.27	0.282219	0.000026	0.000945	0.000021	1184.0	0.2821979	-20.19	5.63	0.28204
CORE_1_66	1.078	0.05	3.4	0.17	0.282282	0.000031	0.001078	0.000065	1660.0	0.2822481	-17.96	18.30	0.28173
CORE_1_67	1.09	0.16	3.68	0.54	0.282169	0.000024	0.00062	0.000059	1504.0	0.2821513	-21.96	11.29	0.28183
CORE_1_68	1.052	0.069	3.34	0.23	0.282231	0.000022	0.000934	0.000046	1207.0	0.2822097	-19.77	6.58	0.28202
CORE_1_69	1.78	0.12	5.64	0.35	0.28215	0.000024	0.000868	0.00003	1293.0	0.2821288	-22.63	5.67	0.28197
CORE_1_70	1.34	0.1	4.3	0.32	0.282166	0.000021	0.000829	0.000011	1336.0	0.2821451	-22.07	7.22	0.28194
CORE_1_71	0.944	0.05	3.18	0.16	0.282072	0.000024	0.00049	0.000019	1359.0	0.2820594	-25.39	4.71	0.28193
CORE_1_72	1.48	0.13	4.76	0.41	0.282243	0.000028	0.000869	0.000029	1301.0	0.2822216	-19.34	9.14	0.28196
CORE_1_73	1.214	0.091	3.91	0.31	0.282167	0.000016	0.000884	0.000066	1364.0	0.2821442	-22.03	7.83	0.28192
CORE_1_74	1.444	0.096	4.6	0.29	0.282178	0.000022	0.000936	0.000028	1444.0	0.2821524	-21.64	9.95	0.28187
CORE_1_75	1.289	0.088	4.26	0.31	0.282151	0.000033	0.000637	0.000047	1482.0	0.2821331	-22.60	10.14	0.28185
CORE_1_76	1.498	0.097	4.86	0.31	0.28216	0.000014	0.000806	0.00001	1363.0	0.2821392	-22.28	7.63	0.28192
CORE_1_77	2.26	0.14	6.47	0.37	0.282129	0.000016	0.001615	0.000063	1315.0	0.2820889	-23.37	4.75	0.28195
Pennsylvanian sandstone, sample 2 (Late Pennsylvanian)													
CORE_3_1	1.008	0.024	3.501	0.086	0.282117	0.000026	0.00018	0.000057	581.0	0.282139	-22.95	-10.07	0.28242
CORE_3_2	1.238	0.064	4.17	0.19	0.28217	0.000027	0.000435	0.000043	1122.0	0.2821858	-21.04	3.80	0.28208
CORE_3_3	0.947	0.036	3.05	0.11	0.282205	0.000026	0.000809	0.000019	679.6	0.2822197	-19.80	-5.00	0.28236
CORE_3_4	1.051	0.053	3.41	0.17	0.28219	0.000031	0.000781	0.00004	1126.0	0.2822004	-20.26	4.40	0.28208

CORE_3_5	1.397	0.072	4.66	0.24	0.281285	0.000021	0.000567	0.000026	1994.0	0.2812915	-52.23	-7.96	0.28152
CORE_3_6	1.263	0.066	4.22	0.2	0.281028	0.000029	0.000447	0.000016	2492.0	0.2810367	-61.25	-5.44	0.28119
CORE_3_7	1.035	0.095	2.78	0.23	0.282228	0.000034	0.00259	0.00011	1404.0	0.2821902	-18.78	10.38	0.2819
CORE_3_8	1.157	0.056	3.8	0.2	0.282218	0.000041	0.000545	0.000049	1337.0	0.2822342	-19.17	10.41	0.28194
CORE_3_9	0.935	0.028	3.09	0.078	0.281073	0.000023	0.000666	0.000042	2739.0	0.2810691	-59.62	1.49	0.28103
CORE_3_10	1.423	0.059	4.43	0.21	0.282502	0.000027	0.000991	0.000074	1217.0	0.2825102	-9.09	17.46	0.28202
CORE_3_11	0.973	0.057	3.34	0.19	0.281325	0.000018	0.000296	0.00001	1862.0	0.2813465	-50.67	-9.05	0.2816
CORE_3_12	1.332	0.065	4.65	0.23	0.282334	0.000031	0.000156	0.0000041	1237.0	0.2823634	-14.96	12.71	0.282
CORE_3_13	0.963	0.044	3.35	0.15	0.281352	0.000019	0.00024	0.000004	1892.0	0.2813764	-49.68	-7.30	0.28158
CORE_3_14	1.382	0.031	4.73	0.11	0.282118	0.000025	0.000324	0.000021	1146.0	0.282145	-22.56	2.89	0.28206
CORE_3_15	1.04	0.14	3.33	0.45	0.282312	0.000033	0.000898	0.000027	810.0	0.2823323	-15.70	1.92	0.28228
CORE_3_16	1.299	0.082	4.09	0.29	0.282224	0.00003	0.000919	0.000072	1004.0	0.2822406	-18.81	3.06	0.28215
CORE_3_17	1.314	0.053	4.12	0.17	0.282233	0.000025	0.000987	0.000026	1168.0	0.2822462	-18.46	6.98	0.28205
CORE_3_18	1.39	0.083	3.44	0.18	0.282622	0.000038	0.002989	0.000078	462.9	0.2826311	-4.70	4.70	0.2825
CORE_3_19	1.401	0.089	4.27	0.27	0.281903	0.00003	0.001282	0.00002	1468.0	0.2819024	-30.13	1.63	0.28186
CORE_3_20	1.646	0.047	5.31	0.15	0.282199	0.000032	0.000761	0.000028	889.0	0.2822223	-19.63	-0.19	0.28223
CORE_3_21	1.07	0.051	3.55	0.16	0.281796	0.000025	0.00051	0.000006	1594.0	0.2818166	-33.88	1.47	0.28178
CORE_3_22	1.1	0.058	3.29	0.21	0.282177	0.00002	0.001435	0.000091	960.0	0.282189	-20.33	0.24	0.28218
CORE_3_23	0.762	0.076	1.88	0.21	0.282635	0.000042	0.00313	0.00021	610.2	0.2826381	-4.10	8.25	0.28241
CORE_3_24	0.84	0.11	2.77	0.36	0.282211	0.000035	0.00061	0.000052	960.0	0.28224	-19.06	2.04	0.28218
CORE_3_25	1.066	0.051	3.7	0.17	0.28244	0.000018	0.000178	0.0000047	573.3	0.2824771	-11.00	1.72	0.28243
CORE_3_26	0.934	0.089	3.26	0.31	0.280982	0.000022	0.000187	0.000019	1732.0	0.2810169	-62.48	-23.75	0.28169
CORE_3_27	1.72	0.085	5.32	0.31	0.282372	0.000034	0.00117	0.0001	588.0	0.2824001	-13.33	-0.67	0.28242
CORE_3_28	1.127	0.02	3.572	0.078	0.282181	0.000028	0.000924	0.000088	1240.0	0.2822014	-20.05	7.03	0.282
CORE_3_29	1.401	0.051	4.5	0.21	0.282191	0.000017	0.00087	0.000088	489.7	0.282225	-19.70	-9.08	0.28248
CORE_3_30	1.283	0.084	4.01	0.28	0.282219	0.000045	0.00097	0.000045	1580.0	0.282234	-18.64	15.97	0.28178
CORE_3_31	1.225	0.048	3.49	0.17	0.281847	0.00004	0.00197	0.00013	1602.0	0.2818312	-31.79	2.18	0.28177
CORE_3_32	1.71	0.13	5.61	0.4	0.282114	0.000022	0.000624	0.000055	1351.0	0.2821431	-22.31	7.50	0.28193
CORE_3_33	1.278	0.05	4.26	0.16	0.281208	0.000021	0.00047	0.000014	1639.0	0.2812384	-54.35	-18.01	0.28175
CORE_3_34	1.542	0.096	4.51	0.29	0.282607	0.000029	0.00191	0.00011	639.0	0.2826291	-4.88	8.58	0.28239

CORE_3_35	1.327	0.065	4.39	0.22	0.28179	0.000036	0.00062	0.0000044	1590.0	0.2818173	-33.74	1.41	0.28178
CORE_3_36	1.232	0.062	4.04	0.17	0.282185	0.000025	0.000633	0.000057	1164.0	0.2822201	-19.66	5.97	0.28205
CORE_3_37	1.148	0.05	3.75	0.16	0.28237	0.000023	0.00067	0.00002	809.0	0.2824078	-13.15	4.58	0.28228
CORE_3_38	0.945	0.056	3.03	0.14	0.282199	0.000024	0.00078	0.00011	1064.0	0.2822324	-19.17	4.13	0.28212
CORE_3_39	1.06	0.079	3.62	0.29	0.282156	0.000017	0.000372	0.000053	670.7	0.2822013	-20.65	-5.85	0.28237
CORE_3_40	1.13	0.17	3.55	0.56	0.282363	0.000029	0.001173	0.000094	501.5	0.282403	-13.30	-2.51	0.28247
CORE_3_41	1.35	0.12	4.58	0.41	0.282439	0.00002	0.000332	0.000012	527.3	0.2824867	-10.61	1.03	0.28246
CORE_3_42	1.008	0.015	3.252	0.028	0.282045	0.000024	0.00082	0.00013	1310.0	0.2820757	-24.54	4.17	0.28196
CORE_3_43	1.01	0.14	3.25	0.48	0.282012	0.00005	0.000826	0.000081	1400.0	0.2820421	-25.67	5.04	0.2819
CORE_3_44	1.4	0.11	4.2	0.34	0.281382	0.000026	0.00135	0.000044	1679.0	0.281391	-47.95	-11.68	0.28172
CORE_3_45	1.389	0.08	4.84	0.28	0.282306	0.000015	0.00012	0.0000008	617.8	0.2823576	-15.24	-1.51	0.2824
CORE_3_46	1.046	0.058	3.45	0.19	0.28236	0.000024	0.000591	0.000012	660.0	0.2824067	-13.30	1.18	0.28237
CORE_3_47	1.386	0.064	4.73	0.21	0.282096	0.000021	0.000316	0.000013	1116.0	0.2821443	-22.60	2.19	0.28208
CORE_3_48	1.227	0.09	3.74	0.28	0.282267	0.000041	0.001317	0.000047	947.0	0.2822995	-16.51	3.86	0.28219
CORE_3_49	1.176	0.08	3.94	0.24	0.282221	0.000028	0.00043	0.000049	1029.0	0.2822697	-18.11	4.66	0.28214
CORE_3_50	0.815	0.04	2.642	0.091	0.282502	0.000022	0.00077	0.00013	478.4	0.2825521	-8.17	2.25	0.28249
CORE_3_51	1.213	0.05	4.07	0.18	0.281702	0.000021	0.000508	0.000035	985.0	0.2817496	-36.46	-14.77	0.28217
CORE_3_52	1.05	0.092	3.48	0.31	0.281907	0.00003	0.000608	0.000028	1132.0	0.281951	-29.21	-4.30	0.28207
CORE_3_53	1.182	0.063	2.9	0.16	0.282361	0.00003	0.00349	0.00014	1270.0	0.2823353	-13.12	12.46	0.28198
CORE_3_54	1.377	0.06	4.35	0.2	0.281932	0.000021	0.000958	0.000049	1349.0	0.2819656	-28.29	1.15	0.28193
CORE_3_55	1.05	0.071	3.33	0.21	0.282401	0.000031	0.000857	0.000015	719.4	0.2824484	-11.67	3.99	0.28234
CORE_3_56	1.49	0.25	4.86	0.8	0.282022	0.000032	0.000683	0.000044	1186.0	0.2820657	-25.07	0.99	0.28204
CORE_3_57	1.25	0.094	4.16	0.32	0.281256	0.000027	0.00056	0.000029	2039.0	0.2812933	-52.16	-6.86	0.28149
CORE_3_58	1.338	0.058	4.32	0.21	0.282108	0.000023	0.000831	0.000063	1015.0	0.2821521	-22.00	0.17	0.28215
CORE_3_59	1.053	0.045	3.05	0.14	0.282737	0.000037	0.001848	0.000064	409.0	0.2827838	0.28	8.90	0.28253
CORE_3_60	1.16	0.12	3.75	0.37	0.282101	0.000019	0.000773	0.000069	1200.0	0.2821435	-22.24	4.07	0.28203
CORE_3_61	1.16	0.24	3.77	0.8	0.282157	0.000037	0.001	0.00012	1299.0	0.2821935	-20.23	8.10	0.28197
CORE_3_62	1.266	0.092	4.44	0.32	0.282322	0.000016	0.000078	0.00001	613.0	0.2823831	-14.36	-0.71	0.2824
CORE_3_63	1.546	0.082	5.34	0.28	0.282311	0.000017	0.000171	0.000023	585.9	0.2823711	-14.75	-1.75	0.28242
CORE_3_64	1.61	0.12	4.97	0.35	0.281504	0.00003	0.001192	0.000046	1918.0	0.2815225	-43.28	-1.51	0.28157

CORE_3_65	1.153	0.069	3.76	0.23	0.282121	0.000036	0.000736	0.000027	928.0	0.2821721	-21.39	-1.09	0.2822
CORE_3_66	1.12	0.13	3.71	0.45	0.282161	0.000025	0.00058	0.000034	1066.0	0.2822133	-19.98	3.50	0.28211
CORE_3_67	1.484	0.064	4.79	0.26	0.281565	0.000045	0.000785	0.000091	1633.0	0.2816057	-41.02	-5.12	0.28175
CORE_3_68	0.921	0.052	3.04	0.17	0.282131	0.000037	0.000552	0.000018	550.6	0.2821903	-21.00	-8.94	0.28244
CORE_3_69	1.18	0.1	3.35	0.34	0.281884	0.00003	0.00253	0.00029	1640.0	0.2818713	-29.70	4.47	0.28175
CORE_3_70	1.136	0.061	3.58	0.19	0.282116	0.00002	0.001012	0.000026	1366.0	0.2821559	-21.50	8.29	0.28192
CORE_3_71	1.249	0.057	4.01	0.17	0.282533	0.000035	0.000836	0.000012	514.0	0.2825919	-6.72	4.46	0.28247
CORE_3_72	1.361	0.064	4.54	0.21	0.282353	0.000016	0.000489	0.000017	608.5	0.2824154	-13.05	0.33	0.28241
CORE_3_73	1.249	0.047	4.15	0.15	0.281634	0.000019	0.000586	0.000035	1658.0	0.2816846	-38.44	-1.74	0.28173
CORE_3_74	0.944	0.05	2.99	0.18	0.282101	0.000025	0.000989	0.000094	1383.0	0.2821451	-21.89	8.30	0.28191
CORE_3_75	1.382	0.066	4.52	0.22	0.282136	0.000029	0.000655	0.000018	1194.0	0.2821922	-20.62	5.66	0.28203
CORE_3_76	1.087	0.062	3.68	0.2	0.282137	0.000025	0.000369	0.00001	1020.0	0.2822019	-20.55	2.05	0.28214
CORE_3_77	1.3	0.11	4.21	0.35	0.28215	0.000027	0.000793	0.000038	1063.0	0.2822071	-20.05	3.21	0.28212
CORE_3_78	1.063	0.035	3.44	0.11	0.28158	0.000022	0.000817	0.0000039	1839.0	0.2816245	-40.21	0.29	0.28162
CORE_3_79	1.6	0.12	4.9	0.38	0.282225	0.000027	0.001223	0.000045	570.6	0.2822849	-17.40	-5.14	0.28243
CORE_3_80	1.28	0.1	4.27	0.35	0.282029	0.000022	0.000495	0.000018	1131.0	0.2820914	-24.33	0.65	0.28207
CORE_3_81	1.217	0.06	3.65	0.17	0.282136	0.000039	0.001469	0.000048	1382.0	0.2821716	-20.51	9.22	0.28191
CORE_3_1	1.426	0.08	4.7	0.26	0.282171	0.000022	0.000605	0.000007	1252.0	0.2821687	-21.46	6.15	0.282
CORE_3_2	1.2	0.2	3.23	0.51	0.282301	0.000031	0.00259	0.00018	590.0	0.2822853	-16.83	-4.69	0.28242
CORE_3_3	1.442	0.093	4.95	0.3	0.282212	0.000025	0.000242	0.000023	895.0	0.2822209	-19.98	-0.10	0.28222
CORE_3_4	1.64	0.15	4.5	0.44	0.280717	0.000041	0.00197	0.00012	3427.0	0.2805988	-72.88	1.03	0.28057
CORE_3_5	1.024	0.027	3.486	0.096	0.281394	0.000037	0.000343	0.000016	2059.0	0.2813926	-48.94	-2.87	0.28147
CORE_3_6	1.55	0.14	4.63	0.51	0.281877	0.000036	0.00171	0.00028	1697.0	0.281834	-31.86	4.46	0.28171
CORE_3_7	1.19	0.11	3.86	0.35	0.282325	0.000033	0.000783	0.000047	1156.0	0.2823199	-16.02	9.32	0.28206
CORE_3_8	1.095	0.075	3.51	0.26	0.281211	0.000019	0.000941	0.000064	2218.0	0.2811832	-55.41	-6.62	0.28137
CORE_3_9	1.008	0.065	3.2	0.21	0.281561	0.000033	0.000994	0.00005	2000.0	0.2815352	-43.04	0.84	0.28151
CORE_3_10	1.261	0.09	4.19	0.3	0.281798	0.00002	0.000609	0.00002	1167.0	0.2817966	-34.65	-8.98	0.28205
CORE_3_11	0.926	0.078	3.07	0.3	0.282144	0.000022	0.000418	0.000043	920.0	0.2821488	-22.42	-2.10	0.28221
CORE_3_12	1.24	0.068	3.66	0.2	0.282169	0.000027	0.001702	0.000071	1397.0	0.282136	-21.54	8.30	0.2819
CORE_3_13	0.789	0.086	2.14	0.24	0.282443	0.000032	0.00272	0.00012	889.5	0.2824085	-11.88	6.42	0.28223

CORE_3_14	1.38	0.12	4.2	0.31	0.281805	0.00003	0.00127	0.00013	1768.0	0.2817744	-34.41	3.98	0.28166
CORE_3_15	1.27	0.17	4.23	0.56	0.281522	0.000022	0.000557	0.000016	1873.0	0.2815142	-44.41	-2.84	0.28159

Biographical Information

Ohood Bader Alsalem was born on September 18, 1982 in the State of Kuwait. She joined Kuwait University in 2000 to start her undergraduate study in the Department of Earth and Environmental Sciences. She received her Bachelor of Science majoring in geology and minoring in petroleum geology in 2005.

Ohood maintained the highest GPA in the Department of Earth and Environmental Sciences during 2001-2005. She was honored to be the head of the students at the field trip to Oman in 2003, a member of the Society of Faculty of Science in Kuwait University in 2004, and a member of the Cultural Committee of the Deanship in the Faculty of Science in Kuwait University in 2004 and 2005. She was also recognized and awarded as the Ideal Student by the Society of Faculty of Science in 2005. Ohood joined Baker Hughes Incorporate immediately after her graduation.

In 2012, Ohood was awarded full education scholarship from Kuwait University to conduct her graduate studies at the University of Texas at Arlington. She joined the Department of Earth and Environmental Sciences at the University of Texas at Arlington for her master degree in petroleum geology in the fall of 2012. In 2014, she was admitted into the PhD program at the University of Texas at Arlington to continue her graduate study. Ohood is currently a member of the Honor Society and Golden Key International Honor Society based on her excellent academic achievement.

Ohood aims to become an academic professor and a researcher in Kuwait University upon finishing her PhD. She has always been dedicated and determined to achieve her ambitions. She is an active, energetic, sociable, and pleasant woman to work with. Her future is bright as long as she keeps her strong faith in herself.